

PHYSICAL HYDROGRAPHY OF THE VIENNA POWER  
PLANT SITE

PART I: COMPUTATIONS OF THE DISTRIBUTION OF  
EFFLUENT DISCHARGED FROM THE VIENNA ELECTRIC  
GENERATING STATION INTO THE NANTICOKE RIVER

PART II: COMPUTATIONS OF THE DISTRIBUTION OF  
CONTAMINANTS INTRODUCED INTO CHICONE CREEK  
IN GROUNDWATER

by Donald W. Pritchard and Robert E. Wilson

Special Report 37\*

July 1980



PHYSICAL HYDROGRAPHY OF THE VIENNA POWER  
PLANT SITE

PART I: COMPUTATIONS OF THE DISTRIBUTION OF  
EFFLUENT DISCHARGED FROM THE VIENNA ELECTRIC  
GENERATING STATION INTO THE NANTICOKE RIVER

PART II: COMPUTATIONS OF THE DISTRIBUTION OF  
CONTAMINANTS INTRODUCED INTO CHICONE CREEK  
IN GROUNDWATER

by Donald W. Pritchard and Robert E. Wilson

Special Report 37\*

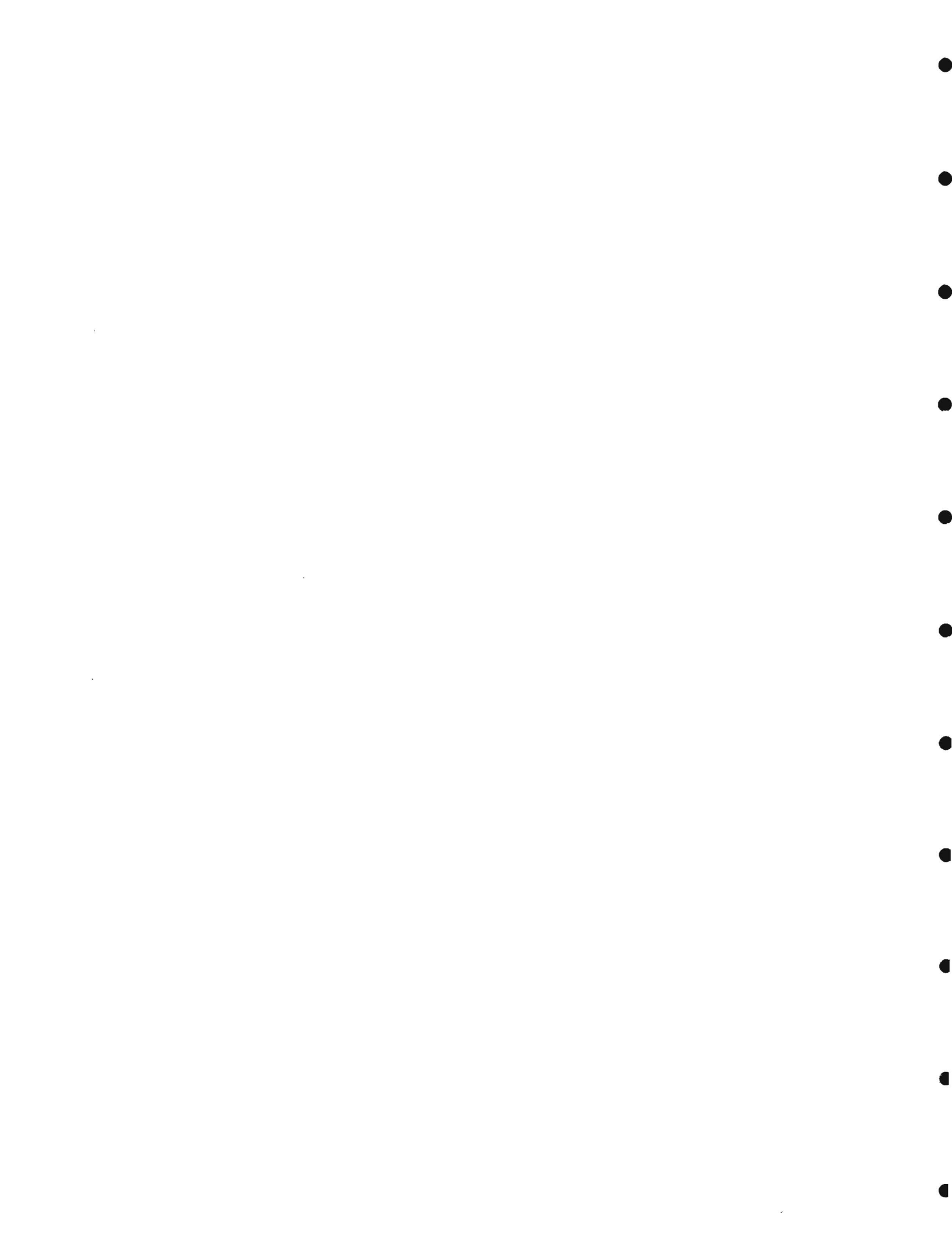
July 1980

Reference 80-4

*Sponsored by the Power Plant Siting Program  
Department of Natural Resources, State of Maryland*

\*Issued Concurrently with JHU-PPSE 8-10





MARINE SCIENCES RESEARCH CENTER  
STATE UNIVERSITY OF NEW YORK  
STONY BROOK, NEW YORK 11794

JHU-PPSE 8-10\*

PHYSICAL HYDROGRAPHY OF THE VIENNA POWER PLANT SITE

PART I: COMPUTATIONS OF THE DISTRIBUTION OF EFFLUENT DISCHARGED  
FROM THE VIENNA ELECTRIC GENERATING STATION INTO THE  
NANTICOKE RIVER

PART II: COMPUTATIONS OF THE DISTRIBUTION OF CONTAMINANTS INTRODUCED  
INTO CHICONE CREEK IN GROUNDWATER

by

Donald W. Pritchard and Robert E. Wilson

July 1980


*Sponsored by the Power Plant Siting Program*

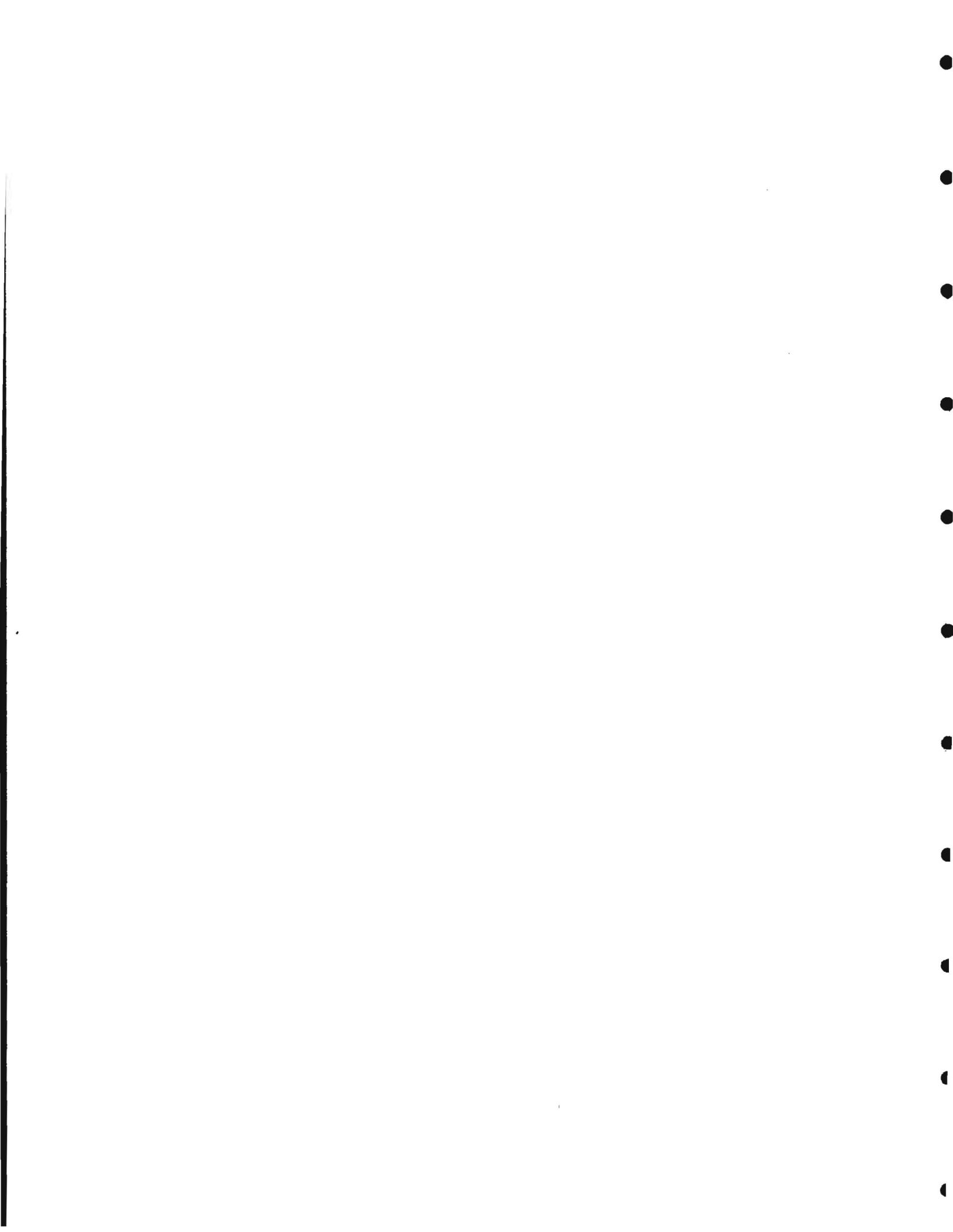
*Department of Natural Resources, State of Maryland*

Special Report 37\*  
Reference 80-4

\* Issued Concurrently

Approved for Distribution

  
\_\_\_\_\_  
J.R. Schubel, Director



Part 1

Computations of the Distribution of Effluent Discharged  
from the Vienna Electric Generating Station  
into the Nanticoke River

INTRODUCTION

The purpose of this part of this report is to present the results of computer computations of the probable concentration of excess heat and contaminants in the Nanticoke River resulting from the combined discharge of blowdown water from existing Unit 8 and Proposed Unit 9 of the Vienna Electric Generating Station.

Computations are made herein for both the 400 MW new unit as originally proposed and for the 600 MW Unit 9 as now proposed in the amended Application for Certificate of Public Convenience and Necessity submitted by the Delmarva Power Company. Presentation of the results of both these cases allows an evaluation of the impact of the plant as now proposed and also the increment increase in impact resulting from the increase in unit size between that originally proposed and that now proposed.

In making the detailed calculations shown graphically in this report it was assumed that the blowdown water from Unit 8 and Unit 9 would be combined into a single discharge. Combining the discharges from the units would provide a smaller nearfield thermal plume than would be the case for the complex interacting plumes which would result from separate discharges. Computational difficulties have

prevented us from determining the shape of the two interacting plumes for the case of separate discharges. However, estimates of the area enclosed within specified isolines of contaminant concentration and of excess temperature have been made, and these results will be compared with the results of the more detailed analysis of the single, combined discharge for the two units.

The detailed results of computations of the character of the thermal plume given here make use of the original design for the discharge pipe, which called for an 8" inside diameter. The present plans call for a discharge pipe with a 10" orifice. The effects of this difference in discharge orifice size will also be discussed in a later section of this part of this report.

#### THE MODEL

The model used to obtain the information on the shape and dimensions of the thermal and contaminant plume presented herein is the MSRC Combined Field Thermal Plume Model. A detailed description of this model is given by Carter *et al.* (1979). The model combines a near field thermal plume model based on the work of Carter and Regier (1974) with a far field diffusion model described by Carter *et al.* (1977). The latter model makes use of the Okubo-Pritchard Diffusion Equations, Pritchard (1960).

The procedure involves the super-position of a large number of sequential small diffusing patches, each from an infinitesimal, instantaneous source, and all moving with the time varying ambient

velocity  $u_a(t)$ . The sequence of infinitesimal sources sum to the continuous rate of discharge of the power plant. The integration of the far field model is carried out over a number of tidal cycles until a pseudo-steady state far field distribution is attained; that is, until the time dependent variations in concentration over the tidal cycle are repeated from tidal cycle to tidal cycle.

The concentration distribution as computed from the far field model, while applicable for locations well removed from the source, is incorrect in the near field plume because the momentum and buoyant entrainment are not included. After pseudo-steady state in the far field computations is reached, the source is turned off, and computations made for several tidal cycles to obtain the background concentration distribution over the near field and intermediate field.

The near field model is then exercised and the distribution of concentration thus obtained is added to the far field distribution. In carrying out this combining of the two models care is taken such that excess heat and contaminant mass are conserved.

An important feature of this model is that it includes the interaction of the far field and near field distributions. In most near field models, the tacit assumption is made that there is an infinite supply of "clean" water available for entrainment into the plume. No account is taken of the fact that quite often some fraction of the water being entrained into the plume as dilution water contains a background of contaminants and excess heat built up from the previous continuous discharges from the plant.

Models are often used without verification that the computed results can be used with reasonable confidence for the specific purpose at hand. Usually this is because the data necessary for such verification are not available. The various parts of the MSRC Combined Field Thermal Plume Model have shown good comparisons with a number of direct plume measurements. The model has been used in its present full configuration in studies associated with an existing power plant on the Hudson River estuary. Good comparison was obtained between computed and observed values of recirculation at the plant, though no detailed comparison of computed and observed plume characteristics were made.

Fortunately, a set of data exists which allows verification of the model's use in the Vienna area of the Nanticoke River. In April 1974 the condenser discharges from the once-through cooling systems of Units 5, 6 and 7, together with the blowdown water from the cooling tower of Unit 8, were tagged with the fluorescent dye Rhodamine WT, as reported by Carter and Regier (1975). We have exercised the MSRC Combined Field Thermal Plume Model under the conditions applicable to the April 1974 field study, and have compared the computed values of dye concentration with the observed values of dye concentration with the observed values reported by Carter. This comparison is presented as final section to this part of this report.

#### INPUT PARAMETERS FOR THE MODEL

The model requires that certain geometric and flow dependent parameters be specified, including the time dependent velocity field.



For our purposes here the velocity was considered to be composed of a time dependent oscillatory component of semi-diurnal tidal period plus a time independent non-tidal mean velocity. An analysis of the current meter records made just upstream from the plant indicated that the amplitude of the oscillatory tidal current for the subject segment of the Nanticoke River is  $55 \text{ cm s}^{-1}$ . The mean non-tidal flow depends on the river flow, but the current meter records do not indicate any significant vertical shear in this mean flow.

Three river flow conditions were considered: (1) A low river flow of 445 cfs, which results in a non-tidal velocity of  $0.84 \text{ cm s}^{-1}$  for the average cross-section in the two-tidal excursion long reach of the river centered on the plant site; (2) a mean river flow of 810 cfs, which corresponds to a mean non-tidal velocity of  $1.53 \text{ cm s}^{-1}$ ; and (3) a high river flow of 1520 cfs, corresponding to a mean non-tidal velocity of  $2.86 \text{ cm s}^{-1}$ .

The diffusion velocity, a coefficient which enters the Okubo-Pritchard Diffusion Equations, was taken to be  $1.5 \text{ cm s}^{-1}$ . This value has been found applicable in other studies in the Chesapeake Bay estuarine system, and on the basis of the verification study described later in this report, this value appears applicable to the Nanticoke in the vicinity of the Vienna Electric Generating Station.

The mean width of the river in the area of interest was taken to be 410 meters, and the mean depth as 3.67 meters.

As pointed out earlier, it was assumed that the blowdown water from Unit 8 and Unit 9 would be combined into a single discharge.

The design features of the discharge structure were taken from the Application for Certificate of Public Convenience and Necessity as originally submitted by the Delmarva Power Company, for a shoreline submerged discharge for Unit 9. The details are given in Section 2.8C.1 and Figure 2.8C.1 of the above captioned document. Briefly, the discharged orifice is assumed to be located at a depth of 10 feet below MLW on the face of a vertical wall at the shoreline. This wall is assumed to extend downwards to a dredged bottom at 12 feet below MLW. The discharge port is taken to be a cylindrical pipe with an inside diameter of 8 inches. The effects on the results described here of increasing this pipe diameter to 10 inches will be discussed in a later section.

Computations were first made using the wintertime blowdown flow from Unit 9, as stated in the above captioned document for a 400 MWE unit, of 1332 gpm, combined with a blowdown discharge from Unit 8 of 381 gpm. This later figure was obtained by scaling the blowdown flow from Unit 9 by the ratio of the make-up flow for Unit 8 of 1460 gpm as given by Carter (1975) to the make-up flow for Unit 9 of 4892 gpm as given in the above captioned application. The total rate of flow to be discharged through the 8" diameter outfall was therefore taken to be  $1713 \text{ gals min}^{-1}$  or  $0.108 \text{ m}^3 \text{ sec}^{-1}$ . The velocity at the discharge orifice was then taken to be  $3.33 \text{ m sec}^{-1}$  (or  $10.9 \text{ ft sec}^{-1}$ ).

The Delmarva Power Company states in their Application for Certificate of Public Convenience and Necessity that the blowdown

water discharge will have a temperature of 68°F in winter when the ambient temperature in the river is 34°F; while in summer the temperature of the discharge will be 85°F when the ambient temperature of the receiving water is 84°F. Hence the excess temperature at discharge in winter would be 34°F, and in summer, only 1°F. The amended document gives slightly different values. However, these differences would not significantly alter the conclusions reached here. The preliminary computations presented here are for the wintertime conditions of a 34°F excess temperature of the discharge. The summertime case for an excess temperature of 1°F is not treated for the following reasons. The distribution of relative concentration in the near field would not be significantly different between summer and winter, other things, such as river flow being equal. In the present form of the MSRG model, computational difficulties arise for the near field computations for very large densimetric Froude numbers such as occur for an excess temperature of only 1°F. We know that the near field plume will be smaller, that is, show more rapid dilution with distance from the source, as the densimetric Froude number increases, other factors being equal. Consequently the case considered here should be more severe in the near field than would occur for the summertime conditions of a 1°F excess temperature. Intermediate conditions will exist in the spring months of April and May when spawning of striped bass occur in this reach of the Nantuxke River. Excess temperatures of the discharge will be

RESULTS

about 15°F in April and 12°F in May. The size of the areas contained within specified isotherms of excess temperature in the thermal plume will thus be less than those computed here for the winter case, by a factor of two or more.

Note that in our computations we deal not with the absolute value of the excess temperature or of the concentration of a contaminant, but with the relative concentration; that is, the ratio of the concentration (or excess temperature) at any point in the plume to the concentration (or excess temperature) at the point of discharge.

Thus, while the excess temperature in the summertime plume will obviously be much less than the excess temperature in the wintertime plume, since the initial undiluted values are 1°F for summer and 34°F for winter, the relative excess temperatures for the two cases will be approximately the same in the far field, and only fractionally lower in summer than in winter for the near field plume. This fact is important since the concentration of chemical contaminants in the undiluted blowdown water may be higher in summer than in winter.

## RESULTS

The computed output from the model for these computations are in terms of the relative concentration, or inverse dilution. Thus, representing the dilution of the effluent by the symbol  $D$ , the concentration of a contaminant at the point of discharge by  $c_o$  and that at any other point in the river by  $c$ , and the excess temperature at the point of discharge by  $\theta_o$  and that at any other point in the river

by  $\theta$ , then the relative concentration is given by

$$D^{-1} = \frac{c}{c_o} = \frac{\theta}{\theta_o} \quad (1)$$

The relative concentration then varies from 1.0 at the discharge to 0.0 at positions sufficiently removed from the source so that no measurable constituents of the effluent occur.

Note that Equation (1) when applied to the excess temperature,  $\theta$ , is correct only if surface cooling to the atmosphere is unimportant. This is certainly the case here where mixing in the near field plume results in a rapid reduction in excess temperature to very low values due to dilution. The integral of the excess temperature over the area of the plume results in a very low driving term for heat loss to the atmosphere.

Computations were made over a reach of the river extending upstream and downstream from the plant site a distance of 5 nautical miles (9.2 km) which is approximately the length of a tidal excursion. The complex geometry of this 10 nautical mile reach of the river was scaled to a rectilinear grid having a width of 410 meters, the mean width of the river over this segment. Values of the relative concentration were printed out at 561 grid positions for the far field computations. The grid points were separated by 0.2 nautical miles in the longitudinal direction and by 41 meters in the lateral direction. The rectilinear grid was distorted in the printout so that there appears to be an equal spacing in the lateral direction and in the

longitudinal direction; that is, the river appears to be wider in relation to its length by the factor of  $370.6/41$  or  $9.04$ .

Printouts were obtained for each of the three river flows (high flow, or 1520 cfs; mean flow, or 810 cfs; and low flow, or 445 cfs), for four different stages of the tide (maximum ebb, maximum flood, near slack before ebb, and near slack before flood). Values are given for near the time of slack water rather than at slack water because the near field model fails to compute for exactly zero ambient current.

The computed relative concentration distributions were contoured by hand, and the resulting far field distributions on the distorted rectangular reach of the river are shown in Figures 1 through 6 for the twelve cases considered (3 river flows, each for 4 phases of the tide).

The near field plume on these figures is somewhat larger than it should be, since the far field computation does not take into consideration dilution by momentum entrainment close to the points of discharge. Near field calculations were carried out for mean river flow, for near slack before ebb and for maximum flood flow. These computations were made on an expanded rectangular grid of 1071 points extending longitudinally 0.2 nautical miles upstream and downstream from the point of discharge, and extending laterally from the western shore of the river outward a distance of only 82 meters. The longitudinal spacing between grid points for this near field calculation was 0.0080 nautical miles, and the lateral spacing was

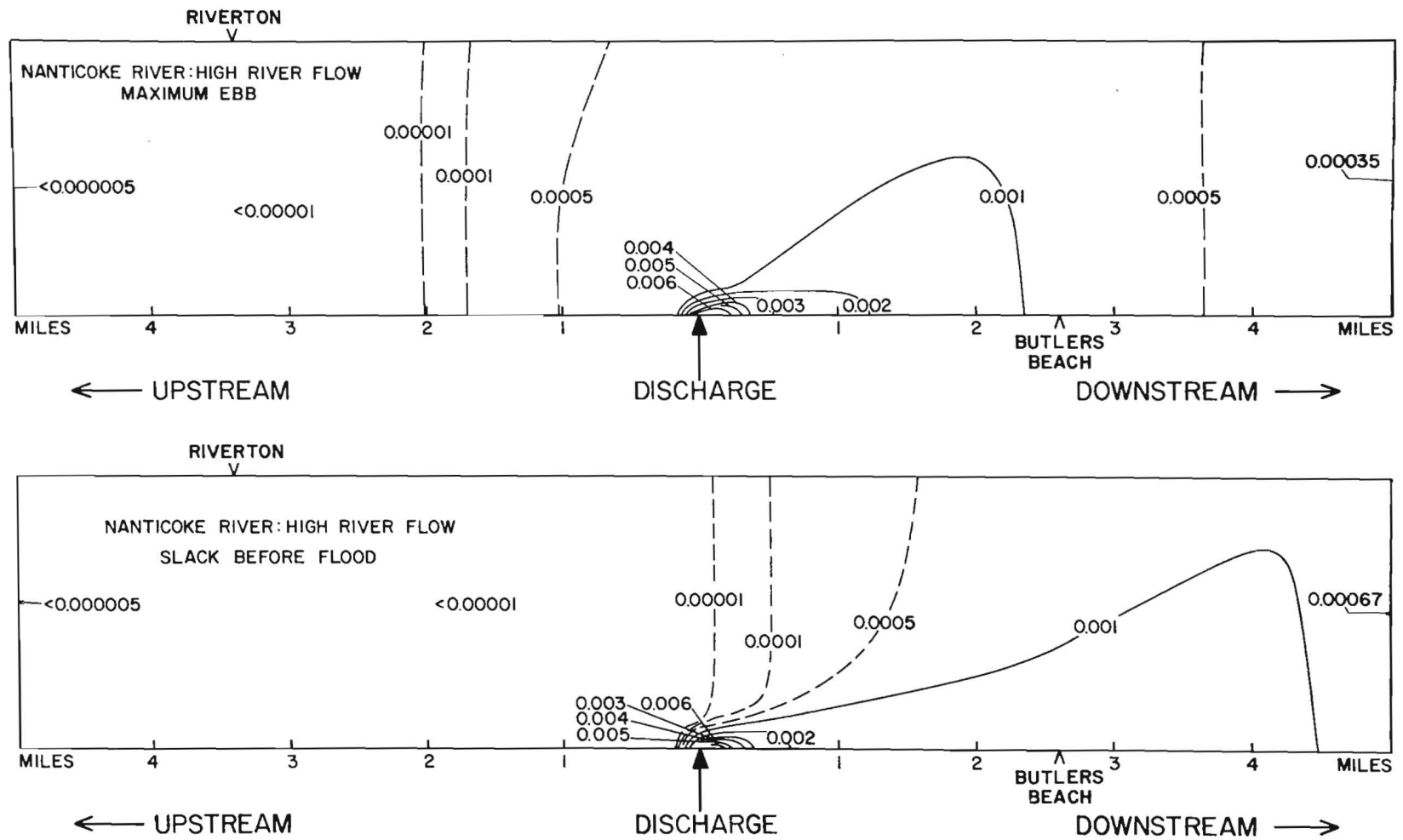


Figure 1. Isolines of relative concentration for high river flow (1520 cfs), for maximum ebb tidal flow and for near slack before flood.



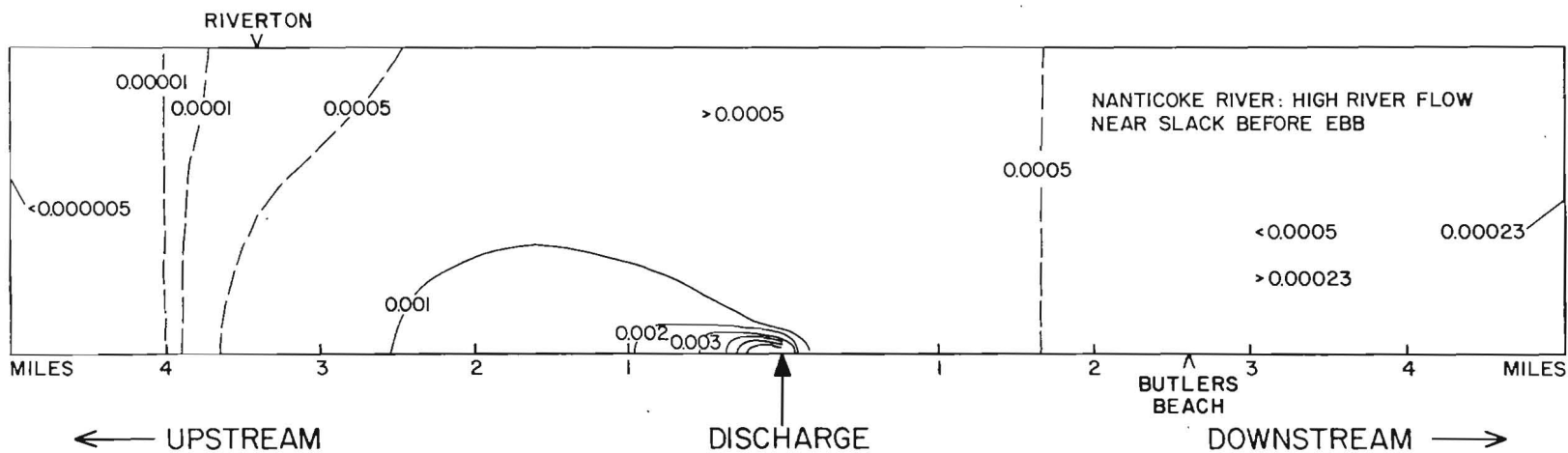
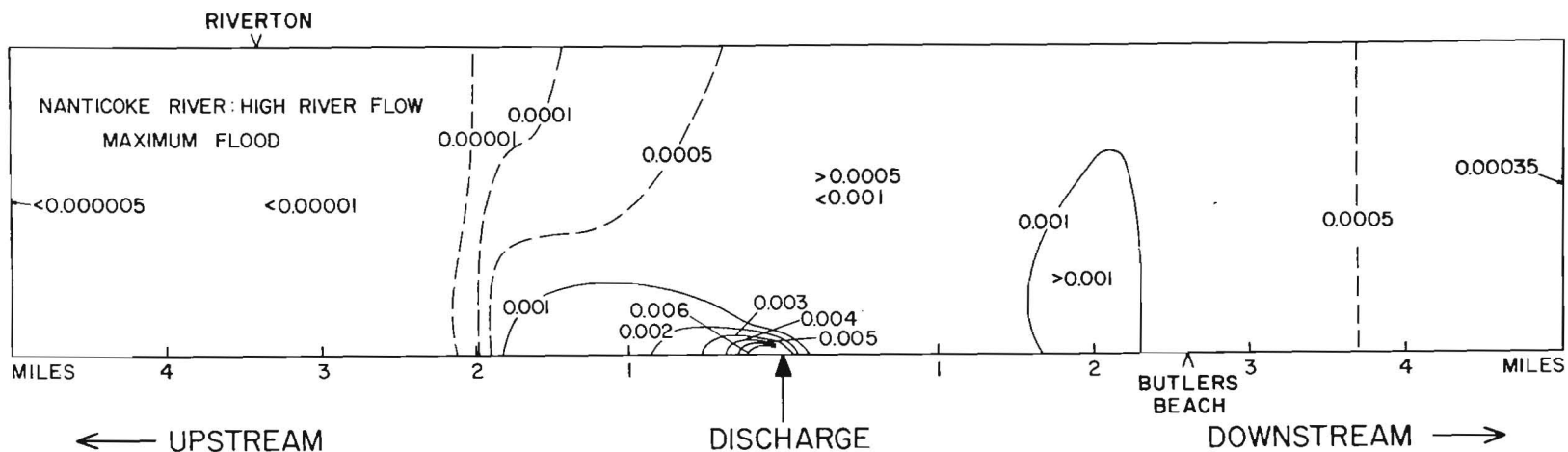


Figure 2. Isolines of relative concentration for high river flow (1520 cmfs), for maximum flood tidal flow and for near slack before ebb.

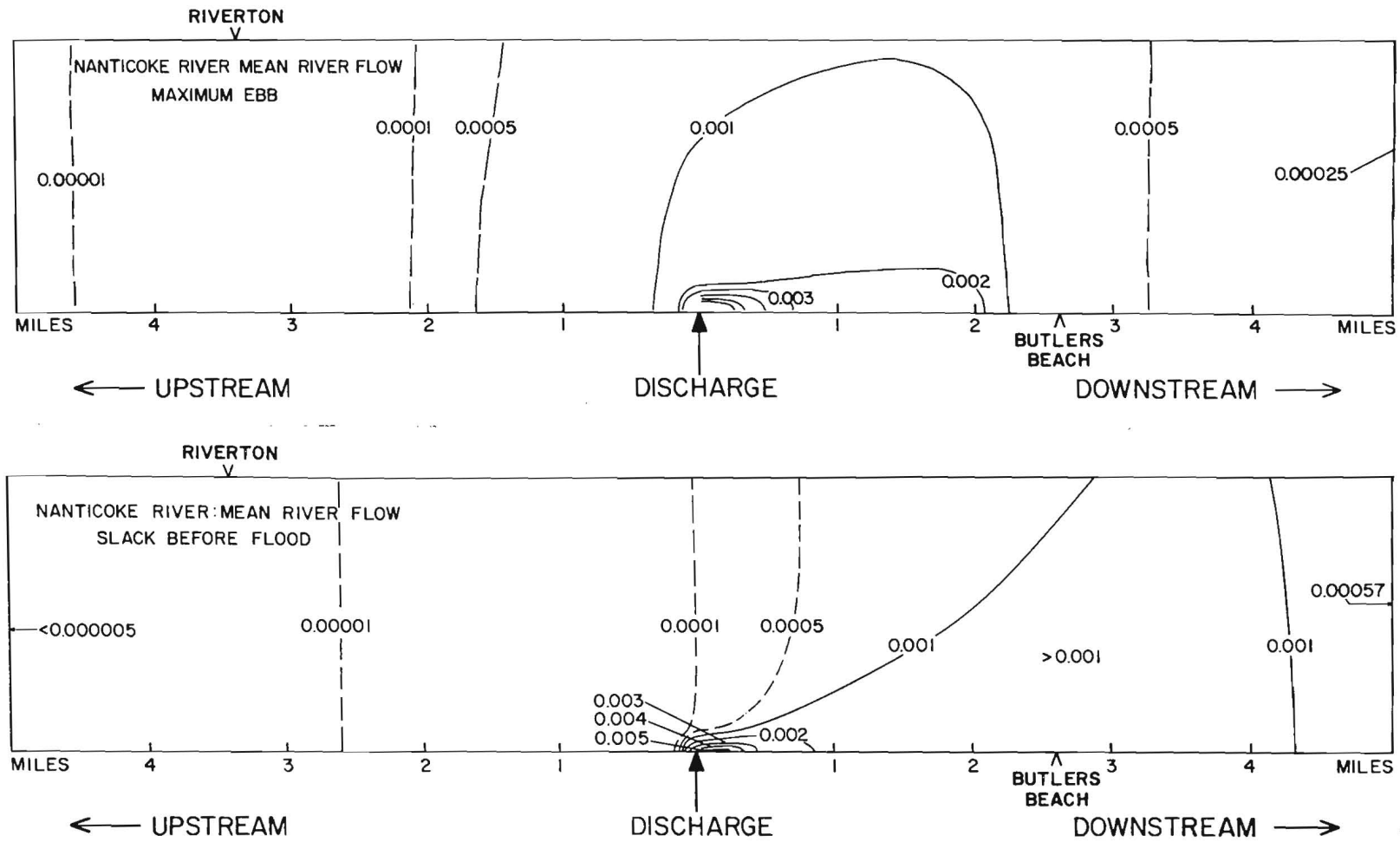


Figure 3. Isolines of relative concentration for mean river flow (810 cfs), for maximum ebb tidal flow and for near slack before flood.

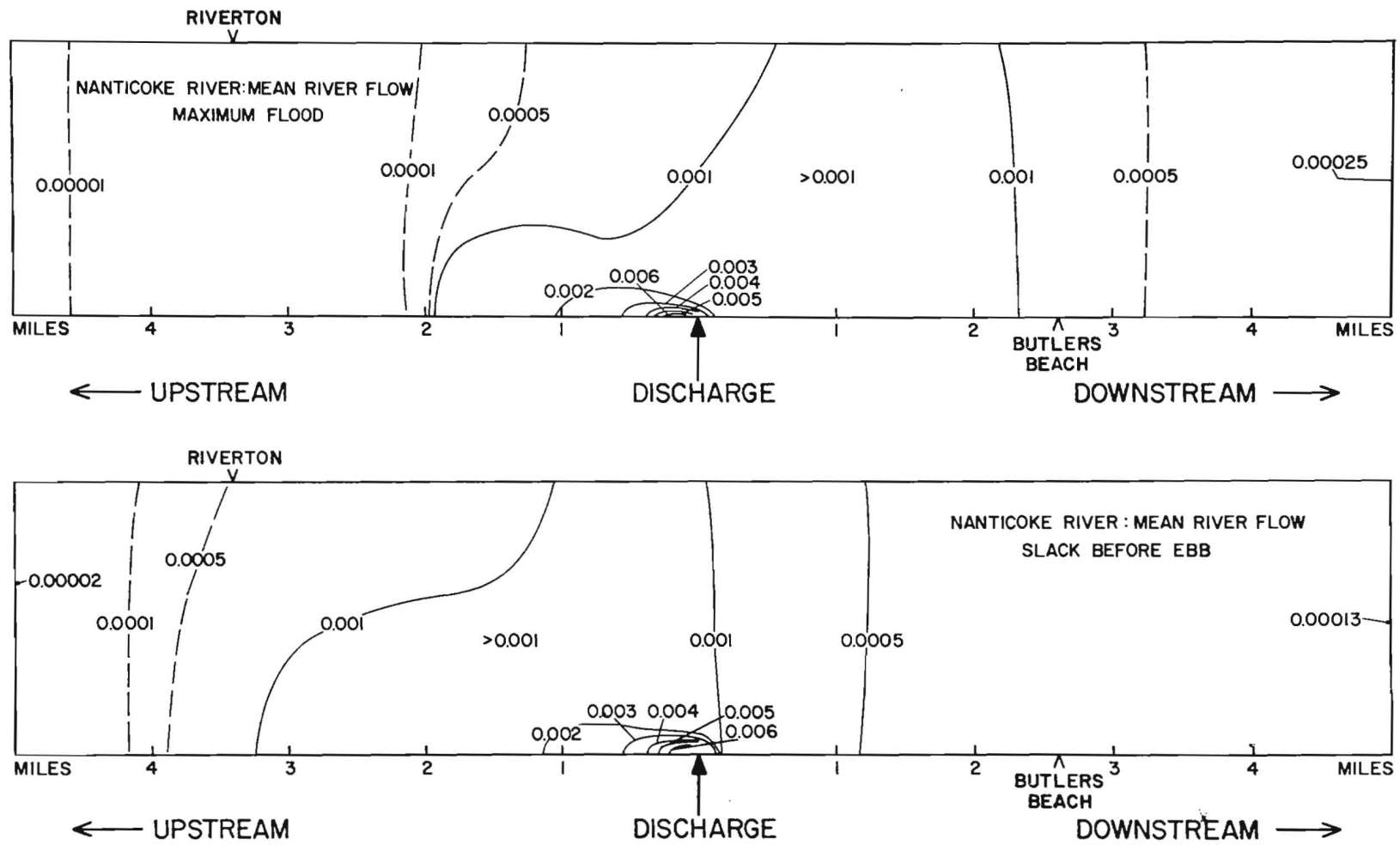


Figure 4. Isolines of relative concentration for mean river flow (810 cfs), for maximum flood tidal flow and for near slack before ebb.

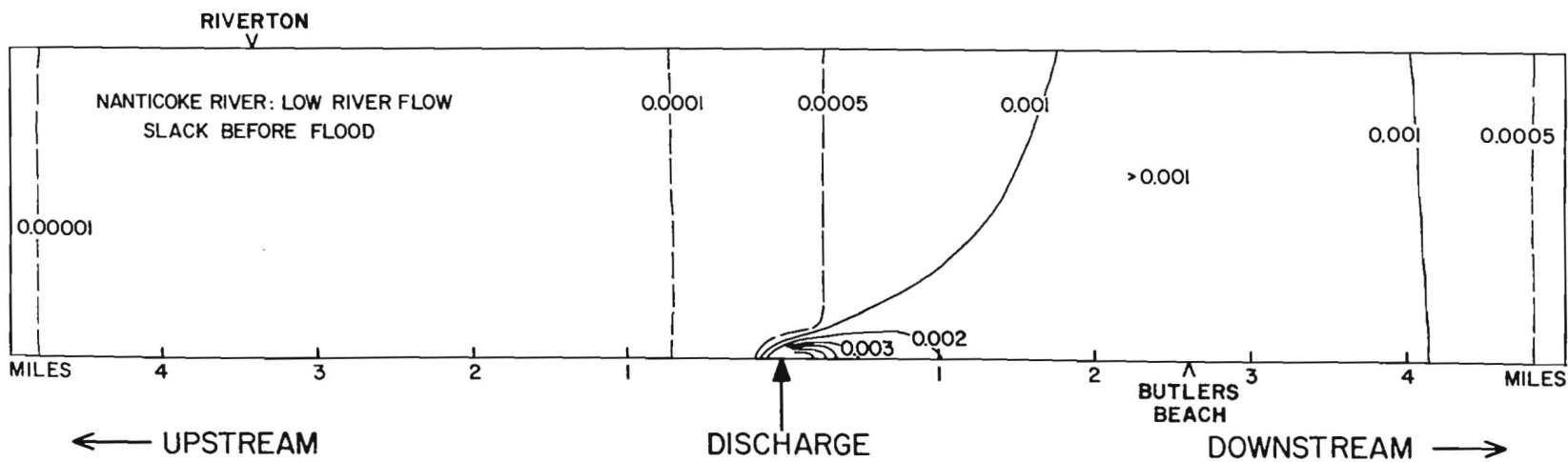
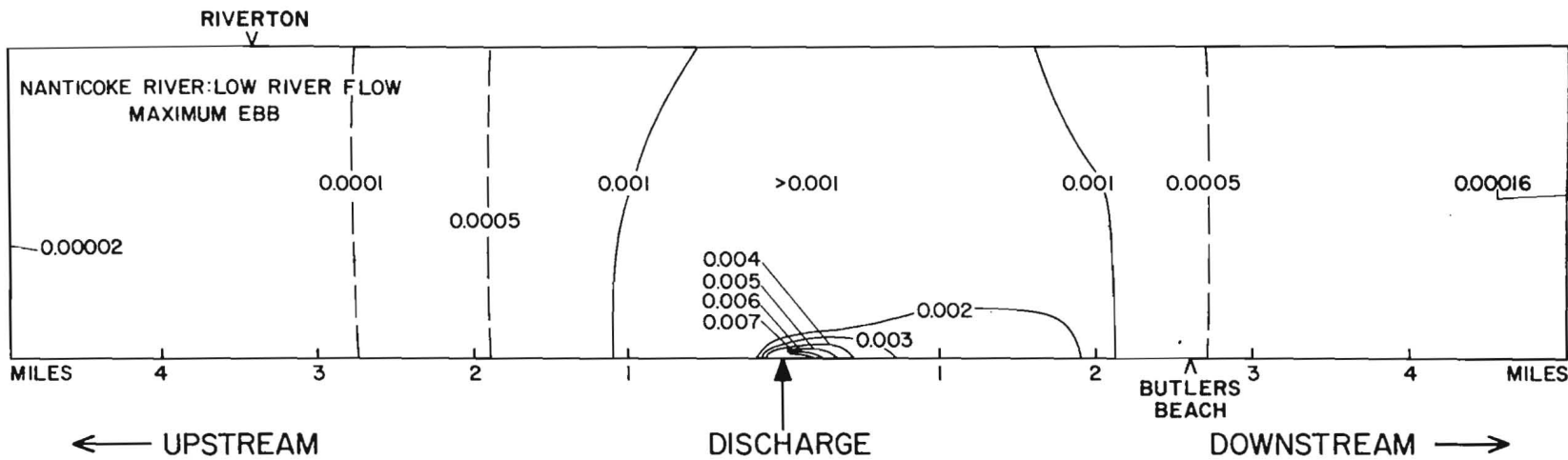


Figure 5. Isolines of relative concentration for low river flow (445 cfs), for maximum ebb tidal flow and for near slack before flood.

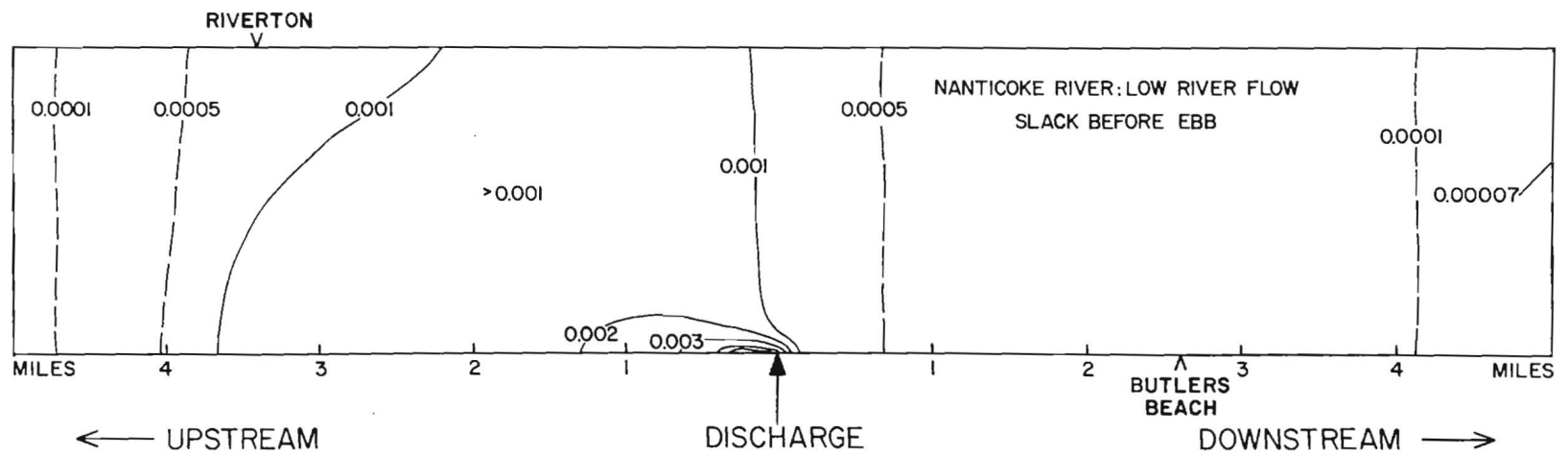
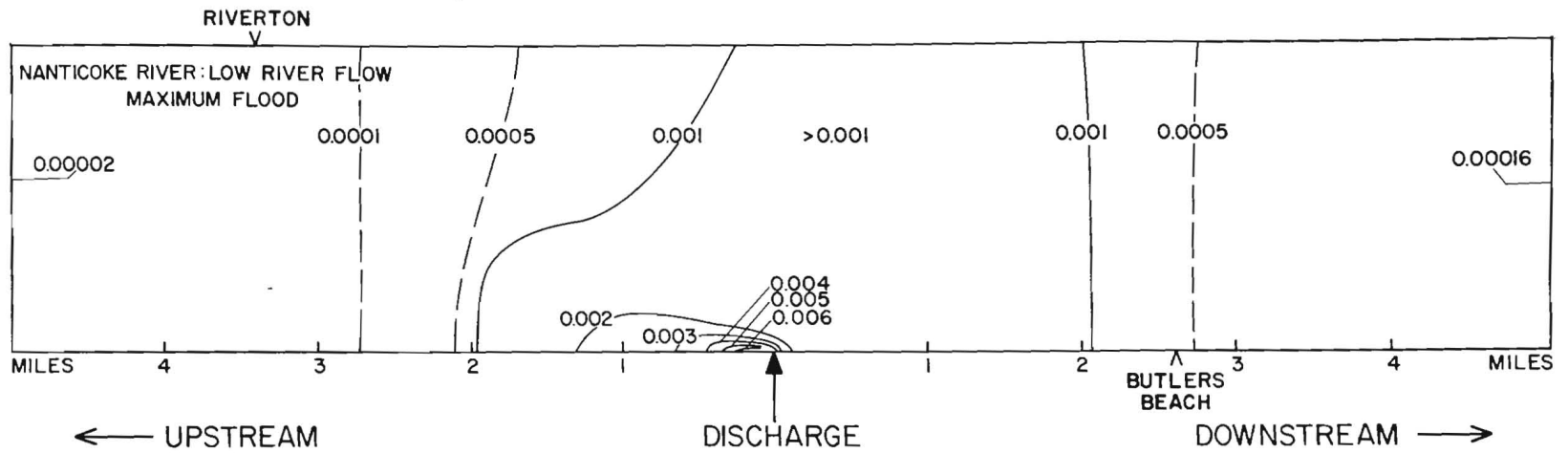


Figure 6. Isolines of relative concentration for low river flow (445 cfs), for maximum flood tidal flow and for near slack before ebb.

4.1 meters. The contoured distributions of relative concentration for these near field plumes are given in Figures 7 and 8.

The far field distributions of relative concentrations have been scaled back to the actual geometry of the river, and the twelve cases are given in Figures 9 through 32. A separate figure is given for the reach of the river up-stream from the point of discharge and for the reach of the river downstream from the point of discharge for each of the twelve cases considered.

Before going further we should mention that we accounted for the influence of the river banks on the far field concentrations by using the method of images. Reflection from the river bank which is on the same side of the river as the original source was accounted for by simply doubling the magnitude of the original source. Reflection from the distant river bank was accounted for by placing an image source behind this bank a distance equal to the width of the river. This image source must itself have an image appropriately placed, and so on. We used in total 6 image sources and the relative far field concentration fields presented in Figures 1 through 6 and 9 through 32 each represent a linear superposition of the field from the original source and the 6 image sources.

The concentration fields in Figures 1 through 6 and 9 through 32 show a well defined plume with relatively high concentrations superposed on a relatively uniform background. The plume is composed of material emitted from the source since the last change in direction of the tidal current. Concentrations within the plume decrease down

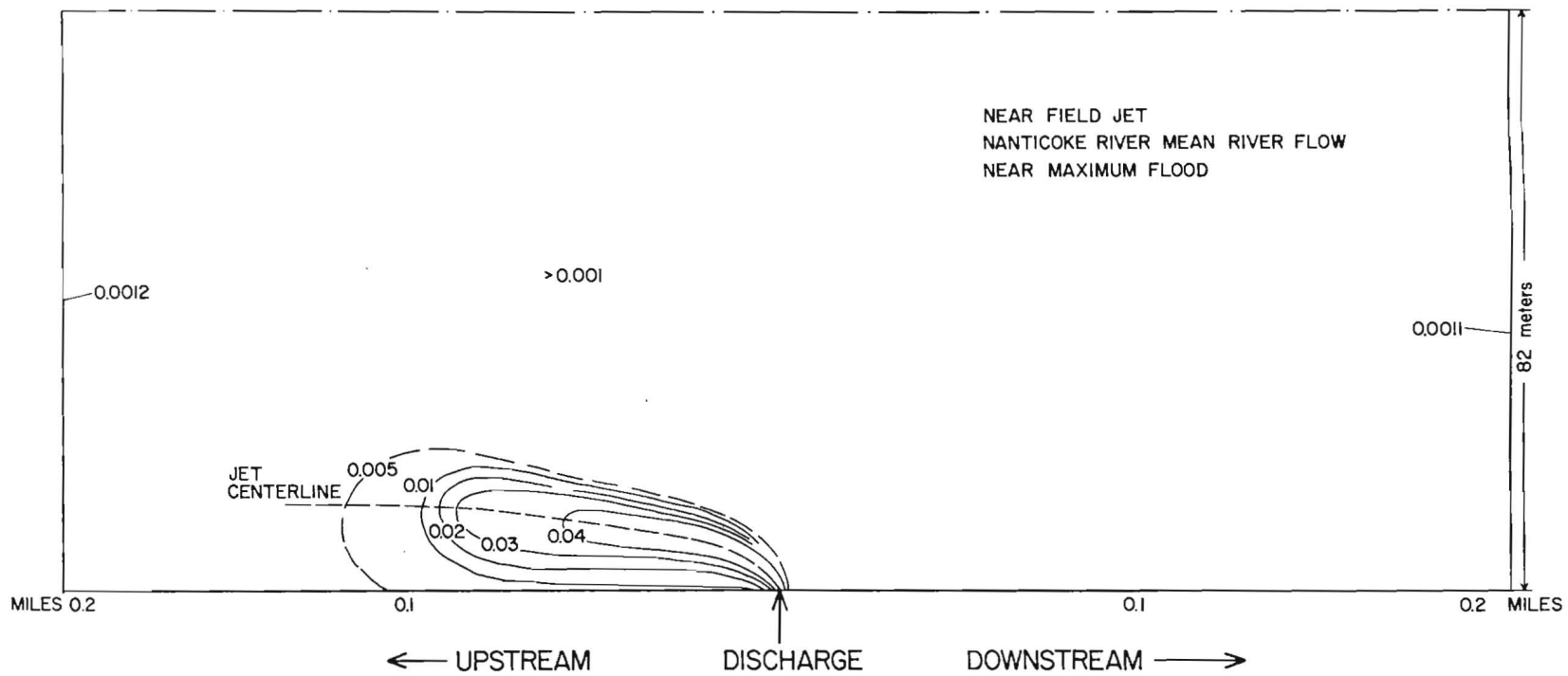


Figure 7. Isolines of relative concentration in the near field plume for mean river flow, for near maximum flood tidal flow.



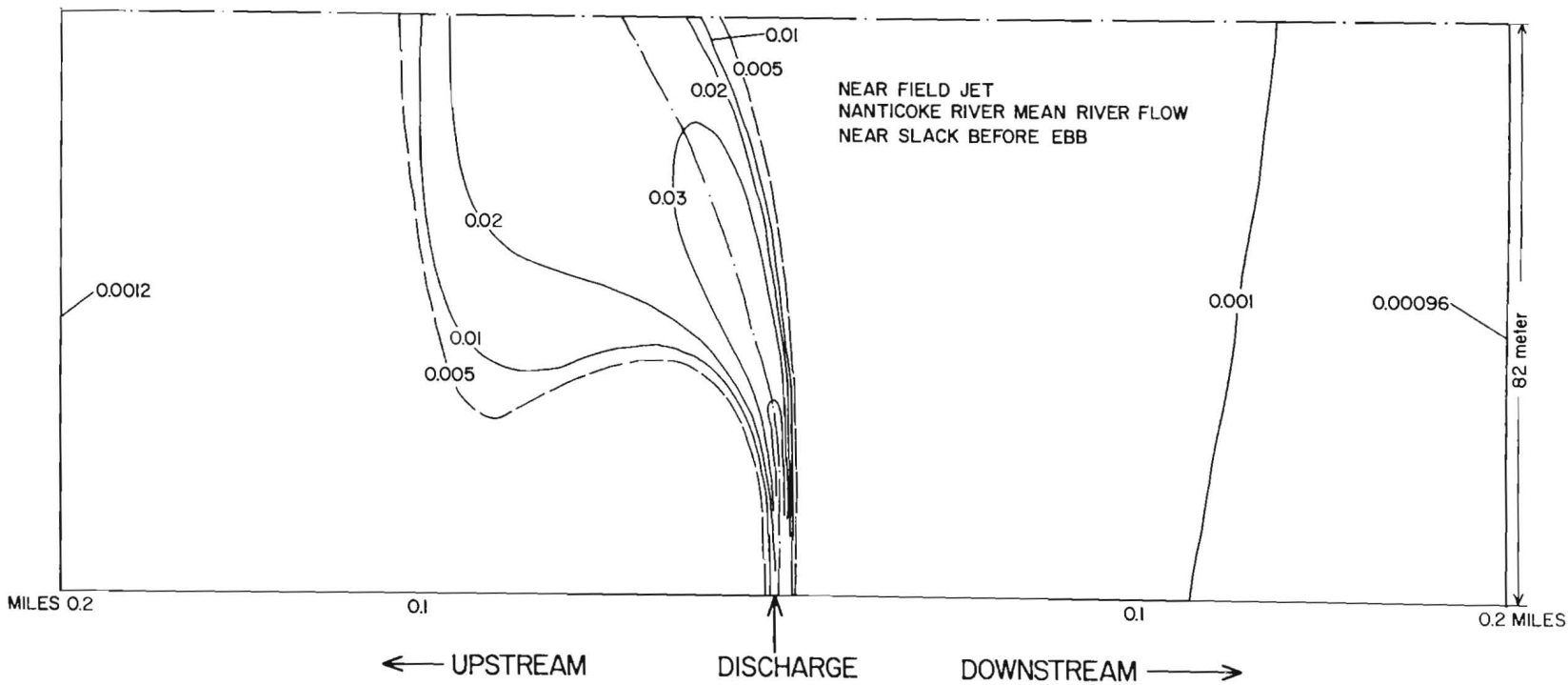


Figure 8. Isolines of relative concentration in the near field plume for mean river flow, for near slack before ebb.

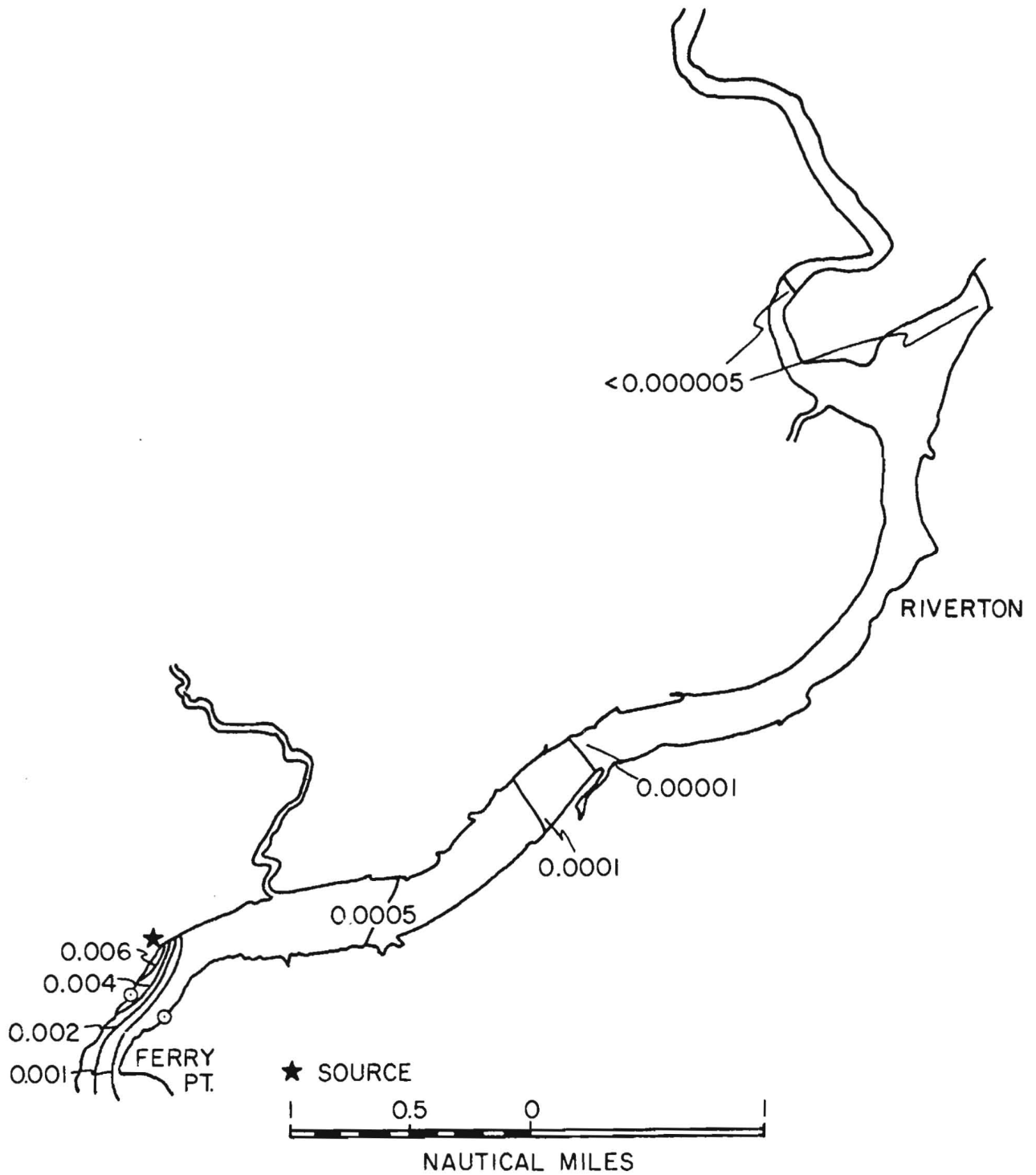


Figure 9. Distribution of relative concentration for a 400 MW plant, at maximum ebb, during high river flow, upstream from the source.

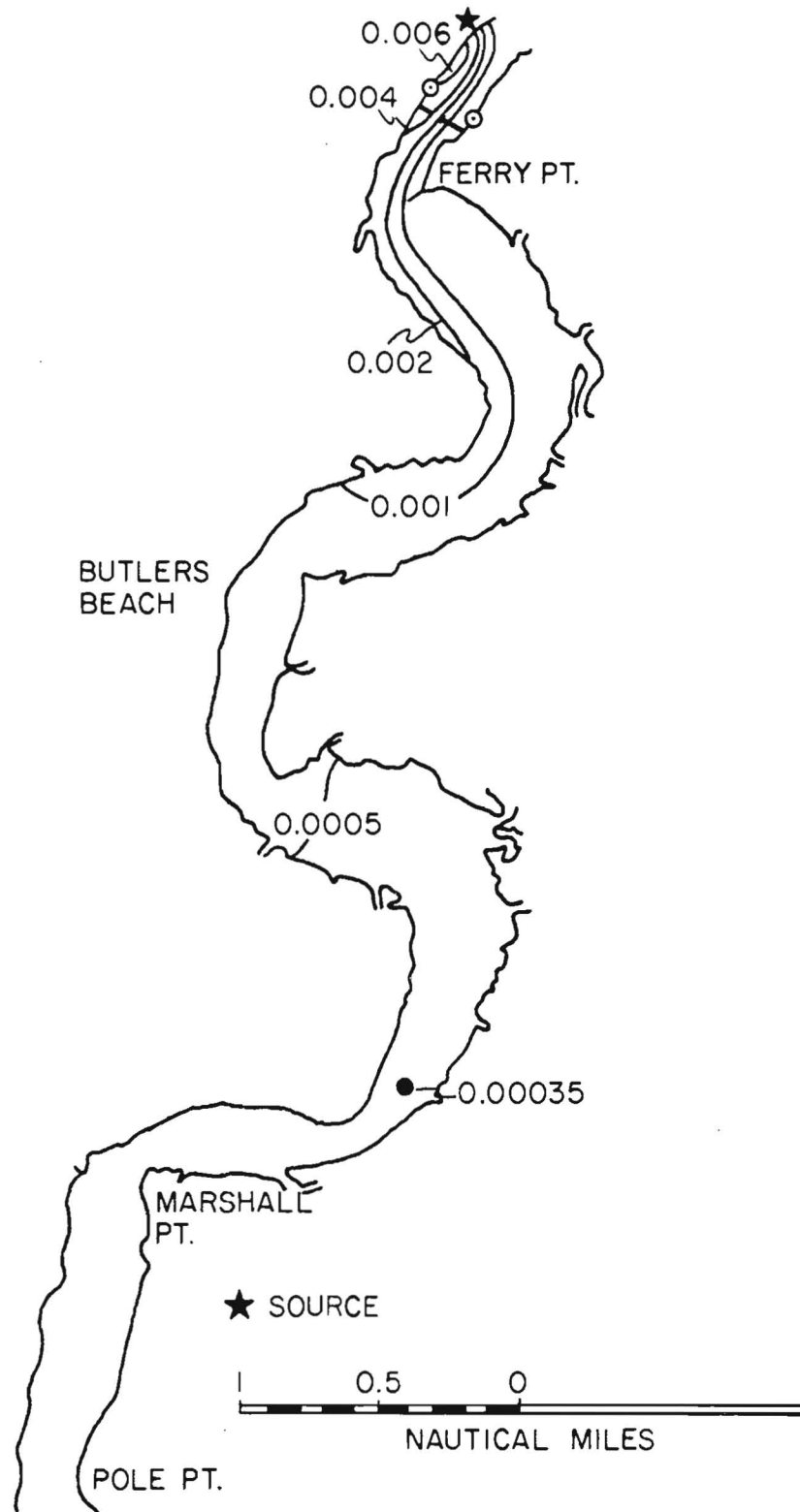


Figure 10. Distribution of relative concentration for a 400 MW plant, at maximum ebb, during high river flow, downstream from the source.

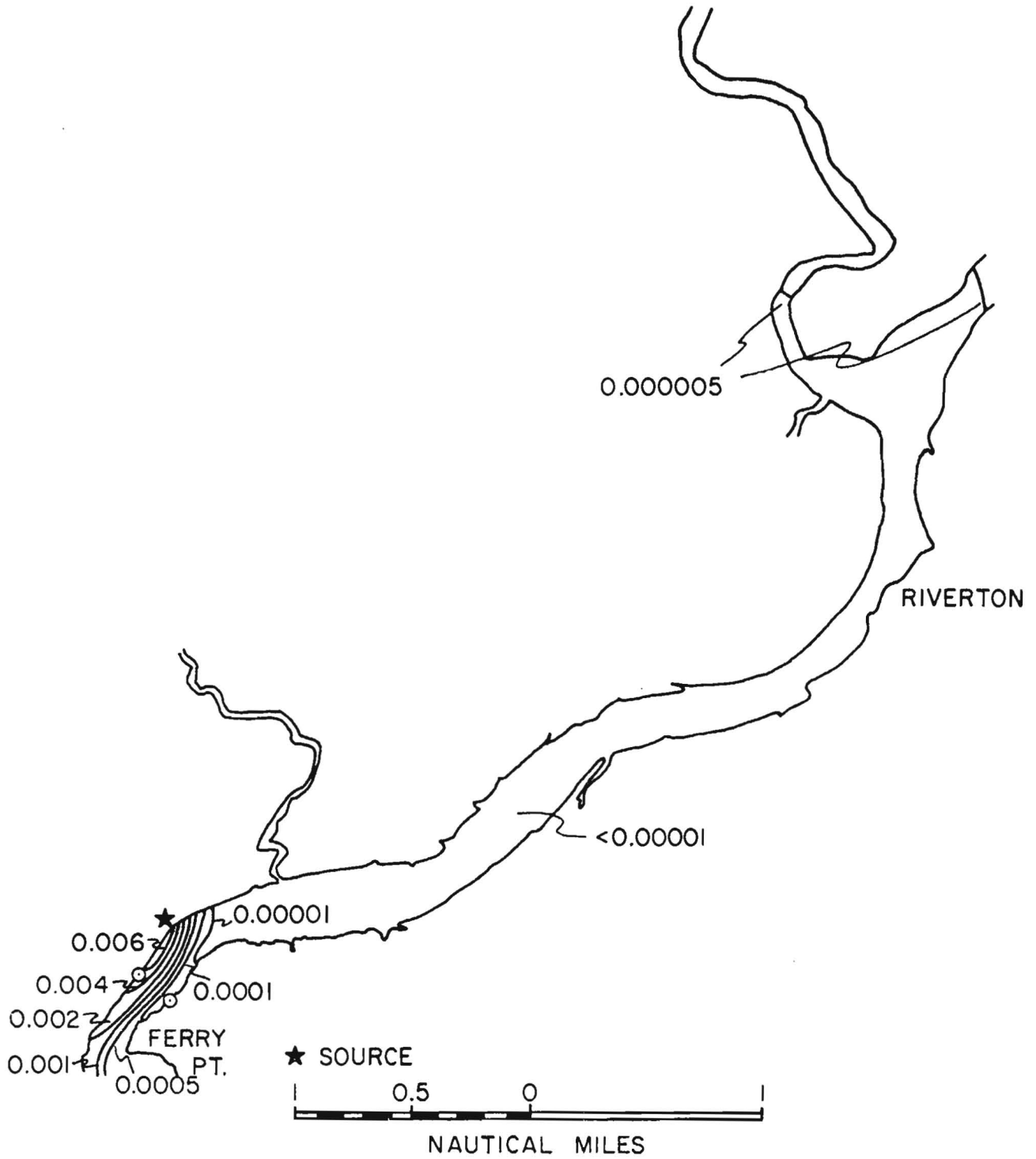


Figure 11. Distribution of relative concentration for a 400 MW plant, near slack before flood, during high river flow, upstream from the source.

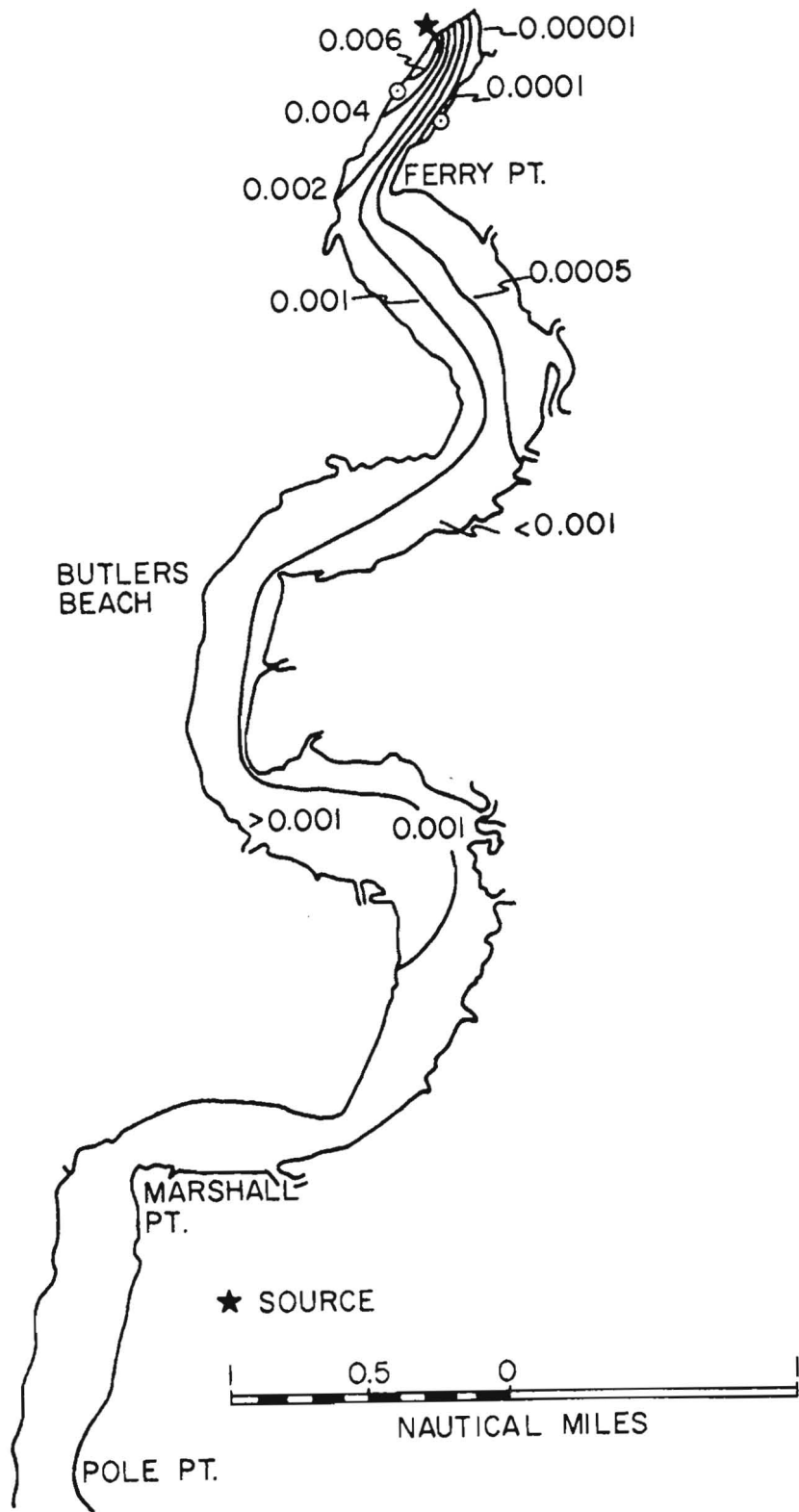


Figure 12. Distribution of relative concentration for a 400 MW plant, near slack before flood, during high river flow, downstream from the source.

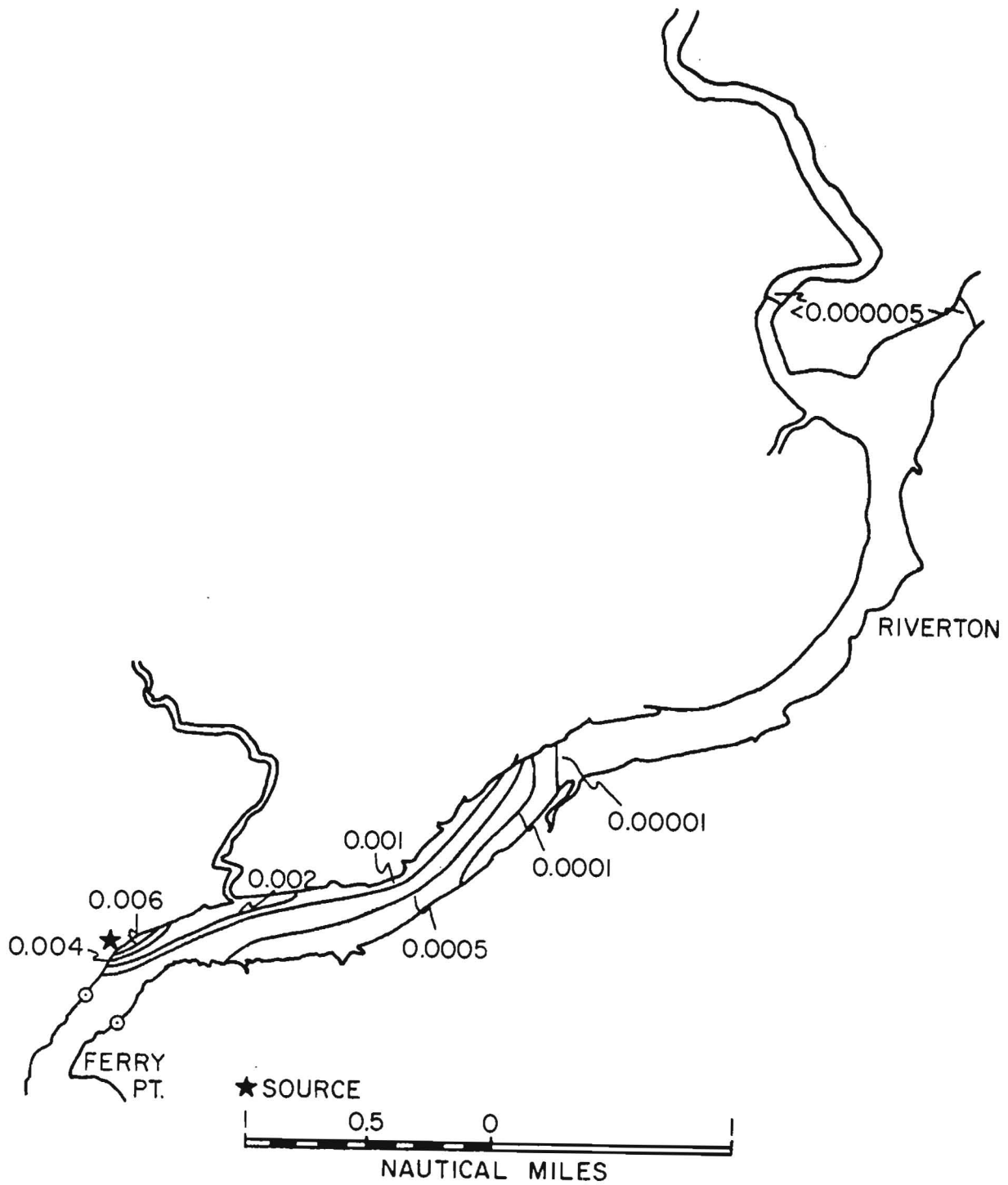


Figure 13. Distribution of relative concentration for a 400 MW plant, at maximum flood, during high river flow, upstream from the source.

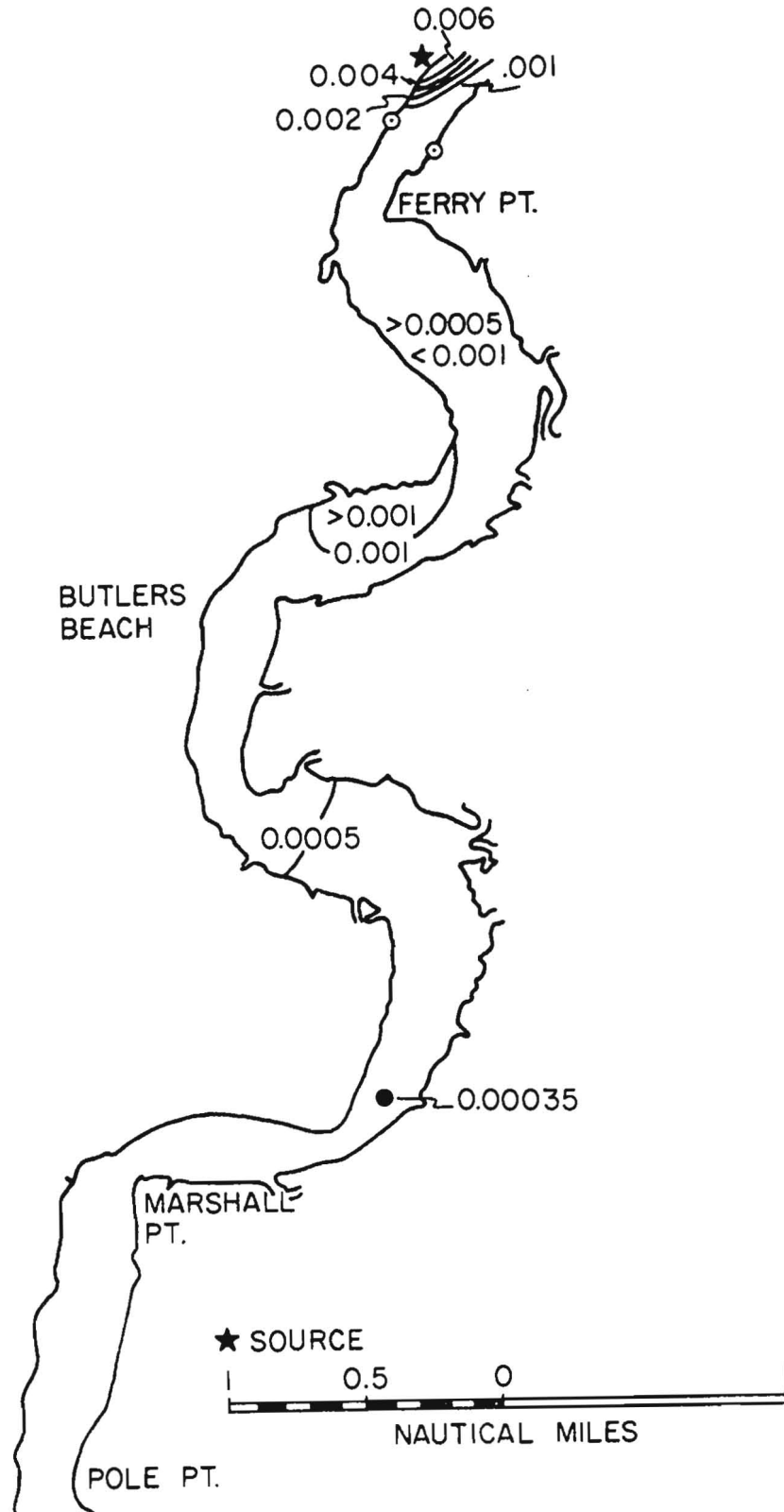


Figure 14. Distribution of relative concentration for a 400 MW plant, at maximum flood, during high river flow, downstream from the source.



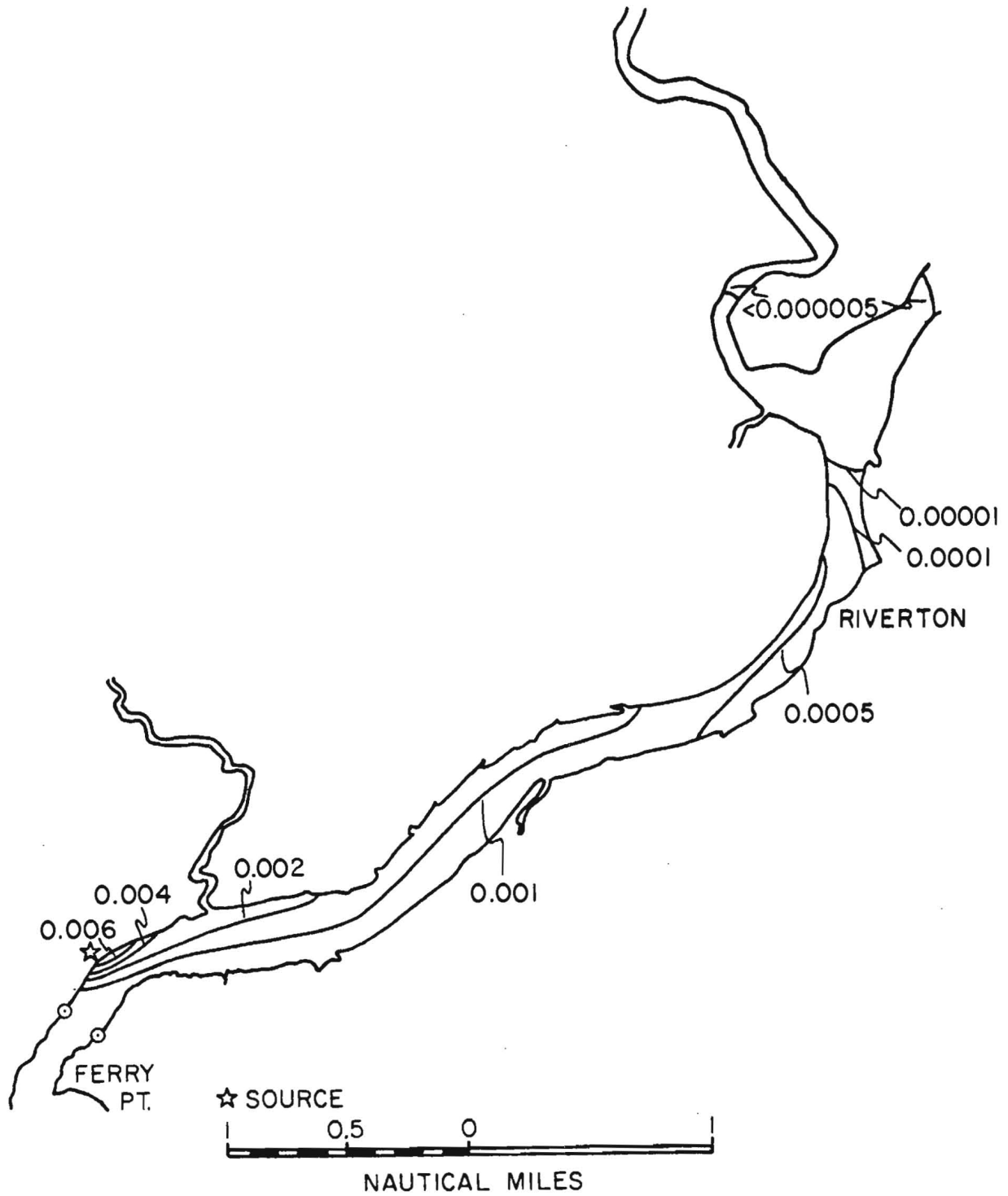


Figure 15. Distribution of relative concentration for a 400 MW plant, near slack before ebb, during high river flow, upstream from the source.

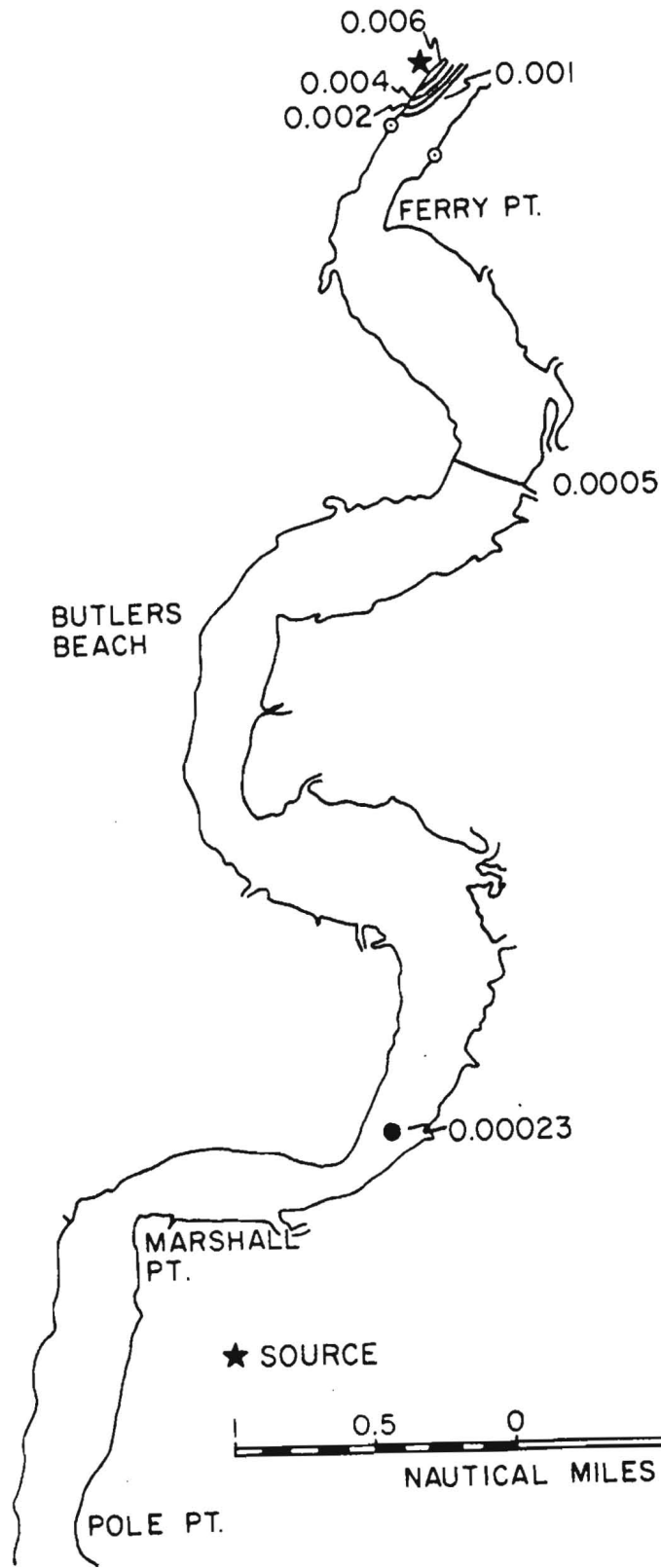


Figure 16. Distribution of relative concentration for a 400 MW plant, near slack before ebb, during high river flow, downstream from the source.

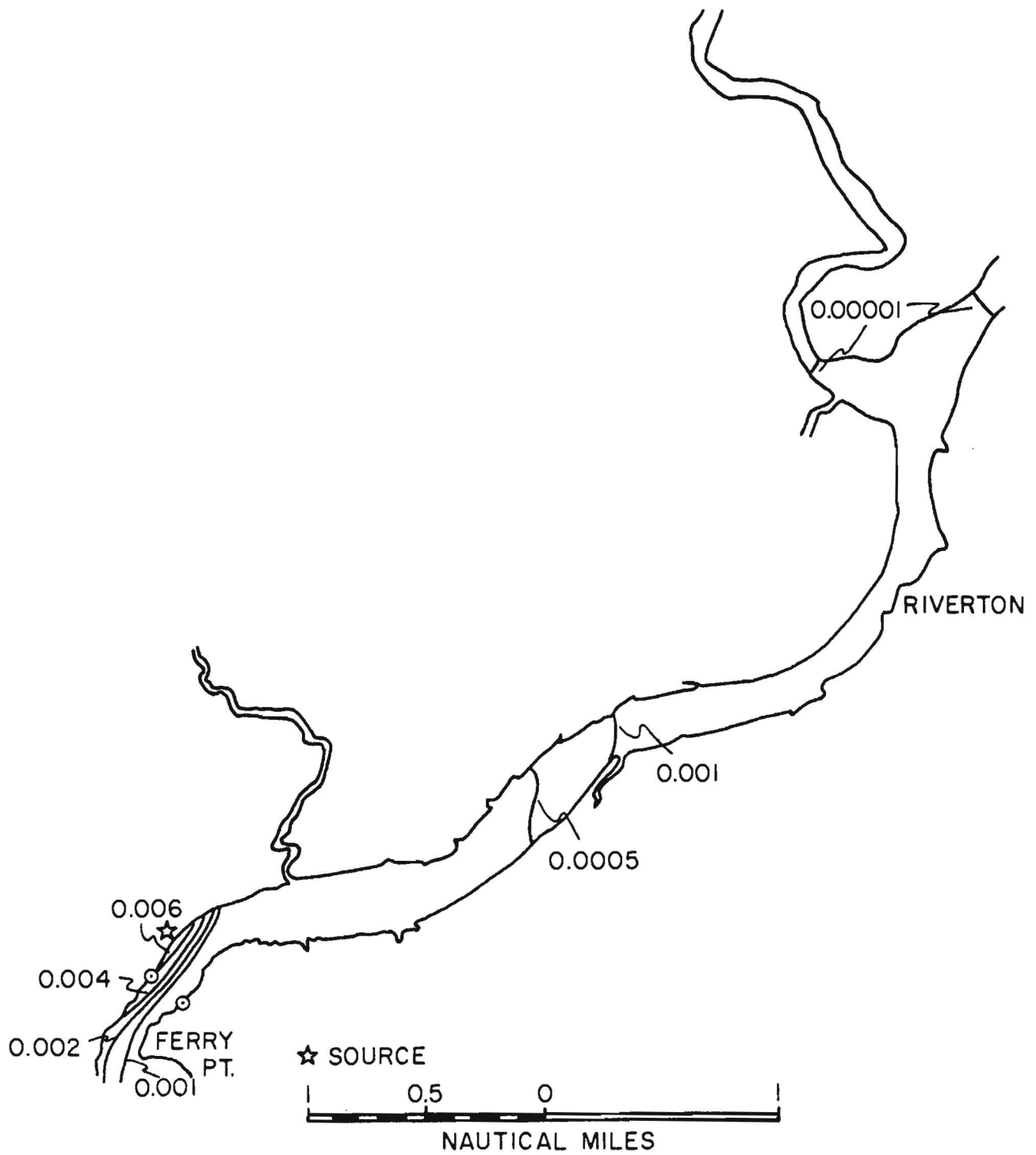


Figure 17. Distribution of relative concentration for a 400 MW plant, at maximum ebb, during mean river flow, upstream from the source.

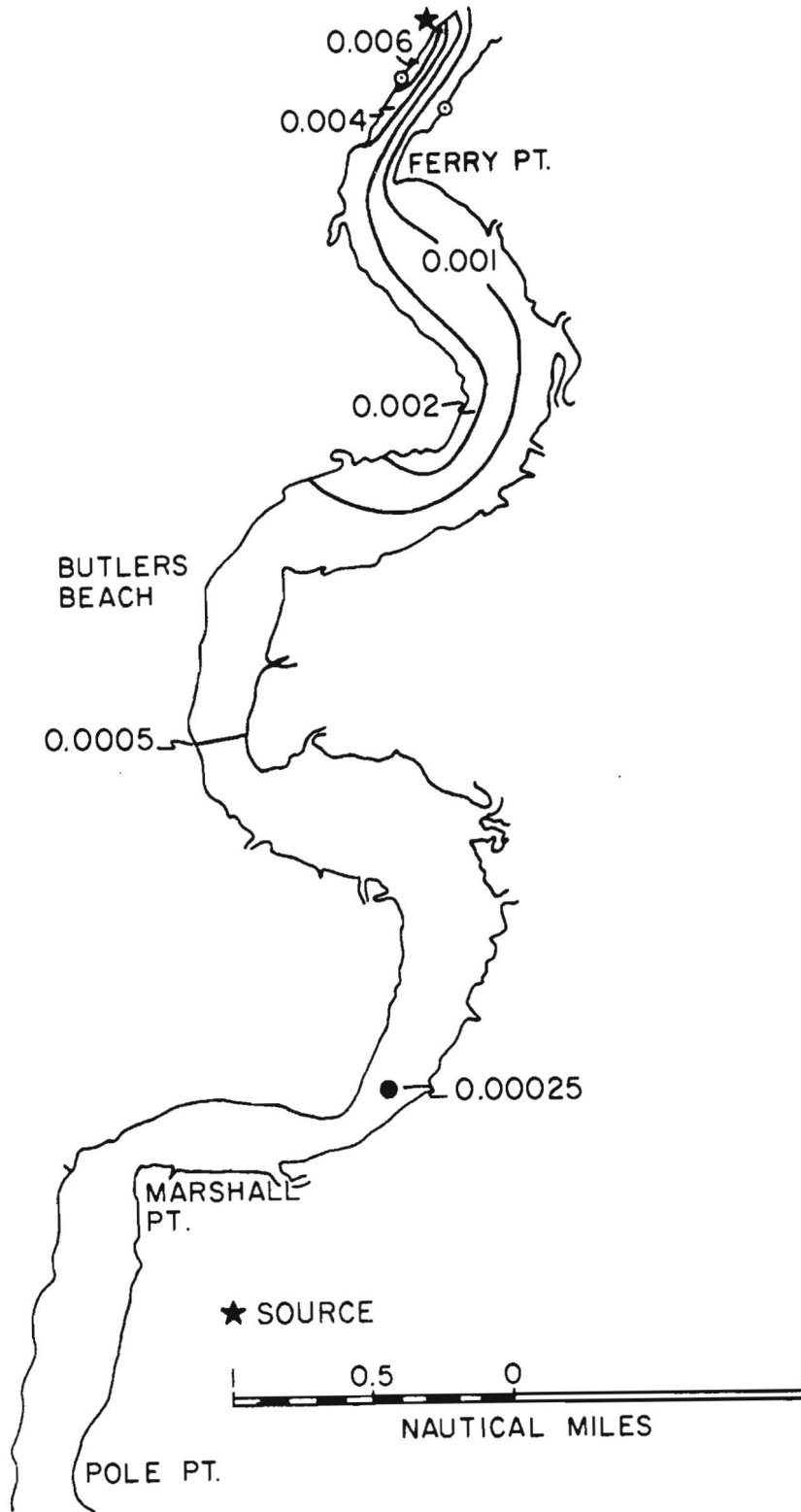


Figure 18. Distribution of relative concentration for a 400 MW plant, at maximum ebb, during mean river flow, downstream from the source.

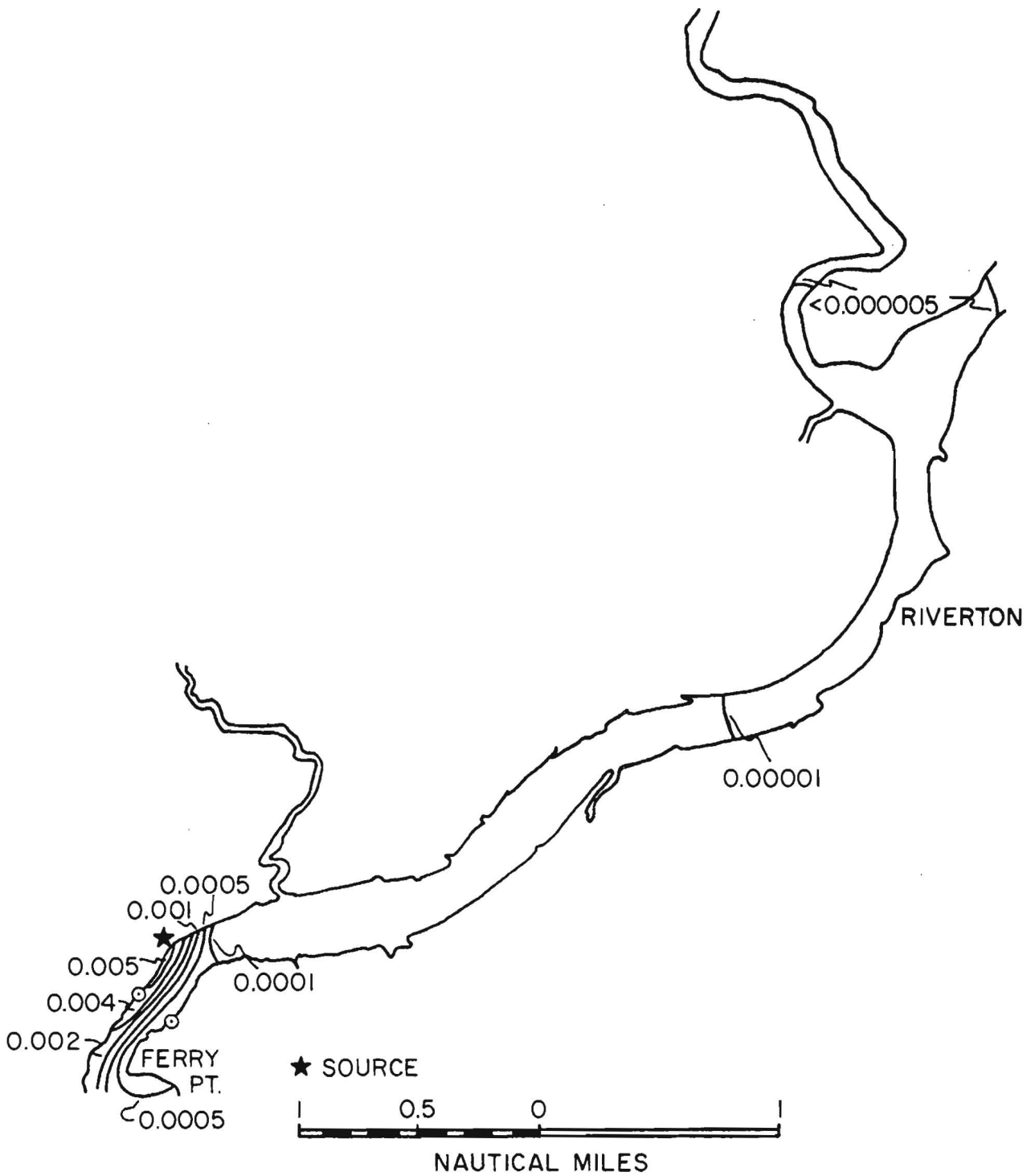


Figure 19. Distribution of relative concentration for a 400 MW plant, near slack before flood, during mean river flow, upstream from the source.

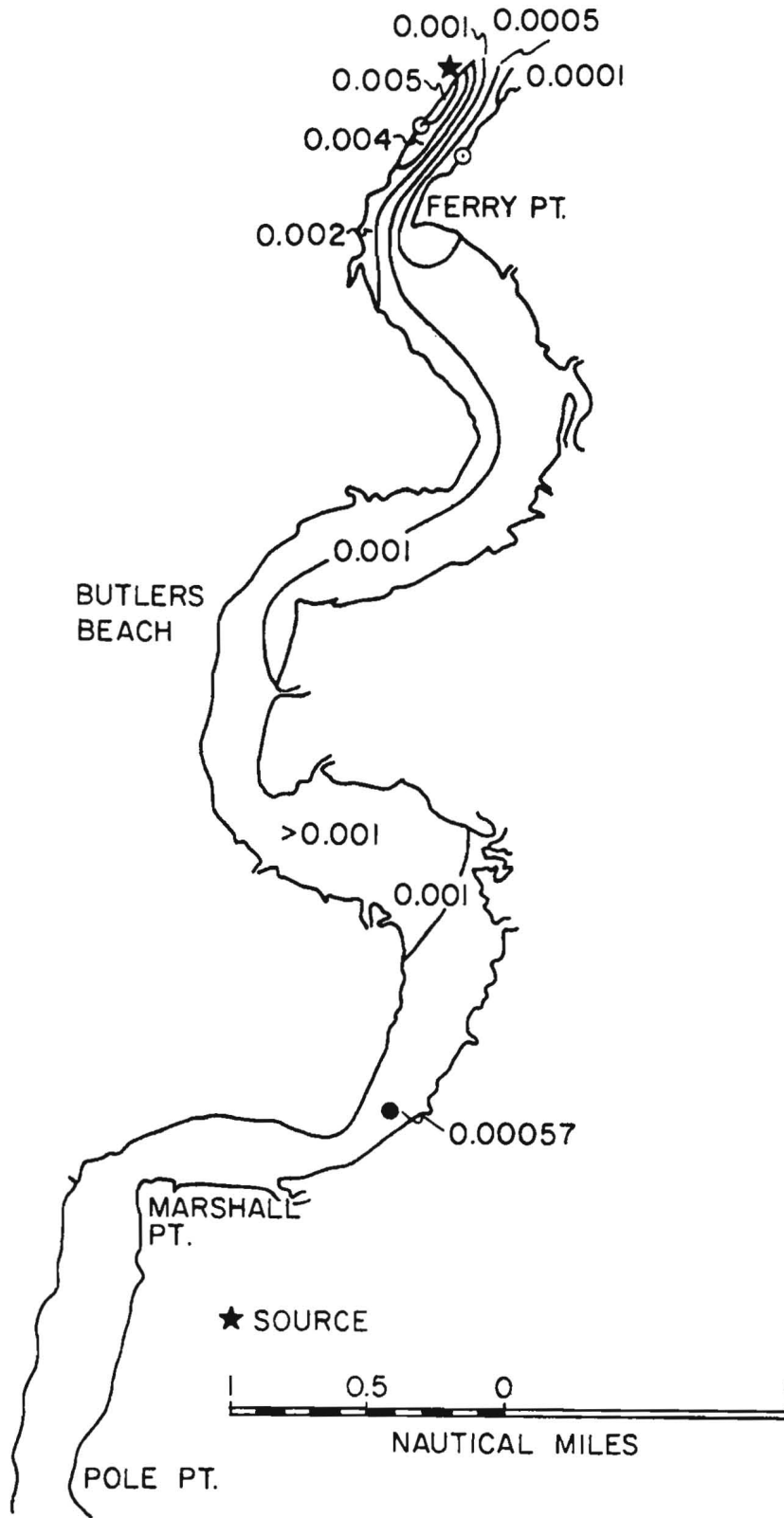


Figure 20. Distribution of relative concentration for a 400 MW plant, near slack before flood, during mean river flow, downstream from the source.

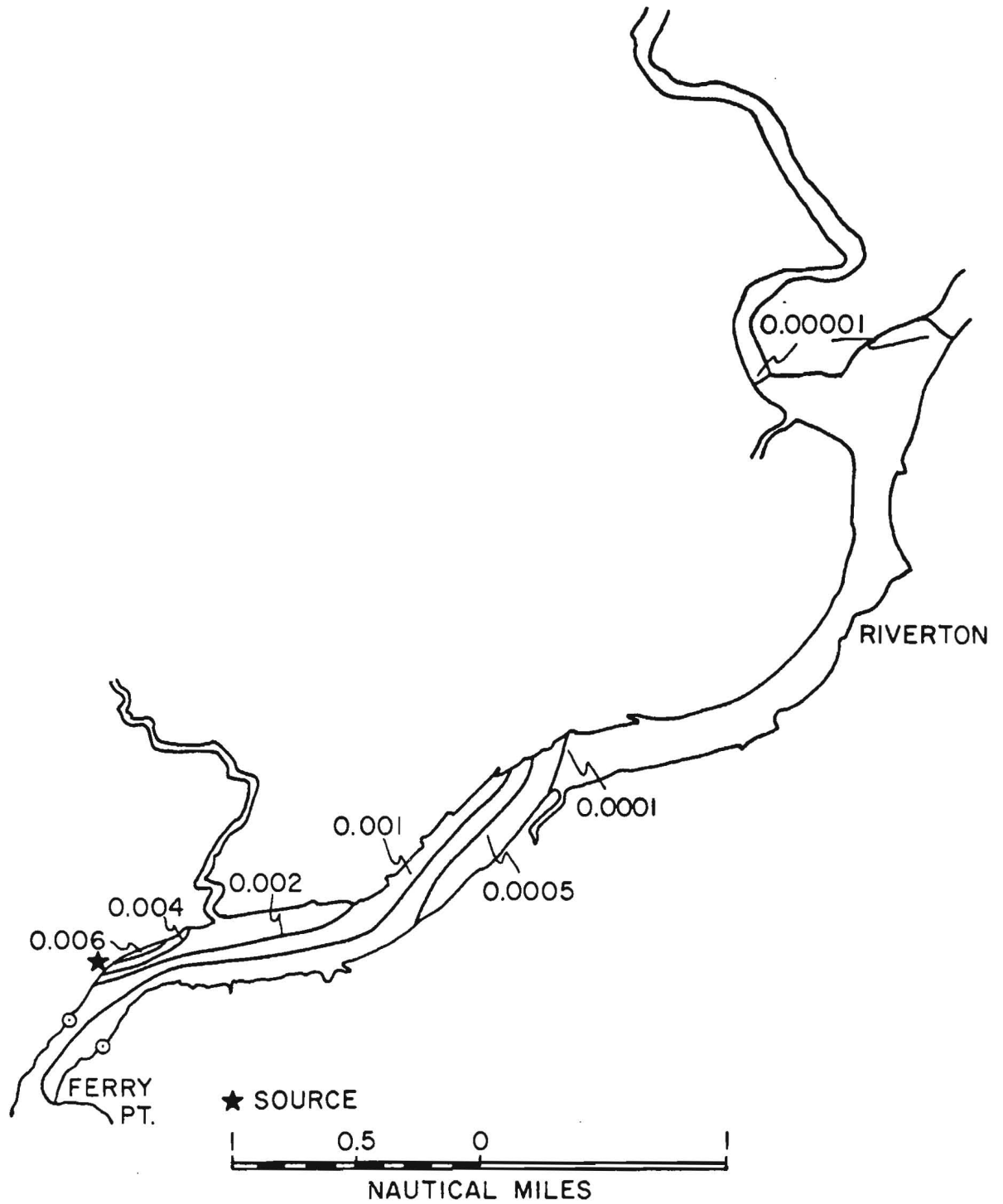


Figure 21. Distribution of relative concentration for a 400 MW plant, at maximum flood, during mean river flow, upstream from the source.

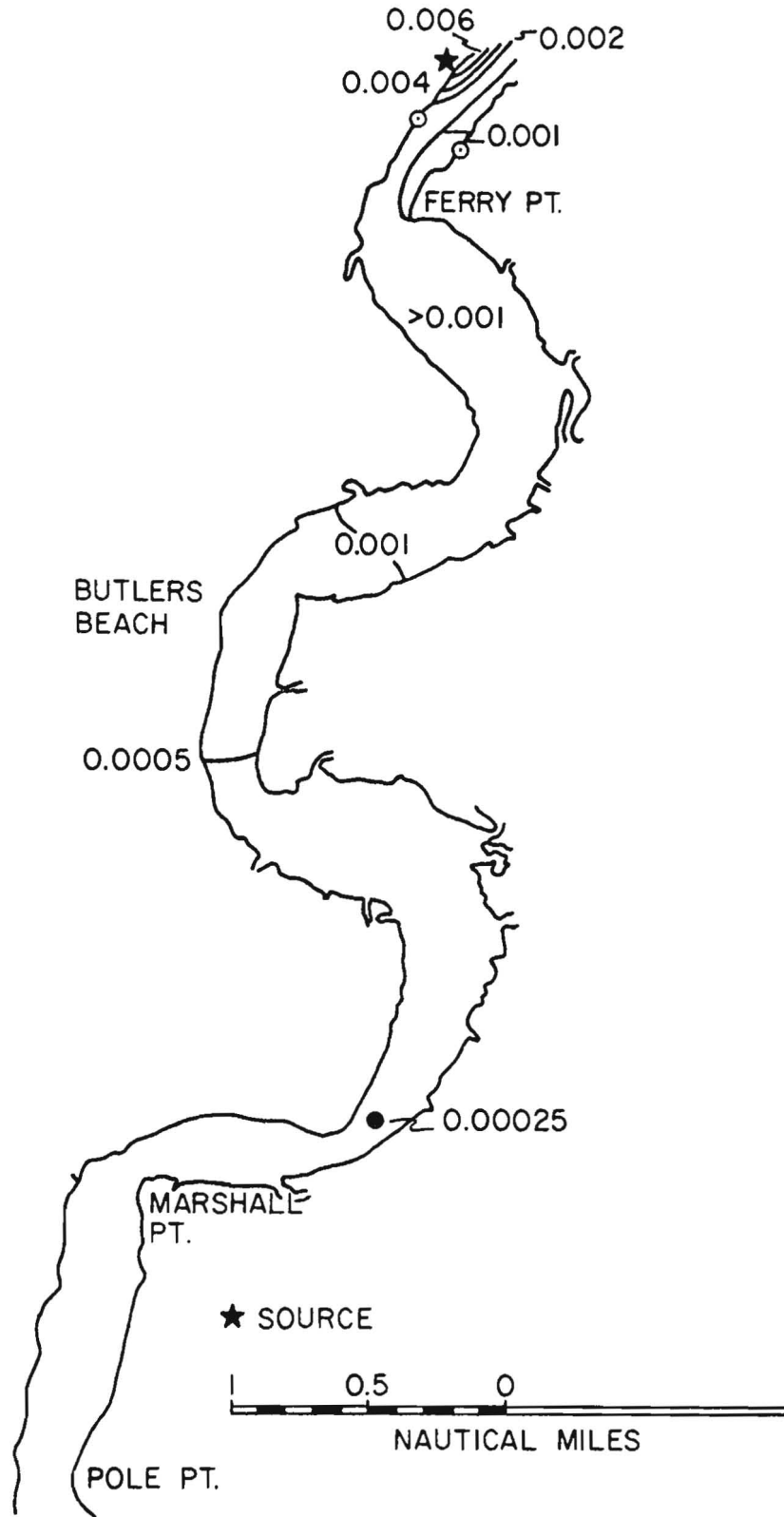


Figure 22. Distribution of relative concentration for a 400 MW plant, at maximum flood, during mean river flow, downstream from the source.



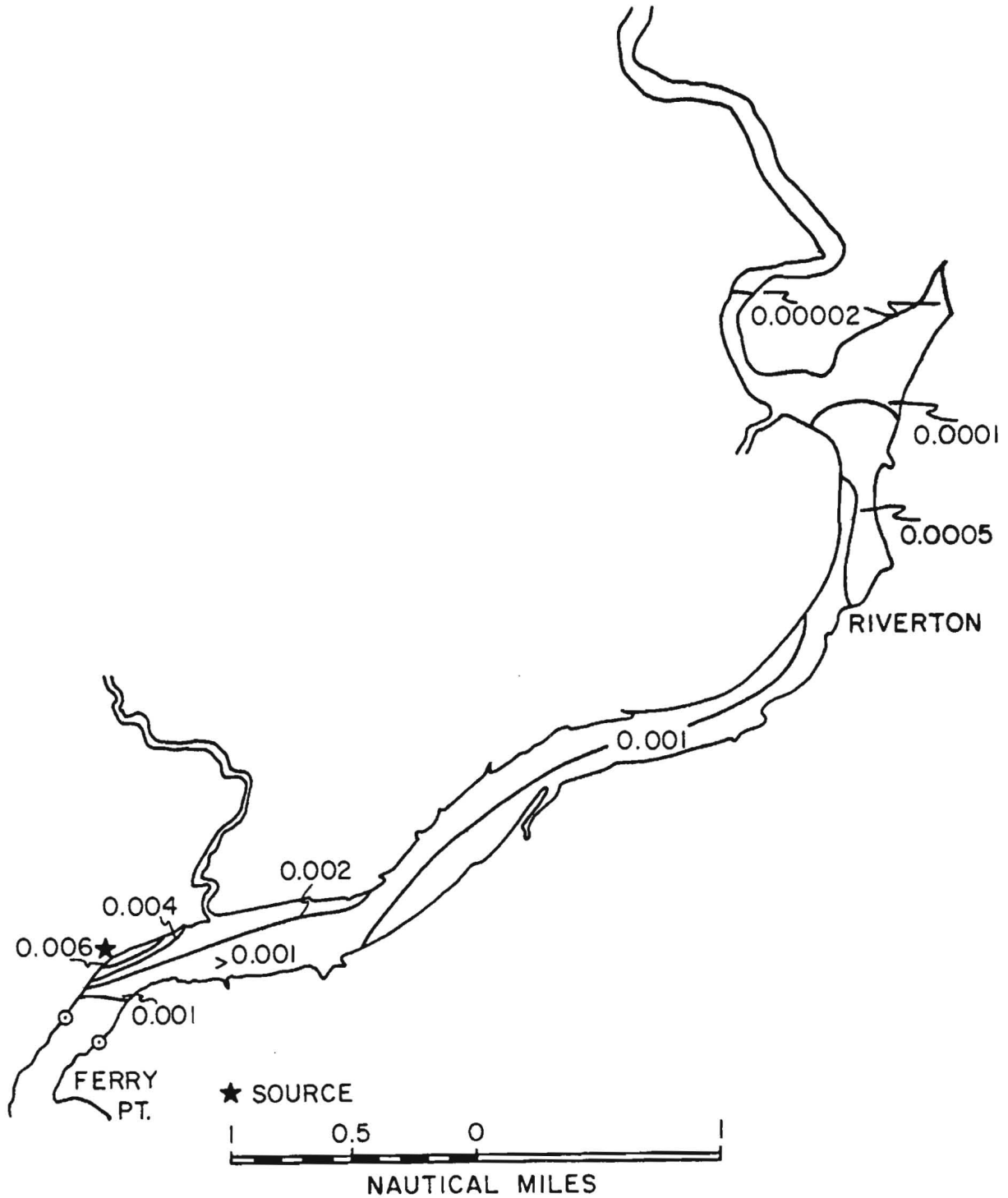


Figure 23. Distribution of relative concentration for a 400 MW plant, near slack before ebb, during mean river flow, upstream from the source.

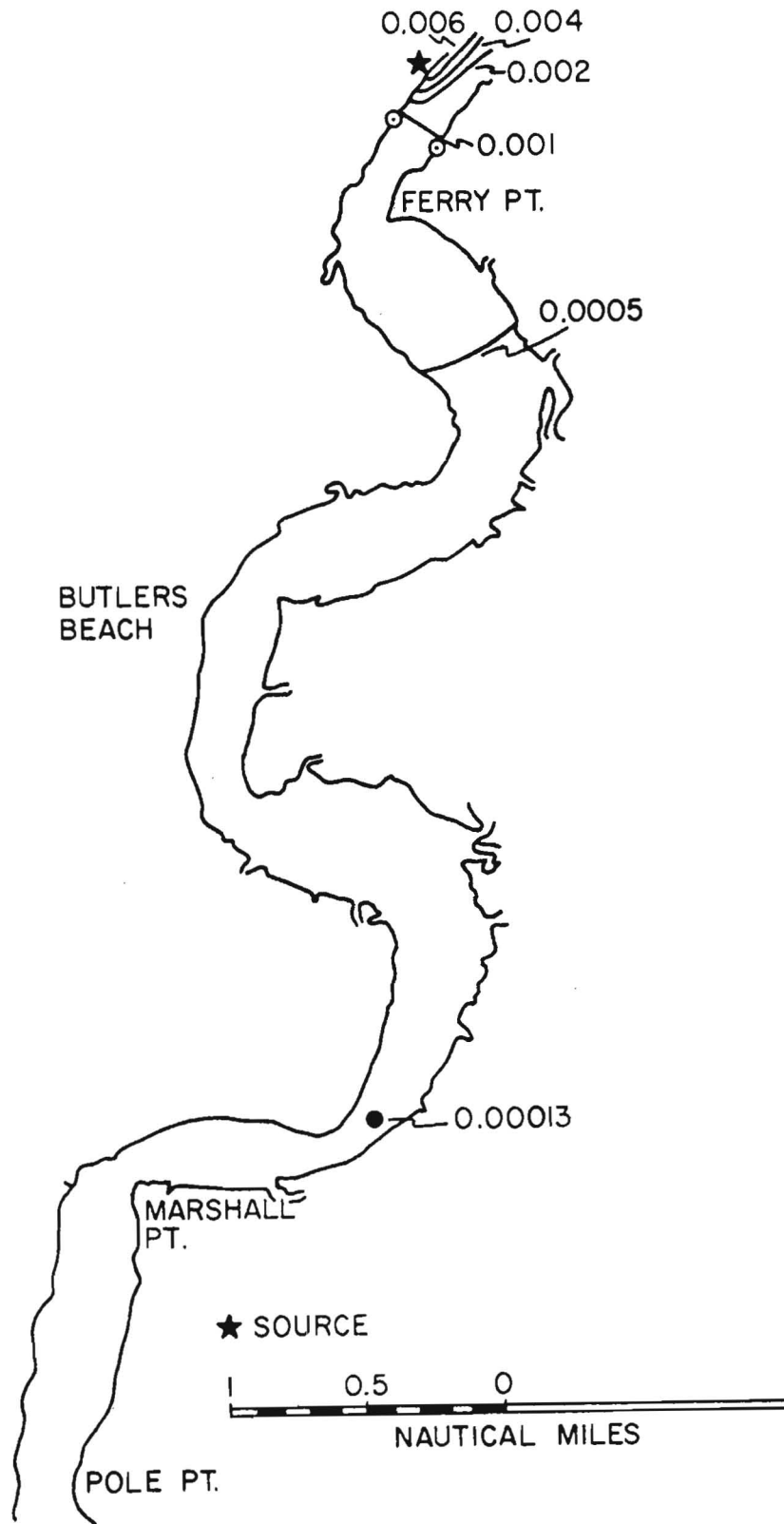


Figure 24. Distribution of relative concentration for a 400 MW plant, near slack before ebb, during mean river flow, downstream from the source.

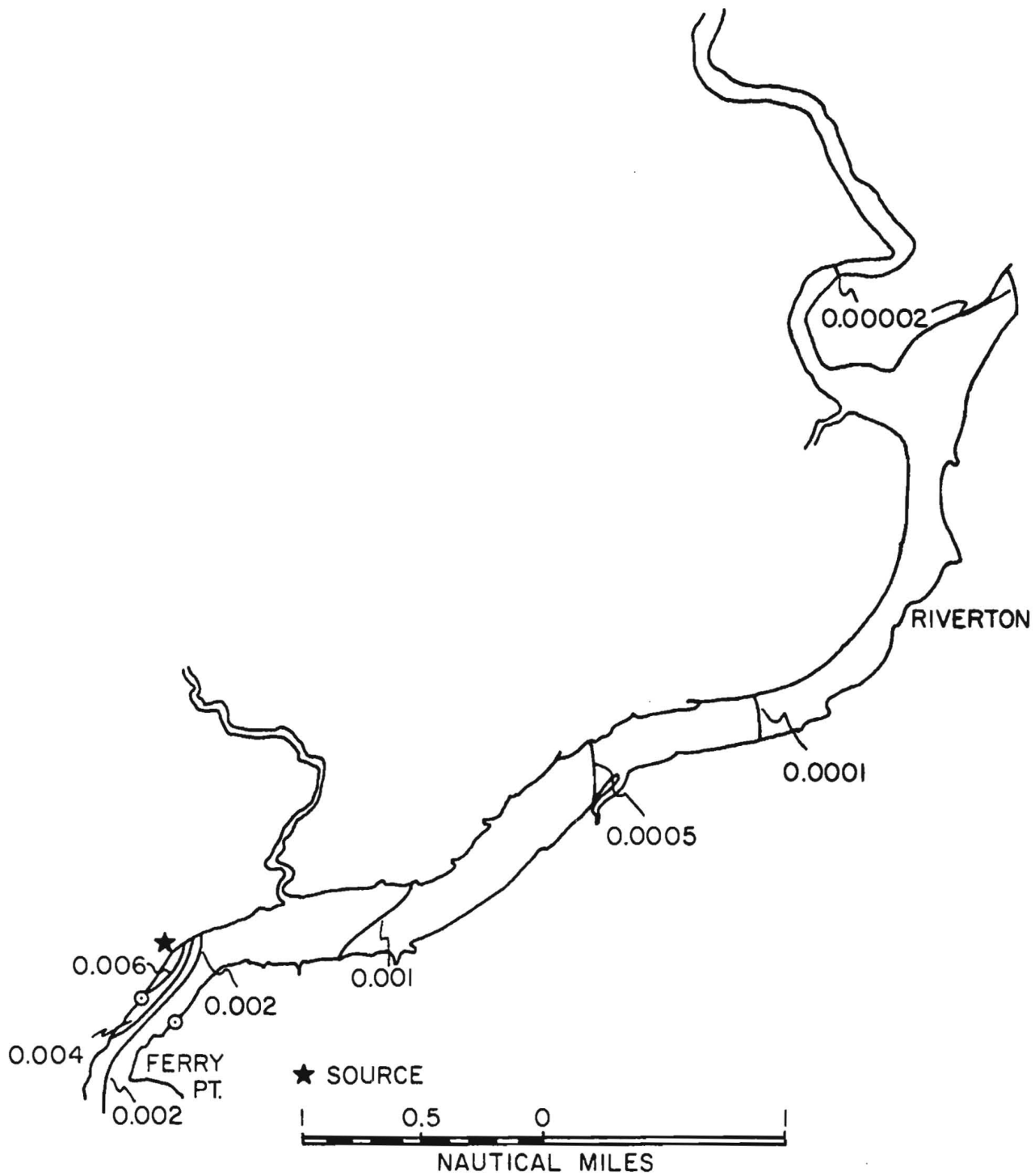


Figure 25. Distribution of relative concentration for a 400 MW plant, at maximum ebb, during low river flow, upstream from the source.

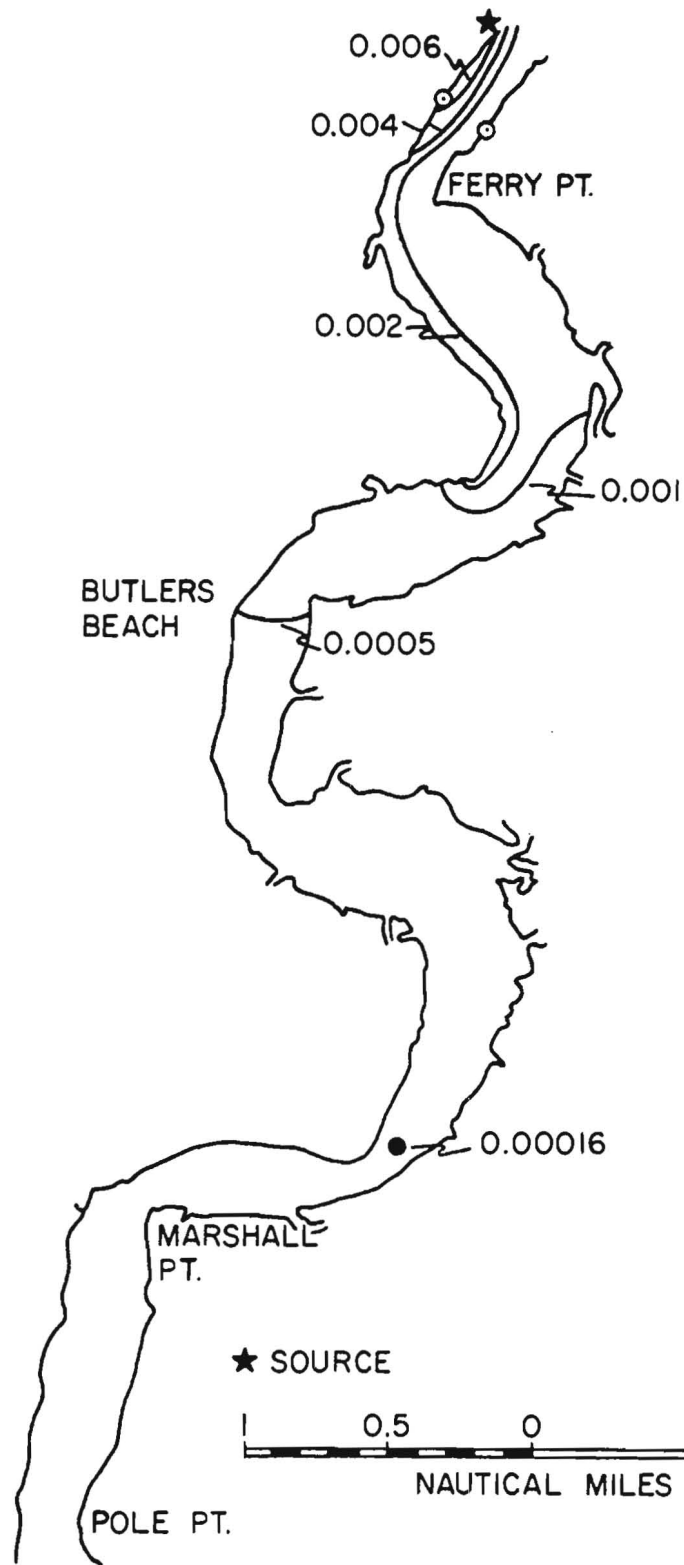


Figure 26. Distribution of relative concentration for a 400 MW plant, at maximum ebb, during low river flow, downstream from the source.

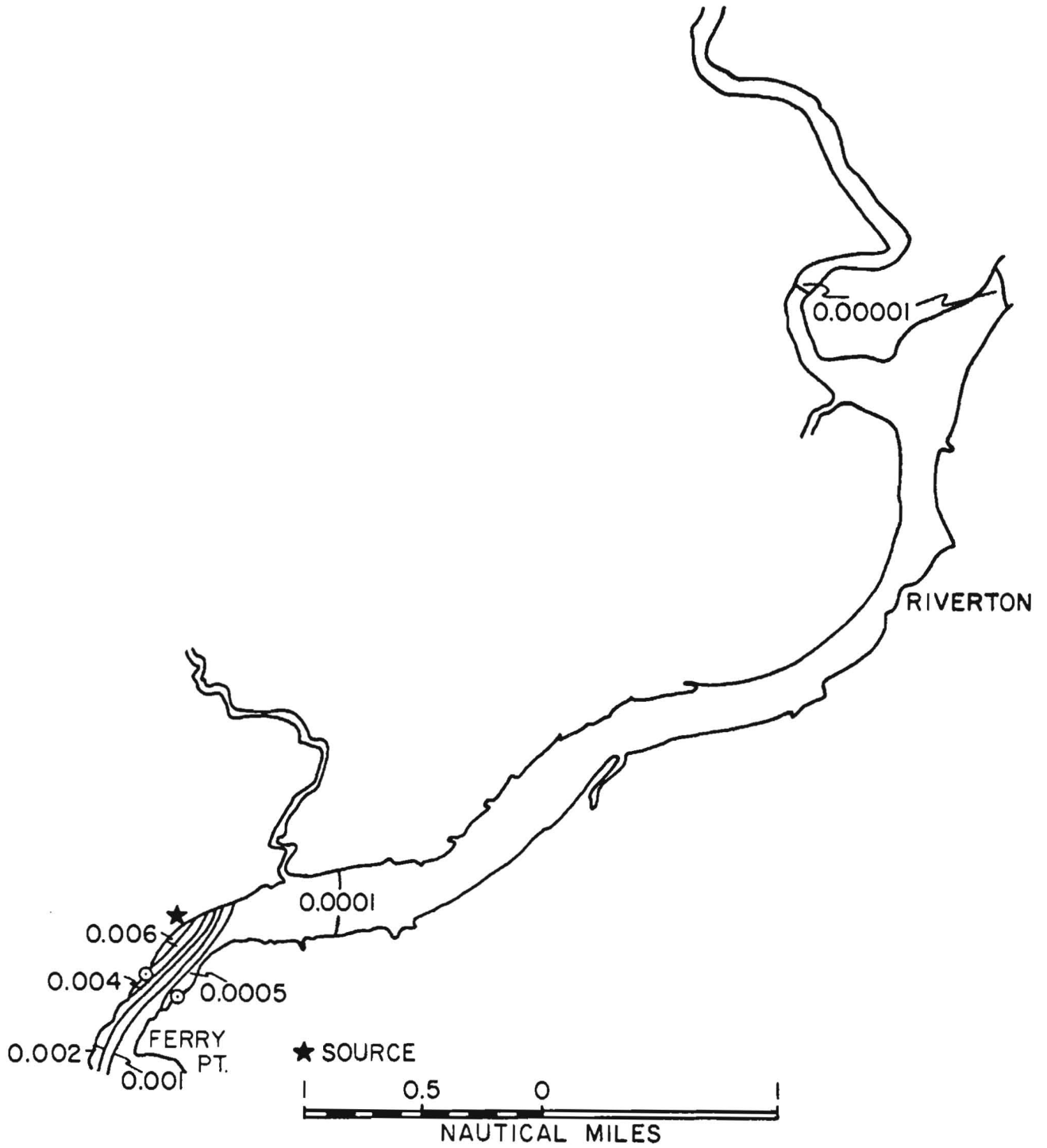


Figure 27. Distribution of relative concentration for a 400 MW plant, near slack before flood, during low river flow, upstream from the source.

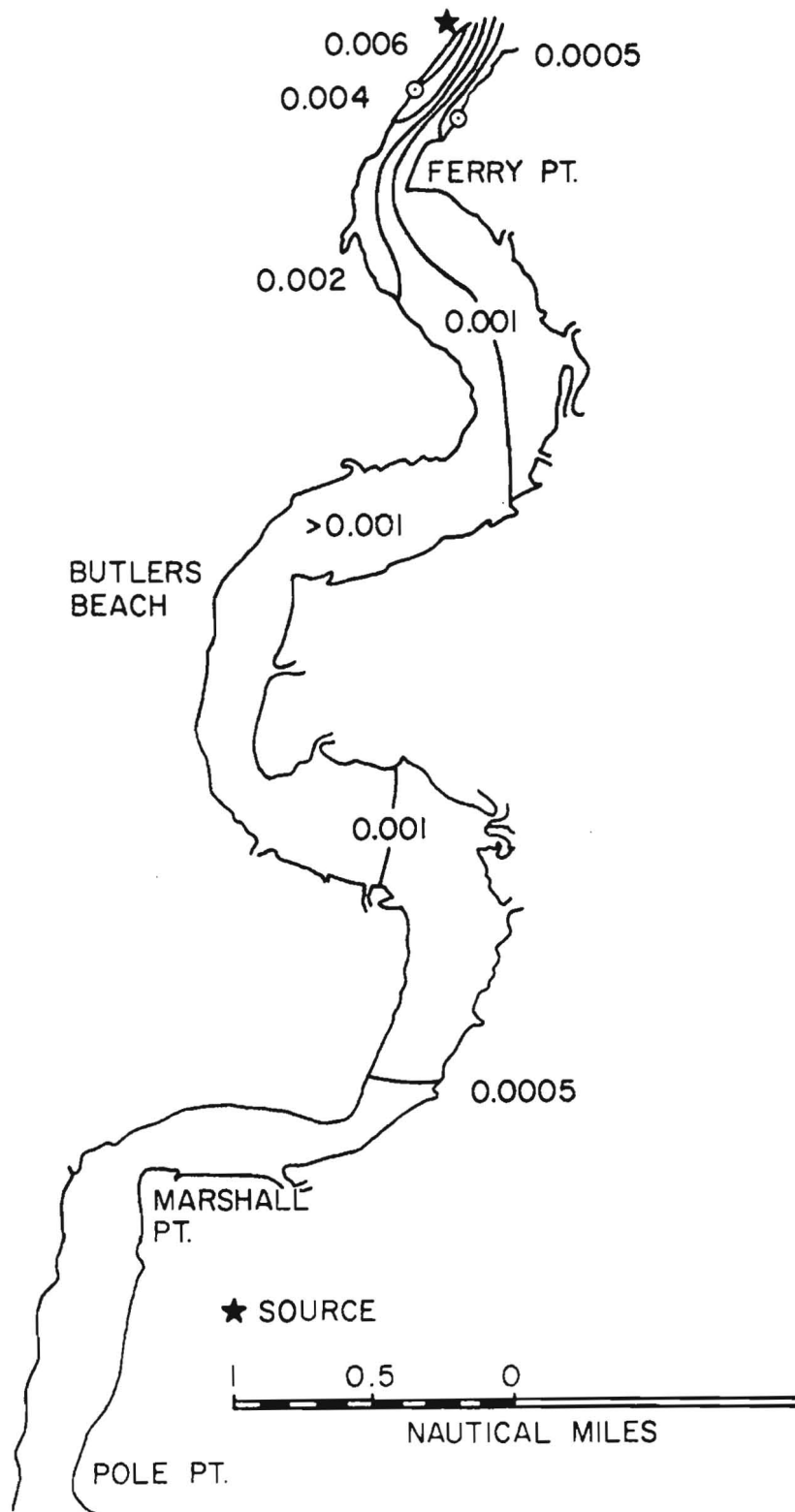


Figure 28. Distribution of relative concentration for a 400 MW plant, near slack before flood, during low river flow, downstream from the source.

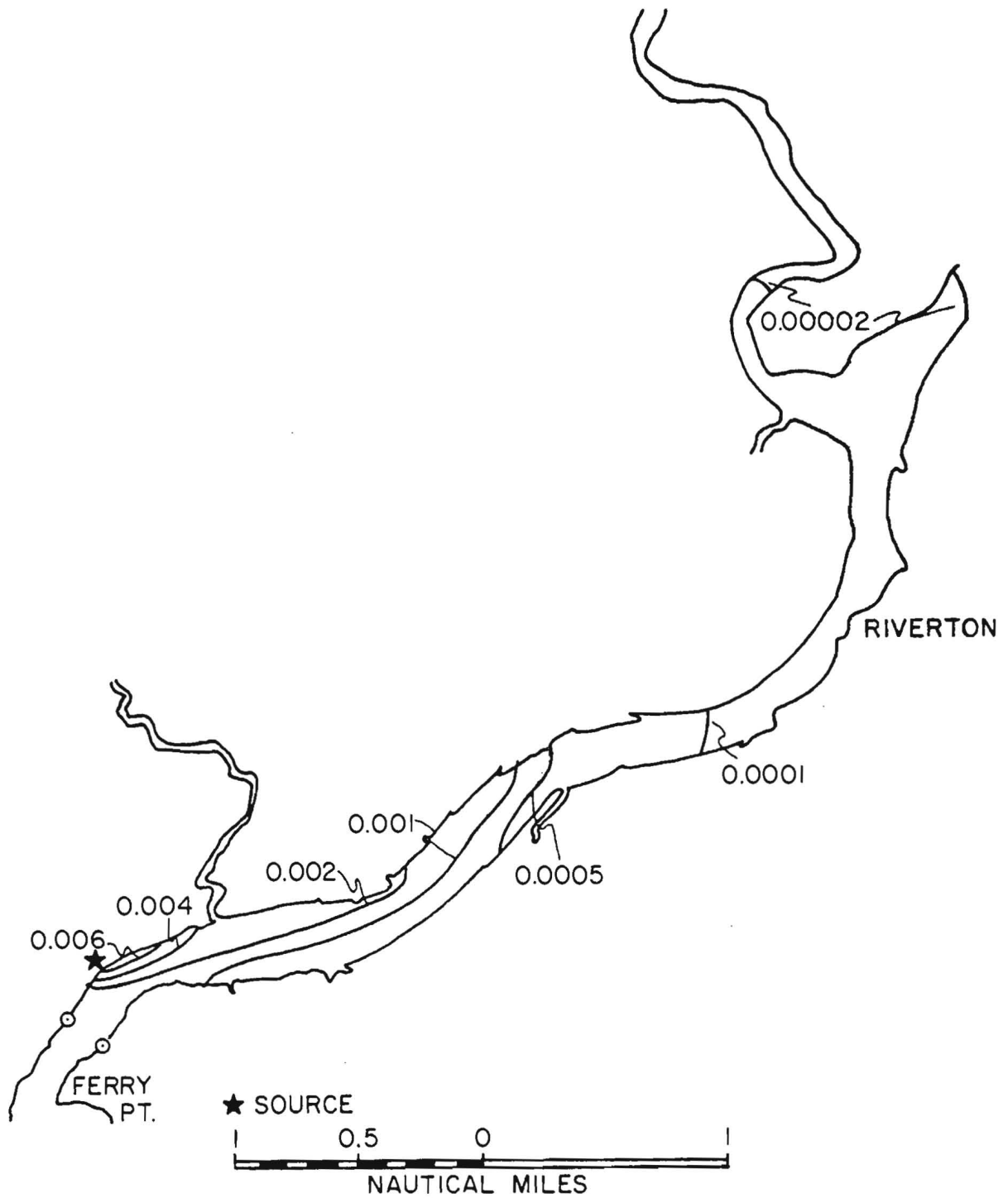


Figure 29. Distribution of relative concentration for a 400 MW plant, at maximum flood, during low river flow, upstream from the source.

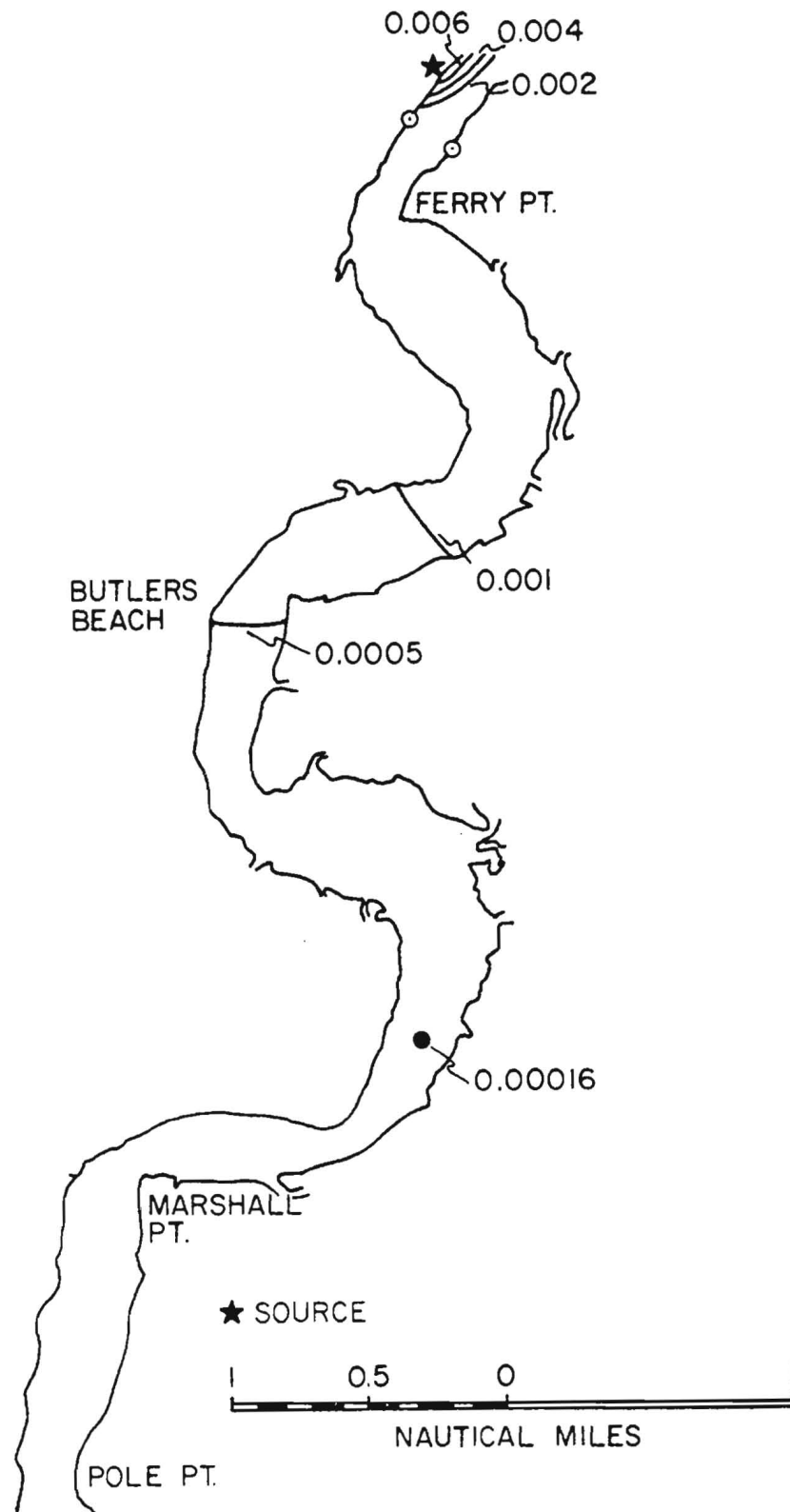


Figure 30. Distribution of relative concentration for a 400 MW plant, at maximum flood, during low river flow, downstream from the source.



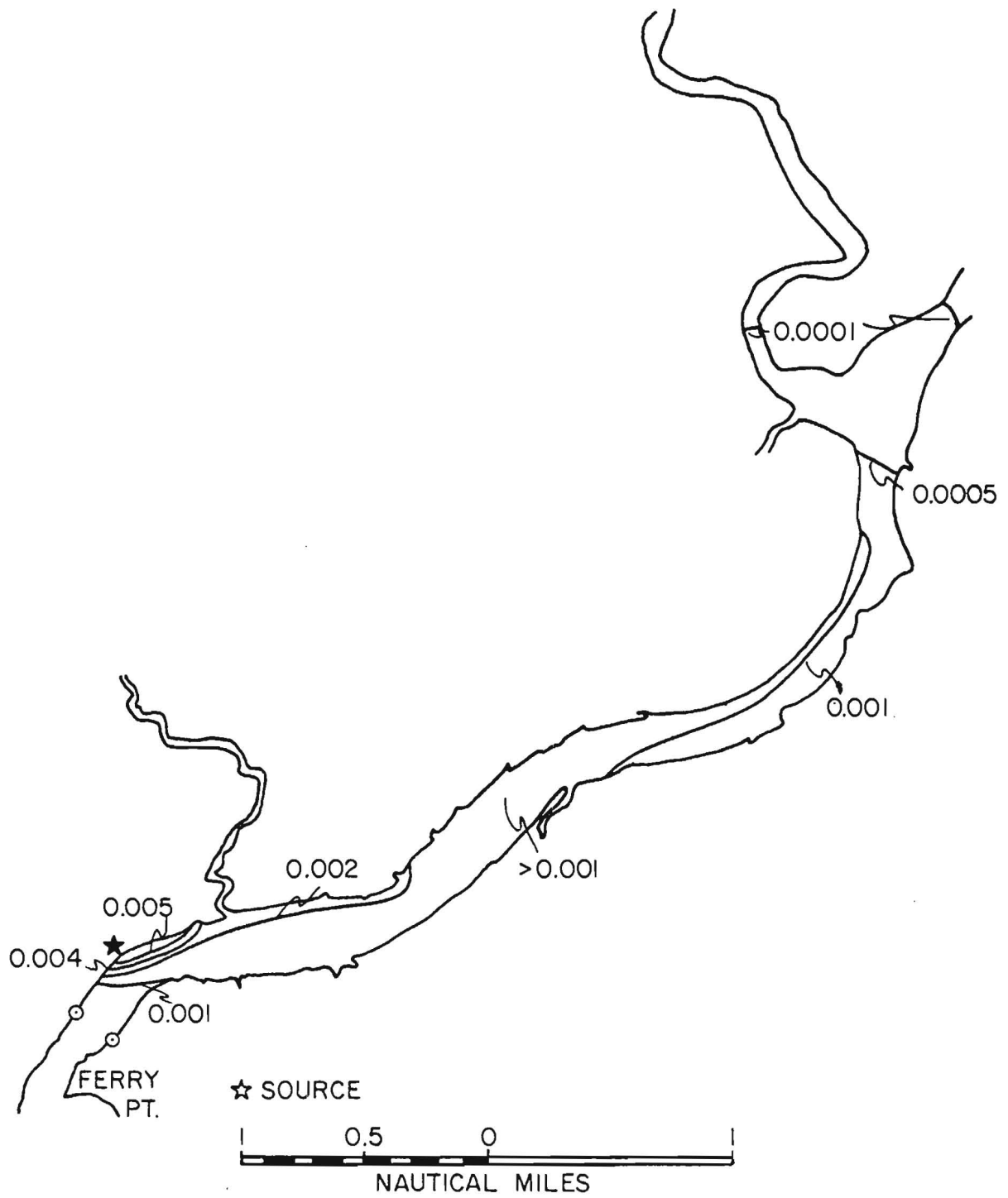


Figure 31. Distribution of relative concentration for a 400 MW plant, near slack before ebb, during low river flow, upstream from the source.

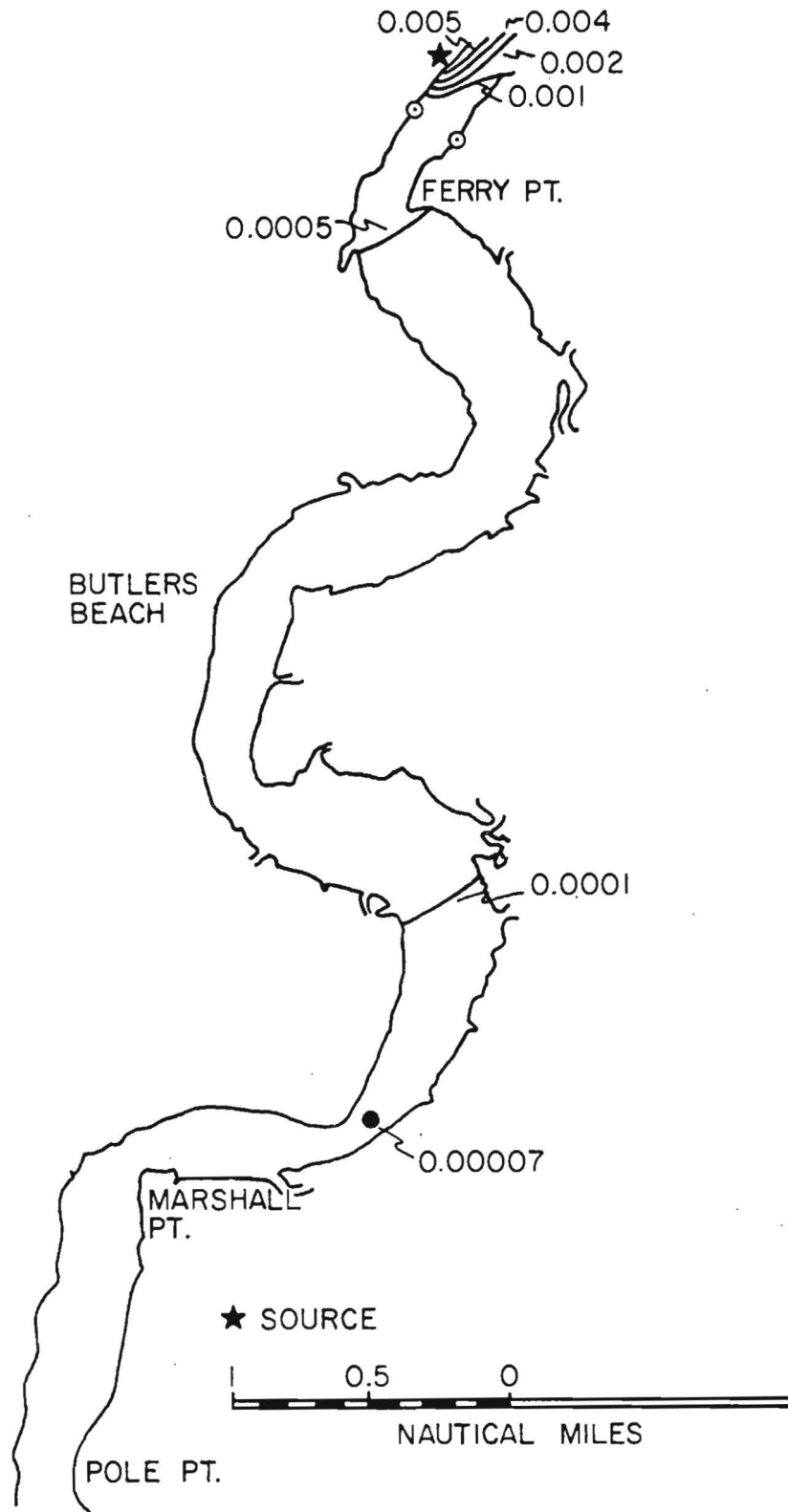


Figure 32. Distribution of relative concentration for a 400 MW plant, near slack before ebb, during low river flow, downstream from the source.

the centerline approximately as one over the distance from the source. The magnitude of concentrations within the plume depend primarily on the strength of the source and the ratio of the tidal current amplitude to the diffusion velocity. When the tide changes, a new plume begins to form and the plume created on the previous stage of the tide diffuses into the background.

The background concentration field is produced by the superposition of these diffusing remnant plumes over many tidal cycles. The background concentration field oscillates with the tidal current but it is very important to note that background concentration levels are dependent on the strength of the source and the magnitude of the *nontidal residual* current velocity rather than the tidal current velocity. Background concentrations are, therefore, quite sensitive to river flow.

As stated in the introduction, computations were also carried out for a source with a flow rate of 2570 gals. min., representing the discharge from Unit 8 combined with a new Unit 9 of 600 MWE.

The computed relative far field concentrations for this increased source on the distorted rectangular grid are presented in Figures 33 through 38. With the exception of the source strength, all input parameters for these computations were the same as those for the 400 MW plant. A comparison of the far field concentrations for the 400 MW and 600 MW plants is afforded by Figures 1 through 6 and 33 through 38. At any specific point, concentrations for the increased source are simply increased by a factor of 1.5 over those

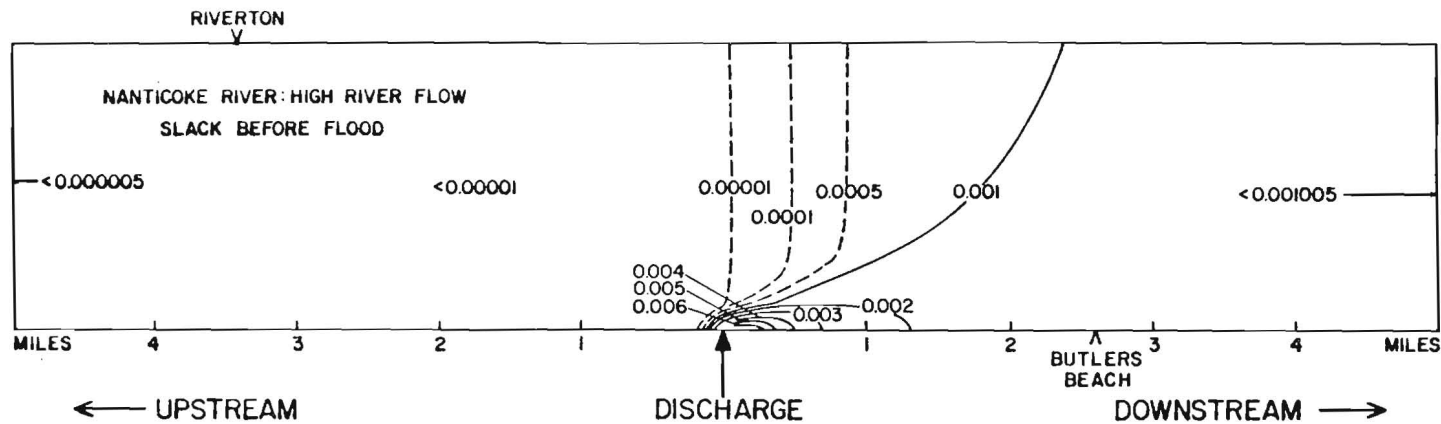
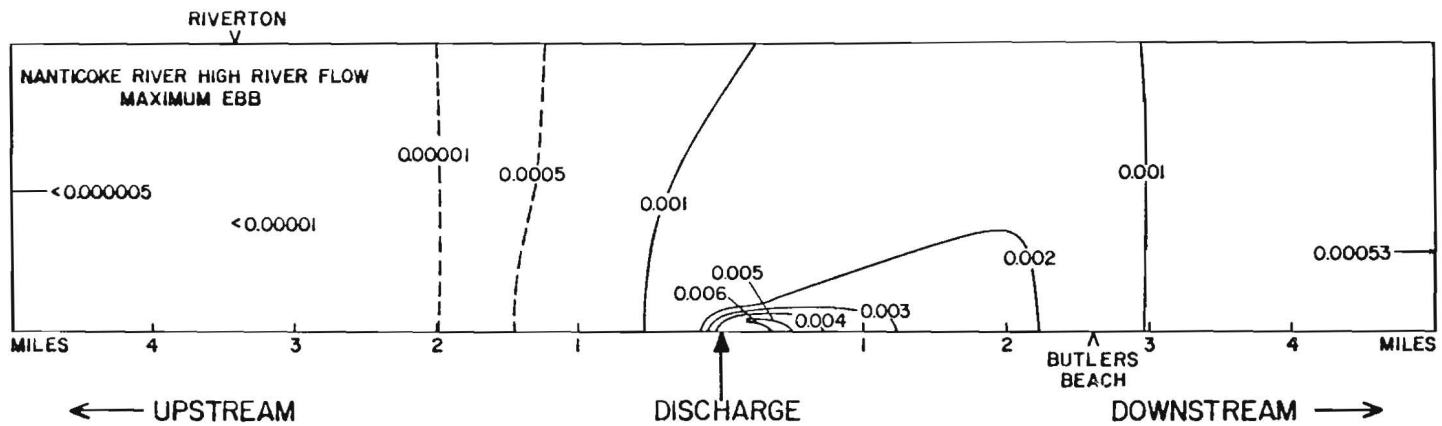


Figure 33. Isolines of relative concentration for high river flow (1520 cfs), for maximum ebb tidal flow and for near slack before flood. Computations are for a discharge flow of 2570 gpm representative of a 600 MW plant (compare with Figure 1 which is representative of a 400 MW plant).

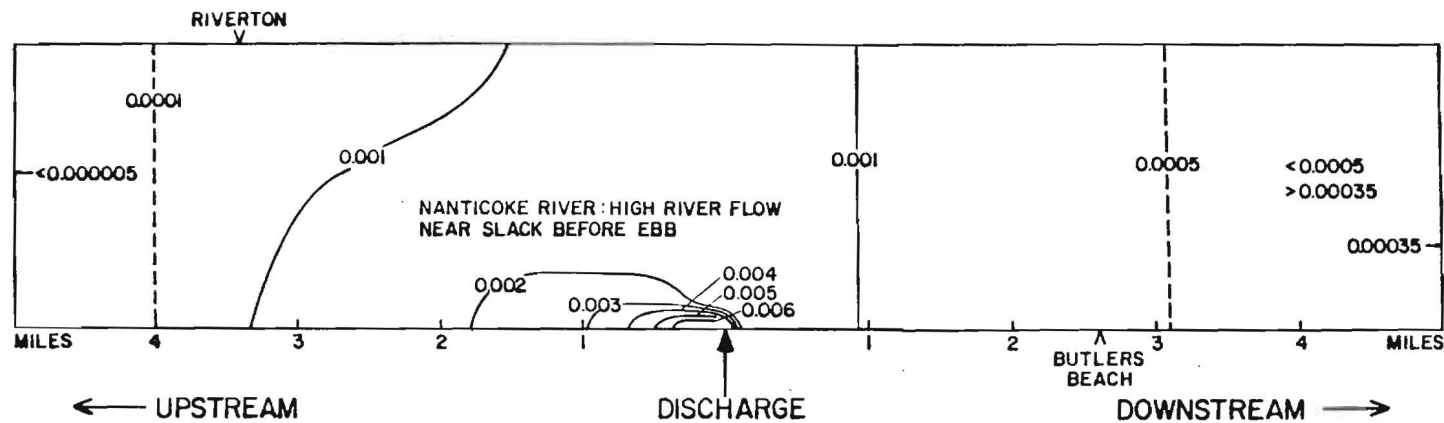
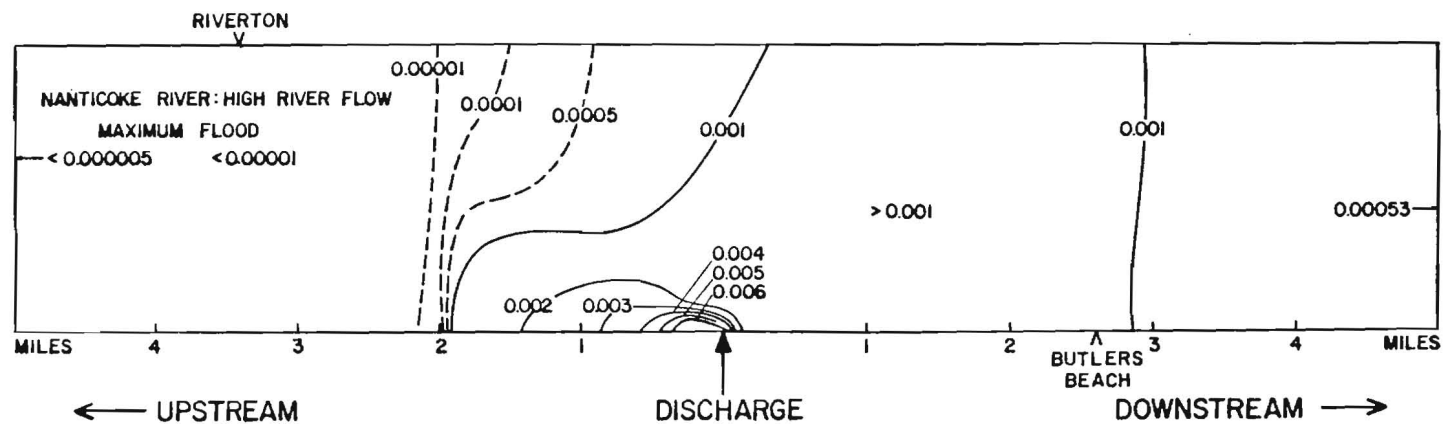


Figure 34. Isolines of relative concentration for high river flow (1520 cfs), for maximum flood tidal flow and for near slack before ebb. Computations are for a discharge flow of 2570 gpm representative of a 600 MW plant (compare with Figure 2 which is representative of a 400 MW plant).

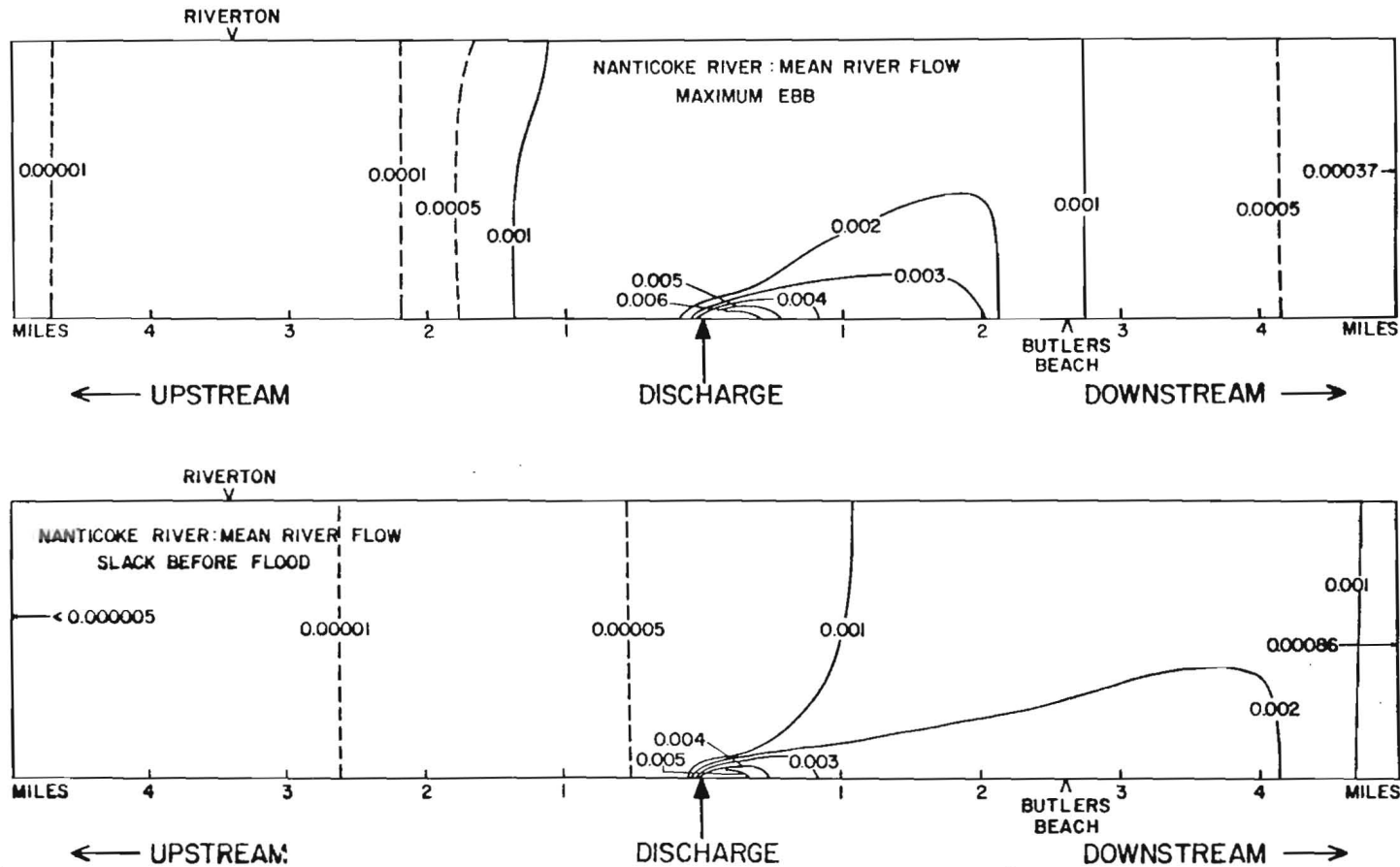


Figure 35. Isolines of relative concentration for mean river flow (810 cfs), for maximum ebb tidal flow and for near slack before flood. Computations are for a discharge flow of 2570 gpm representative of a 600 MW plant (compare with Figure 3 which is representative of a 400 MW plant).

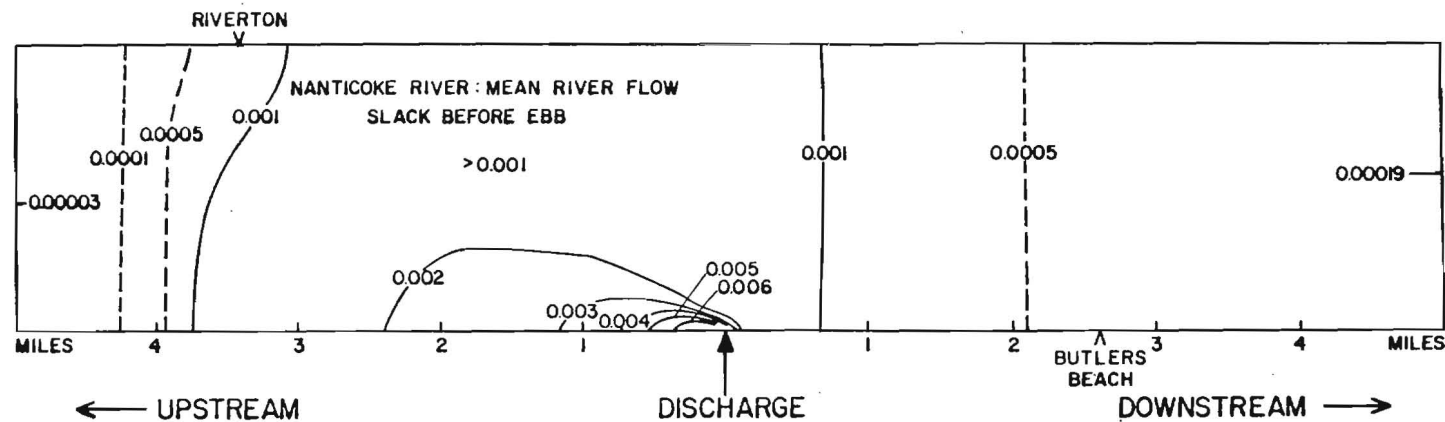
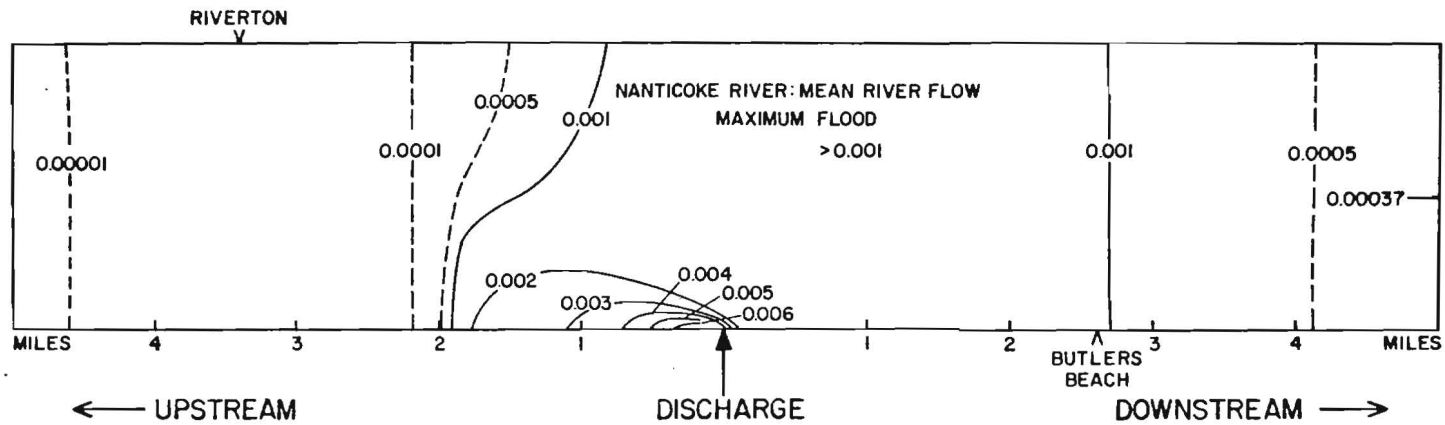


Figure 36. Isolines of relative concentration for mean river flow (810 cfs), for maximum flood flow for near slack before ebb. Computations are for a discharge flow of 2570 gpm representative of a 600 MW plant (compare with Figure 4 which is representative of a 400 MW plant).

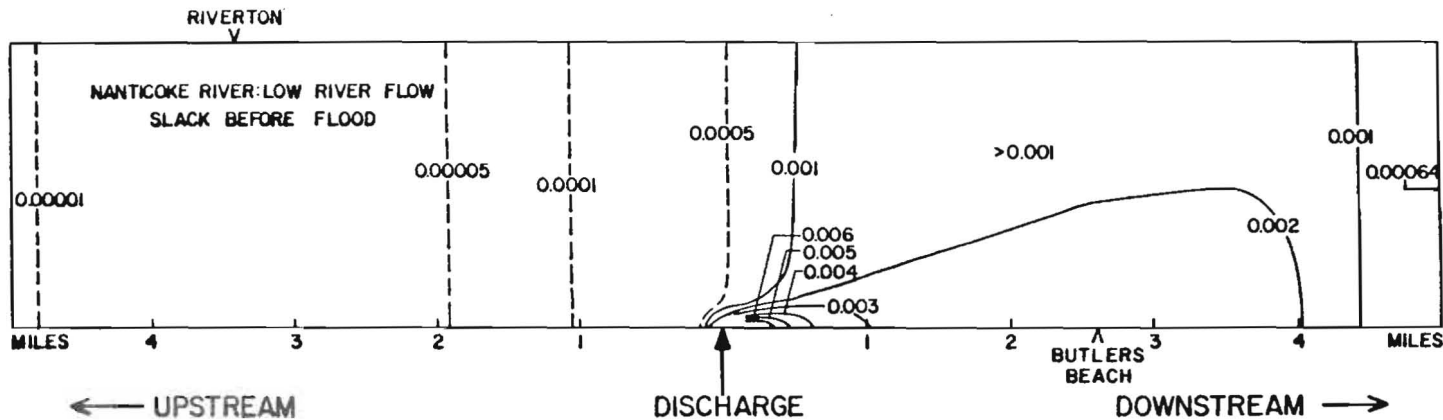
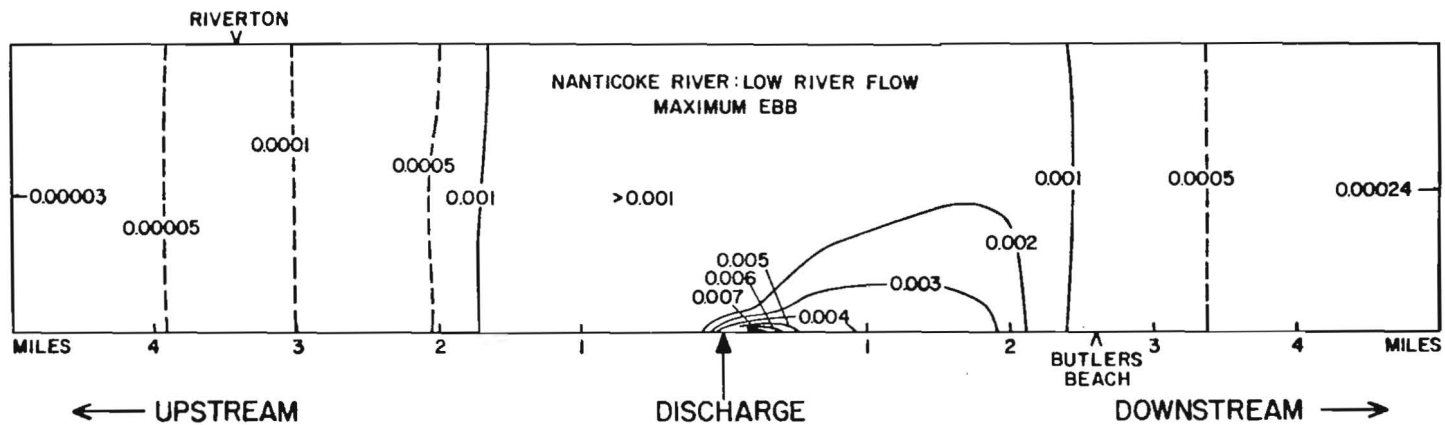


Figure 37. Isolines of relative concentration for low river flow (445 cfs), for maximum ebb tidal flow and for near slack before flood. Computations are for a discharge flow of 2570 gpm representative of a 600 MW plant (compare with Figure 5 which is representative of a 400 MW plant).



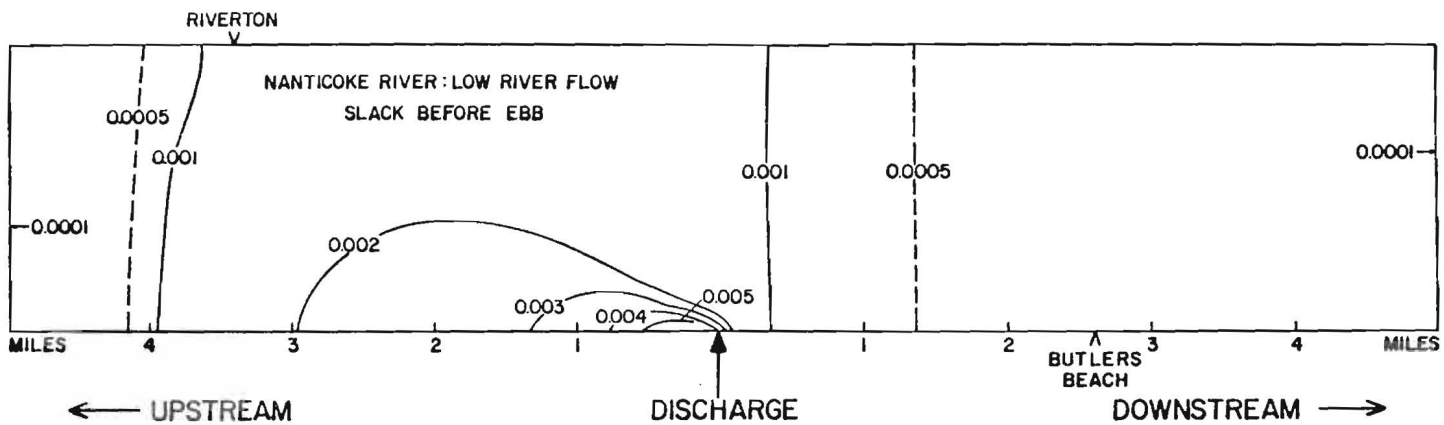
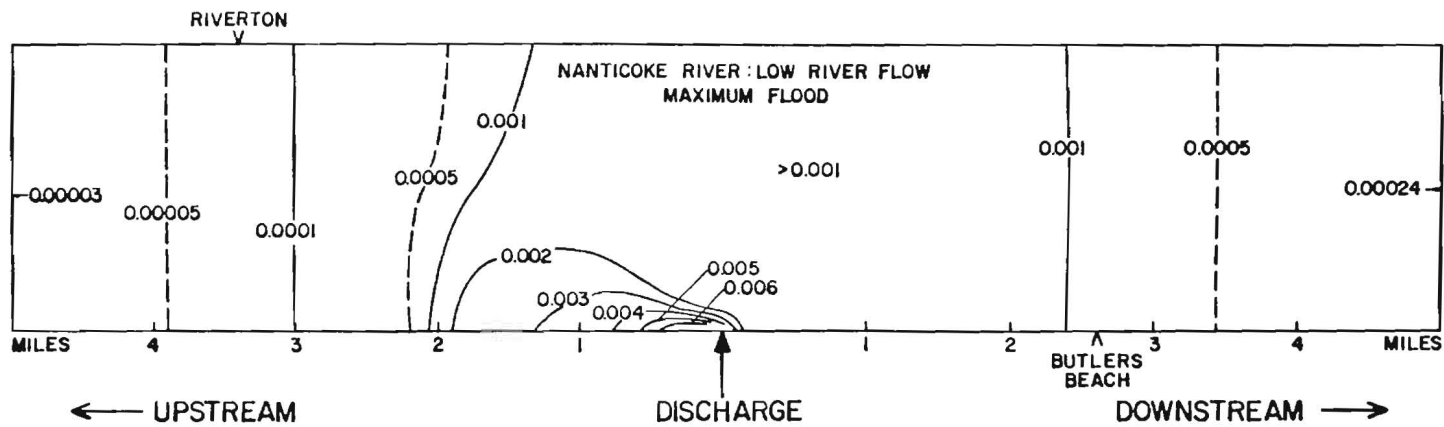


Figure 38. Isolines of relative concentration for low river flow (445 cfs), for maximum flood tidal flow and for near slack before ebb. Computations are for a discharge flow of 2570 gpm representative of a 600 MW plant (compare with Figure 6 which is representative of a 400 MW plant).

concentrations computed for the original source; concentrations at a fixed point are linearly proportional to source strength. The area enclosed by a given isoline of concentration is not, however, linearly proportional to source strength and may exhibit very significant increases which are greater than a factor of 1.5.

The far field distributions of relative concentration computed for the increased source have been scaled back to the actual river geometry; they are presented in Figures 39 through 62. These figures are to be compared to Figures 9 through 32 for the 400 MW plant.

The near field distribution for this 600 MW case are given in Figures 63 and 64. It is evident that these figures are not markedly different from Figures 7 and 8, which give the nearfield distributions of relative concentration for the 400 MW case. The only clear difference between these two sets of figures is that in the 600 MW case (Figure 63), the plume extends further offshore before bending to become parallel to the axis of the estuary.

The reasons for both the similarities and the differences can be found in the assumed input conditions for the two cases. In making the computation for the larger discharge the diameter of the discharge orifice was kept the same as in the 400 MW case. The consequent larger velocity and momentum of the discharge resulting in extending the plume further offshore and also in increasing the densimetric Froude number, and hence increasing the relative rate of mixing in the near field.

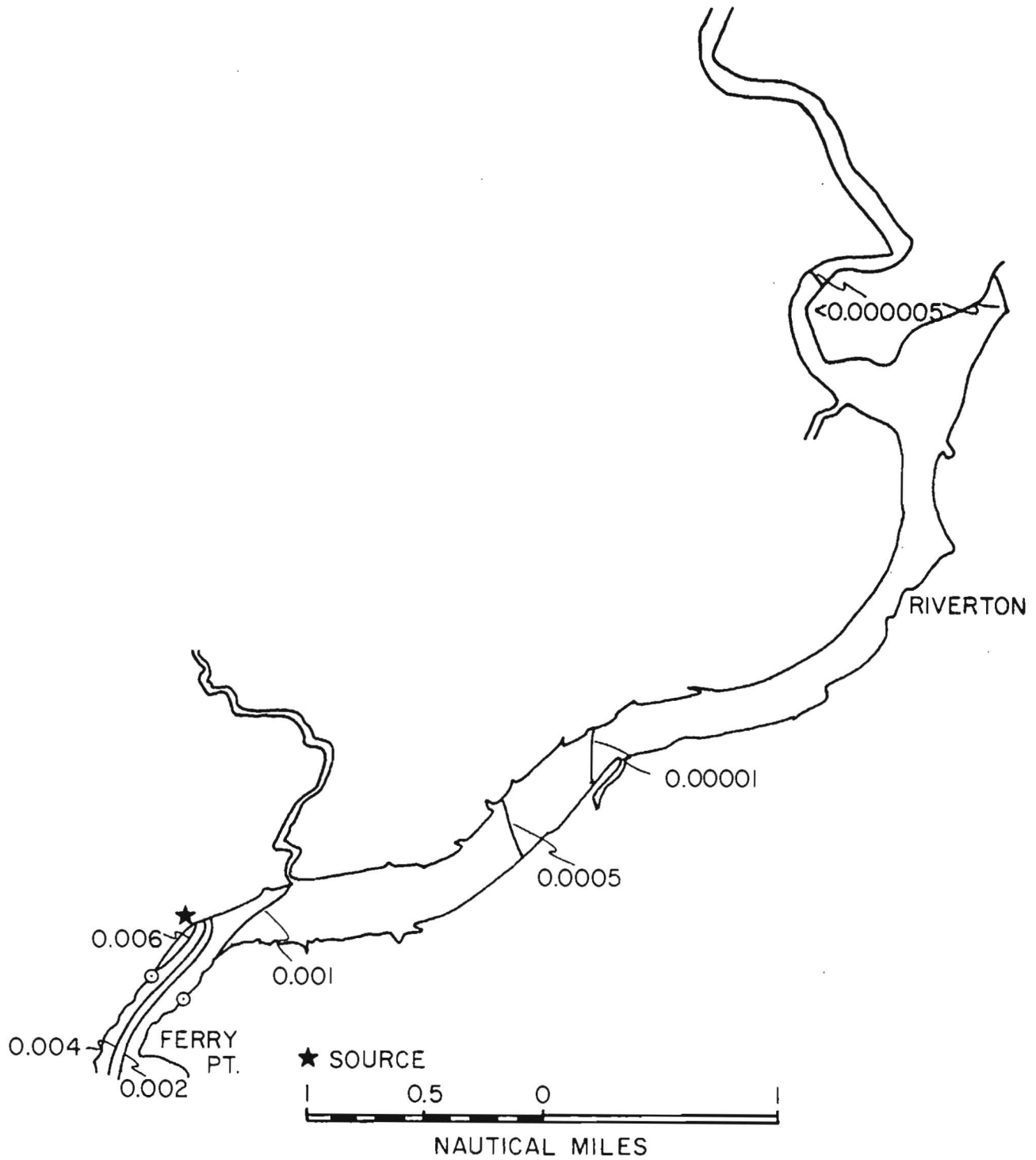


Figure 39. Distribution of relative concentration for a 600 MW plant, at maximum ebb, during high river flow, upstream from the source.

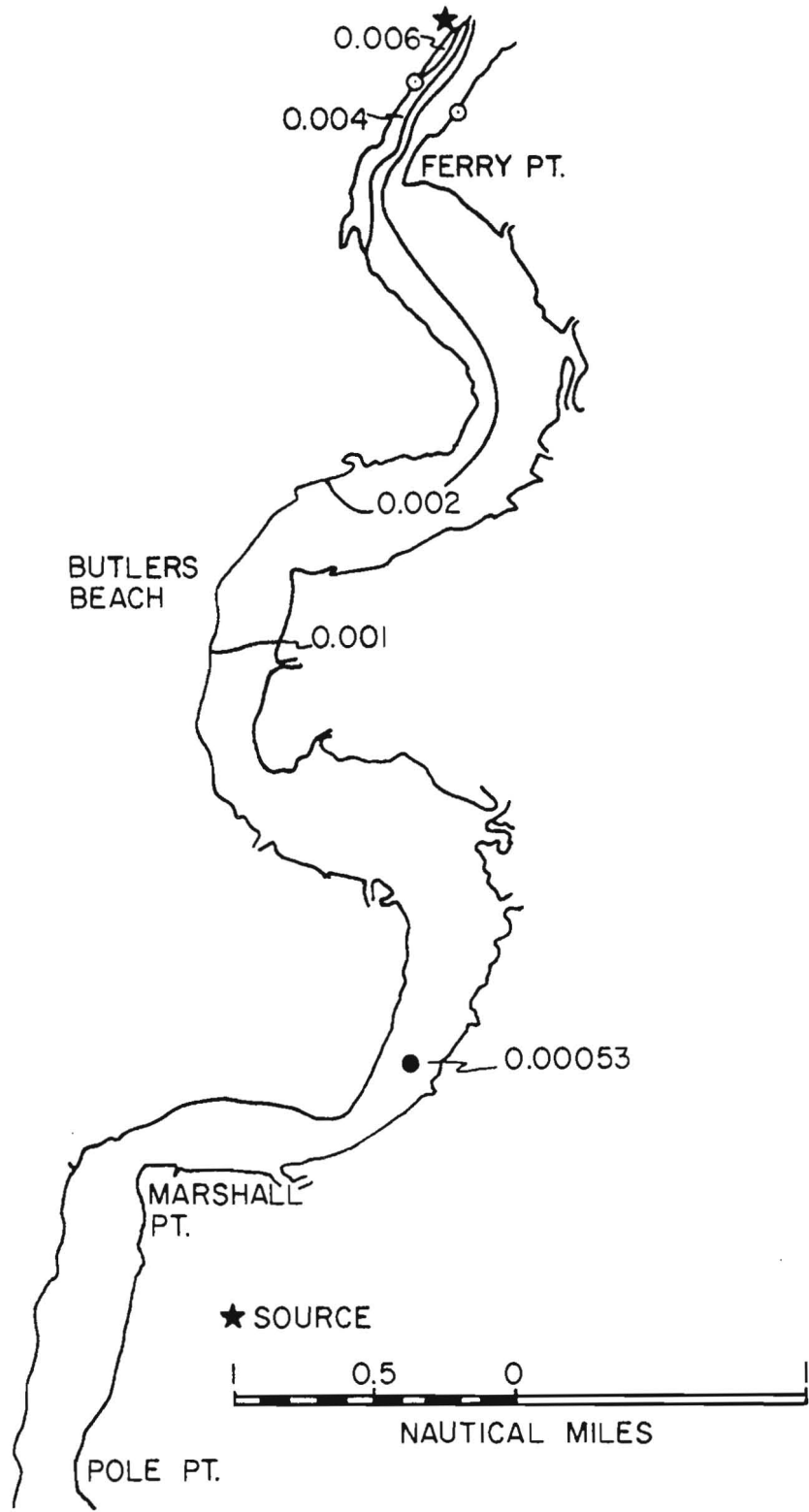


Figure 40. Distribution of relative concentration for a 600 MW plant, at maximum ebb, during high river flow, downstream from the source.

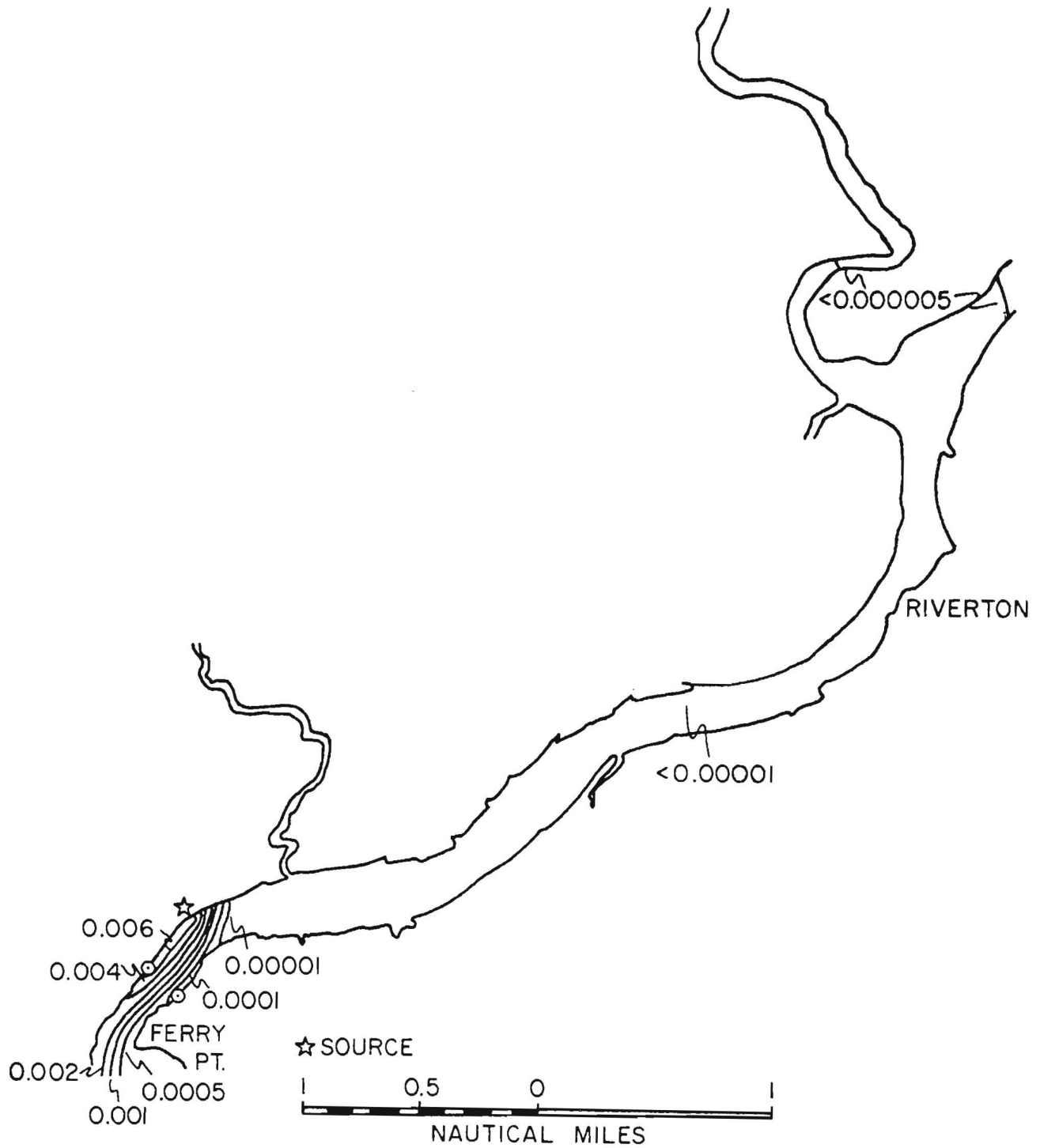


Figure 41. Distribution of relative concentration for a 600 MW plant, near slack before flood, during high river flow, upstream from the source.

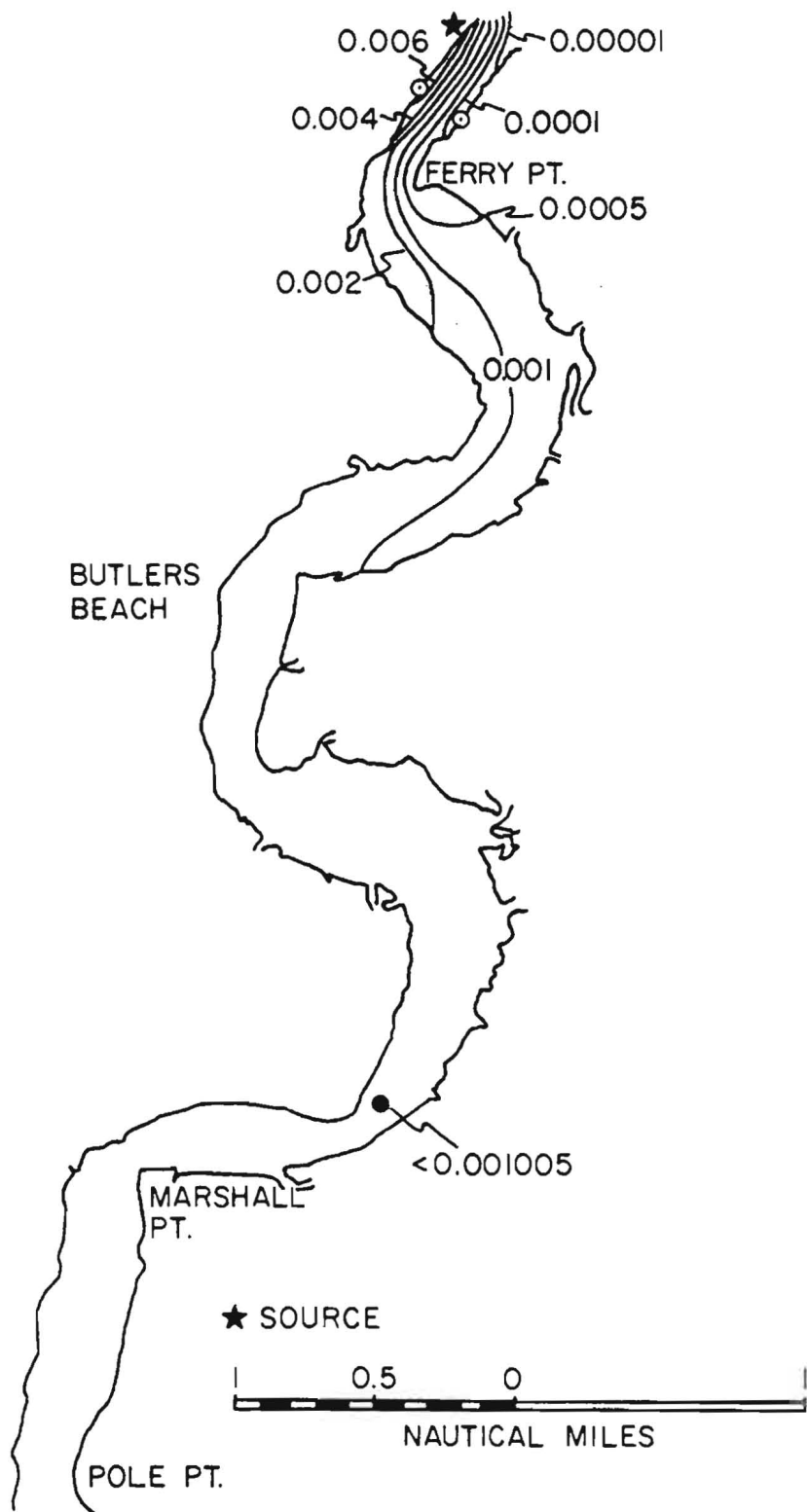


Figure 42. Distribution of relative concentration for a 600 MW plant, near slack before flood, during high river flow, downstream from the source.

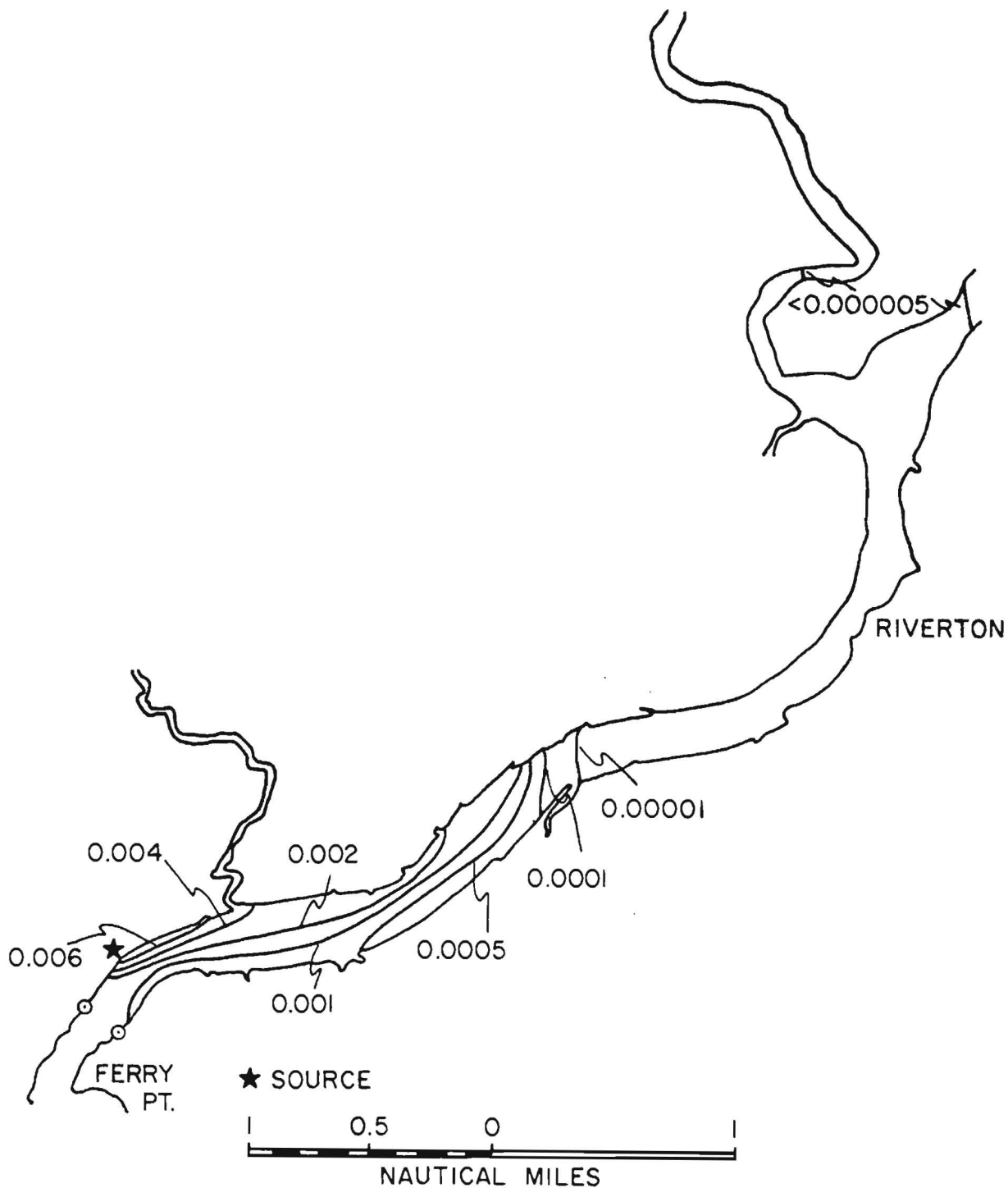


Figure 43. Distribution of relative concentration for a 600 MW plant, at maximum flood, during high river flow, upstream from the source.

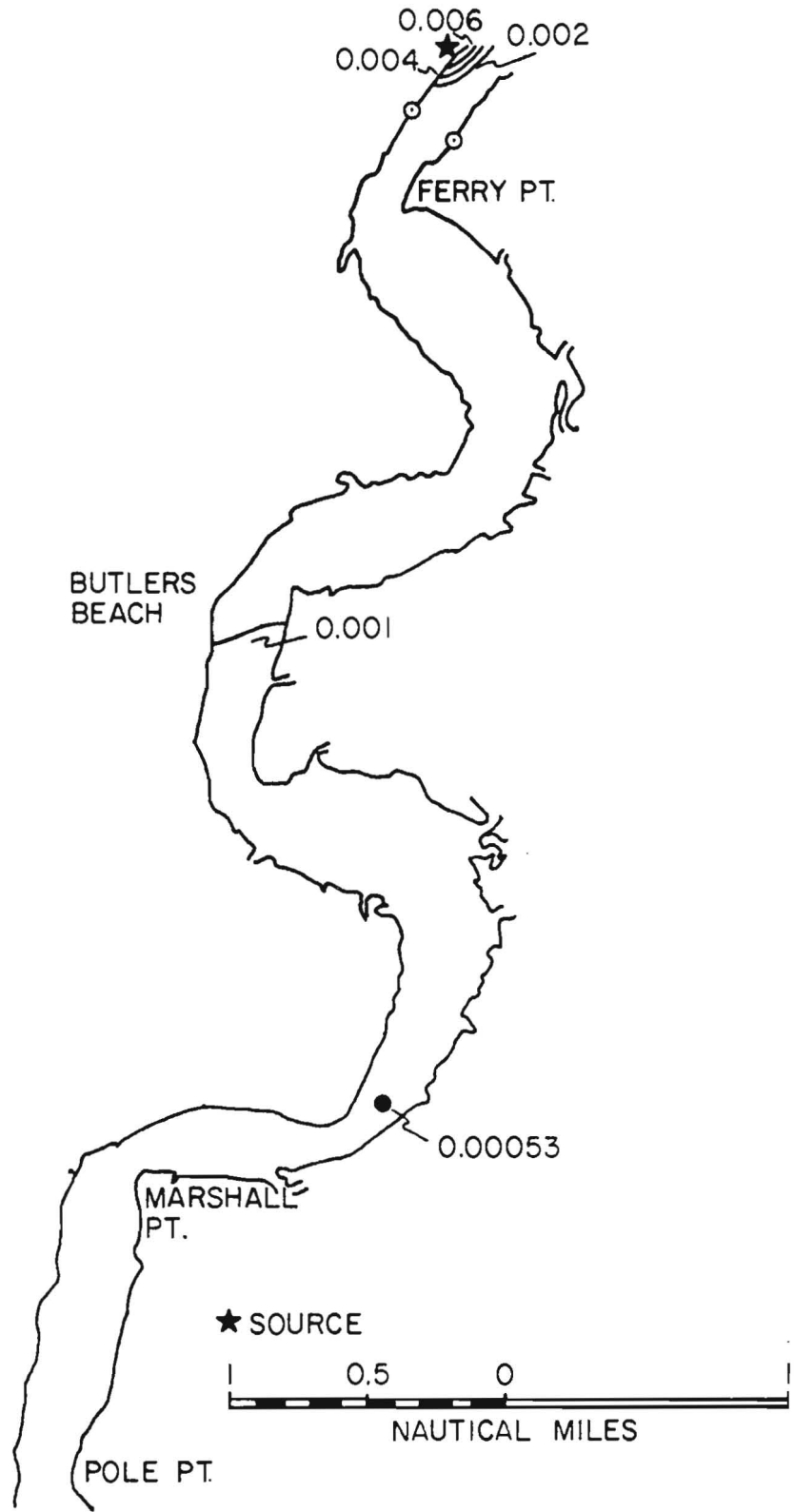


Figure 44. Distribution of relative concentration for a 600 MW plant, at maximum flood, during high river flow, downstream from the source.



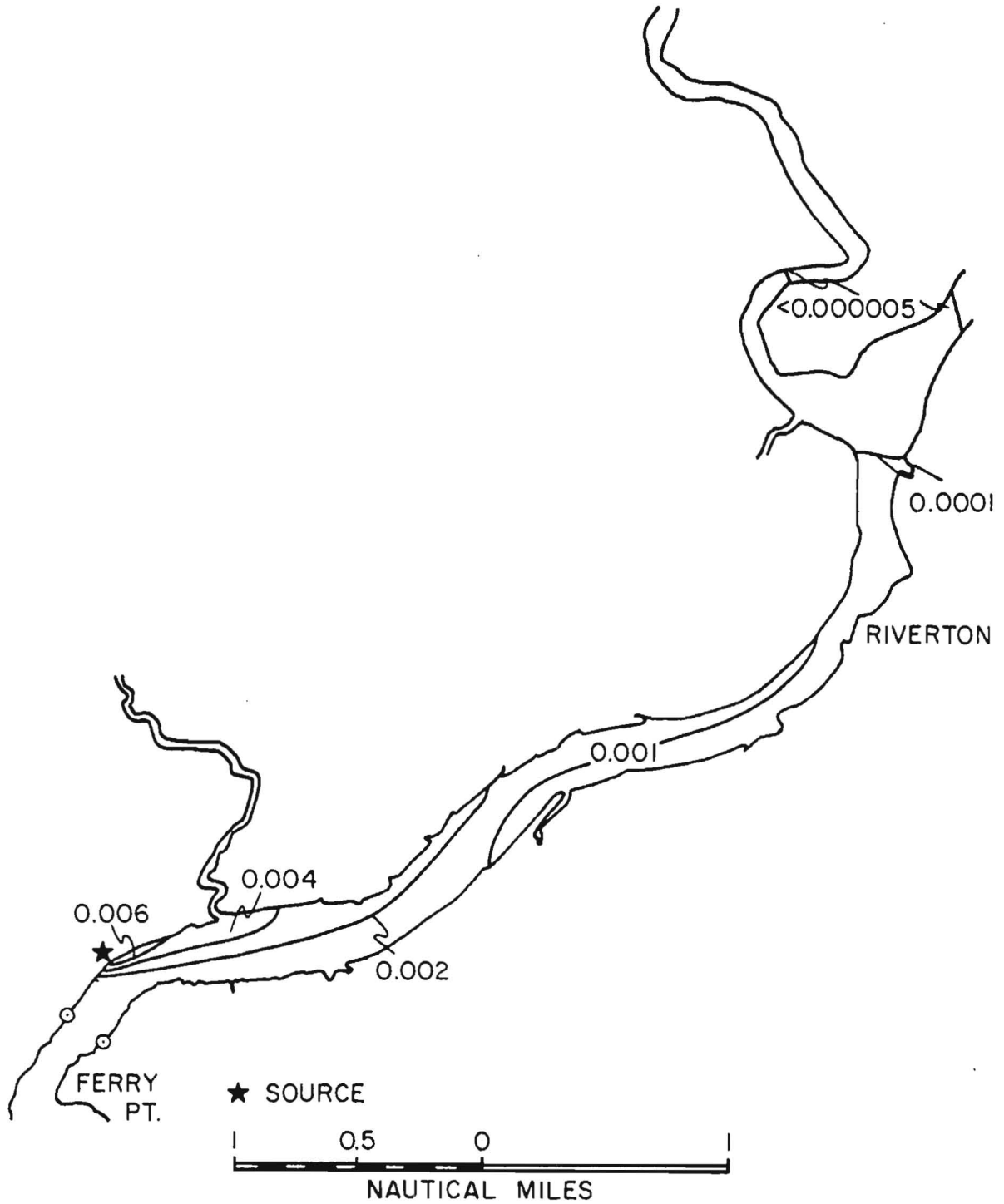


Figure 45. Distribution of relative concentration for a 600 MW plant near slack before ebb, during low river flow, upstream from the source.

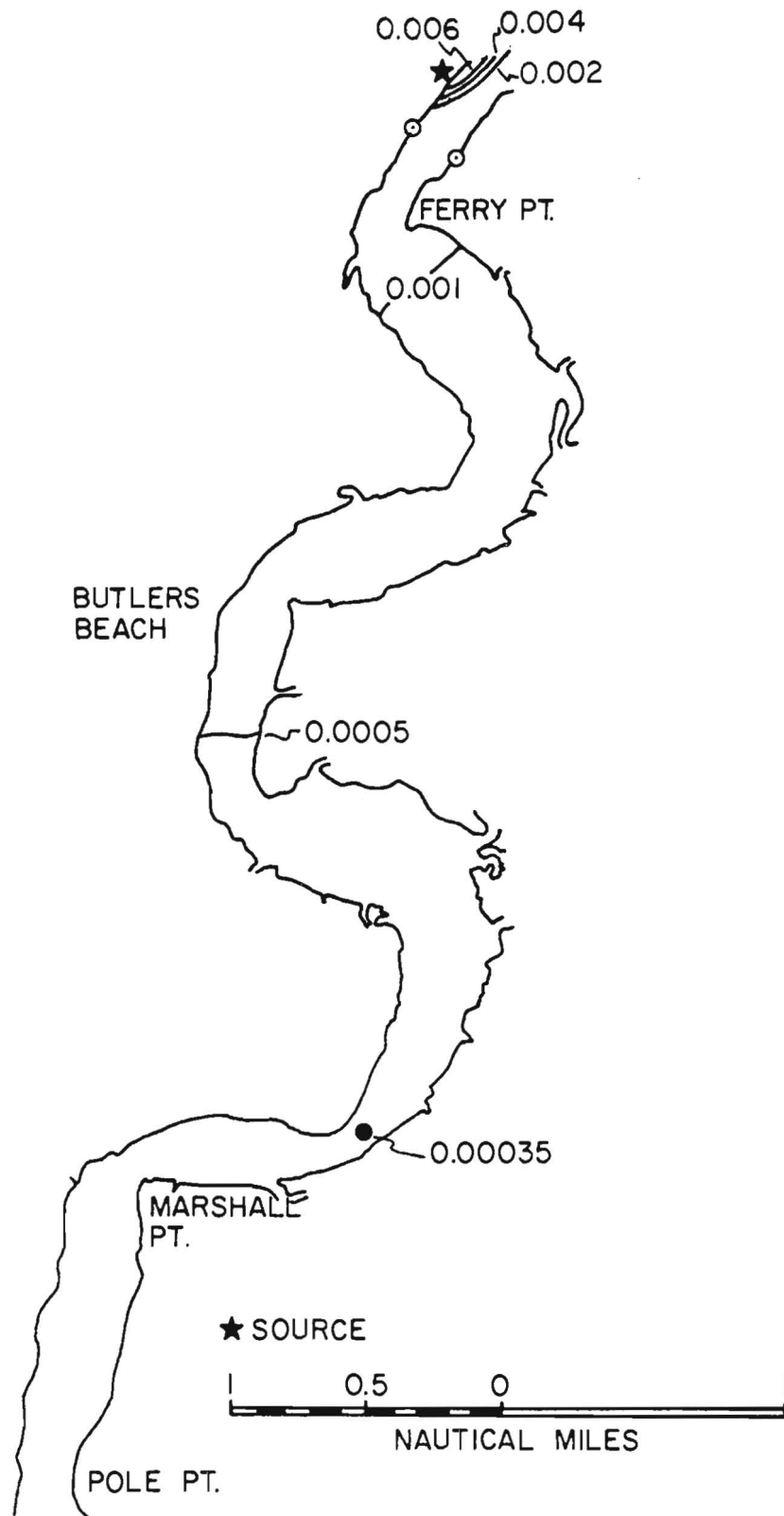


Figure 46. Distribution of relative concentration for a 600 MW plant, near slack before ebb, during high river flow, downstream from the source.

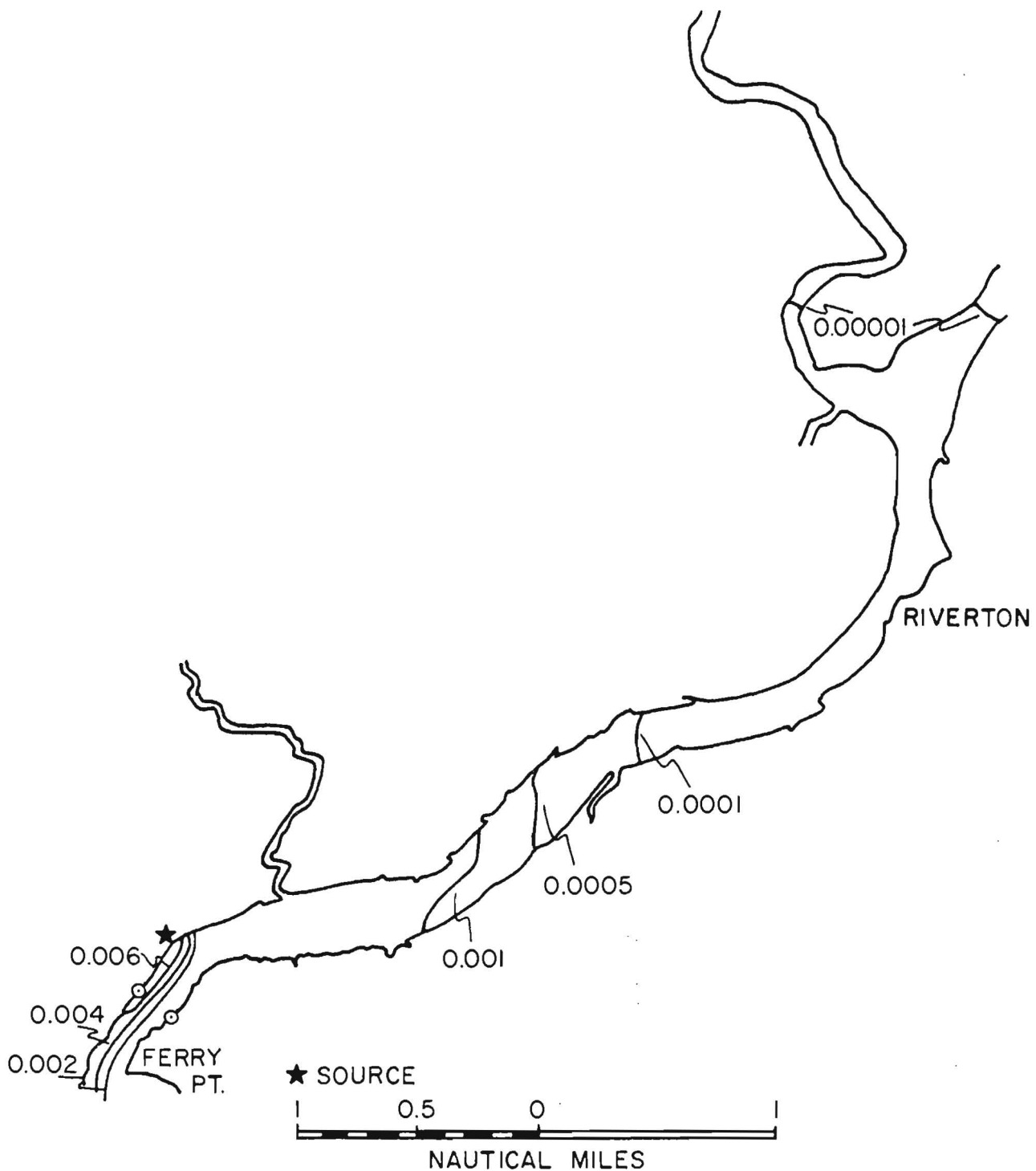


Figure 47. Distribution of relative concentration for a 600 MW plant, at maximum ebb, during mean river flow, upstream from the source.

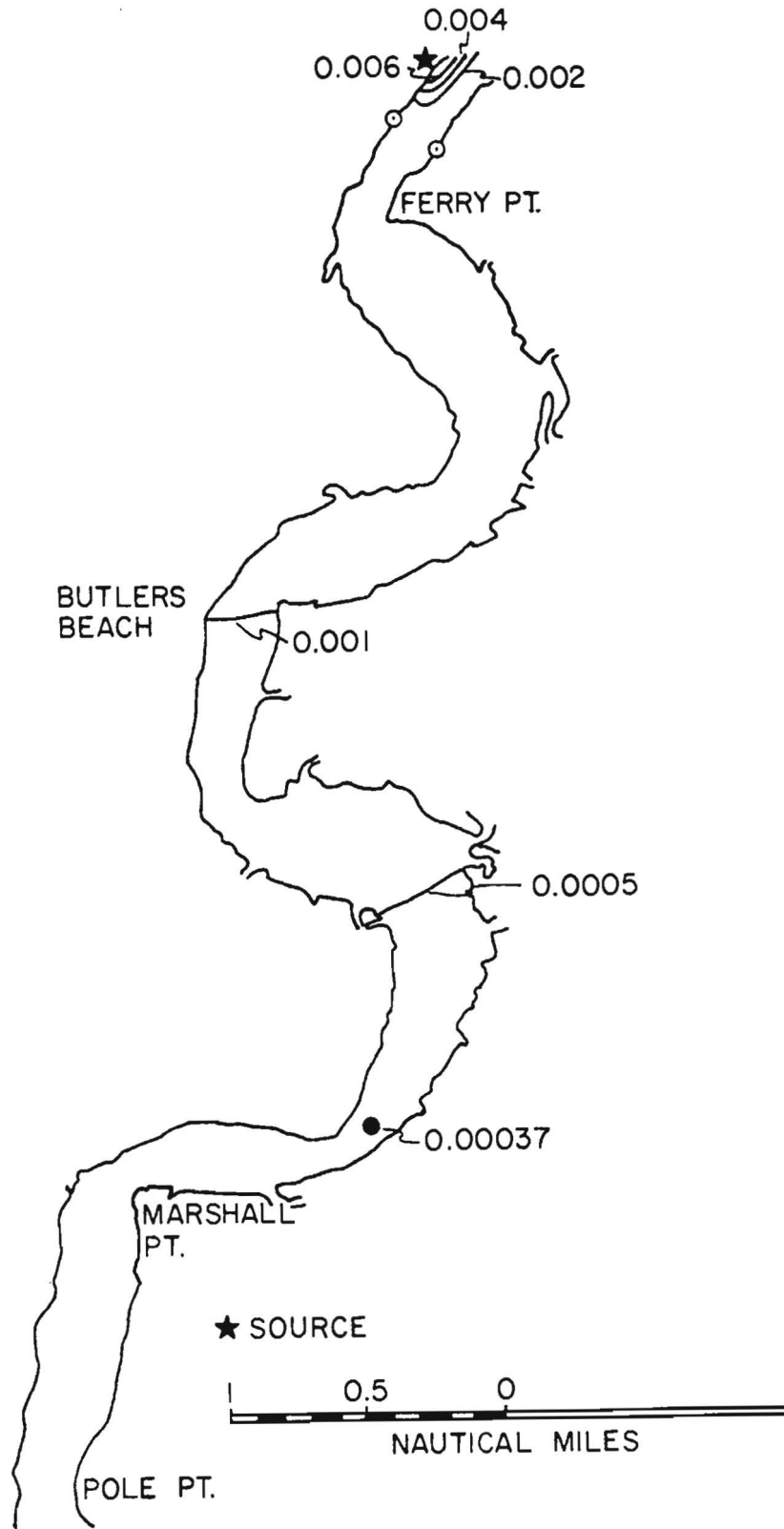


Figure 48. Distribution of relative concentration for a 600 MW plant, at maximum ebb, during mean river flow, downstream from the source.

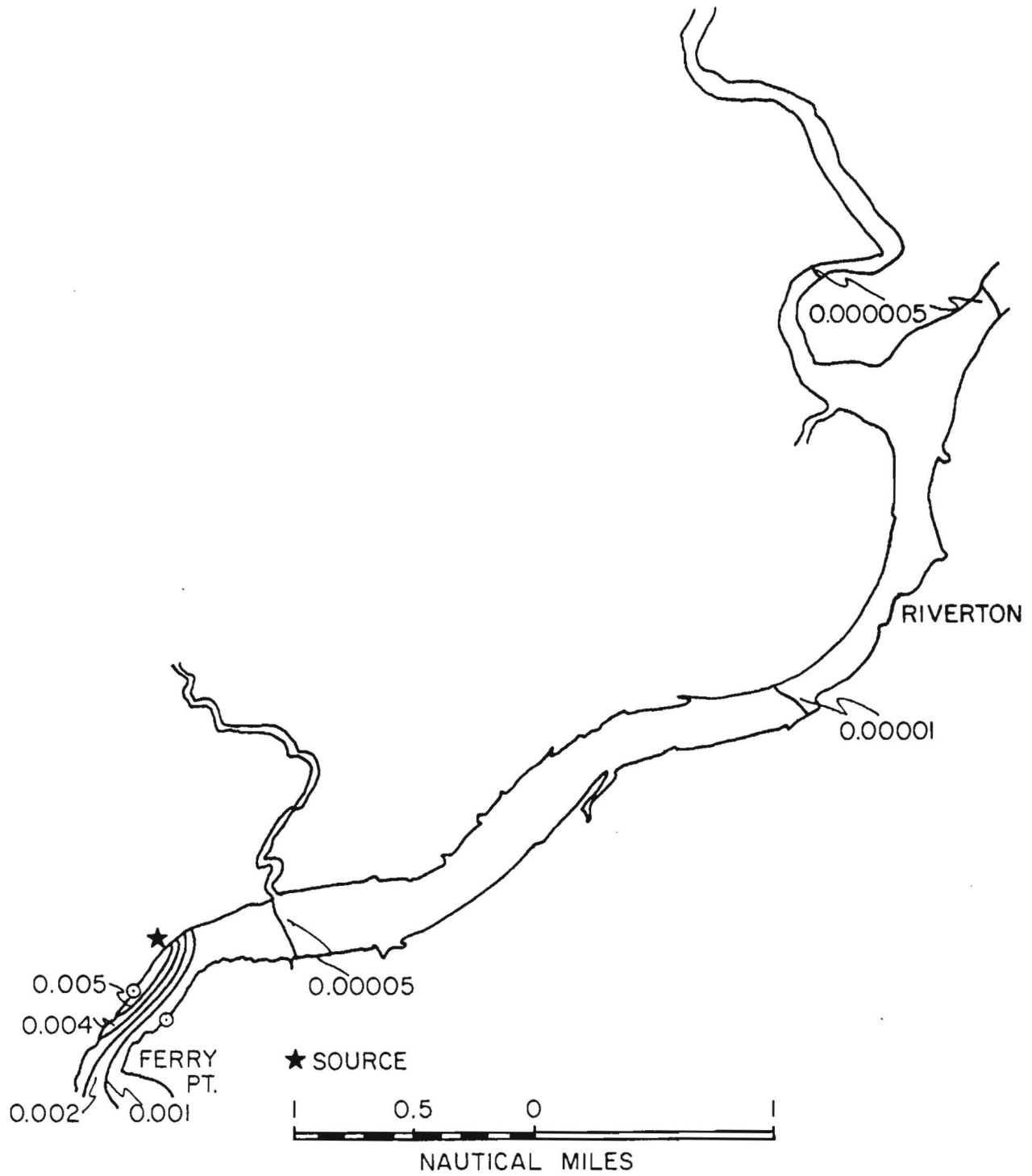


Figure 49. Distribution of relative concentration for a 600 MW plant, near slack before flood, during mean river flow, upstream from the source.

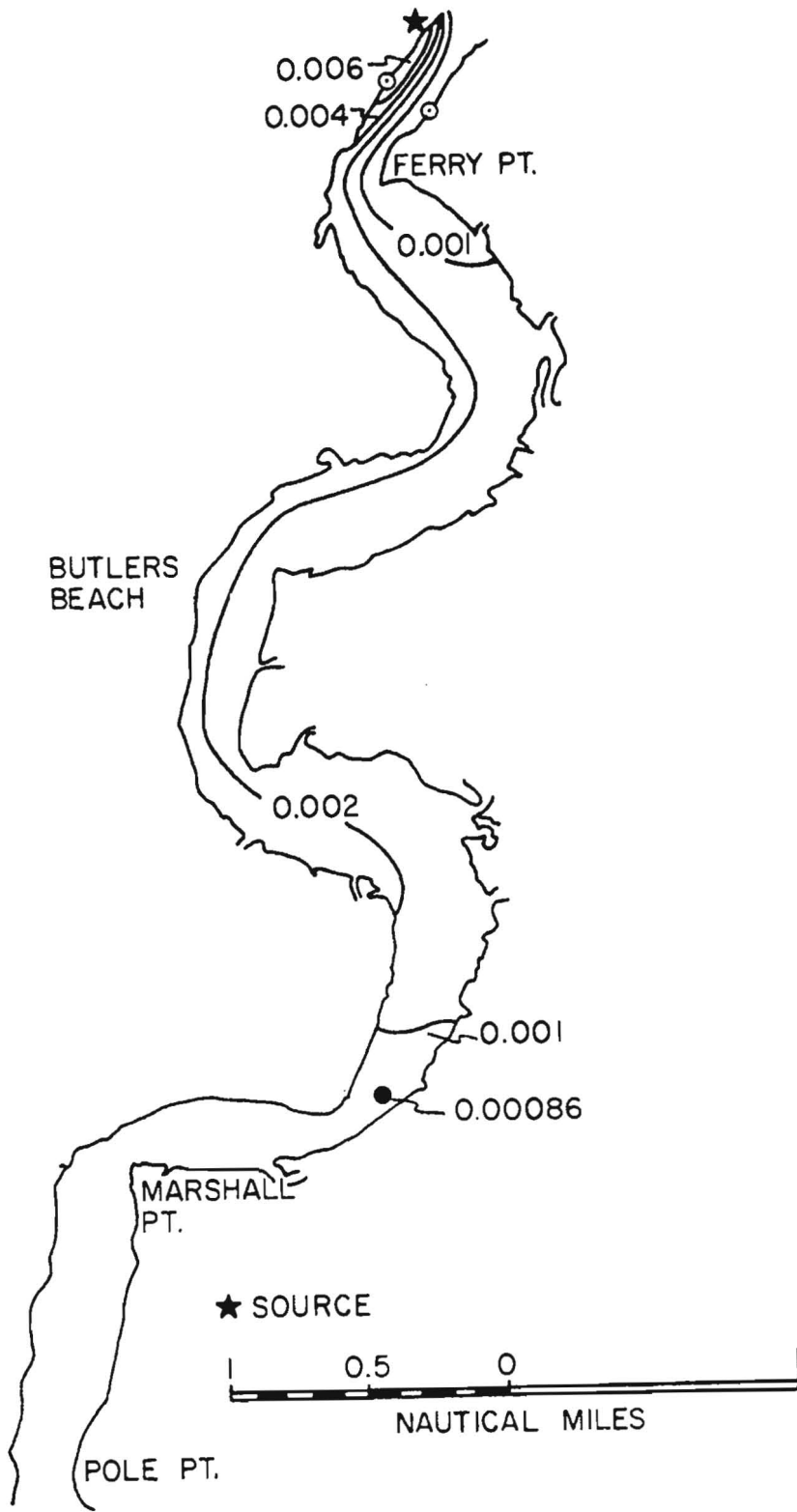


Figure 50. Distribution of relative concentration for a 600 MW plant, near slack before flood, during mean river flow, downstream from the source.

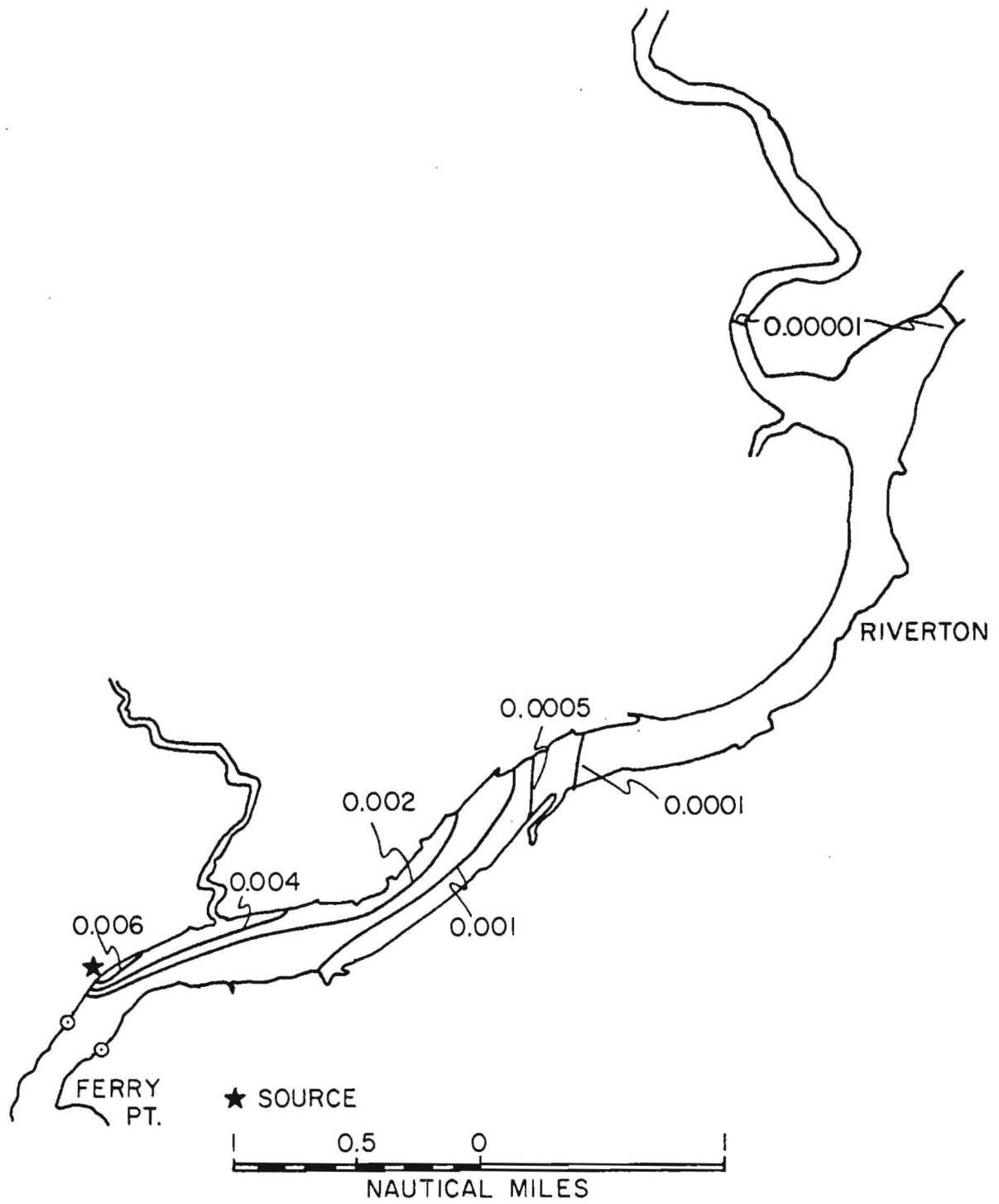


Figure 51. Distribution of relative concentration for a 600 MW plant, at maximum flood, during mean river flow, upstream from the source.

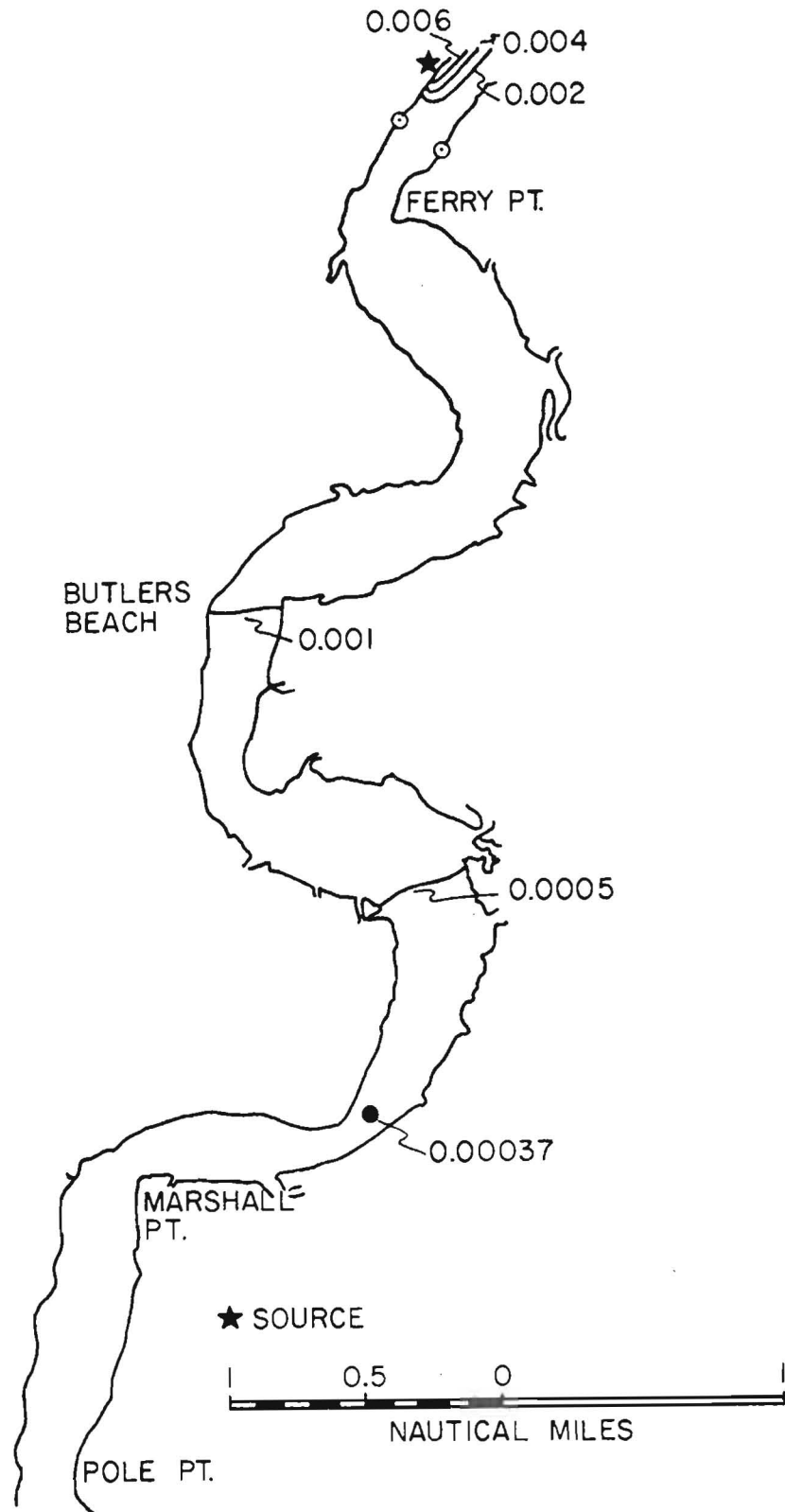


Figure 52. Distribution of relative concentration for a 600 MW plant, at maximum flood, during mean river flow, downstream from the source.



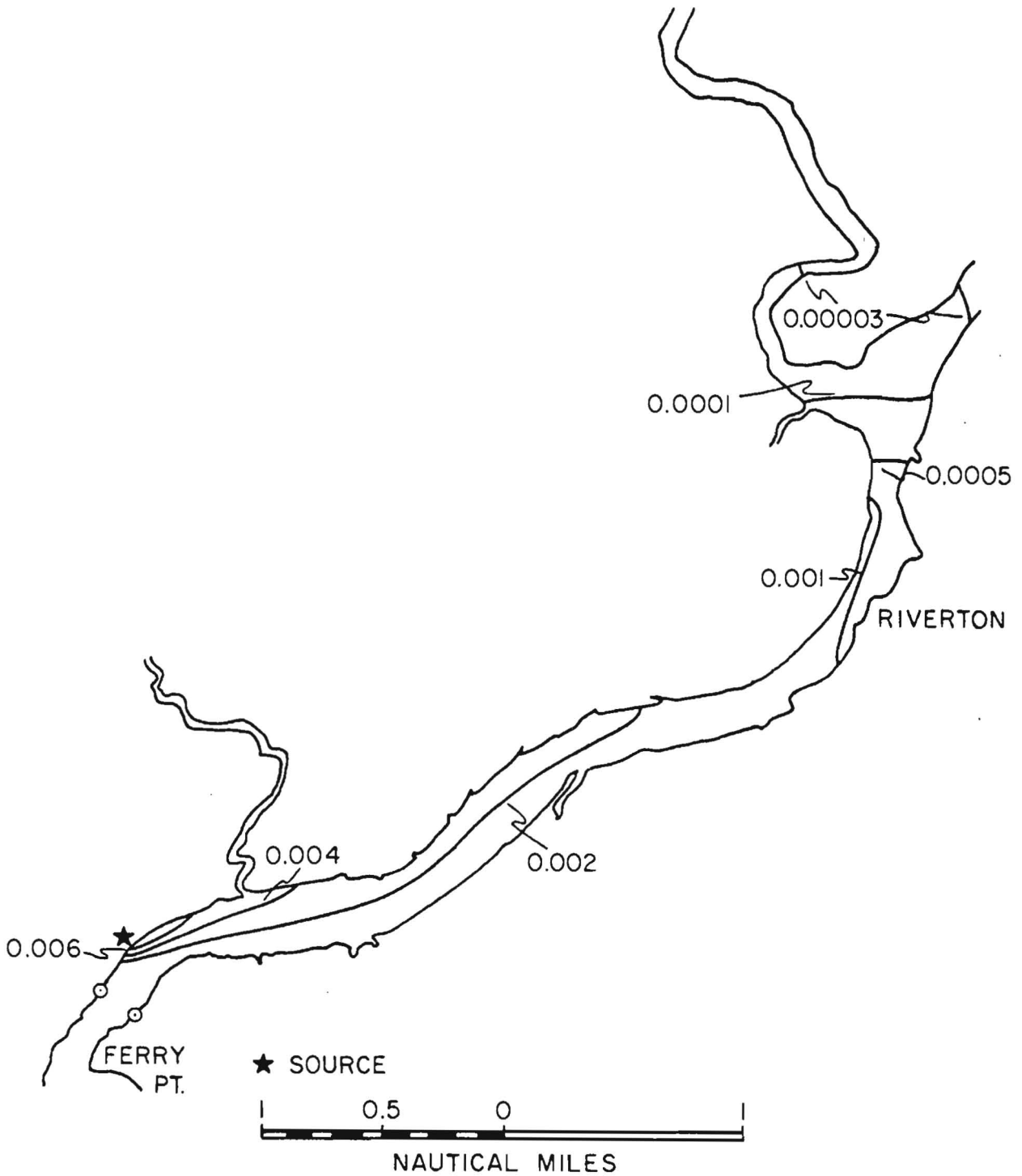


Figure 53. Distribution of relative concentration for a 600 MW plant, near slack before ebb, during mean river flow, upstream from the source.

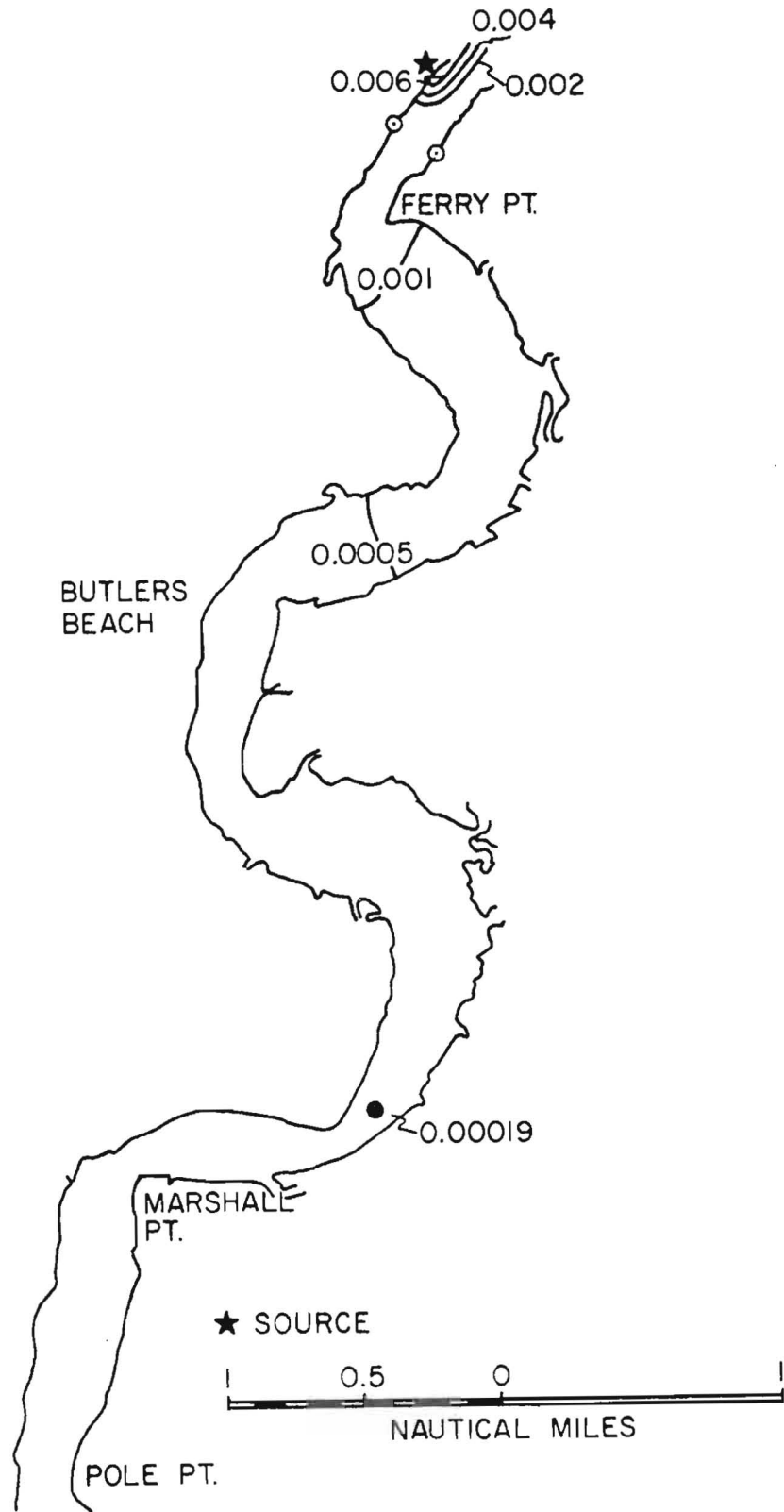


Figure 54. Distribution of relative concentration for a 600 MW plant, near slack before ebb, during mean river flow, downstream from the source.

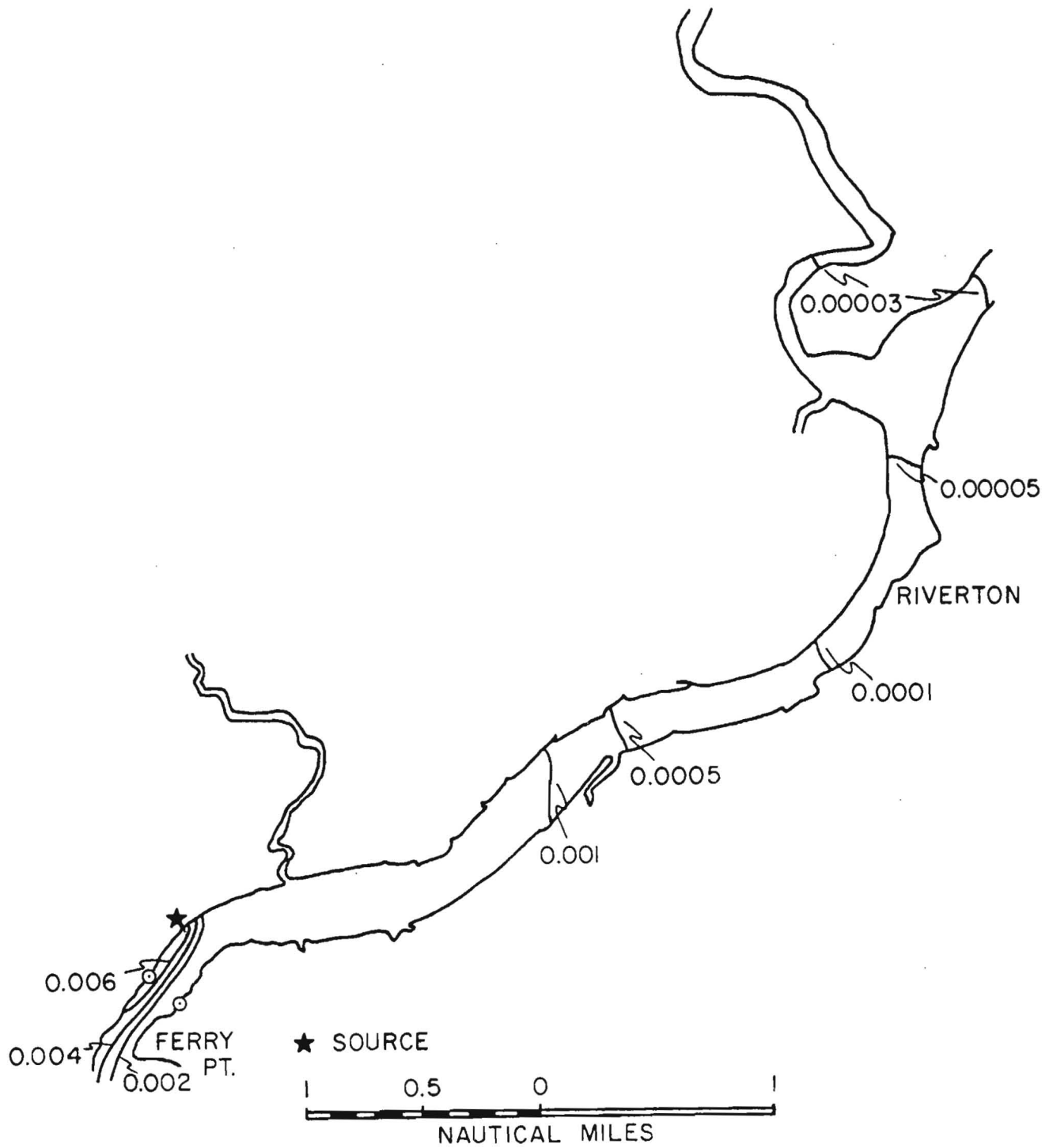


Figure 55. Distribution of relative concentration for a 600 MW plant, at maximum ebb, during low river flow, upstream from the source.

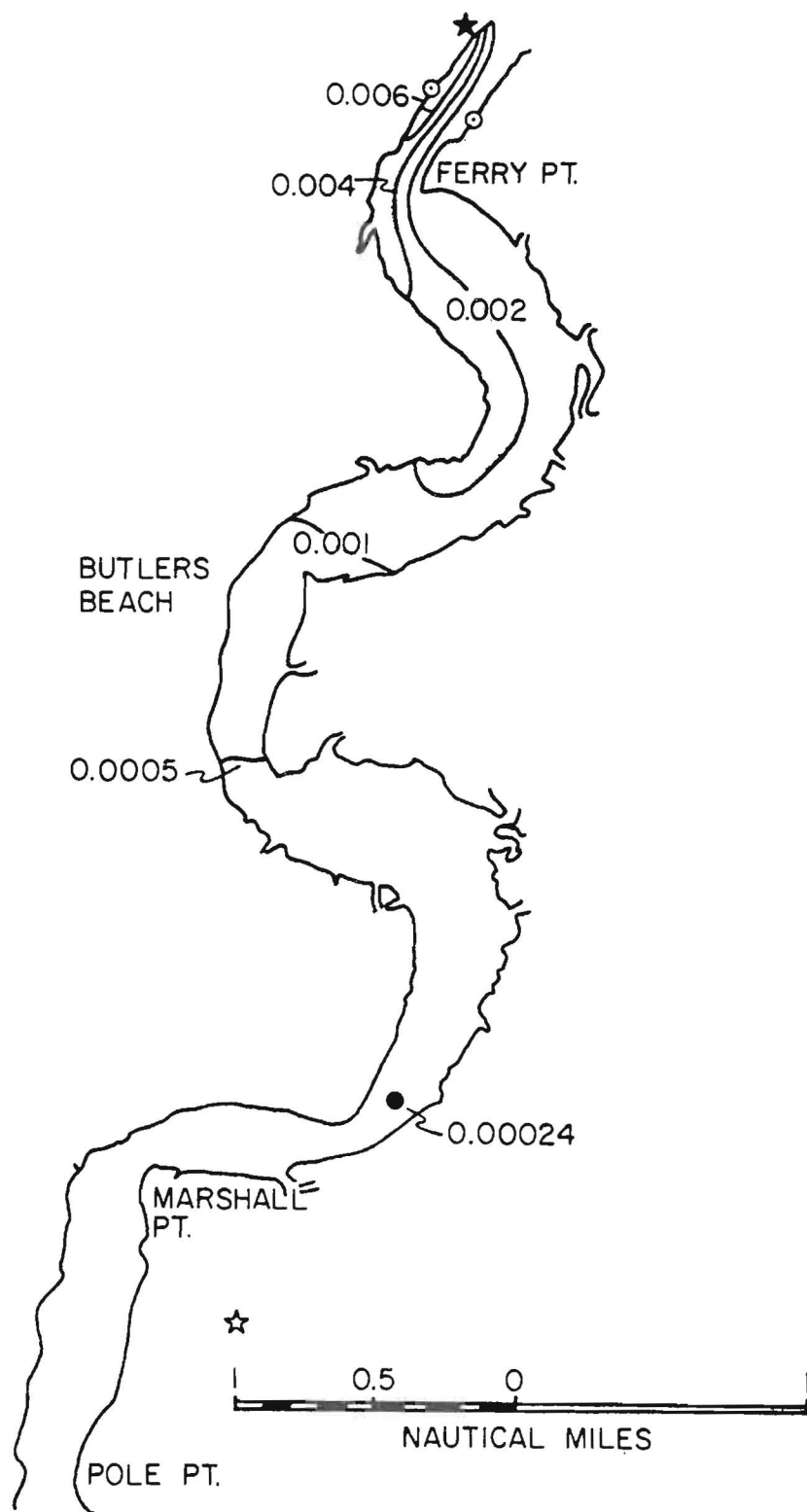


Figure 56. Distribution of relative concentration for a 600 MW plant, at maximum ebb, during low river flow, downstream from the source.

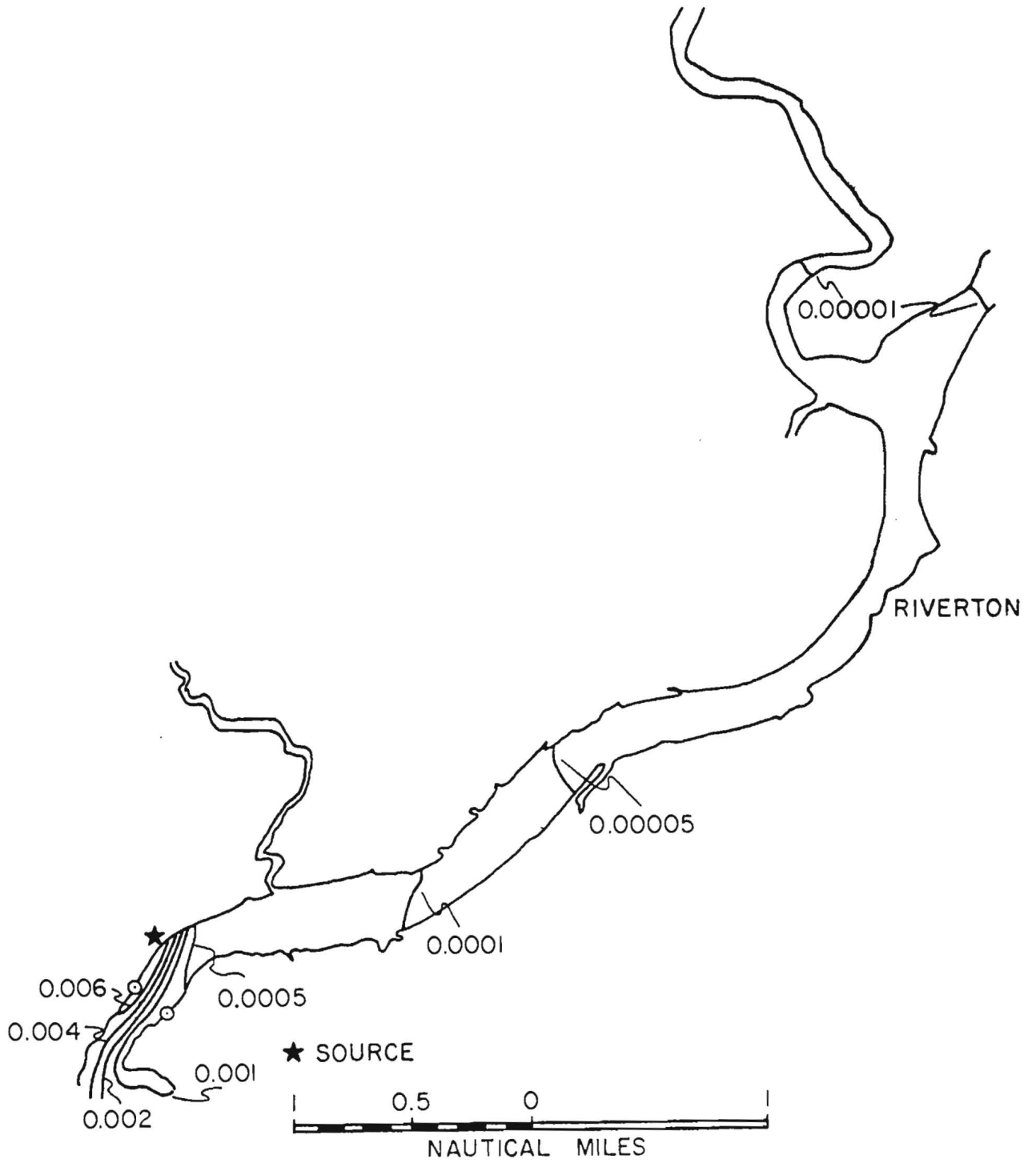


Figure 57. Distribution of relative concentration for a 600 MW plant, near slack before flood, during low river flow, upstream from the source.

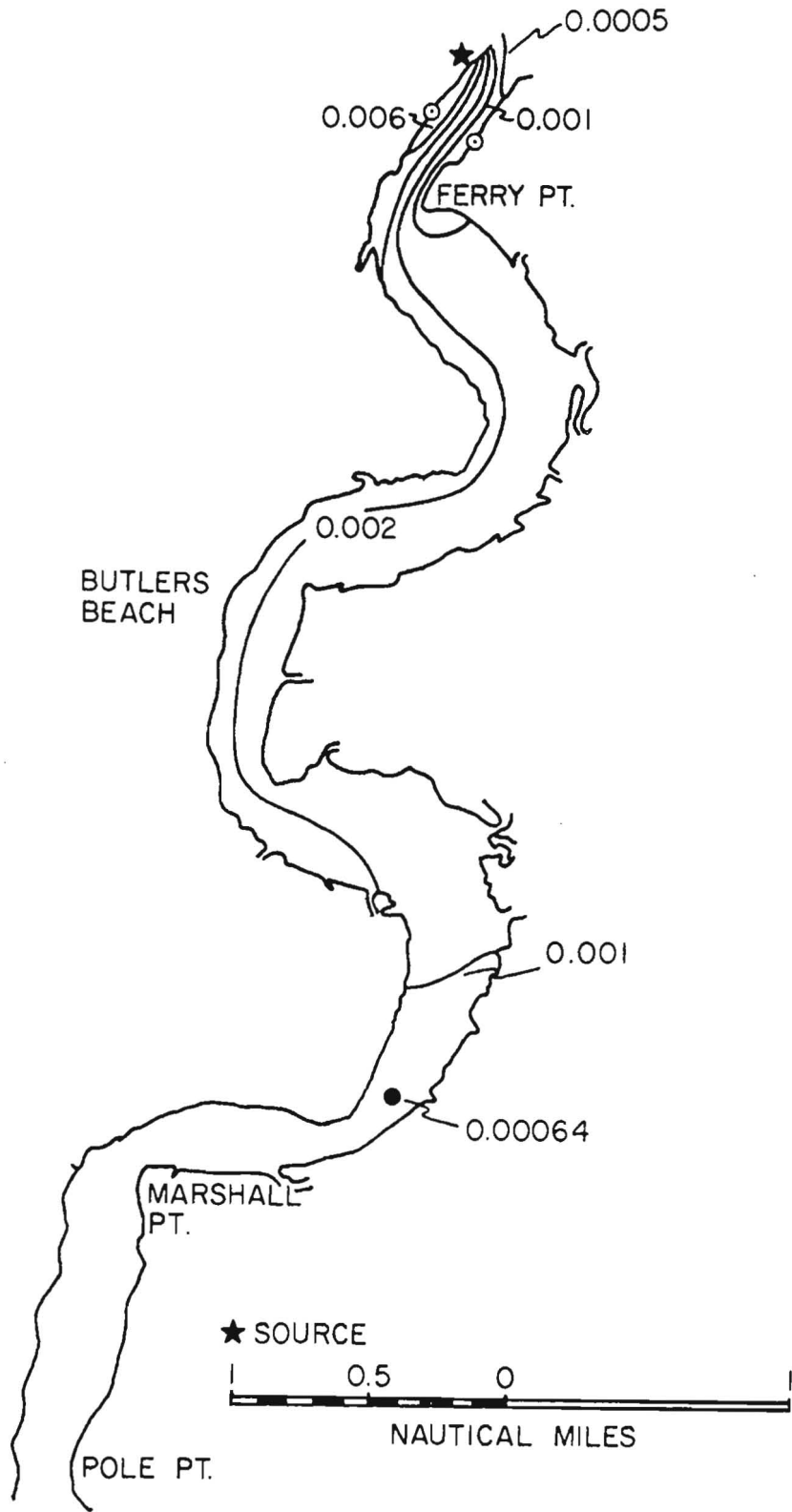


Figure 58. Distribution of relative concentration for a 600 MW plant, near slack before flood, during low river flow, downstream from the source.

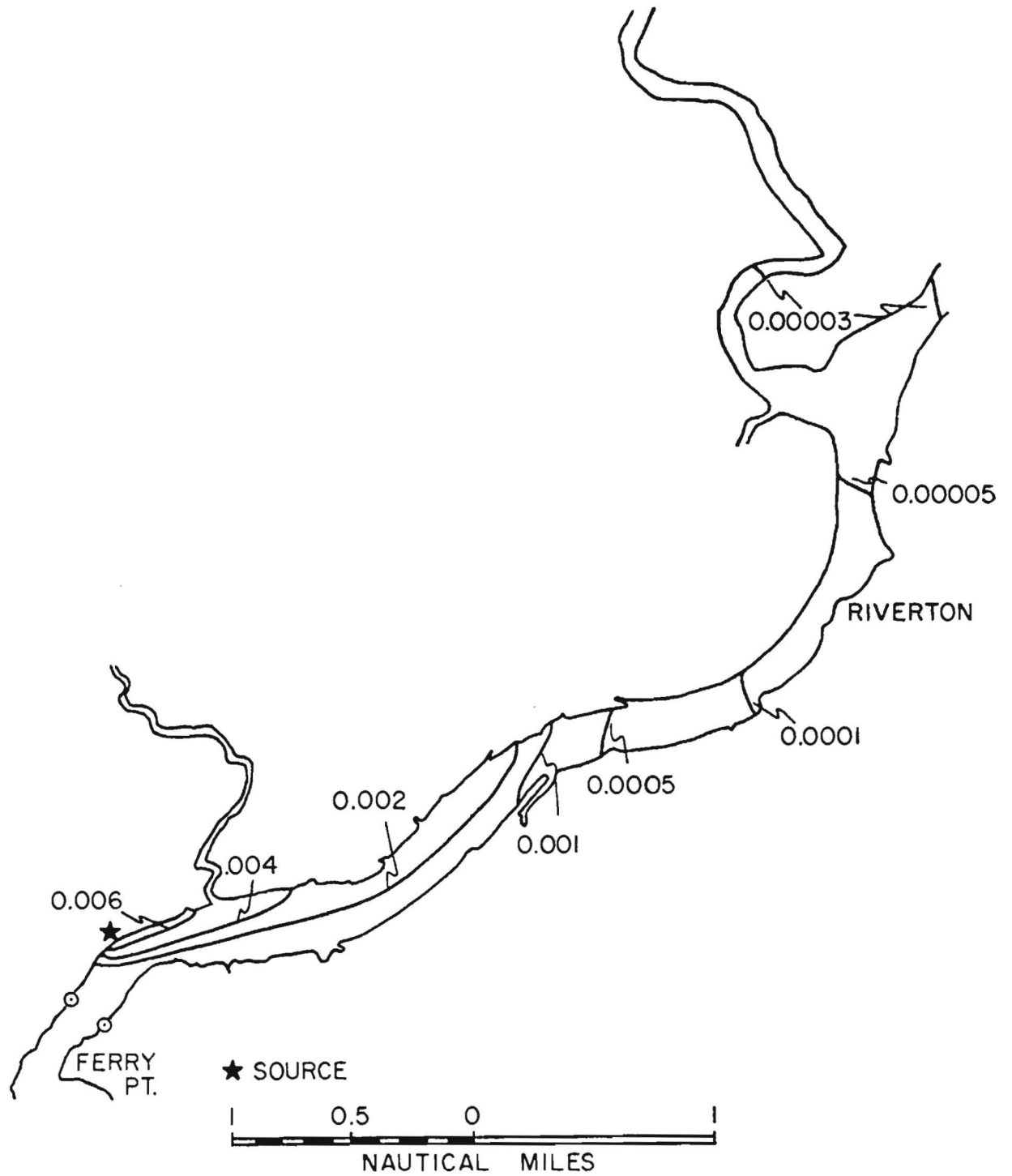


Figure 59. Distribution of relative concentration for a 600 MW plant, at maximum flood, during low river flow, upstream from the source.

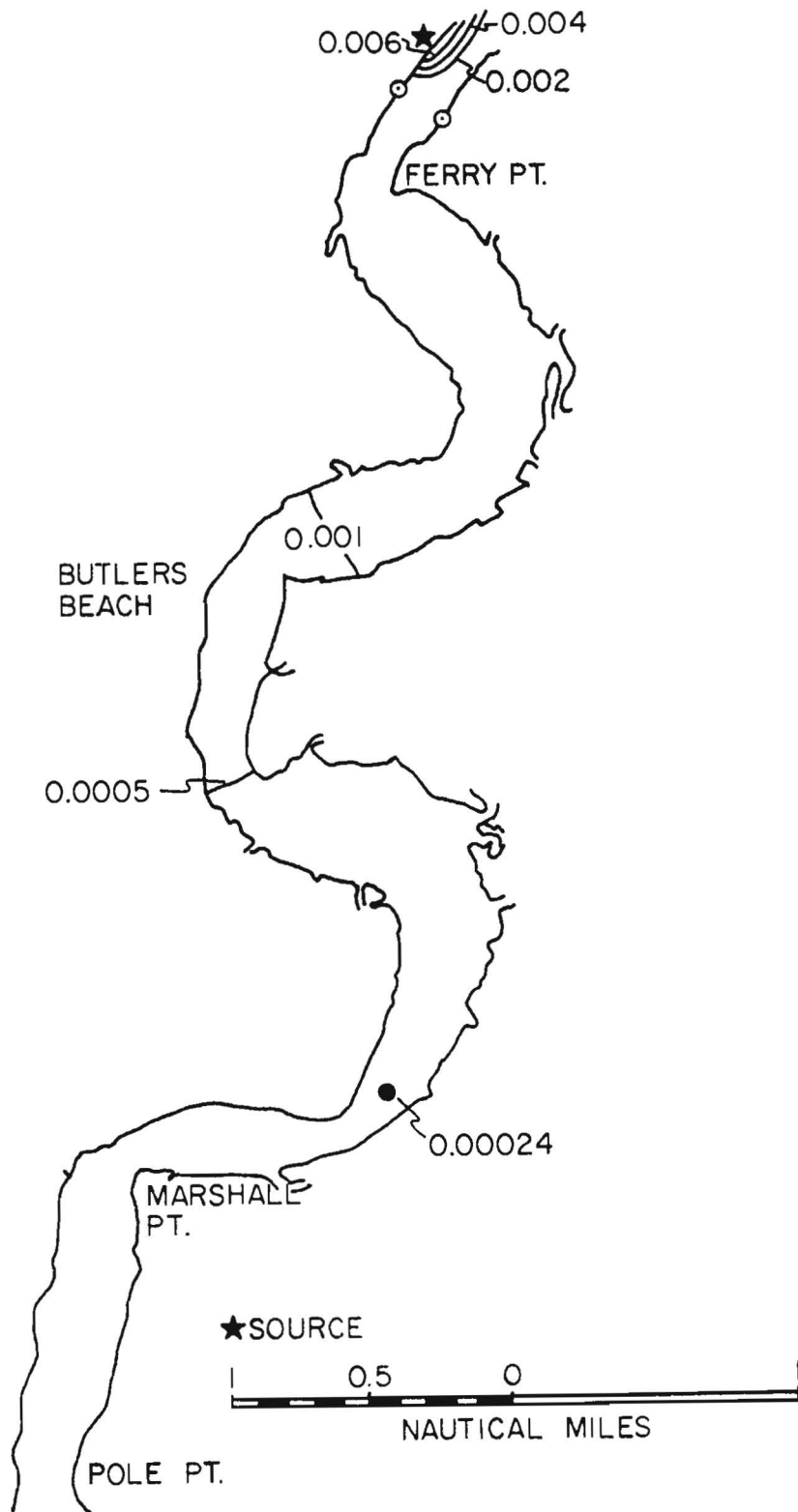


Figure 60. Distribution of relative concentration for a 600 MW plant, at maximum flood, during low river flow, downstream from the source.



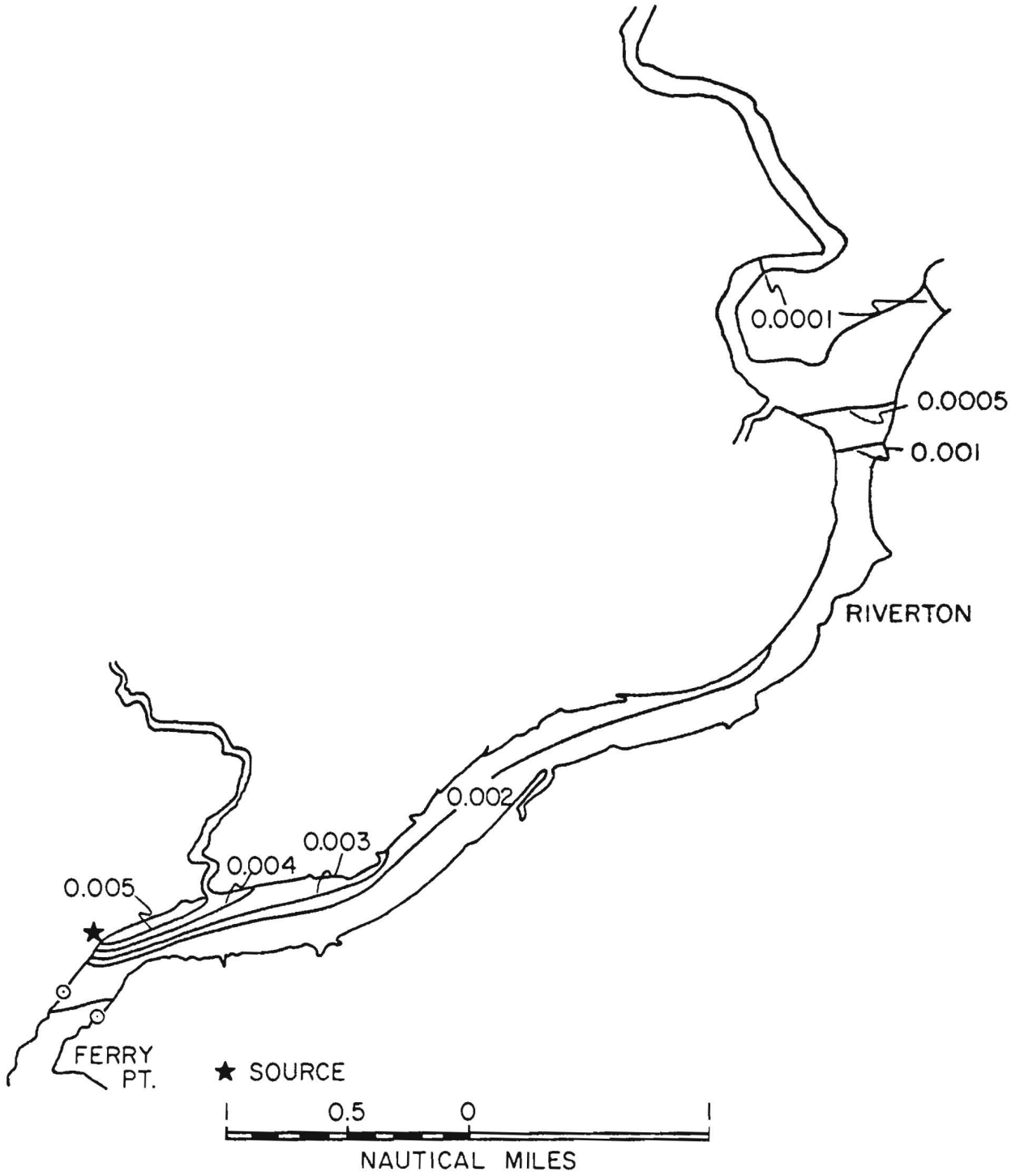


Figure 61. Distribution of relative concentration for a 600 MW plant, near slack before ebb, during low river flow, upstream from the source.

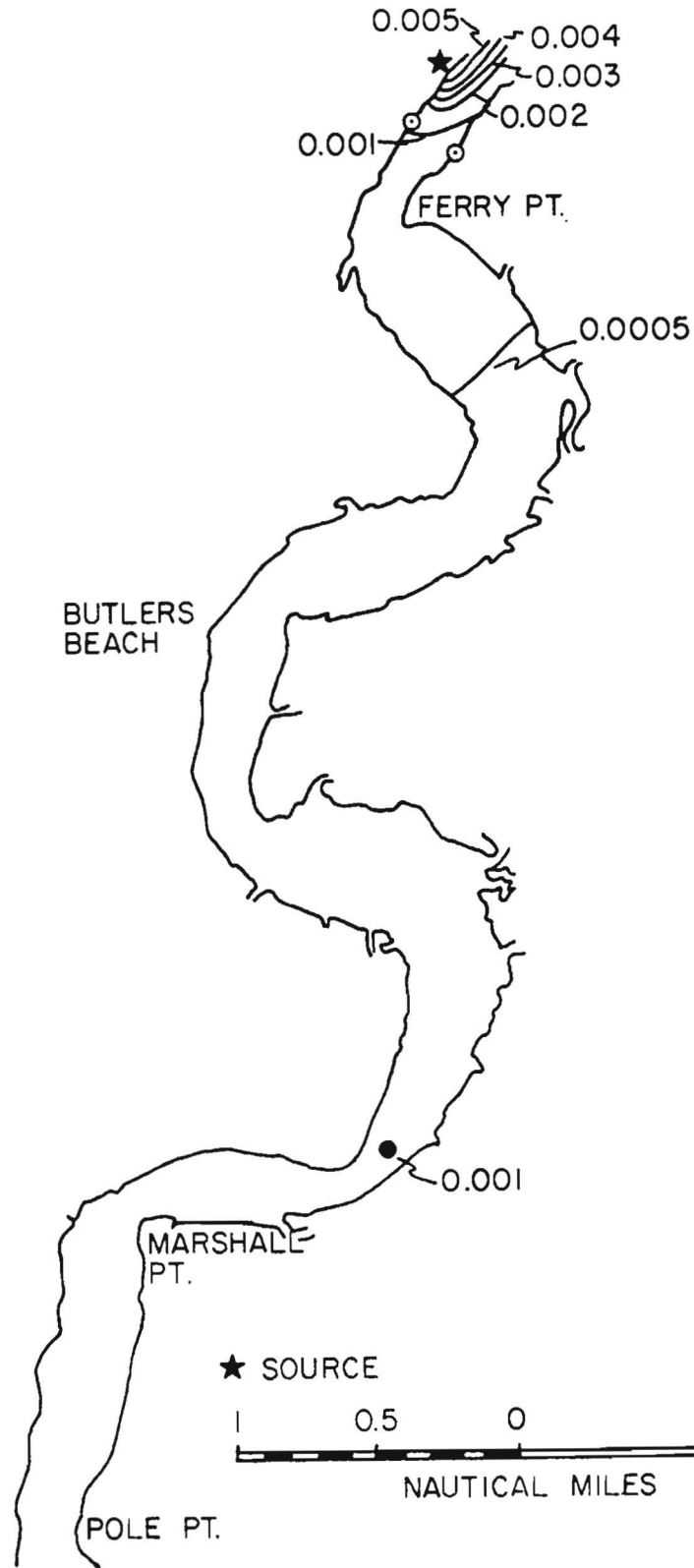


Figure 62. Distribution of relative concentration for a 600 MW plant, near slack before eff, during low river flow, downstream from the source.

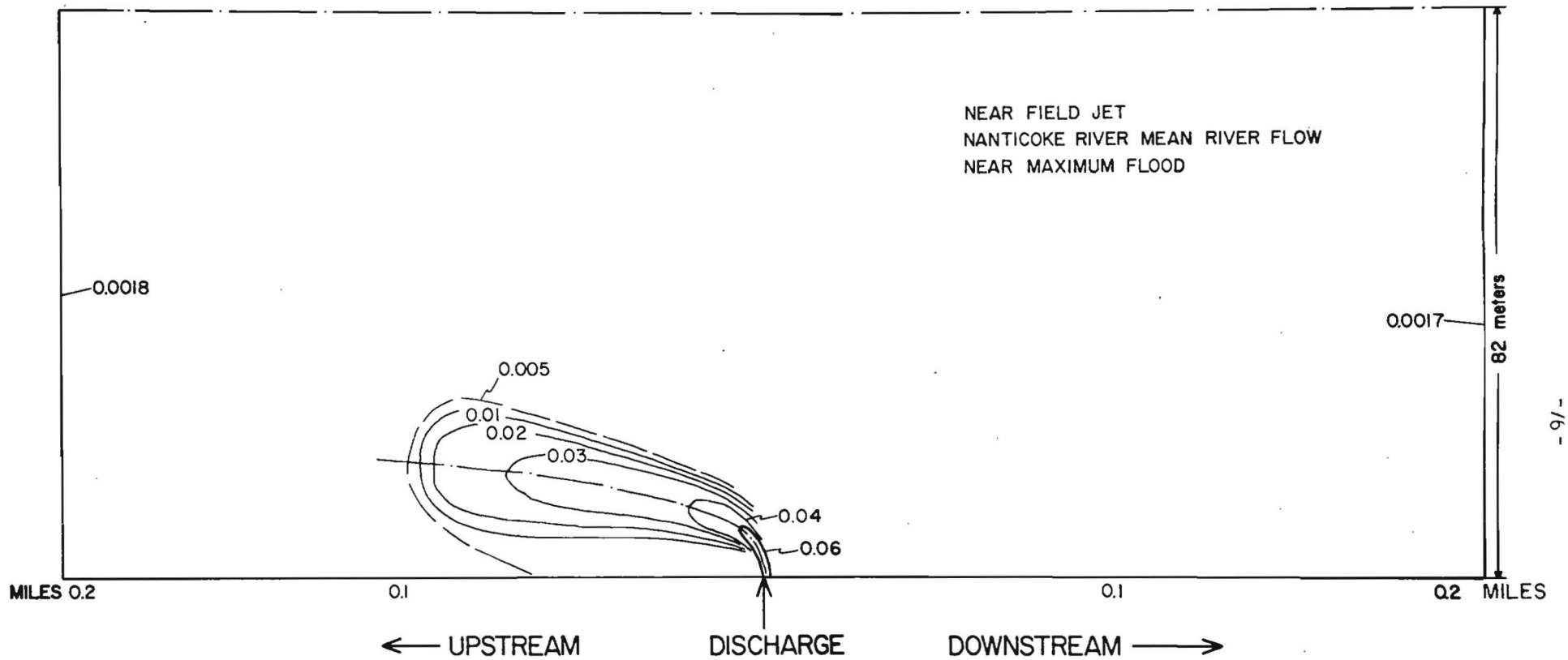


Figure 63. Isolines of relative concentration in the near field plume for a 600 MW plant for mean river flow, for near maximum flood tidal flow.

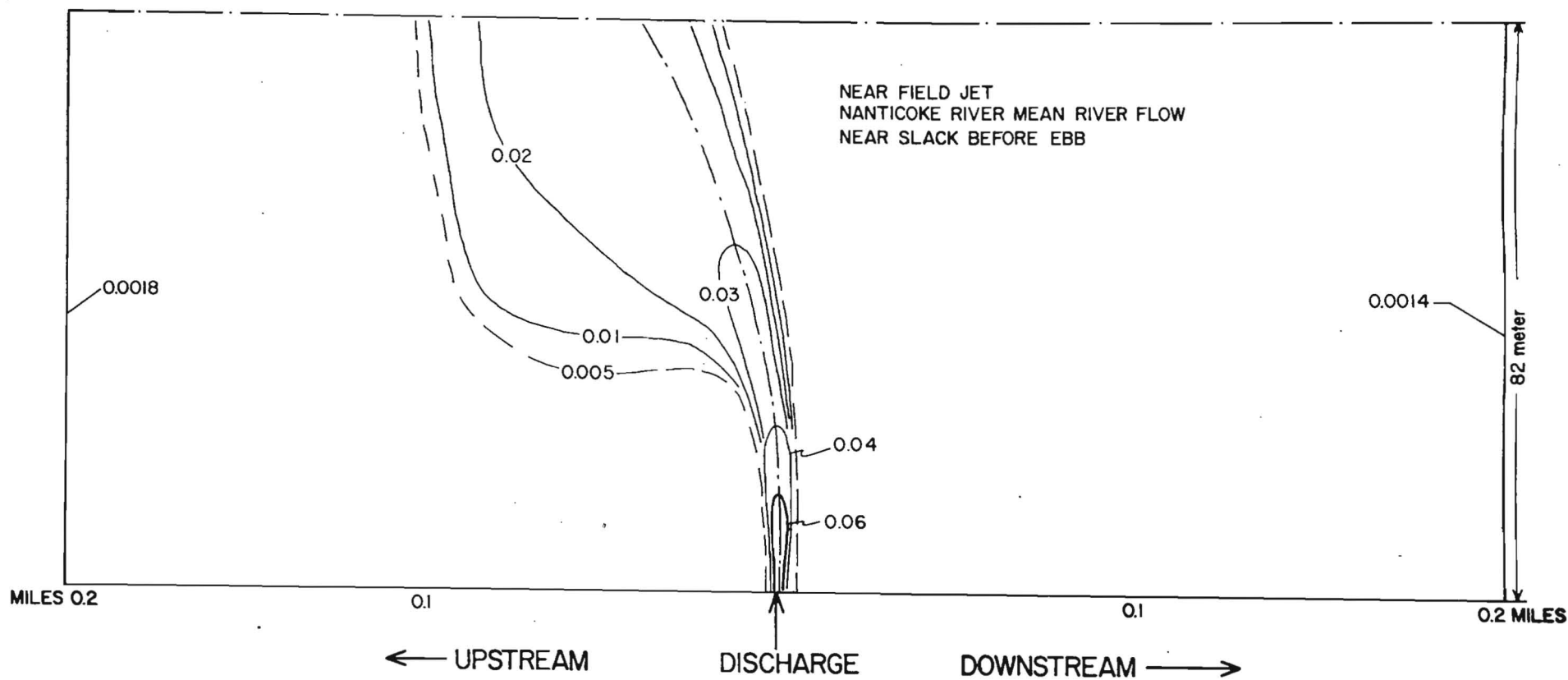


Figure 64. Isolines of relative concentration in the near field plume for a 600 MW plant for mean river flow, for near slack before ebb.

The length, width and area enclosed by specified values of relative concentration, or inverse dilution have been determined from the contours shown in Figure 7 and Figure 63, and are given in Table 1. Values of excess temperature (rounded to the nearest tenth of a degree) corresponding to these values of inverse dilution, for the case of an excess temperature at discharge of 34°F, are also listed in the table. The tabulation is made only for the flood tide data and not for the near slack data because: (1) the slack case represents an event of very short duration during the tidal cycle; and (2) for inverse dilutions greater than 0.03, the flood tide case gives larger areas than does the slack tide case. This statement may appear to be contrary to the impression given by visual comparison of Figure 7 with Figure 8, or of Figure 63 with Figure 64. However, the distortion of the lateral scale in comparison with the horizontal scale also tends to distort one's visual impression of these figures. Note that the values of the dimensions and areas as given in this table depend on contours of inverse dilution drawn from data plotted at grid points on a rectilinear grid. The distance between grid points in the longitudinal direction is 14.83 meters, and in the lateral direction, 4.1 meters. Because of this fact the longitudinal dimensions of the plume as listed are uncertain by about  $\pm 3$  meters, and the lateral dimensions by about  $\pm 1$  meter. Keeping these figures in mind, we note that:

(a) The size of the area enclosed within the 0.06 relative concentration isoline (2.0°F isotherm of excess temperature) is larger

Table 1

Dimensions and Areas contained Within Isolines of Various Concentration and Excess Temperature values in the Nanticoke River at the Time of Maximum Flood Flow, for Combined Discharges from Existing Unit 8 and Proposed Unit 9, Wintertime Conditions.

A. FOR UNIT 9 OF 400 MWE

1/Dilution (c/Co)	Excess Temp. (°F)	Length (m)	Width (m)	Area (m <sup>2</sup> )	Area (ft <sup>2</sup> )	Area (Acres)
0.06	2.0	19	3	46	491	0.011
0.04	1.4	110	4	352	3787	0.087
0.03	1.0	177	7	991	10664	0.245
0.02	0.7	186	14	2083	22412	0.515
0.01	0.3	204	17	2774	29848	0.685
0.005	0.2	236	20	3776	40624	0.933

B. FOR UNIT 9 OF 600 MWE

1/Dilution (c/Co)	Excess Temp. (°F)	Length (m)	Width (m)	Area (m <sup>2</sup> )	Area (ft <sup>2</sup> )	Area (Acres)
0.06	2.0	23	5	92	990	0.023
0.04	1.4	64	6	307	3305	0.076
0.03	1.0	157	8	1005	10810	0.248
0.02	0.7	191	15	2292	24658	0.566
0.01	0.3	197	20	3152	33910	0.778
0.005	0.2	206	25	4120	44325	1.018

for the 600 MW case than for the 400 MW case. Though the difference in the lengths and widths of the area enclosed by this isotherm are only marginally greater than the values of uncertainty in measurement from the contoured charts as given above, such an enlargement is consistent with the fact that the larger momentum will result in a larger zone of flow establishment, an initial reach of the discharge jet within which no centerline dilutions occur.

(b) The individual lengths and widths of the areas contained within the specified inverse dilution values in the range between 0.04 and 0.005 differ between the two cases, with the length for the 400 MWE case being slightly larger than in the 600 MWE case, while the difference in widths is in the opposite direction. However, the difference in the areas between the two cases as given in Table 1 for this range of values of inverse dilution is not significant. This is because, due to the fact that the area of the discharge orifice was kept constant, the larger discharge velocity for the 600 MWE case resulted in an increase in entrainment and hence relative dilution which just balanced the increase in source strength for this range of inverse dilutions. It should not be concluded that *in general* the size of the plume would remain constant with an increase in source strength by merely keeping the size of the discharge orifice constant. This particular situation resulted from a unique combination of input parameters.

(c) While not evident from the contours given in these figures of the near field distribution, the size of the areas contained

within isolines of inverse dilution for values of this parameter less than 0.005 for the 600 MWE case become steadily larger (as the values of inverse dilution decrease) in comparison to the 400 MWE case, until the full effect of the larger source strength is felt. This feature is evident in the diagrams for the far field.

#### THE EFFECTS OF VARYING PLANT DESIGN SPECIFICATIONS

As pointed out earlier, the computations presented in detail in this part of this report are based in part on the assumption that the blowdown water from Unit 8 and from Unit 9 are combined into a single discharge. Also, the input to the model included the assumption that the diameter of the pipe to be used for this single discharge would be 8 inches (0.67 feet). The Delmarva Power Company now propose to release the blowdown water from Unit 9 through a pipeline having a diameter at the point of discharge of 10 inches (0.83 ft).

As mentioned earlier, computational difficulties preclude the computation of the distribution in space and time of two interacting plumes. If the two discharges are far enough apart so that no interaction occurs, computations may be carried out, and if the two discharges are sufficiently close together so that they can be considered as a single discharge, then computations may also be made. At intermediate separations the two plumes interact hydrodynamically. Such interaction results in a loss of some excess momentum from both plumes which is then not available to drive the entrainment mechanism. Even if no hydraulic interaction occurs, mixed water, with some



concentration of contaminant or excess heat, from one plume may be entrained into the other. This process is equivalent to re-entrainment of partially contaminated water in a single plume. Re-entrainment is probably the most significant factor with regard to the failure of some thermal discharges to produce plumes having areas within specified isolines of concentration or excess heat as small as had been predicted.

If the discharge structures are separated sufficiently so that during the period of ebb flow the lower reaches of the plume with an upstream source do not encroach on the upstream end of the downstream plume, and, *vica versa* for flood flow, then there is some advantage to separation of the two discharges. However, the discharge velocity in each of the separate discharges should be kept at least as high as would occur for the combined discharge. In any case, the far field distribution will not be significantly affected whether or not, within the limits of the station property, the discharges are separated or are combined.

Computations have been made for the purpose of comparing the size of the areas within specified isolines of inverse dilution for the plume from the blowdown discharge for Unit 9, for a discharge orifice diameter of 10 inches and of 8 inches. For inverse dilutions less than 0.05, corresponding to an excess temperature for the wintertime case of 1.7°F, our calculations show no effect of this difference in discharge pipe size. However, for relative concentrations greater than 0.05 the computed areas for the larger pipe diameter were

significantly larger than for the smaller pipe diameter. For example, the area contained within the 0.06 isoline of relative concentration, which corresponds in winter to the 2.0°F excess temperature is calculated to be 3.7 times larger in the case of discharge from a 10 inch diameter pipeline than in the case of discharge from an 8 inch diameter pipeline. Note, however, that the plume size as defined by this isoline is still only a fraction of an acre in area.

#### MODEL VERIFICATION

In order to assess the validity of our predicted far field distributions of relative concentration we have made comparisons of computed distributions with the observed distributions of relative concentration from the dye tracer experiment conducted by Carter and Regier (1975) (Chesapeake Bay Institute Technical Report 90). This experiment was conducted with the specific objective of delineating the field of excess temperature resulting from the cooling water discharge of the Delmarva Power and Light Company Vienna, Maryland generating station into the Nanticoke River.

We have compared the observed time histories of relative dye concentration with time histories predicted by our simple model for a total of four separate model runs. We made three separate runs corresponding to low river flow, mean river flow and high river flow conditions. The model parameters used in these simulations were the same as those used in the simulations represented in Figures 9 through 32 and 39 through 64 with the exception of the source strength. For the

fourth simulation we altered both the diffusion velocity and the tidal current amplitude from values used earlier to better represent the dye data. All parameters used in the simulations are discussed below.

In all of the simulations discussed here we used a source strength which represented the actual volume rate of discharge of cooling water from the Vienna generating station into the Nanticoke River at the time the dye tracer experiment was conducted. The design operating parameters for the Vienna generating station at the time of the dye tracer experiment are discussed by Carter and Regier (1975). The total condenser cooling water flow for units #5, 6, 7 and 8 is approximately  $7.6 \text{ m}^3 \text{ s}^{-1}$ . This is the volume rate of discharge which we used as a source term for all simulations which were compared with dye data. It should be noted, however, that Carter and Regier (1975) mentioned that there were brief periods during the dye tracer experiment when pumps for units #5 and 7 were turned off and that only infrequently were units #5, 6, and 7 operating at rated capacity.

Figures 65 through 67 show simulated time histories for relative concentration corresponding to low river flow conditions (445 cfs). For this river flow a mean velocity of  $.838 \text{ cms}^{-1}$  was used; the diffusion velocity and tidal current amplitude used were, respectively,  $1.5 \text{ cms}^{-1}$  and  $55 \text{ cms}^{-1}$ . These values for mean velocity, diffusion velocity and tidal current amplitude are consistent with values used for the previous simulations. Figures 65 through 67

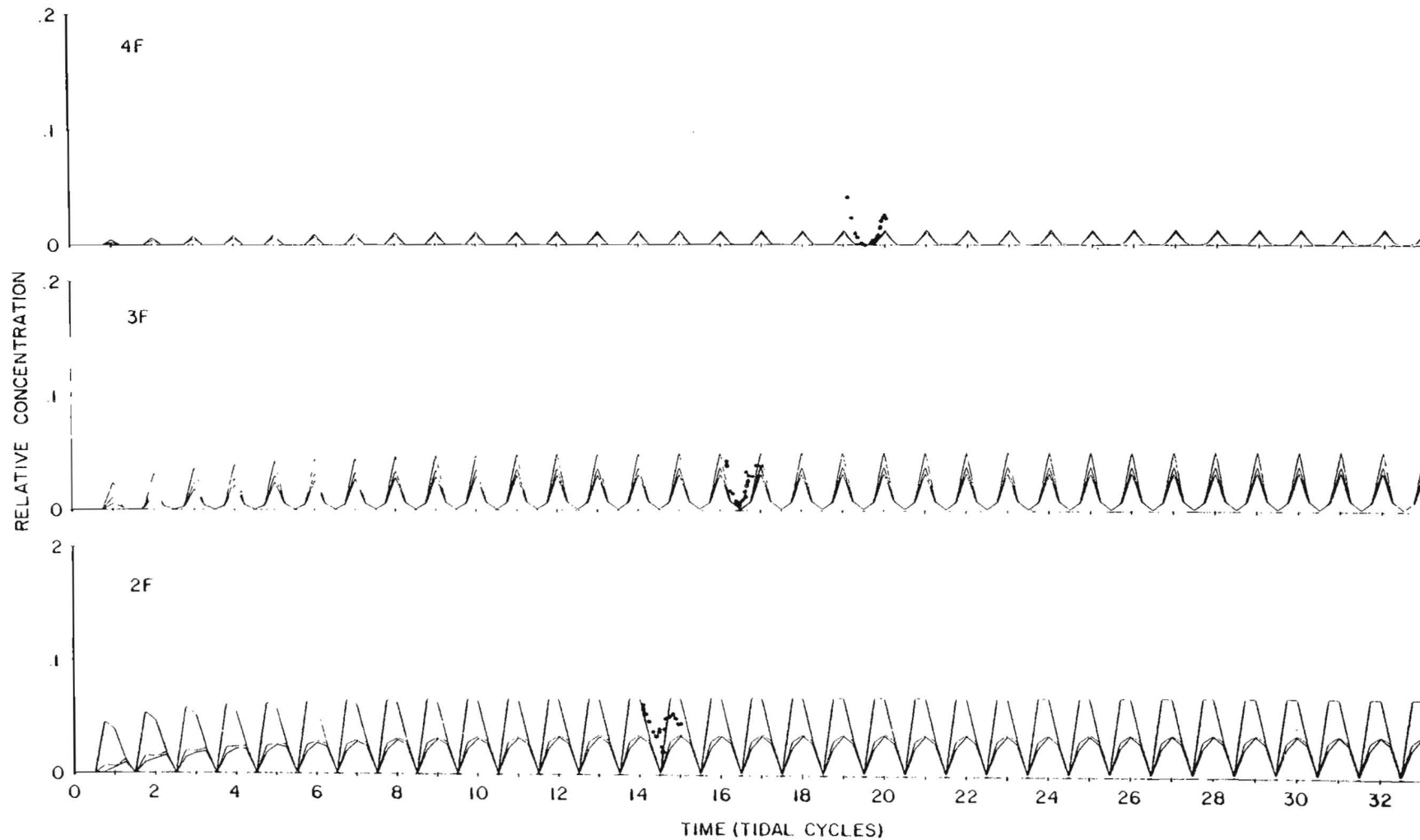


Figure 65. A comparison of observed time histories of relative dye concentration (solid circles) with simulated time histories at sections 4F, 3F, 2F for low river flow conditions (445 cfs) and for a diffusion velocity of  $1.5 \text{ cm s}^{-1}$  and tidal current amplitude of  $55 \text{ cm s}^{-1}$  (see text).

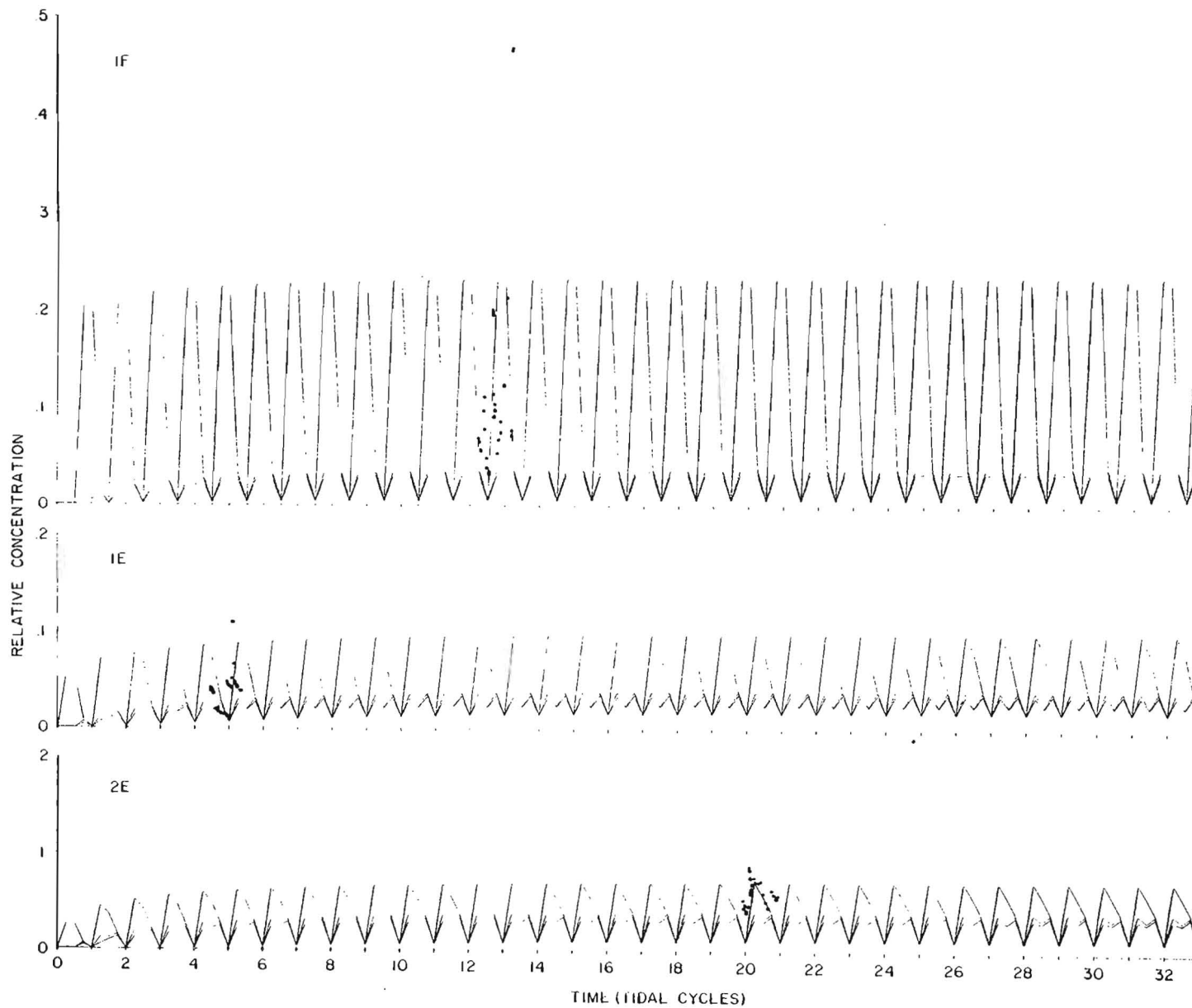


Figure 66. A comparison of observed time histories of relative dye concentration (solid circles) with simulated time histories at sections IF, IE and 2E. (See caption for Figure 65).

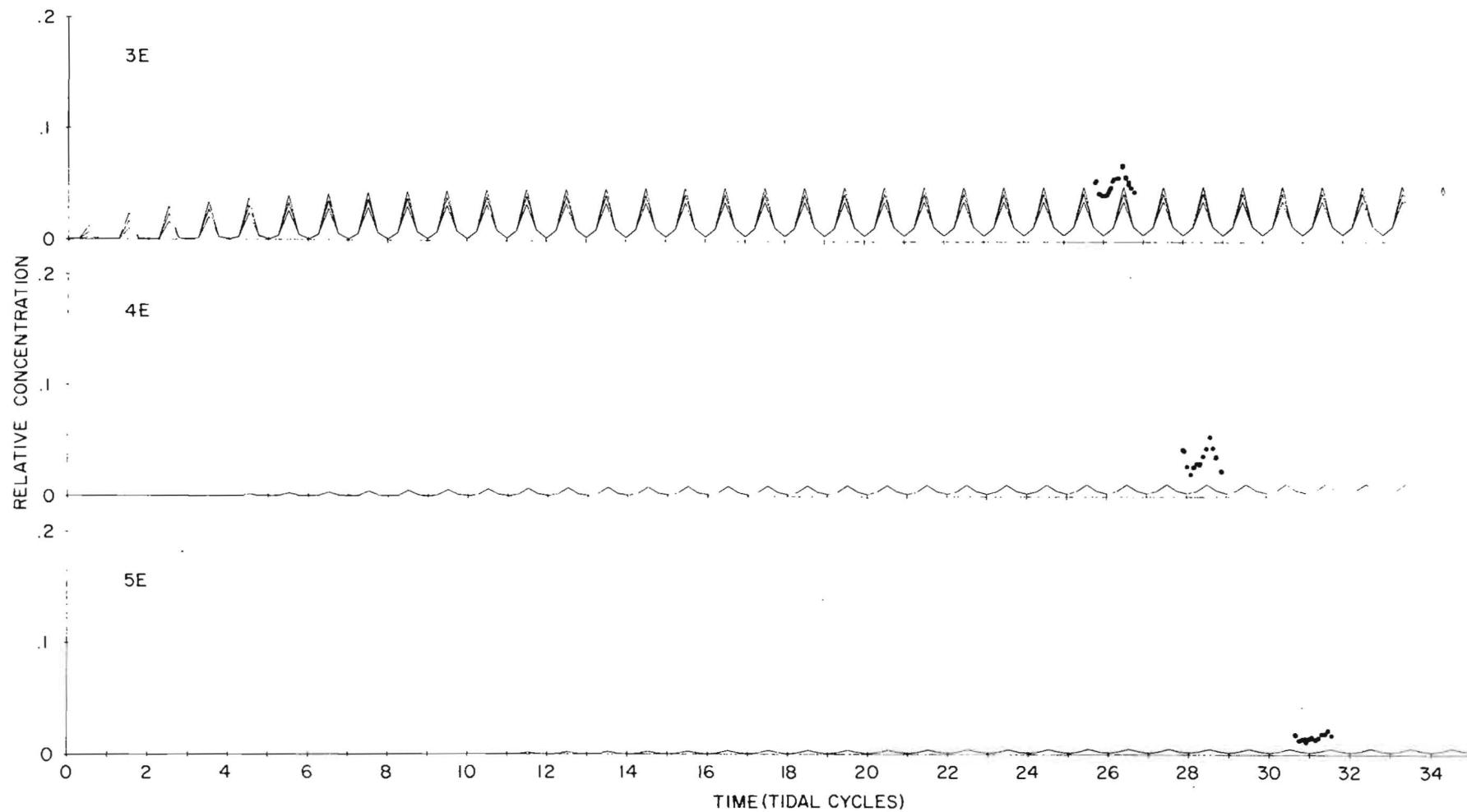


Figure 67. A comparison of observed time histories of relative dye concentration (solid circles) with simulated time histories at sections 3E, 4E and 5F. (See caption for Figure 65).

show simulated time histories for 35 tidal cycles following the initiation of a continuous release at a total of 9 separate sections at different longitudinal positions from the source. The length of the simulations was determined by the length of the dye tracer experiment; dye was dispensed from 1828 on 9 April until 1310 on 26 April. The longitudinal positions at which simulations were performed were fixed to correspond to the positions of the lateral sections at which repetitive sampling was performed during the tracer experiment. We have reproduced Table 2 from Carter and Regier below which provides section designations, distances from the source and the dates of sampling.

Table 2  
(From Carter and Regier, 1975)

Distances from the Source of the Various Sampling Sections  
Together with Sampling Dates.

	Section	Miles/km from Source	Date of Sampling
upstream	4F	4.2/7.78	April 19
	3F	2.1/4.08	18
	2F	1.2/2.22	17
	1F	0.2/0.37	16
	Plant	0	
downstream	1E	0.7/ 1.30	12, 26
	2E	1.5/ 2.78	20
	3E	3.3/ 6.11	23
	4E	5.8/10.75	24
	5E	8.0/14.82	25

At each of the 9 sections in Figures 65 through 67 we have presented the predicted time history for a point on the near shore,

for a point in the center of the river and for a point on the far shore for 35 tidal cycles. We have presented the approximately one tidal cycle of dye data at each section taken from the figures in the above referenced report by Carter and Regier of scaled excess temperature as a function of time. The values in these figures represent the peak value in the section which in almost every instance occurred on the nearshore bank. These scaled excess temperatures at each section were converted to relative concentration by dividing by  $12.0^{\circ}\text{C}$  during the flood part of the tidal cycle and by  $14.4^{\circ}\text{C}$  during ebb (see Carter and Regier).

Figures 65 through 67 show that there is reasonably good agreement between predicted and observed relative concentrations at most of the sections. The agreement is best at sections near the source. The agreement is poor at section 4F far upstream; agreement is not good at sections 4E and 5E which are the two sections furthest downstream.

Figures 68 through 70 provide a comparison between predictions for mean river flow conditions (810 cfs) and the same dye data presented in Figures 65 through 67. For this river discharge we used a mean velocity in our simulations of  $1.525 \text{ cms}^{-1}$ ; the diffusion velocity and tidal current amplitude were kept at  $1.5 \text{ cms}^{-1}$  and  $55 \text{ cms}^{-1}$ , respectively. For mean river flow conditions the simulations show a reduction in concentration at the upstream section 4F, a slight increase in concentrations at the downstream sections 4E and 5E and little change at the other sections from the simulations for low flow.



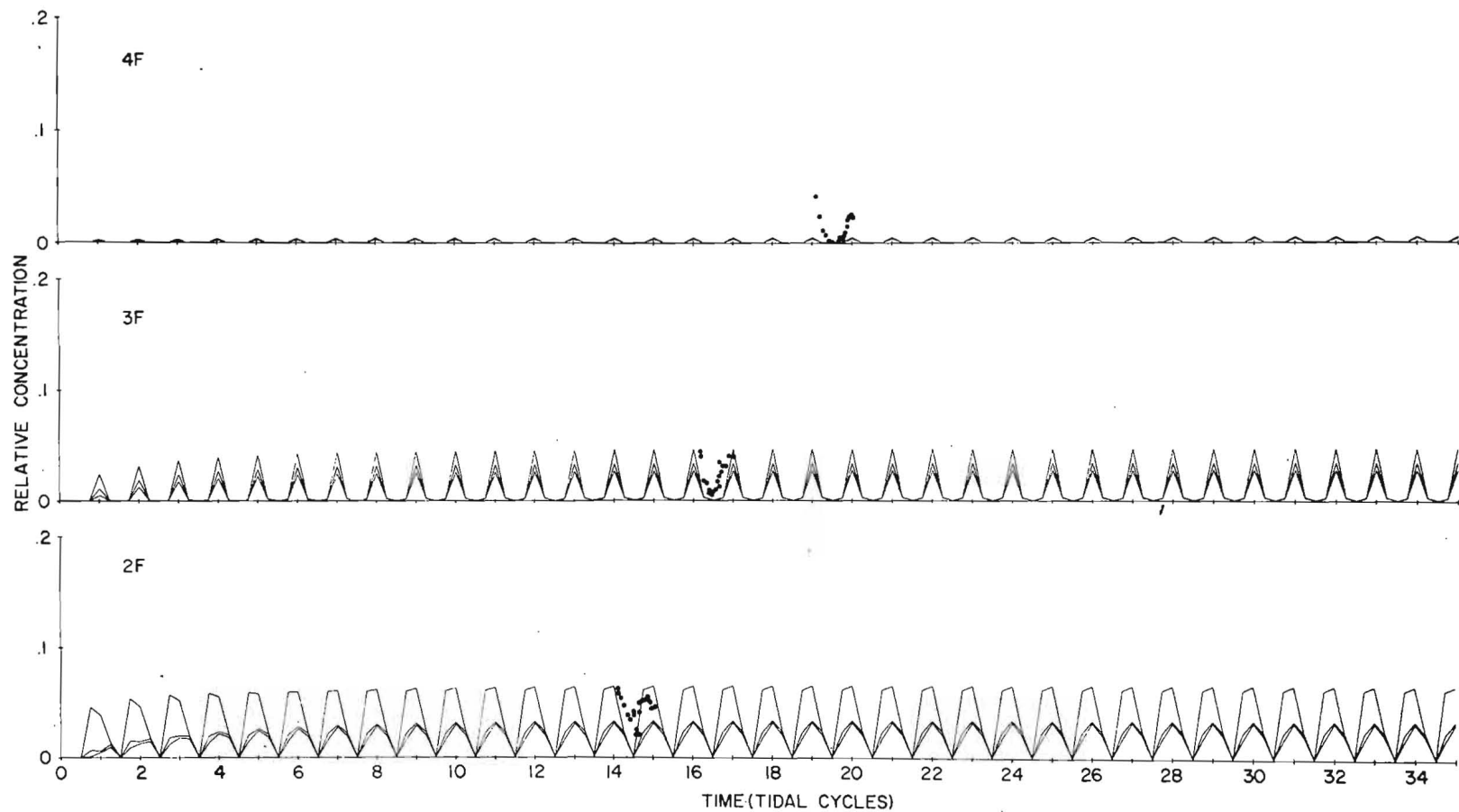


Figure 68. A comparison of observed time histories of relative dye concentration (solid circles) with simulated time histories at sections 4F, 3F, 2F for mean river flow conditions (810 cfs) and for a diffusion velocity of  $1.5 \text{ cm s}^{-1}$  and tidal current amplitude of  $55 \text{ cm s}^{-1}$  (see text).

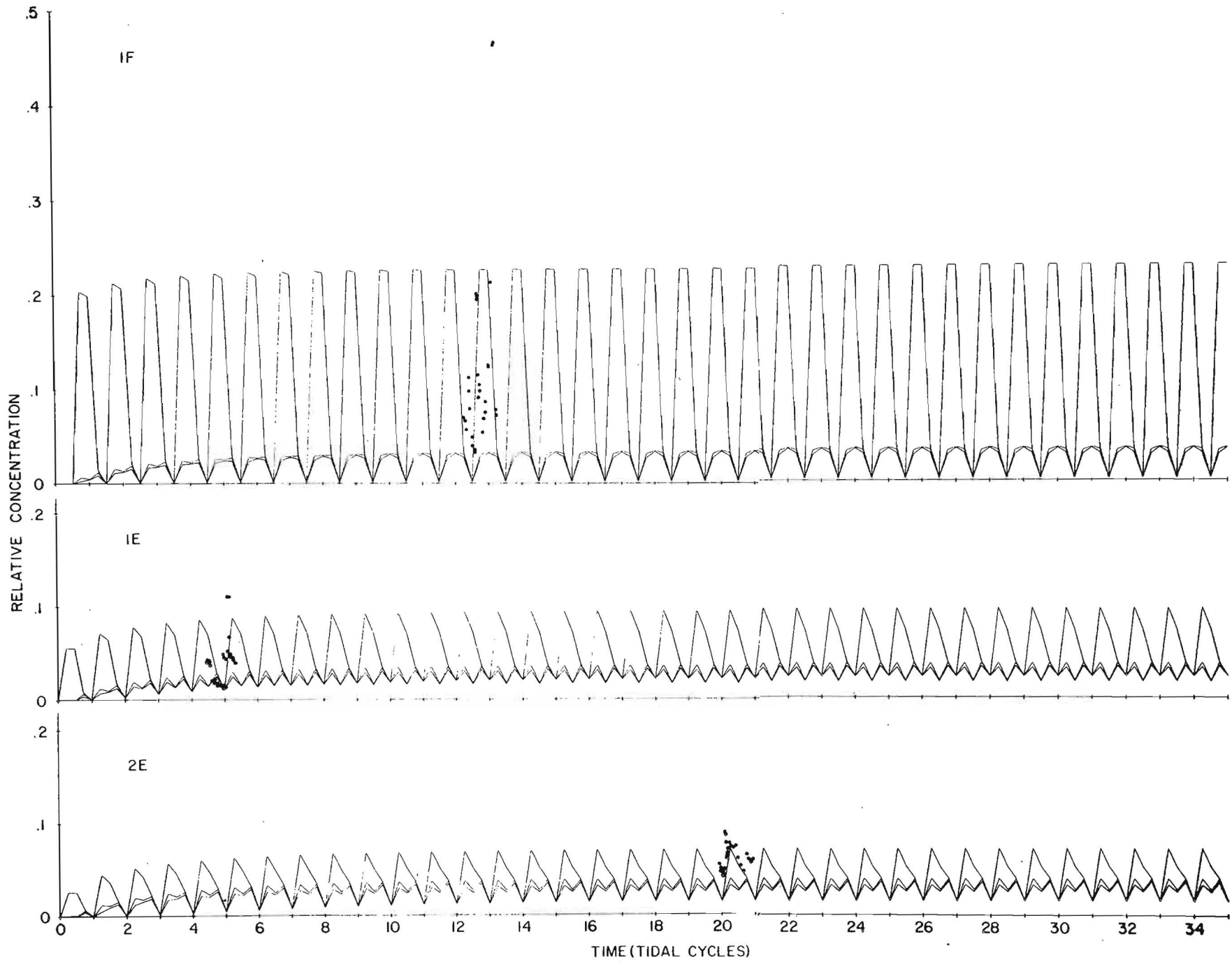


Figure 69. A comparison of observed time histories of relative dye concentration (solid circles) with simulated time histories at sections IF, IE and 2E. (See caption for Figure 68).

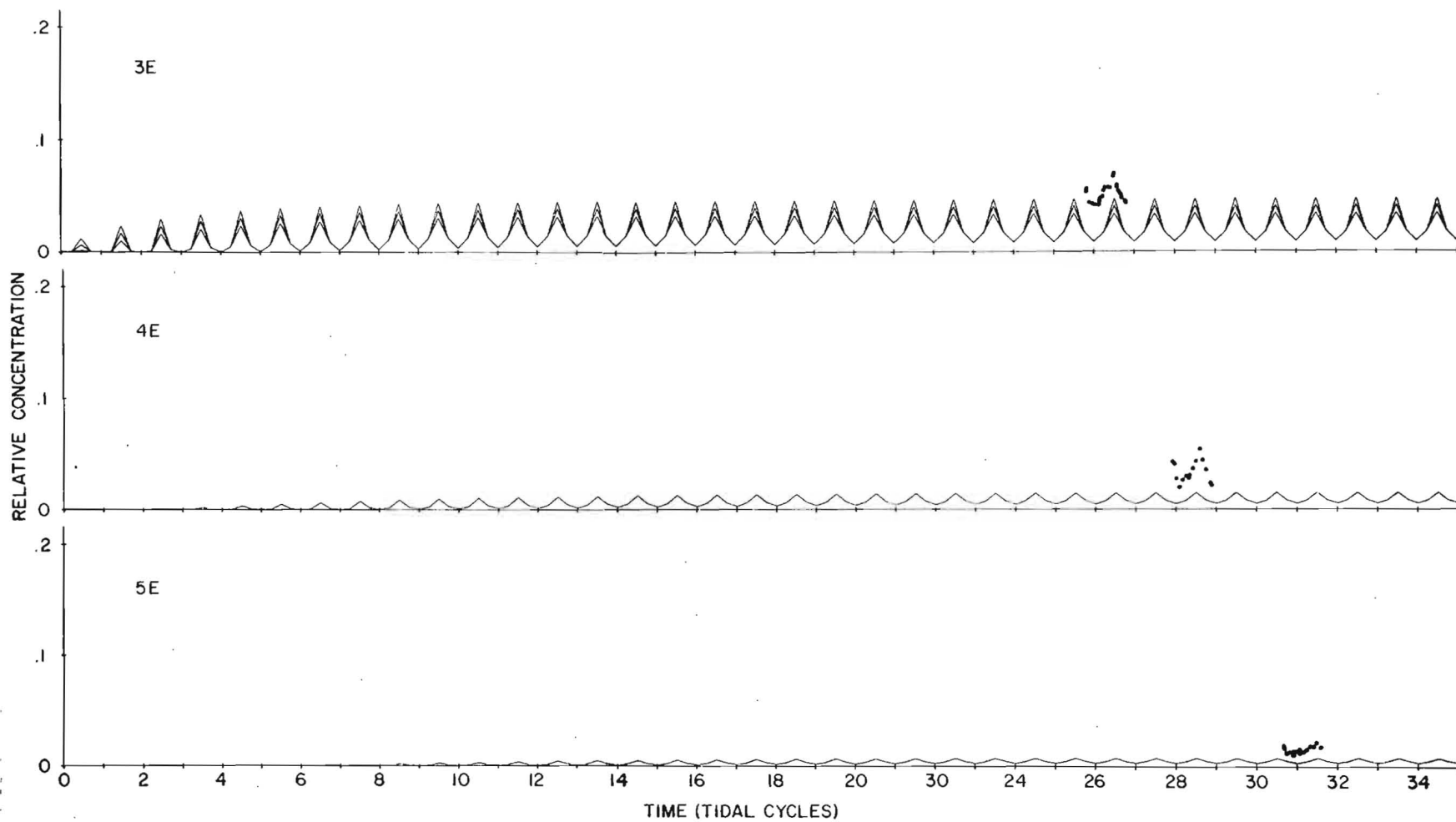


Figure 70. A comparison of observed time histories of relative dye concentration (solid circles) with simulated time histories at sections 3E, 4E and 5F. (See caption for Figure 68).

Overall, with the exception of section 4F, the agreement with the dye data is somewhat improved.

Figures 71 through 73 provide comparisons between predictions for high river flow conditions (1520 cfs) and the dye data. For these simulations we used a mean velocity of  $2.862 \text{ cms}^{-1}$  and the same diffusion velocity and tidal current amplitude used earlier. The simulations show a further reduction in concentrations at section 4F and a slight increase in concentrations at sections 4E and 5E. Simulations for high river flow show, however, that concentrations at sections closer to the source are reduced with this increased mean velocity.

In Figures 74 through 76 simulations for high river flow conditions are shown, but with a reduced diffusion velocity ( $1.0 \text{ cms}^{-1}$ ). The agreement between the predictions and the dye data is improved at all sections except 4F for this reduced diffusion velocity. It should be noted that the amplitude of the tidal current was also reduced from 55 to  $40 \text{ cms}^{-1}$  in an attempt to be more consistent with the current meter observations made off the Vienna generating station by Carter and Regier during the dye tracer experiment. The appropriate tidal current amplitude is uncertain; this should not, however, be of major concern because the predictions are relatively insensitive to changes in the tidal current amplitude. Of more concern are low frequency fluctuations in the mean or nontidal current caused by meteorological forcing. It is clear that the only mechanism by which significantly quantities of dye could have reached upstream to section 4F

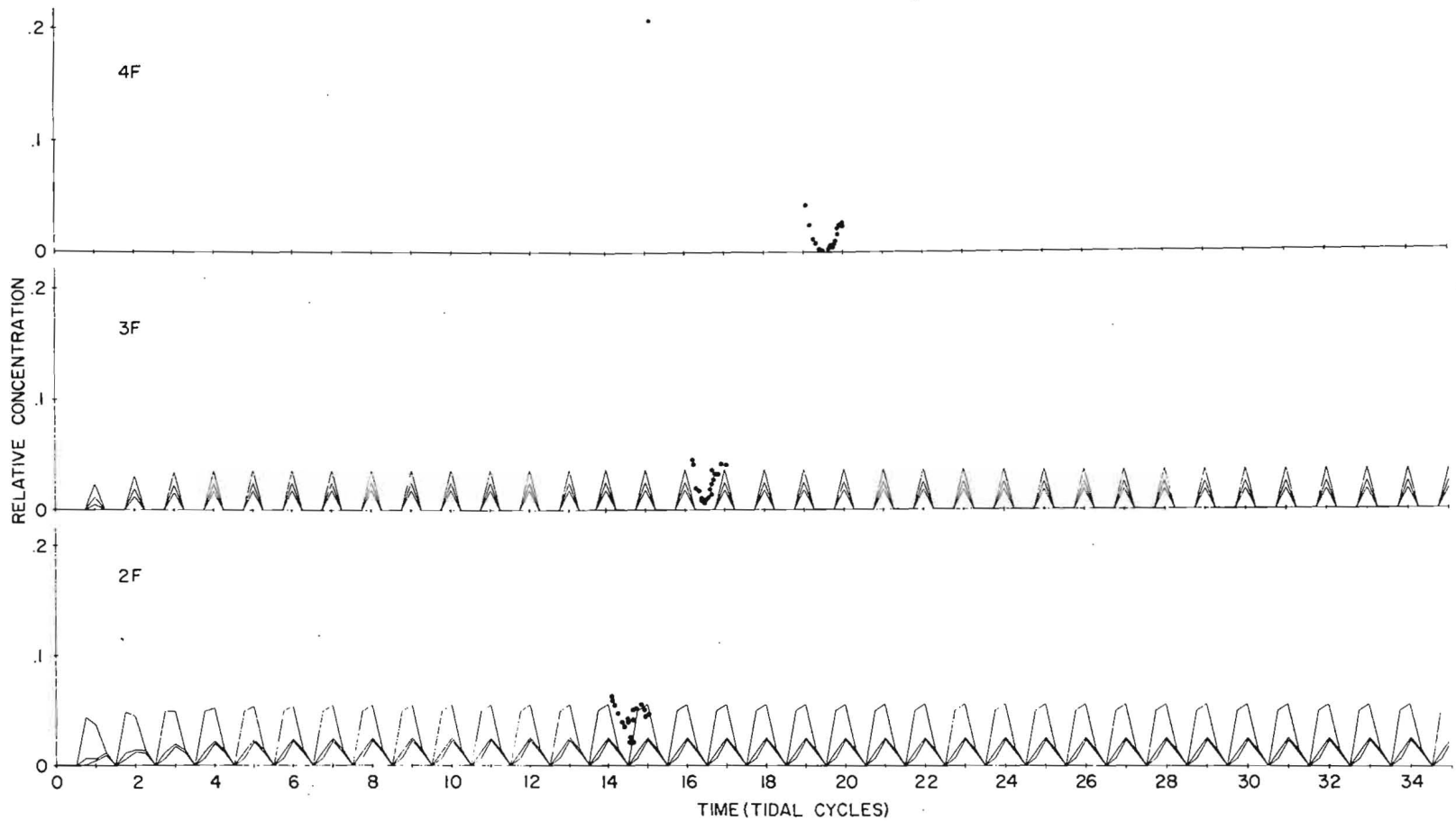


Figure 71. A comparison of observed time histories of relative dye concentration (solid circles) with simulated time histories at sections 4F, 3F, 2F for high river flow ( $1520 \text{ cfs}$ ) and for a diffusion velocity of  $1.5 \text{ cm s}^{-1}$  and tidal current amplitude of  $55 \text{ cm s}^{-1}$  (see text).

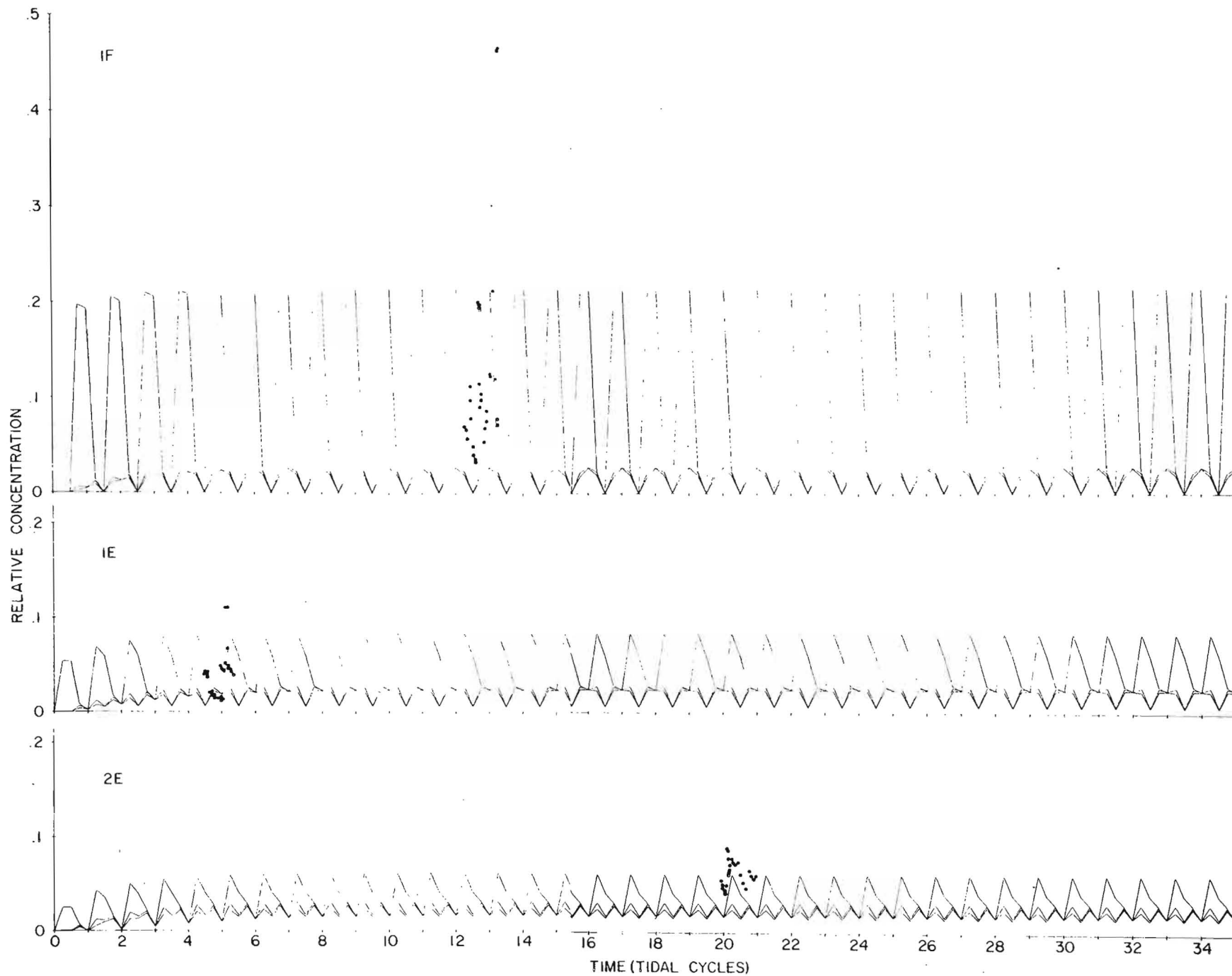


Figure 72. A comparison of observed time histories of relative dye concentration (solid circles) with simulated time histories at sections 1F, 1E and 2E. (See caption for Figure 71).

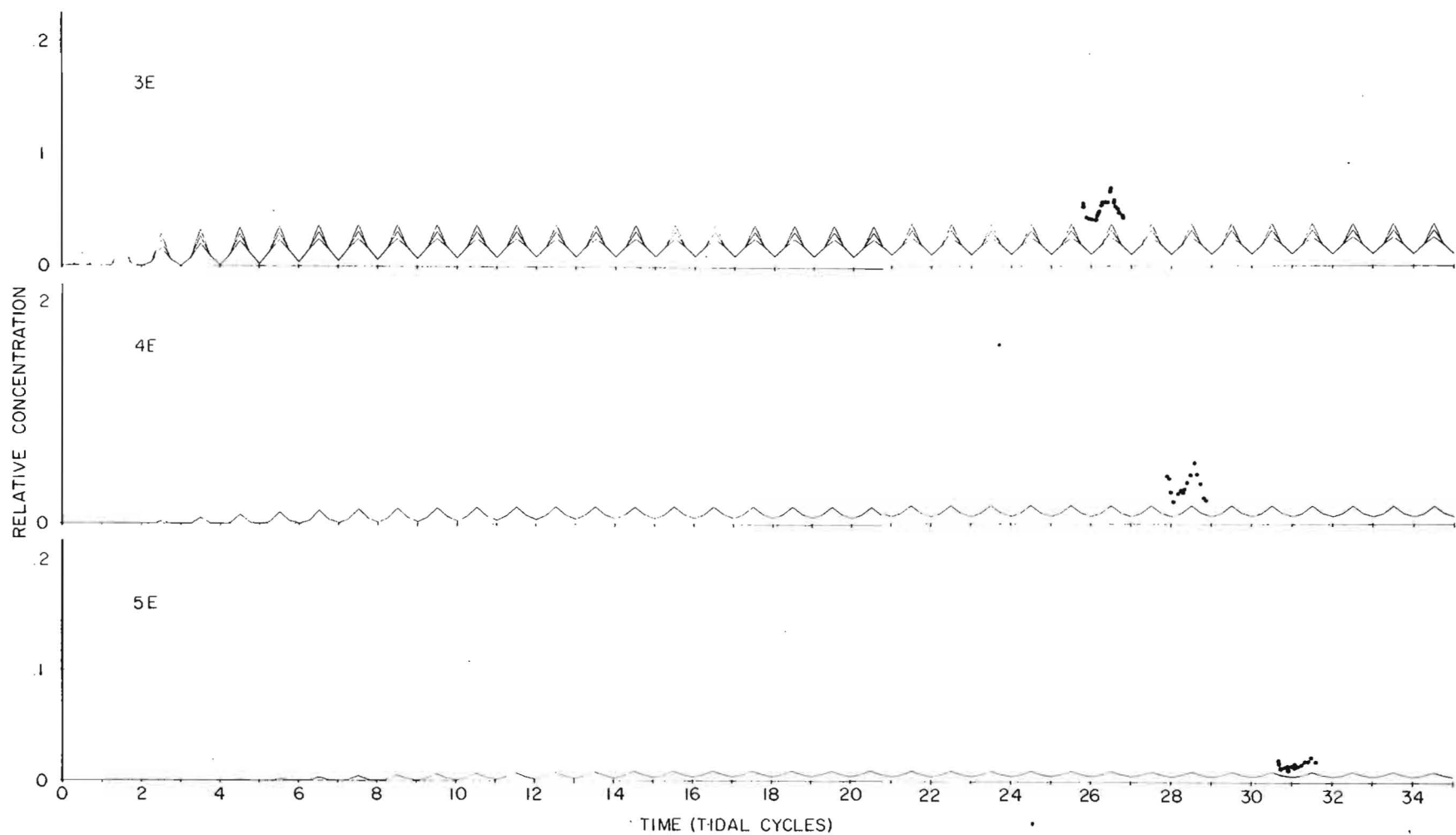


Figure 73. A comparison of observed time histories of relative dye concentration (solid circles) with simulated time histories at sections 3E, 4E and 5F. (See caption for Figure 71).

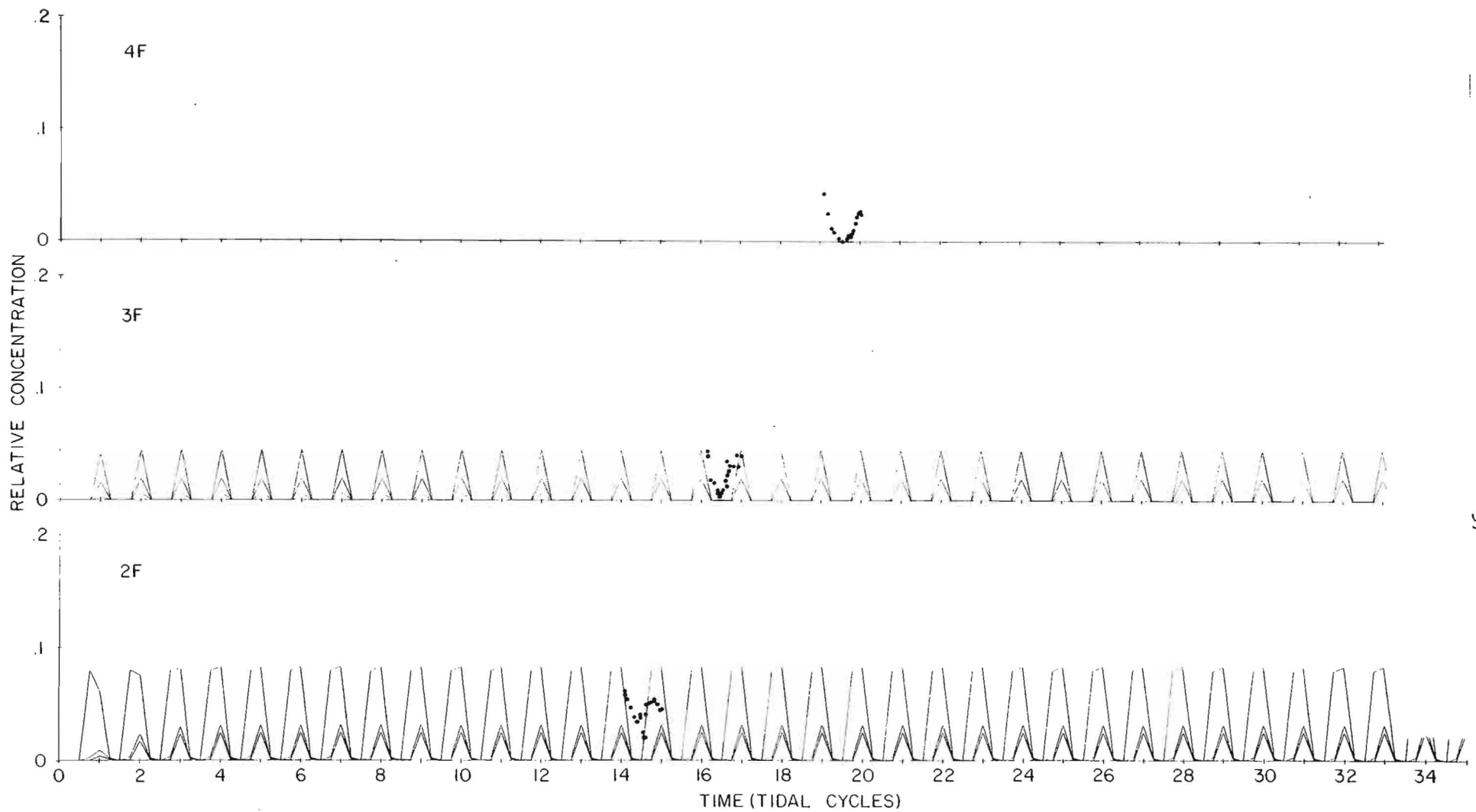


Figure 74. A comparison of observed time histories of relative dye concentration (solid circles) with simulated time histories at sections 4F, 3F, 2F for high river flow conditions (1520 cfs) and for a diffusion velocity of  $1 \text{ cm s}^{-1}$  and a tidal current amplitude of  $40 \text{ cm s}^{-1}$  (see text).



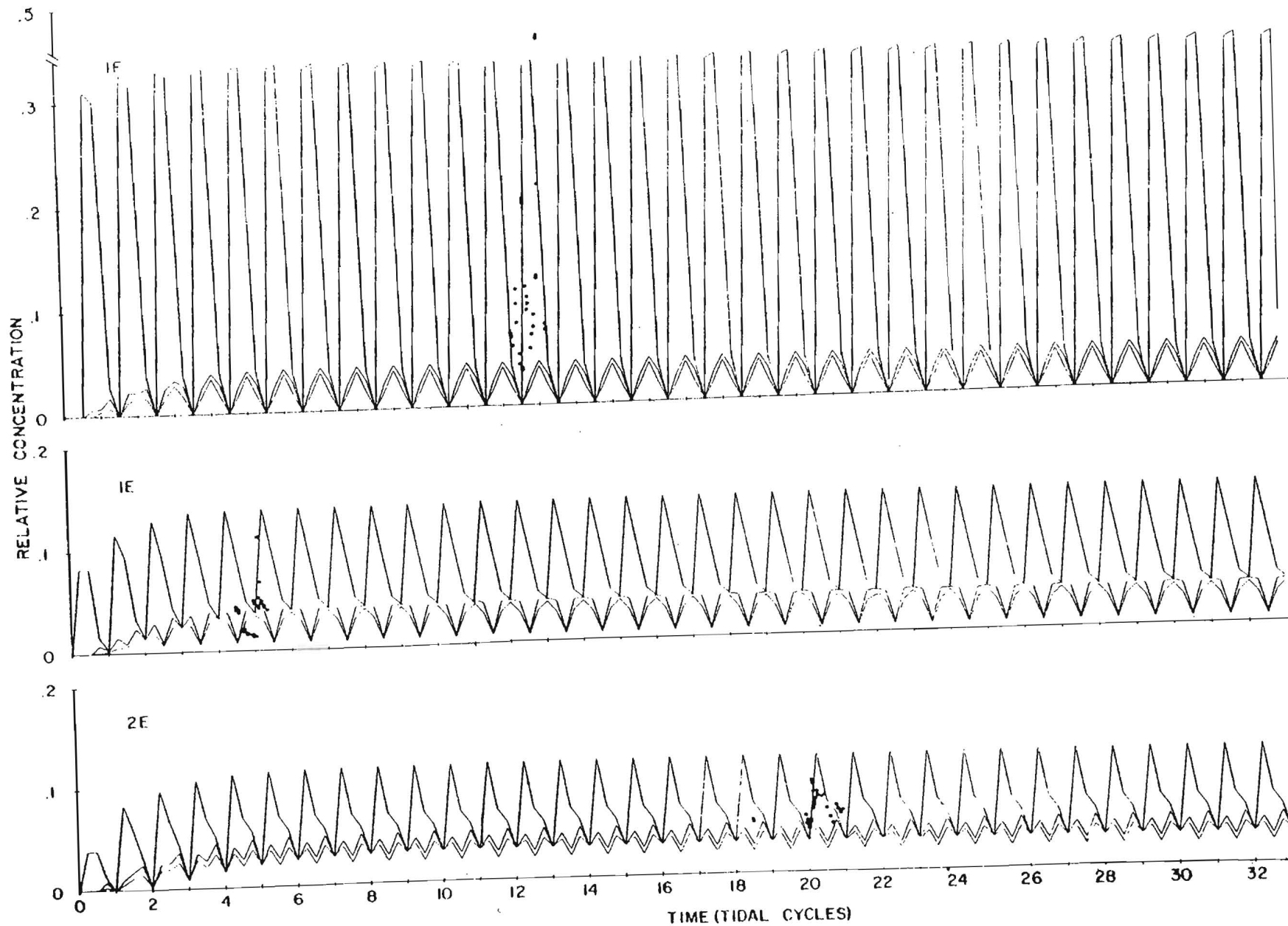


Figure 75. A comparison of observed time histories of relative dye concentration (solid circles) with simulated time histories at section 1F, 1E and 2E (see caption for Figure 74).

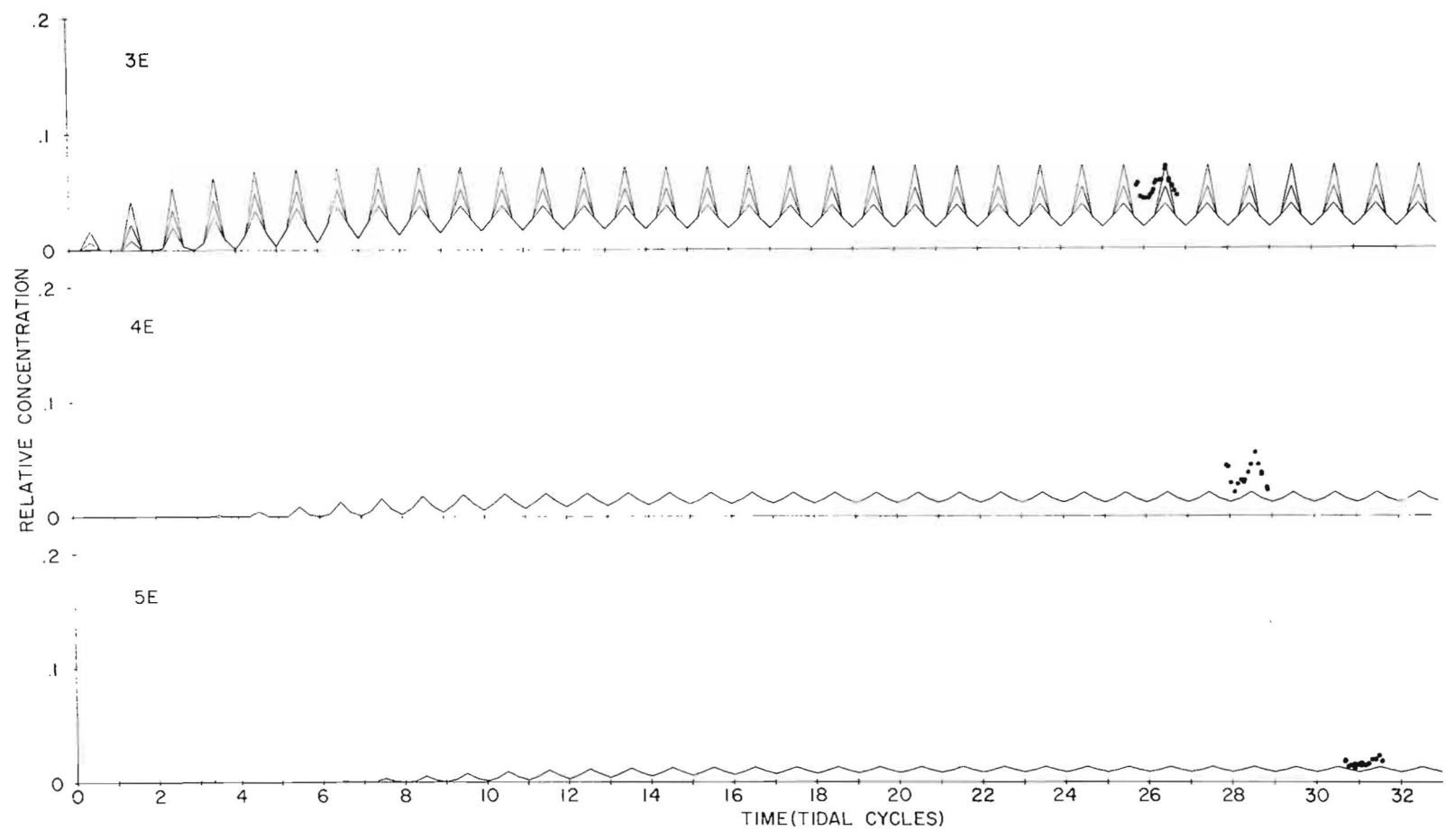


Figure 76. A comparison of observed time histories of relative dye concentration (solid circles) with simulated time histories at sections 3E, 4E, and 5E (see caption for Figure 74).

is for there to have been a prolonged period for which the mean flow was directed upstream. There is in fact some evidence that this did happen during the dye tracer experiment from the current meter records.

We conclude then that our simple kinematic model for diffusion from a continuous source is capable of representing the major features of the observed distribution of relative concentration determined from the dye tracer experiment. Best agreement was obtained for a diffusion velocity of the order  $1 \text{ cm s}^{-1}$  and for a mean velocity of the order  $2.86 \text{ cm s}^{-1}$  characteristic of high river flow conditions. Improved simulations would require information on the low frequency variations in the mean (subtidal) flow. We do not at this time have data from which the actual river flow for April 1974 at Vienna can be determined. However, it should be noted that the month of April falls within the normal spring period of high flow for rivers entering the Chesapeake Bay. Also, though the best agreement occurred for a diffusion velocity of  $1.0 \text{ cm/sec}$ , the difference between the runs using this value and those using a value of  $1.5 \text{ cm/sec}$  were not so great as to suggest negation of our earlier computations of the plume from the proposed Unit 9.

Part II

Computations of the Distribution of Contaminants  
Introduced into Chicone Creek in Groundwater

INTRODUCTION

Chicone Creek is a relatively small tidal waterway tributary to the Nanticoke, extending northerly from the river only a short distance west northwest of the site of the Vienna Electric Generating Station. The West Branch of Chicone Creek runs adjacent to the eastern and northeastern boundaries of the proposed waste disposal site for the power plant. This site is to receive the combined stack scrubber waste and the fly ash from the power station. In this part of this report, the possible fate of any contaminant from the disposal site which might enter the groundwater, which in turn seeps into the West Branch of Chicone Creek, is considered.

A branched one-dimensional real time tidal hydraulic and water quality model is applied to Chicone Creek and its several branches for the purpose of determining the temporal and spatial distribution of concentration of contaminant, relative to the mass rate of addition of the contaminant to the groundwater. The groundwater in turn is considered to be in communication with the West Branch of Chicone Creek.

THE AREA

Figure 1 is a sketch map showing the location of Chicone Creek and its several branches with respect to the Vienna Electric

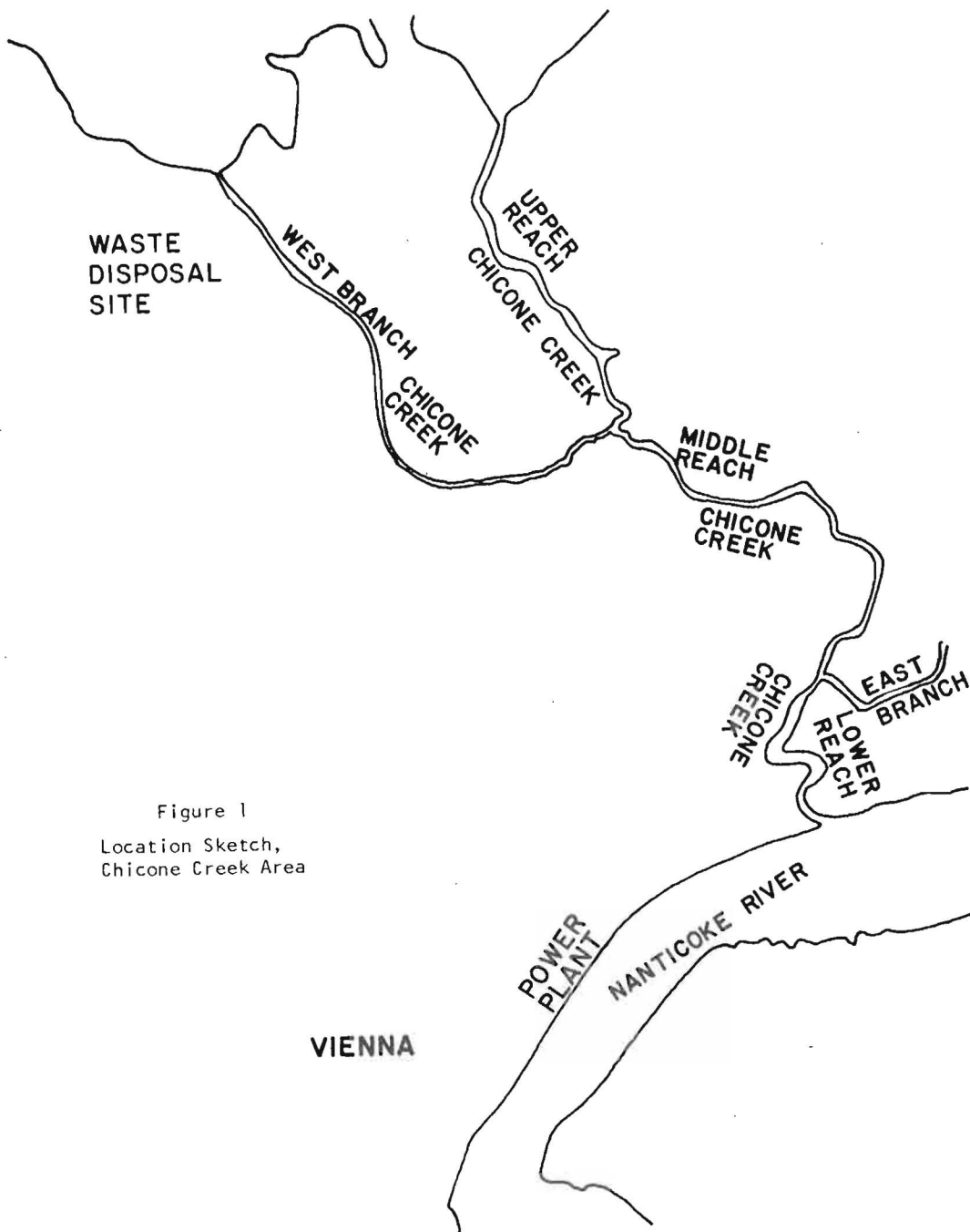


Figure 1  
Location Sketch,  
Chicone Creek Area

Generating Station, and also to the proposed waste disposal area. For our purposes here the Chicone Creek system is considered to be composed of a Main Branch, a West Branch, and an East Branch. The Main Branch is further sub-divided into three reaches. The Upper Reach extends from the head of tide to the junction of the Main Branch with West Branch. The Middle Reach extends in a meandering, southerly direction from the junction of West Branch to the junction of East Branch. The portion of the Main Branch extending between the junction of the East Branch and the mouth of the creek at the Nanticoke River is designated the Lower Reach.

A topographic chart on a scale of 1" = 500' was used to determine the surface width of Chicone Creek and its two major tributaries, at intervals of about every 200 feet. The exact interval between sections at which such measurements were made depended upon the variation in the surface width with distance along the axis of the creek. An areal mosaic of the region, showing the creek and a portion of the tributaries, was used as a check on the data taken from the topographic chart.

Only a very limited amount of data is available on the channel depth and cross-sectional shape of the waterway. Detailed measurements were made at two cross-sections. Information on channel depth along the main stem was provided by word of mouth from field biologists who are studying the waterway. These limited data were interpolated and extrapolated to provide the necessary hydraulic input geometry to the model. The character of this input will be described below. Some comments of the effect of uncertainties in the geometry of the system will also be made in a later section.

### THE MODEL

The model used for the computations carried out on the flushing of Chicone Creek was the M.I.T. Transient Water Quality Network Model. A detailed description of the practical application of this model is contained in Harleman *et al.*, (1977). This model computes the cross-sectionally averaged surface elevation, discharge, axial component of the velocity, salinity, and the concentration of any introduced contaminant, as a function of distance along the axis of the estuary, and as a function of time. It allows for the branching of the computational network describing the waterway into as many tributaries and/or distributaries as are required by the actual geomorphology of the estuary. The model also allows for a distributed lateral input of fresh water and of contaminant as might occur with groundwater seepage. The model computes in real time, that is, at time steps short compared to the tidal period.

### INPUT TO THE MODEL

The model requires as input information on the depth and cross-sectional area along the length of the waterway. It allows for separation of the cross-section into a conveyance segment, which carries the tidal and non-tidal transports, and a storage segment which allows for lateral storage of a portion of the intertidal volume but which does not participate in the longitudinal transport of water volume, mass of salt, or mass of contaminant. Also required as input is the tidal rise and fall at the mouth of the waterway, the

input of fresh water into the head of the main branch and of any tributaries, the salinity and contaminant concentration of the ocean or other parent water body at the mouth of the system being modeled, and of the volume rate of flow per unit distance of any distributed (non-point source) lateral inflow. Also required is the concentration of any contaminant in the lateral inflow.

In the present case the tidal variation of water surface elevation at the mouth of Chicone Creek was considered to be sinusoidal in character, with a range of 2.4 feet, and a period of 12.42 hours, that is, of the semi-diurnal lunar tide. The fresh water inflow to the waterway was computed from the measured drainage area using the run-off factor of 1.0 cfs per square mile characteristic of this region. The average annual inflow of 12.3 cfs computed in this manner was distributed as follows: (a) 2.0 cfs into the head waters of the Main Branch of Chicone Creek; (b) 2.0 cfs into the head waters of West Branch; (c) 4.0 cfs distributed uniformly along the 4000 foot length of the Upper Reach as lateral inflow; (d) 3.5 cfs distributed uniformly along the 3500 foot length of West Branch as lateral inflow; (e) the remaining 0.3 cfs into the head of East Branch.

A contaminant was assumed to be introduced into the waterway in the lateral inflow to West Branch, at a rate of  $m$  pounds per day. The value of  $m$  need not be specified for the model runs, since the results of the computations of contaminant concentration are expressed as a concentration ratio, that is, the ratio of concentration in parts per billion (ppb) over the rate of input of contaminant in pounds per



day. Thus at any later time it will be possible to simply multiply the values of concentration ratio produced in the model runs by the constant factor  $m$  to obtain concentration in ppb.

#### FRICITION AND DISPERSION COEFFICIENTS

The hydraulic portion of the model requires as input values of a bottom friction coefficient, in the form of Manning's  $n$ . The values may be set constant for each reach or different values may be assigned to each cross-section. Experience in other tidal waterways give good verification of the tidal hydraulics for Manning's  $n$  values of between 0.018 to 0.020, though higher values have been found necessary for waterways in which flow is strongly damped by aquatic vegetation.

The hydraulic portion of the model was exercised a number of times with various values of Manning's  $n$  assigned to the various reaches. It was found that the model became unstable in East Branch as Manning's  $n$  values smaller than 0.028, indicating that the flow in this Branch must be heavily damped by some high friction producing factors such as aquatic vegetation. Otherwise the model ran quite well with values of Manning's  $n$  for the other four reaches of between 0.018 and 0.020.

On the basis of the work by Rives and Pritchard (1978) in the C.&D. Canal, it is felt that the value of 0.020 for Manning's  $n$  in the reaches of Chicone Creek other than East Branch is the most appropriate value. However, in order to determine the sensitivity

of the results of the computations of the water quality to variations in the value of Manning's  $n$ , hydraulic runs were made for two cases, one in which Manning's  $n$  was set at 0.0200 everywhere but in East Branch, where the value of 0.0280 was used, and a second in which Manning's  $n$  was set at 0.0180 everywhere except in East Branch, where again the value of 0.0280 was used. The outputs of these runs were then used as input for duplicate runs of the water quality portion of the model.

The water quality portion of the model requires as input values of the estuarine dispersion parameter, designated by  $K$ , and of the Taylor's multiplication factor for bends and channel irregularities, designated  $m$ . Thatcher and Harleman (1972) give the experimental and theoretical evidence for the equations utilizing these parameters. On the basis of studies carried out in other waterways,  $K$  was set at  $50 \text{ ft}^2 \text{ sec}^{-1}$  and  $m$  at 3.0 for these model studies of Chicone Creek.

#### BOUNDARY CONDITIONS AT THE MOUTH

The water quality computations require that a value for the concentration of the contaminant be set at the seaward boundary of the modeled waterway. The model computes the concentration at the mouth during the ebb phase of the tide, but assumes that during the flood phase the concentration decreases exponentially to some fixed value assigned to the "clean" water of the parent water body. In the present case the parent water body is the Nanticoke River. The volume

of the Nanticoke in the tidal excursion reach adjacent to the mouth of Chicone Creek is sufficiently large so that the concentrations of a contaminant discharged from Chicone Creek which would be found in Nanticoke River water entering Chicone Creek at the end of the flood cycle can be considered to be close to zero. The model allows the rate constant, which determines the exponential rate at which the concentration at the mouth decreases from its maximum value at the end of ebb to close to its assigned value in the parent water body (in this case, zero) at the end of flood, to be set by the user. This rate constant, designated TCON in the Model, does affect the concentration distribution within the waterway.

A number of model runs were made with TCON varying from a value of  $0.00780 \text{ sec}^{-1}$ , which results in the contaminant concentration at the mouth reaching the set boundary value of zero in less than one-tenth of the flood tide interval, to a value of 0.00013, which results in the concentration at the mouth decreasing over the entire flood period to a value at the end of flood equal to 5% of the maximum concentration which had occurred at the end of the previous ebb period. We conclude that the value of 0.00021 for TCON is most appropriate. This gives a concentration value at the mouth at the end of the flood period of 1% of its maximum value at the end of the previous ebb period. However, the results of the runs for TCON set at 0.00780 and TCON set at 0.00013 are presented graphically and discussed in the following section.

The salinity at the mouth is assumed to vary in an analogous but inverse manner to that described for a contaminant. That is,

the model computes the salinity during the ebb phase, when it will be decreasing with time as the lower salinity water from the interior of the waterway is being advected to the mouth. At the beginning of flood the salinity is assumed to start increasing exponentially to approach the assigned "ocean" value at the end of flood. The assigned value for the salinity of the Nanticoke River (which is the "ocean" as far as this model of Chicone Creek is concerned) adjacent to the mouth of Chicone Creek was, for these model runs, set at 1‰, (1000 ppm). The reach-node network used in the model runs is shown schematically in Figure 2.

#### RESULTS

The results of four runs of the model, each made over a time interval of 10 tidal cycles, are presented here. Only the data for the last, or 10th, tidal cycle is given, since the purpose of running the model for that number of tidal cycles was simply so that pseudo steady-state conditions could be attained. By pseudo steady-state is meant that the variation of the values of each parameter over a tidal cycle is repeated from one tidal cycle to the next. The results of the 8th and 9th tidal cycles were examined to determine that pseudo steady-state had in fact been attained.

The four water quality runs were made to demonstrate the influence of the several free parameters on the results. For the first two runs the value of TCON was set at  $0.00021 \text{ sec}^{-1}$ . In one of these runs the hydraulic input was obtained from running the

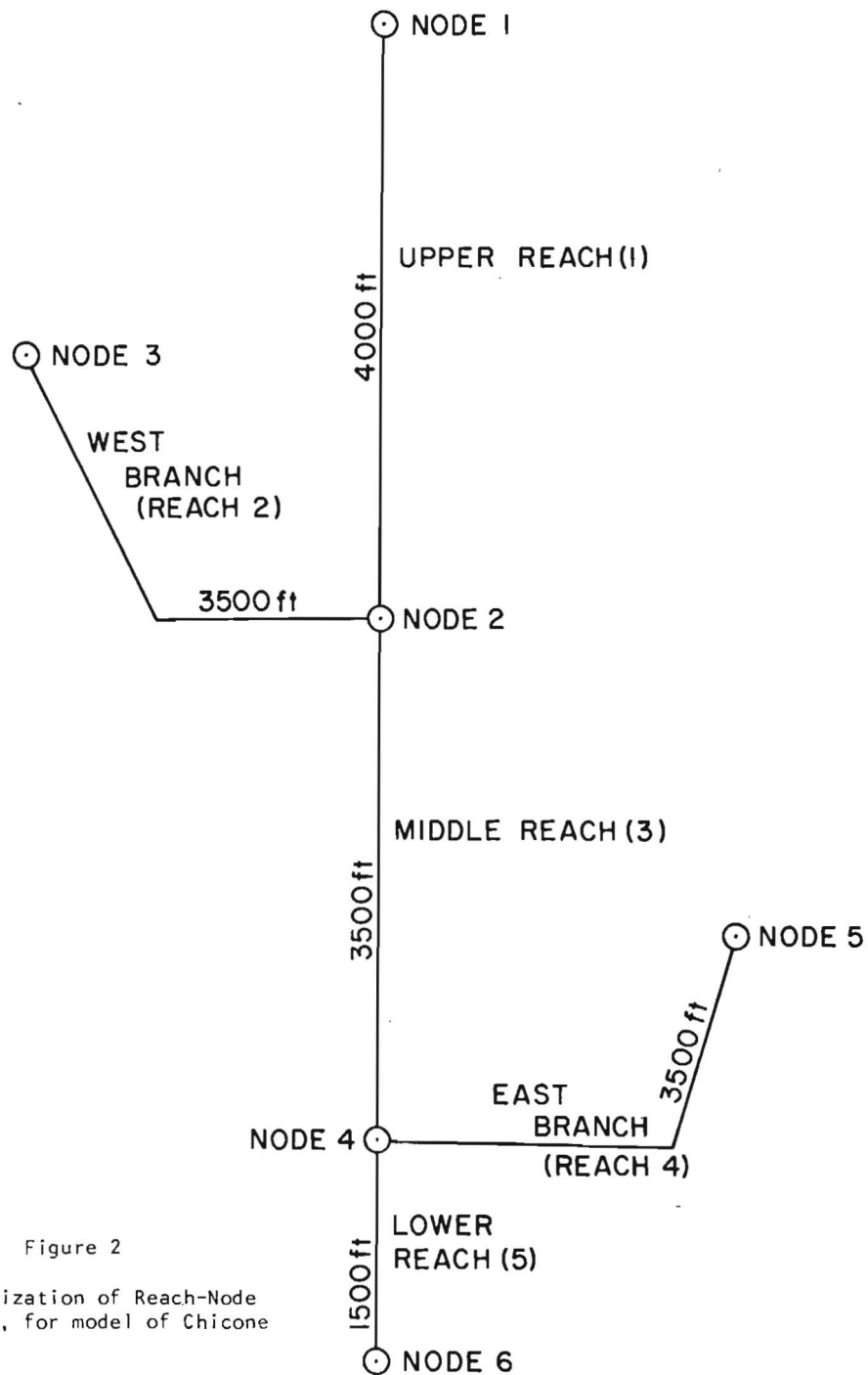


Figure 2  
Schematization of Reach-Node  
Network, for model of Chicone  
Creek

hydraulic portion of the model with the value of Manning's  $n$  set at 0.0200 for all reaches of Chicone Creek except East Branch, where the value set to 0.0280. This hydraulic input is designated CCHS1 for purposes of later reference. In the second of the two water quality runs the hydraulic input was obtained from a hydraulic run made with Manning's  $n$  set at 0.0180 everywhere but in East Branch, where again it was set at 0.0280. This hydraulic input is designated CCHS2 for later reference.

In the other two water quality runs the CCHS1 hydraulic input was used in both cases. For one of these runs the exponential time constant at the seaward boundary, TCON, was set at  $0.00780 \text{ sec}^{-1}$ , while in the final run TCON was set at  $0.00013 \text{ sec}^{-1}$ .

Figure 3 shows the tidal variations in water surface elevation at a position 500 feet below the head of the Upper Reach of the Main Branch of Chicone Creek. The tide in the creek is very nearly a pure standing wave, and is almost uniform in amplitude and phase throughout the tidal waterway. The HW and LW values for the input tide at the mouth of Chicone Creek have also been entered on Figure 3, and are designated by the "X" symbol on that figure. The elevation data is referenced to a datum surface set at 8 feet below mean sea level.

Figure 4 shows the variation in discharge through three cross-sections located at different positions along the length of Chicone Creek. Positive values represent ebb flow and negative values, flood flow. The symbol "\*" is used to designate the data points for a position 500 feet up from the mouth of Chicone Creek.

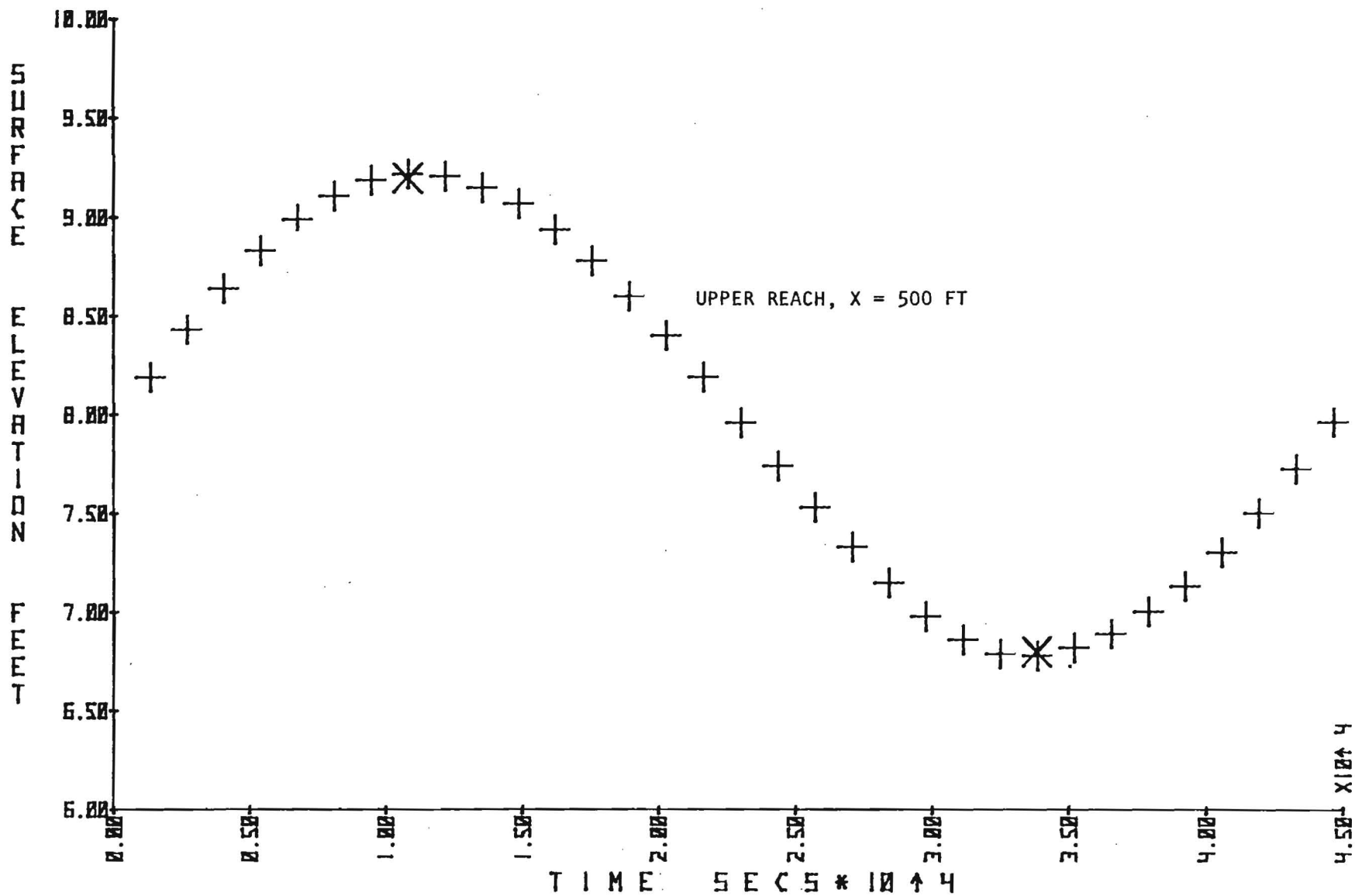


Figure 3. Tidal variation in water surface elevation as computed for a position 500 feet below the head of the Upper Reach of the Main Branch of Chicone Creek. Also, marked with an X, are the HW and LW values of the input tide at the mouth.

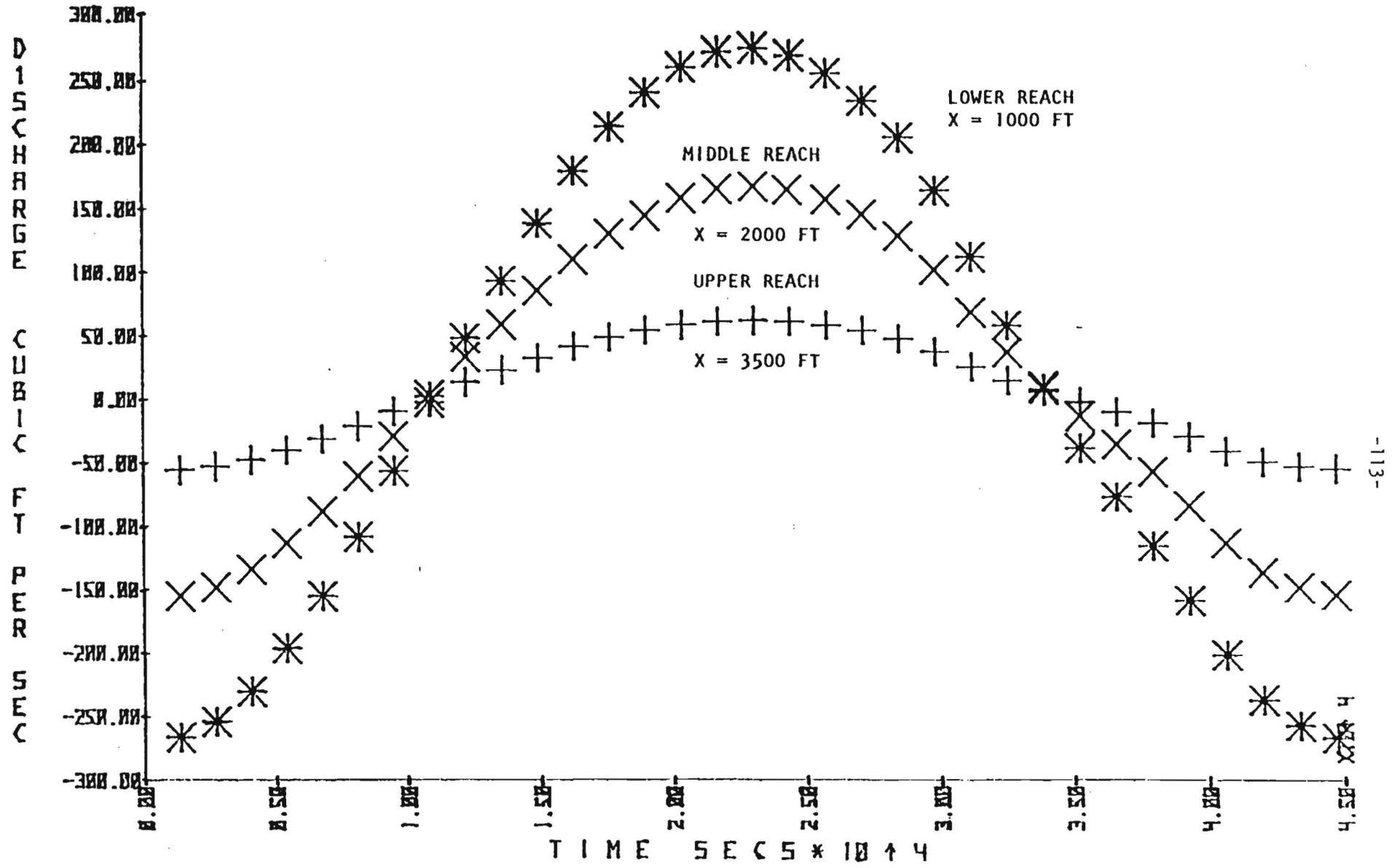


Figure 4. Variations in the discharge over a tidal cycle through three cross-sections at different positions, as labeled, along the length of Chicone Creek.



The symbol "X" designates data points for a position 3000 feet from the mouth, and hence 6000 feet below the head of the Main Branch of Chicone Creek. The symbol "+" is similarly used for a position 5500 feet up from the mouth and hence 3500 feet below the head of the Main Branch.

In both the West Branch and the East Branch the amplitude of the variations in discharge over the tidal period show a decrease with distance analogous to that shown for the Main Branch. At the head of each branch the tidal variations in discharge are zero. The discharge at these three upstream boundary nodes is thus set constant and equal to the volume rate of inflow of fresh water from the upland drainage areas.

Comparison of Figures 3 and 4 clearly demonstrates that the tide in Chicone Creek is a standing wave, since maximum flood flow occurs one-quarter of a tidal cycle, or 3.06 hours, prior to high water, and maximum ebb flow occurs one-quarter of a tidal cycle before low water.

Figures 5 through 11 give the concentration ratio (PPB/lbs per day) as a function of time over the tidal cycle for two water quality runs. For each run, hydraulic input CCHSI was used. One set of data points plotted on these figures represent the results of a water quality run with the exponential time constant at the mouth, TCON, set at 0.00780, and the other set of data points represent the results for TCON set at 0.00013. For Figures 5 and 7, the upper set of points are for TCON = 0.00780, while for Figures 6, 8, 9, 10 and 11,

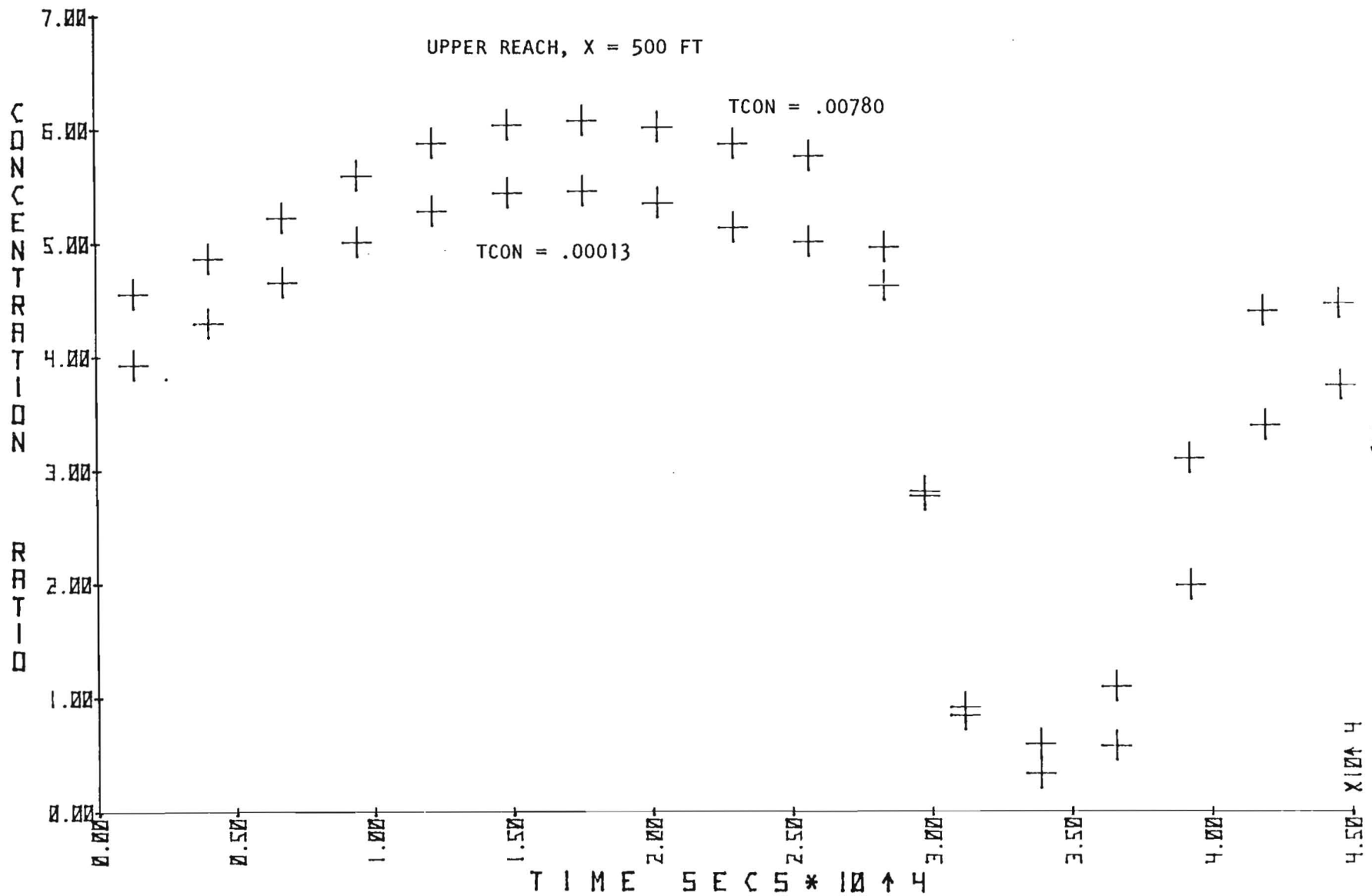


Figure 5. Variation in concentration ratio (PPB/lbs per day) over a tidal cycle at the location and for the test conditions given in the body of the figure.

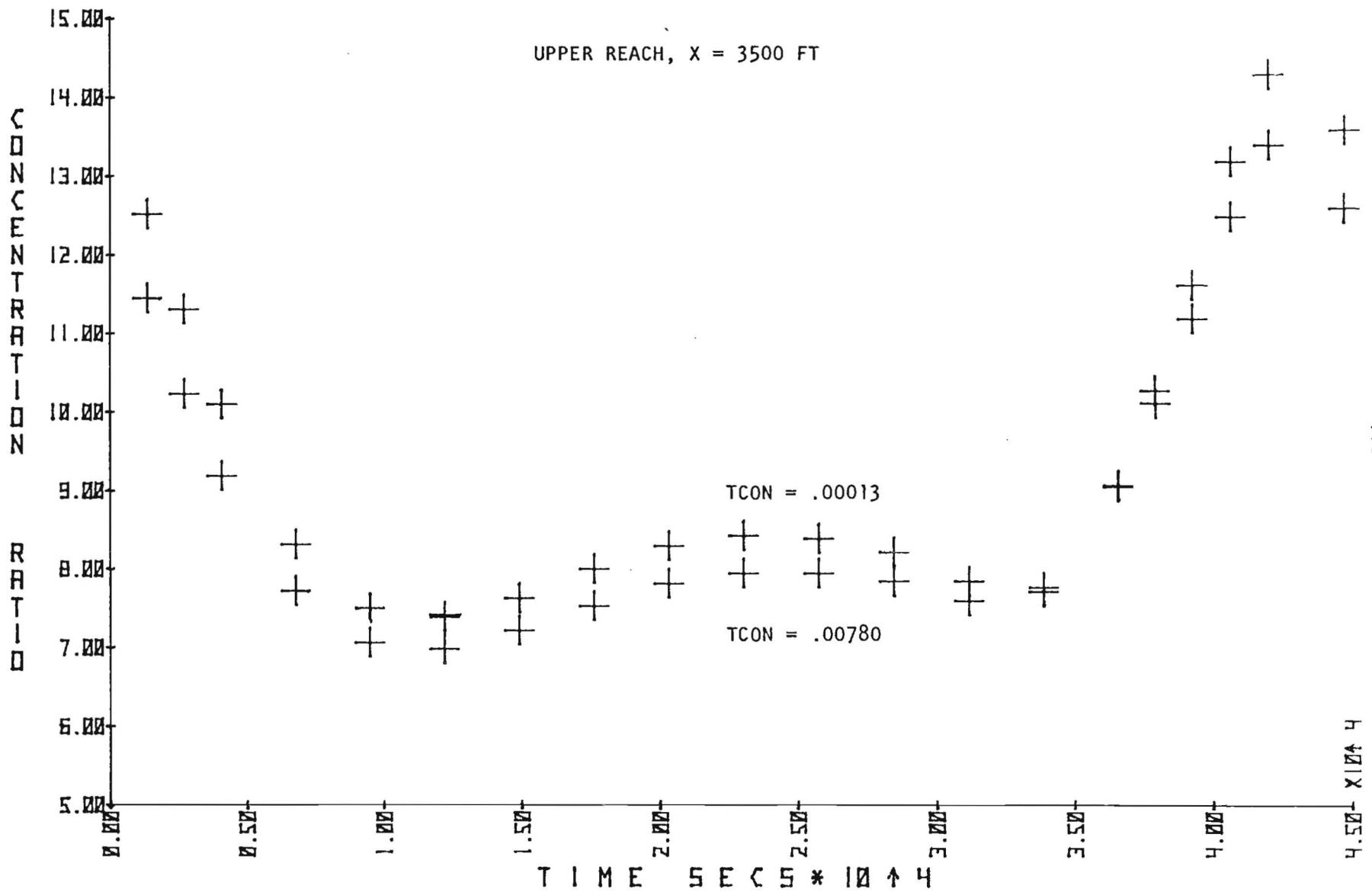


Figure 6. Variation in concentration ratio (PPB/lbs per day) over a tidal cycle at the location and for the test conditions given in the body of the figure.

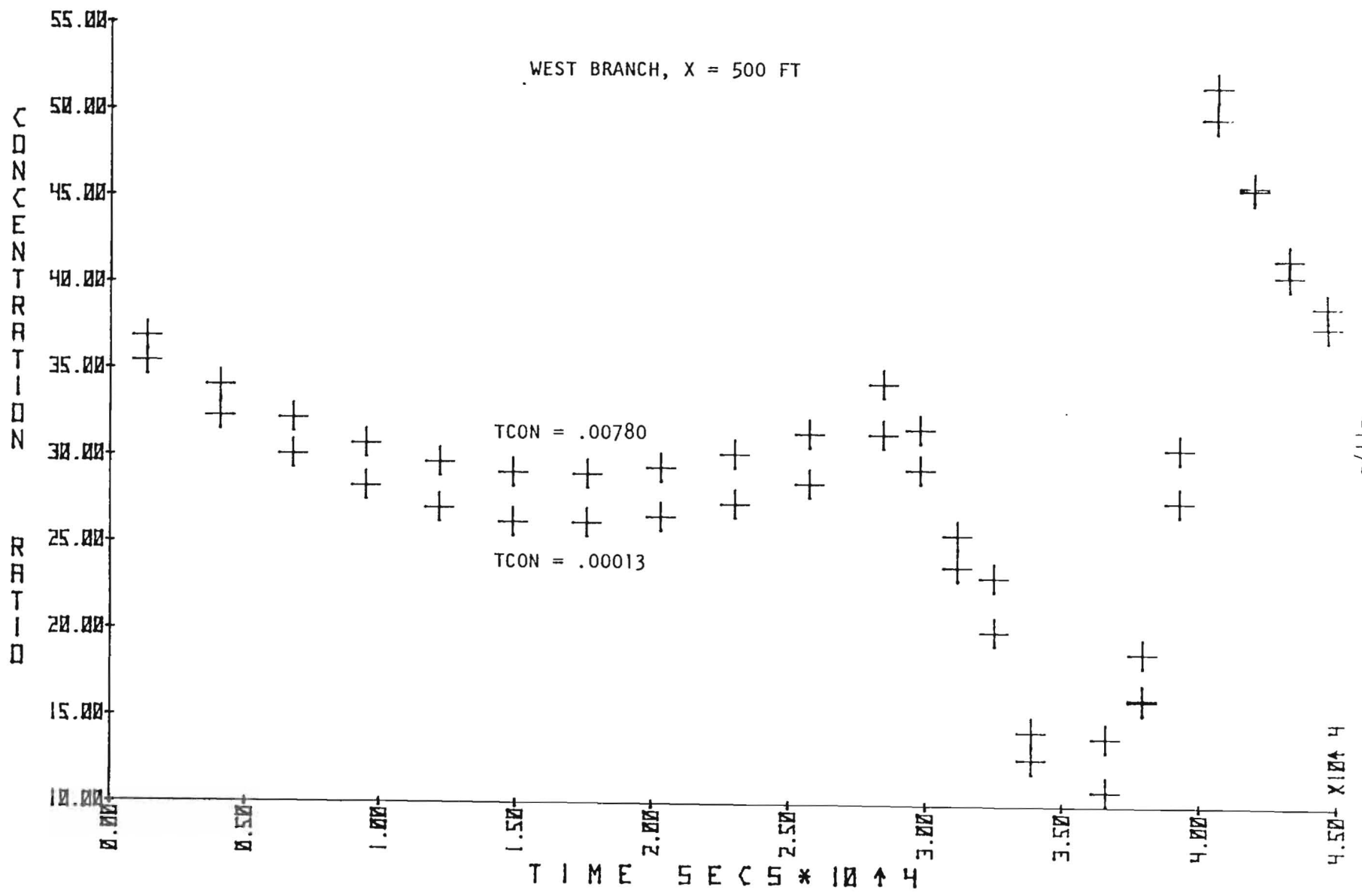


Figure 7. Variation in concentration ratio (PPB/lbs per day) over a tidal cycle at the location and for the test conditions given in the body of the figure.

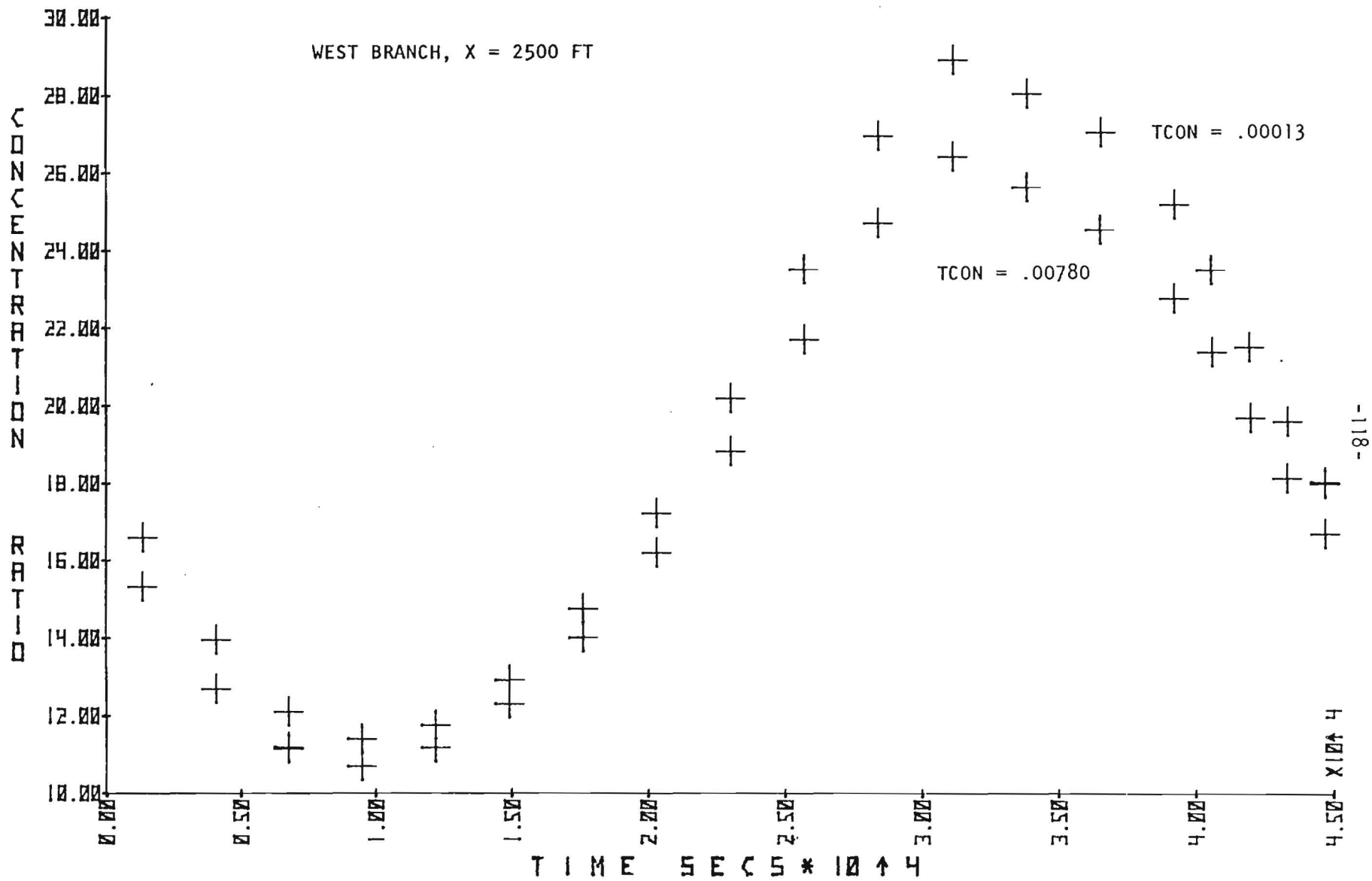


Figure 8. Variation in concentration ratio (PPB/lbs per day) over a tidal cycle at the location and for the test conditions given in the body of the figure.

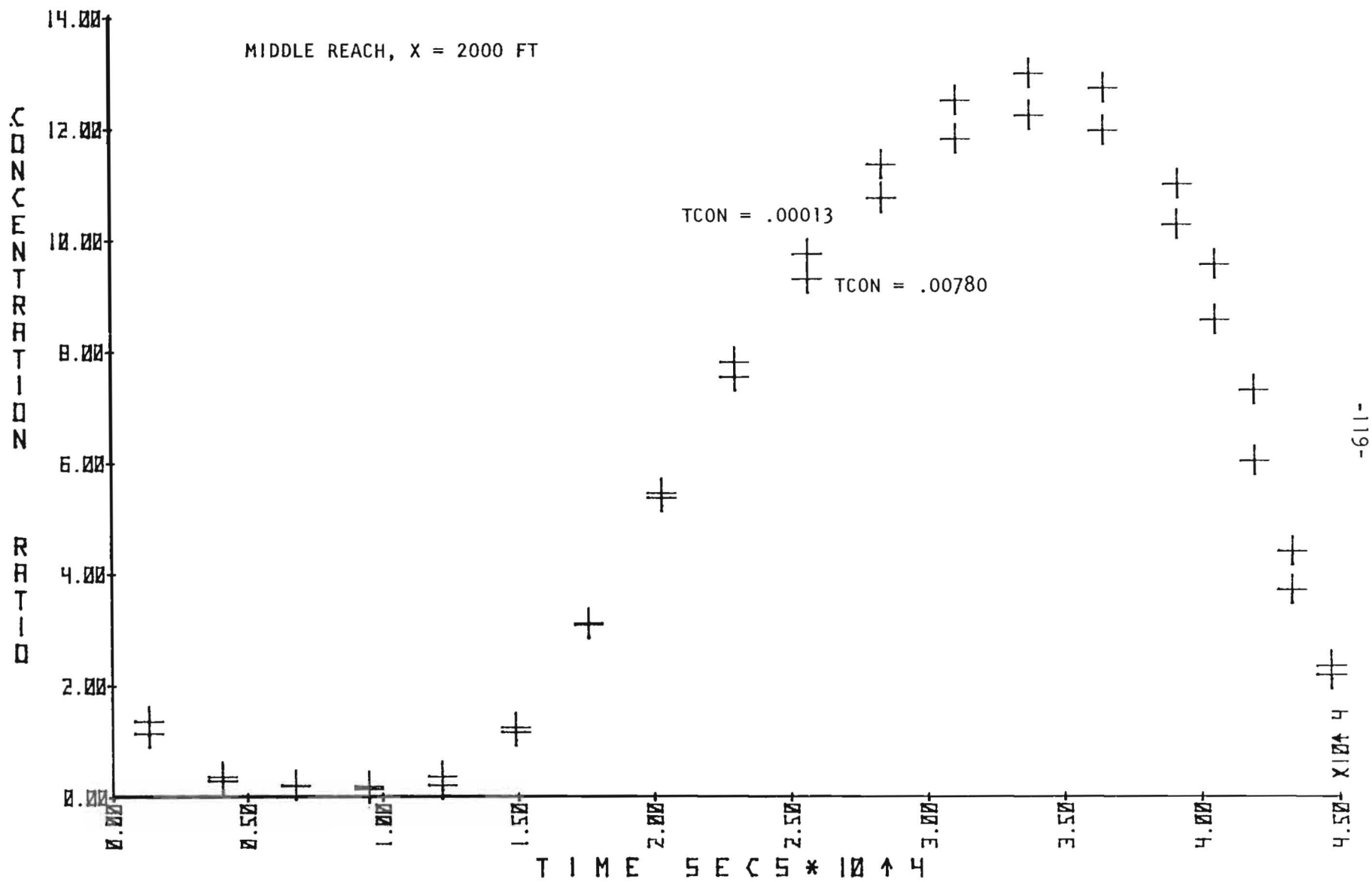


Figure 9. Variation in concentration ratio (PPB/lbs per day) over a tidal cycle at the location and for the test conditions given in the body of the figure.

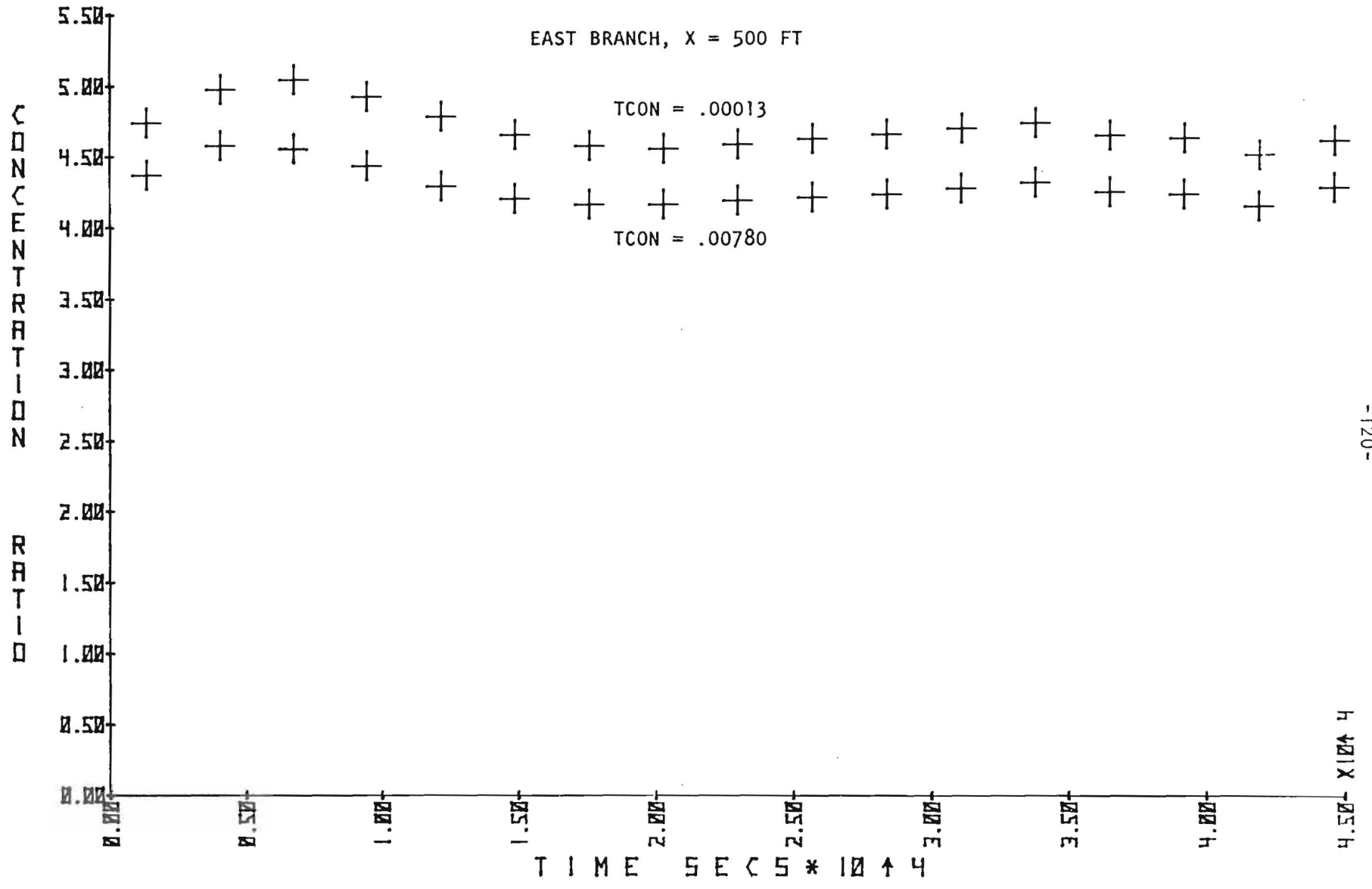


Figure 10. Variation in concentration ratio (PPB/lbs per day) over a tidal cycle at the location and for the test conditions given in the body of the figure.

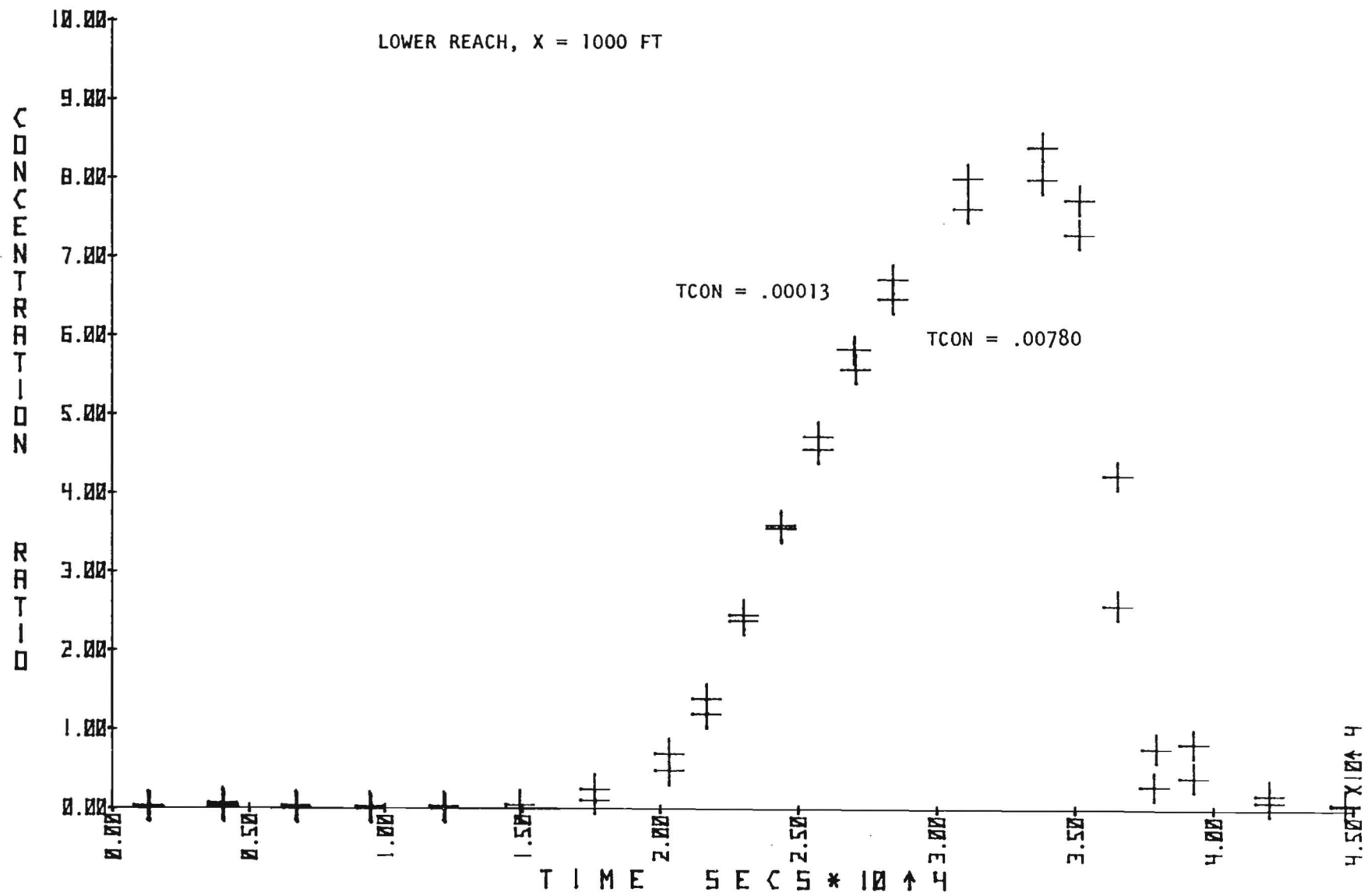


Figure 11. Variation in concentration ratio (PPB/lbs per day) over a tidal cycle at the location and for the test conditions given in the body of the figure.



the upper set of points are for  $TCON = 0.00013$ .

The difference between the maximum values for each case as shown in Figures 5 through 11 ranges from 4% to 11% of the absolute values. Thus variations in  $TCON$  over a reasonable range does not lead to marked difference in the results of the water quality computations.

Figures 12 through 18 give the concentration ratio (in PPB/lb per day) as a function of time over a tidal cycle for two additional water quality runs. In each of these runs  $TCON$  was set at 0.00021, which means that at the end of the interval of flood flow the concentration of contaminant at the mouth had decreased to 1% of its maximum value, which had occurred at the end of the previous interval of ebb flow. The hydraulic input to one of these runs was CCHS1 and to the other it was CCHS2. On all these figures (12 to 18) the uppermost set of points represent the results of the water quality run using CCHS2 for hydraulic input. The differences between the maximum values from each curve shown on each of these figures varies from 1% to 6% of the absolute values of the concentration ratio. Thus variation in Manning's  $n$  over the expected range does not result in very large differences in the results of the water quality computations.

After analysis of the results described above, and review of studies in other areas, we conclude that the water quality runs most appropriate for use in the present case are those for which the hydraulic input is provided by CCHS1 and for which  $TCON = 0.00021$ . All the remaining discussion will be limited to the result of computation made under these conditions.

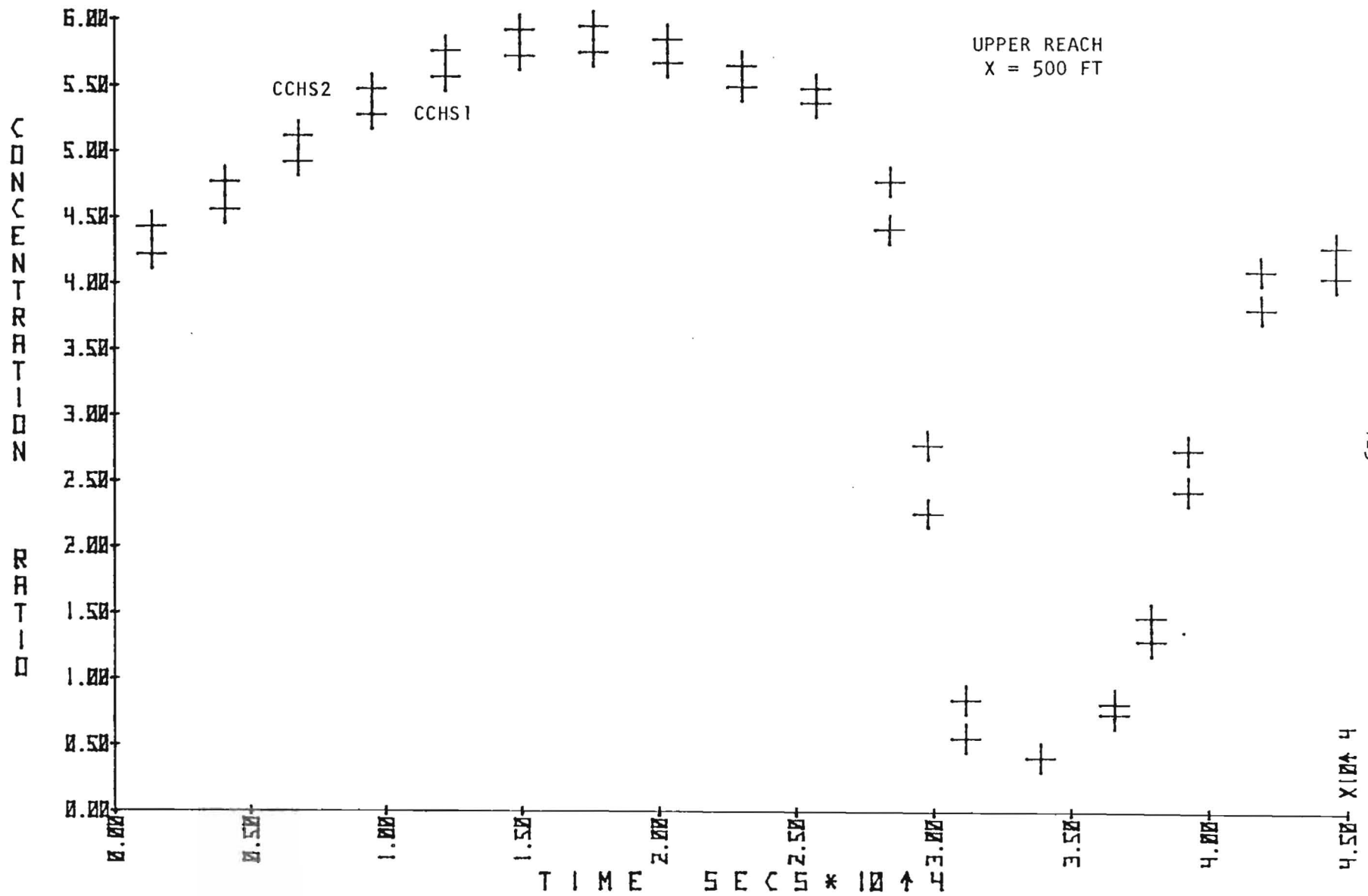


Figure 12. Variation in concentration ratio (PPB/lbs per day) over a tidal cycle at the location and for the test conditions given in the body of the figure.

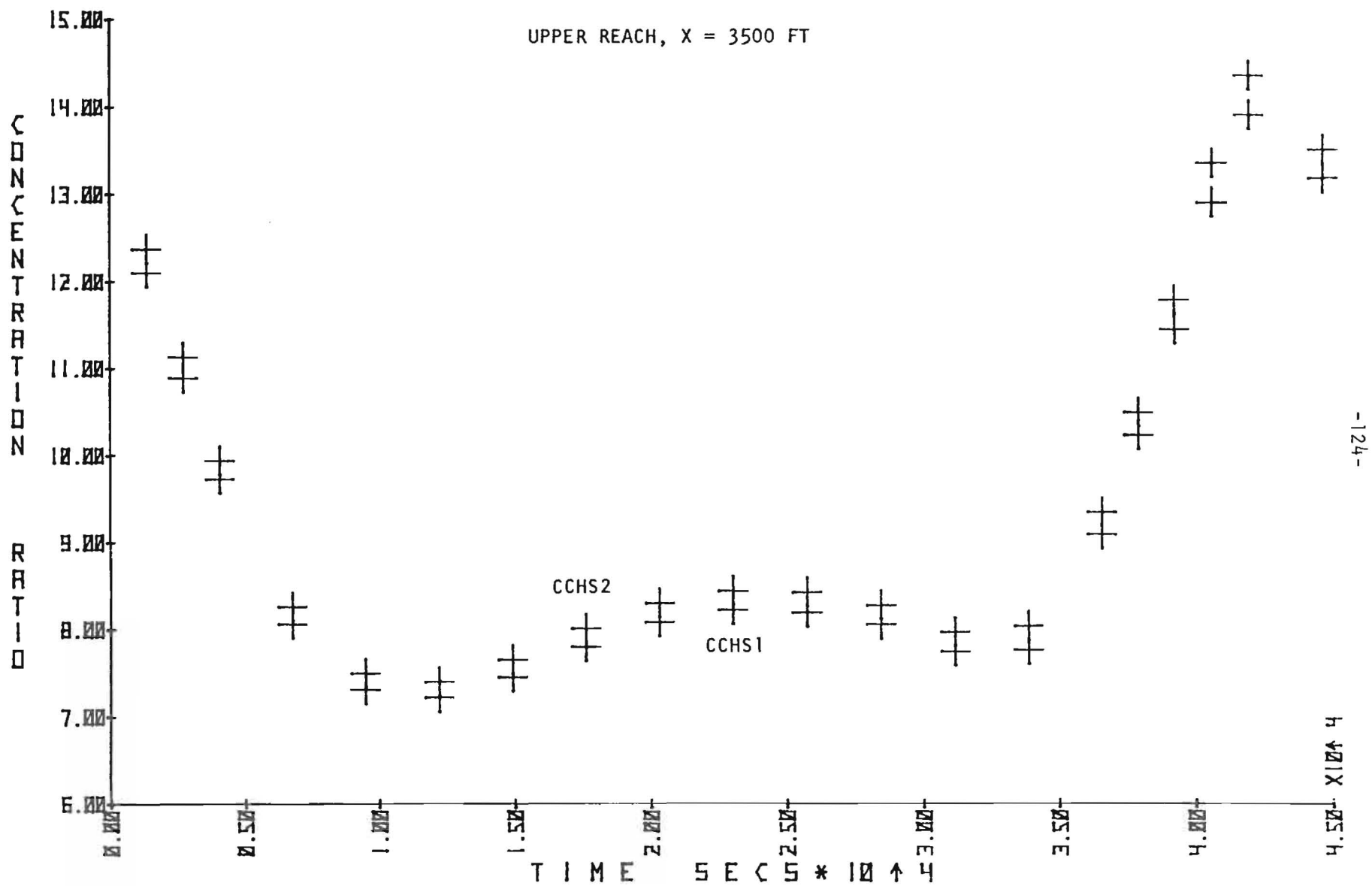


Figure 13. Variation in concentration ratio (PPB/lbs per day) over a tidal cycle at the location and for the test conditions given in the body of the figure.

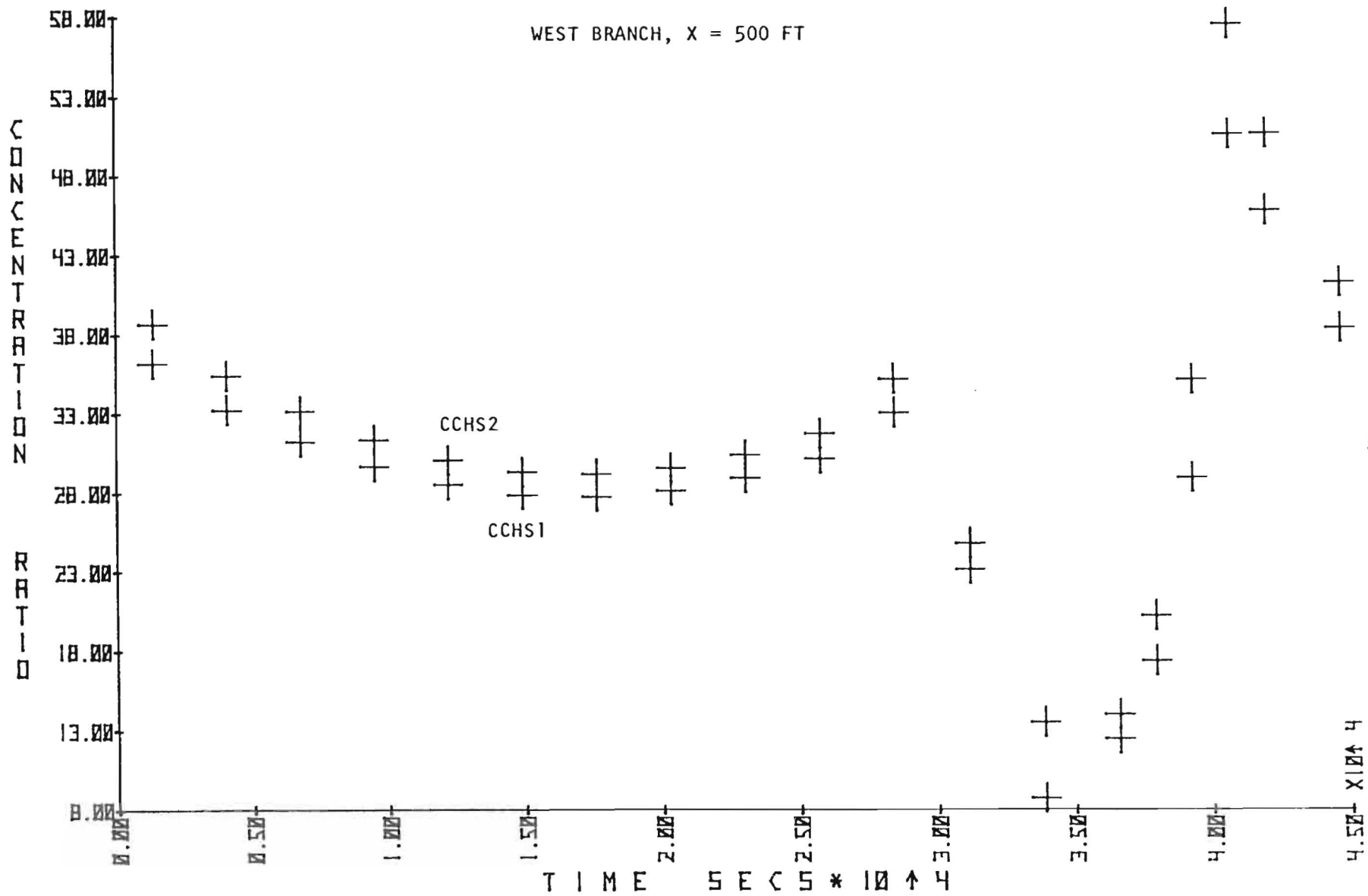


Figure 14. Variation in concentration ratio (PPB/lbs per day) over a tidal cycle at the location and for the test conditions given in the body of the figure.

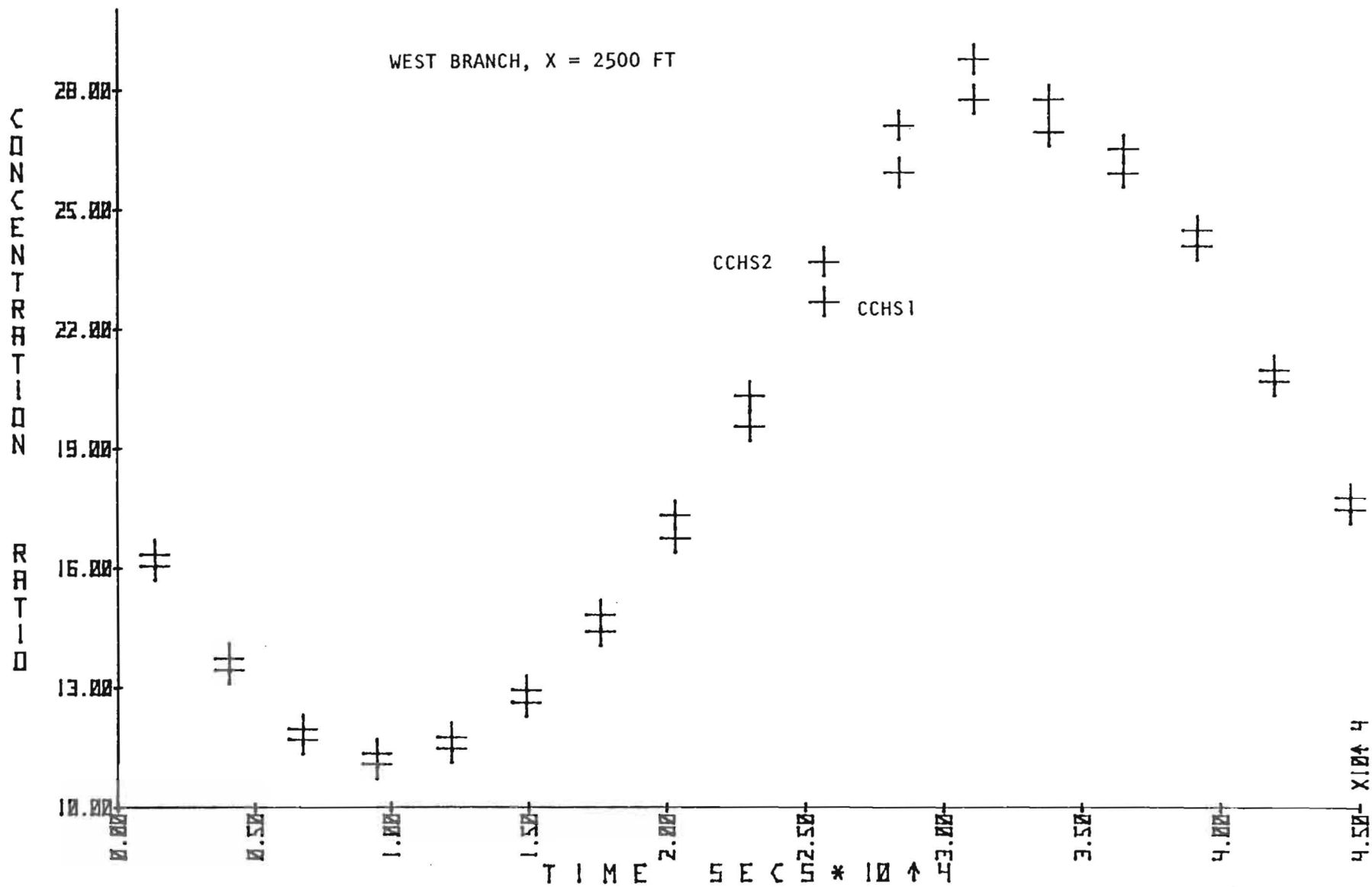


Figure 15. Variation in concentration ratio (PPB/lbs per day) over a tidal cycle at the location and for the test conditions given in the body of the figure.

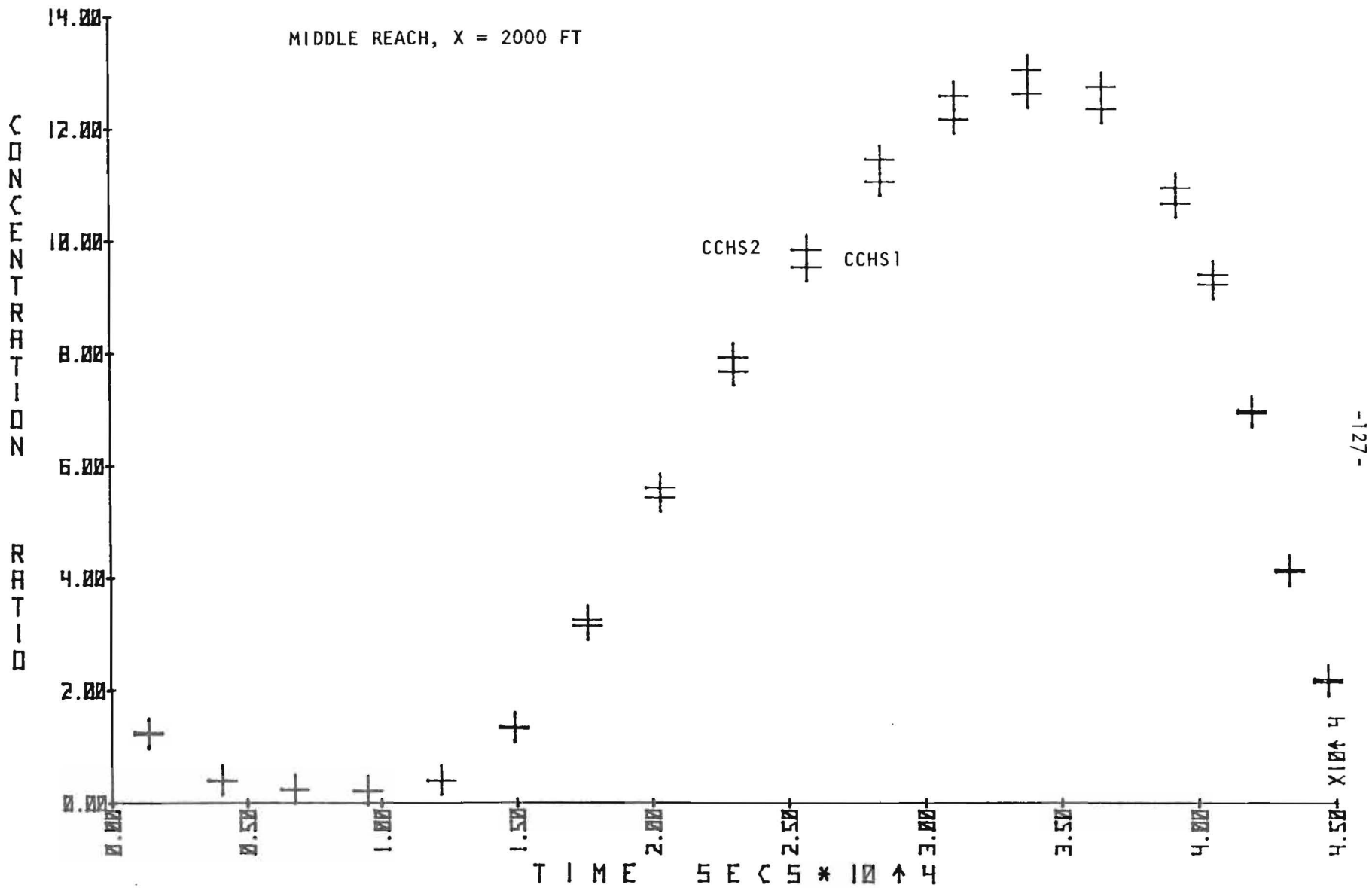


Figure 16. Variation in concentration ratio (PPB/lbs per day) over a tidal cycle at the location and for the test conditions given in the body of the figure.

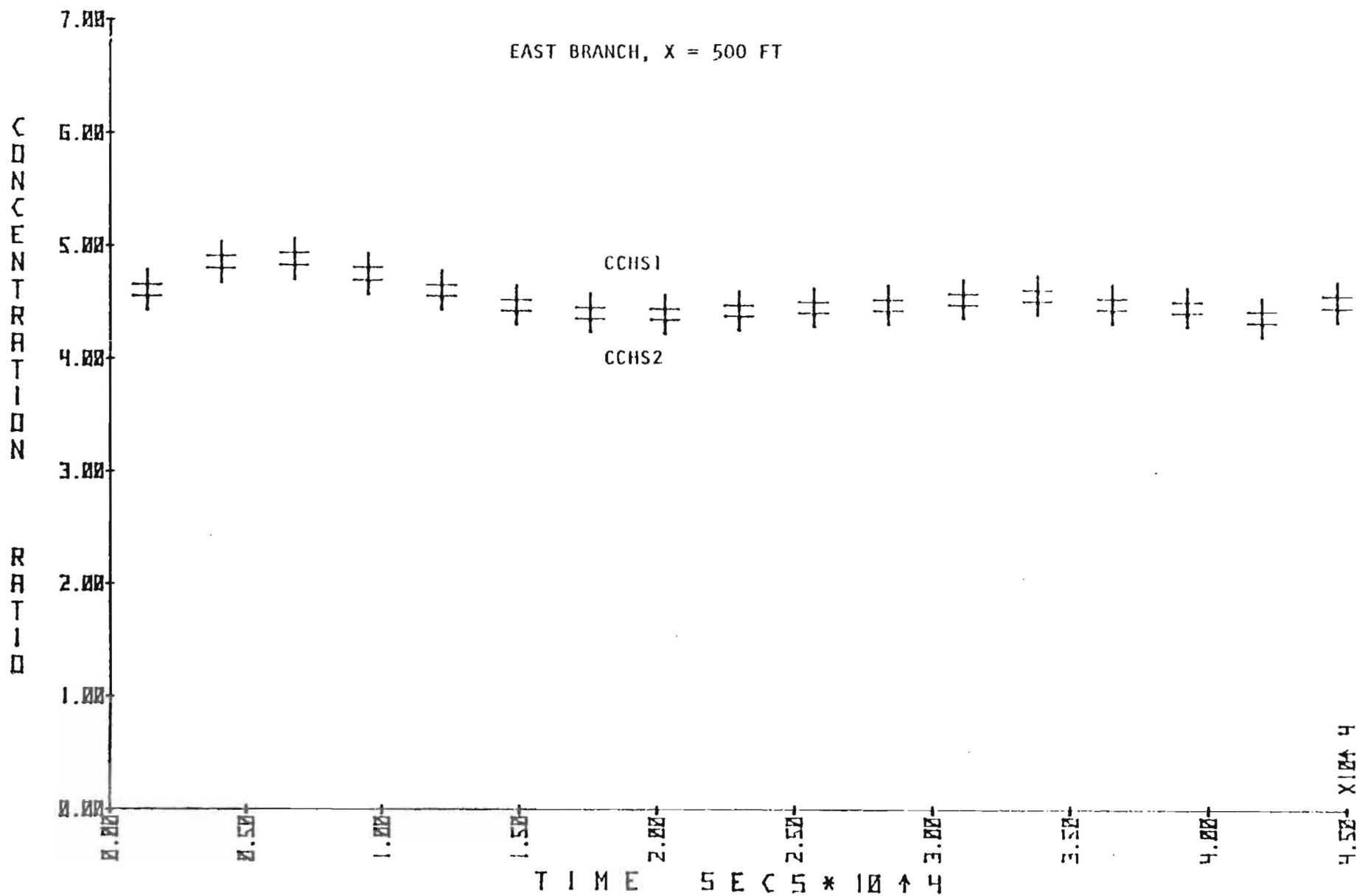


Figure 17. Variation in concentration ratio (PPB/lbs per day) over a tidal cycle at the location and for the test conditions given in the body of the figure.

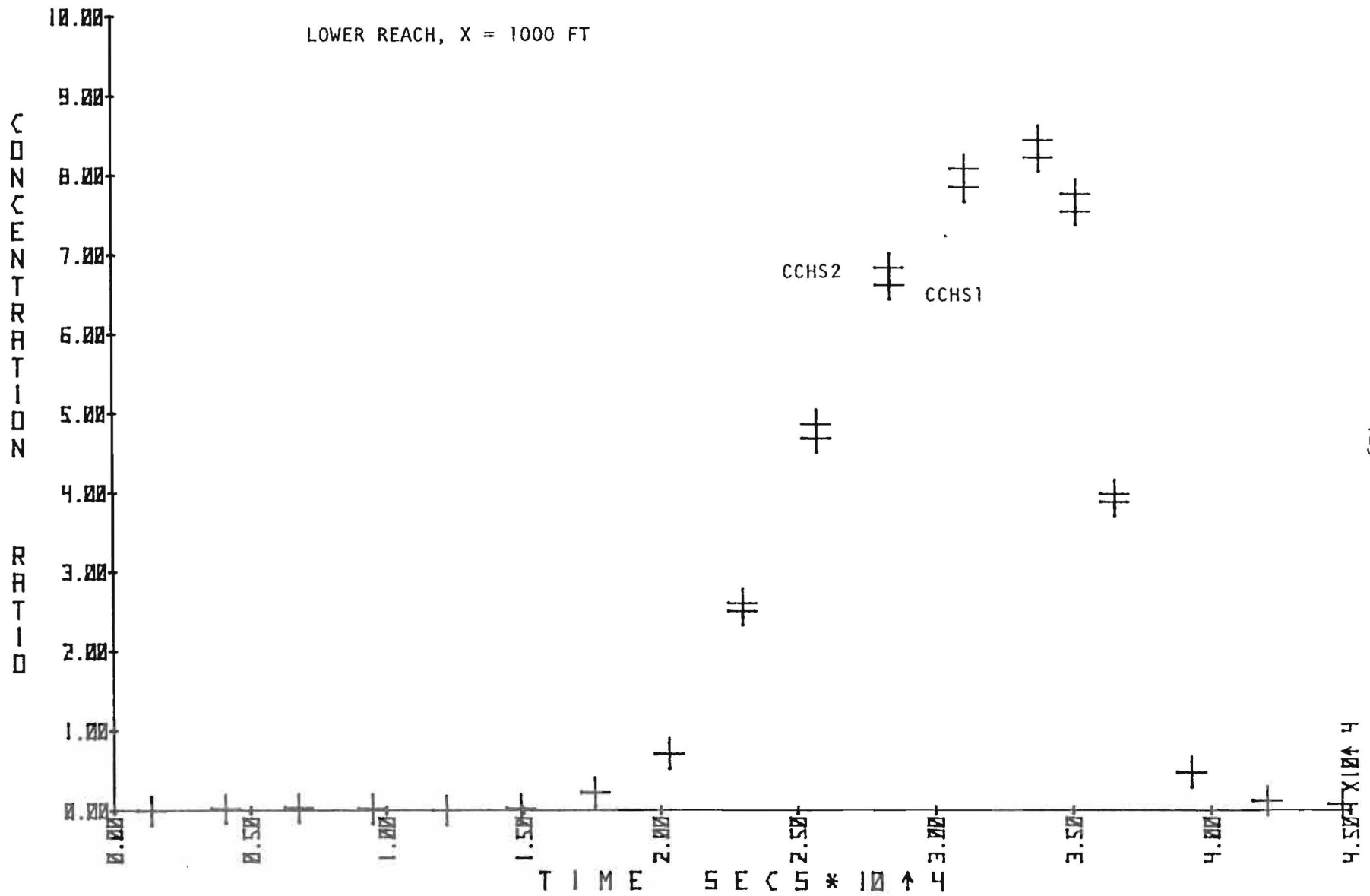


Figure 18. Variation in concentration ratio (PPB/lbs per day) over a tidal cycle at the location and for the test conditions given in the body of the figure.



Figures 19 through 21 show the variation of concentration ratio as a function of distance along the axis of Chicone Creek and of its tributary branches, for a time during the 10th tidal cycle near the time of High Water. Figure 19 covers the Main Branch of Chicone Creek, with the head of tide to the left and the mouth at the Nanticoke to the right. Figure 20 covers the West Branch, with the head of tide to the left of the figure and the junction of the West Branch with the Main Branch to the right. Figure 21 covers the East Branch, with the head of tide to the left of the figure and the junction of the East Branch with the Main Branch to the right.

Figures 22 through 24 are the same as Figures 19 through 21, except that they are for a time close to the time of Low Water.

Tables 1 through 12 give the tabulated output of the water quality model. The first 8 of these tables give the concentration ratio for each time step (169.4 secs) over the tenth tidal cycle, at various positions in Chicone Creek and in its tributary branches. Tables 9 and 10 give the concentration as a function of distance for each of the five reaches, at a time close to High Water, while Tables 11 and 12 give the same information for a time close to Low Water.

These graphs and tables show that for an input of 1.0 lbs per day of a contaminant into the groundwater entering the West Branch of Chicone Creek as a lateral seepage, the following distribution of concentration of the contaminant would occur under mean tide and fresh water inflows:

(a) The concentration at a distance of 500 feet from the upper end of the main stem of Chicone Creek would vary from a

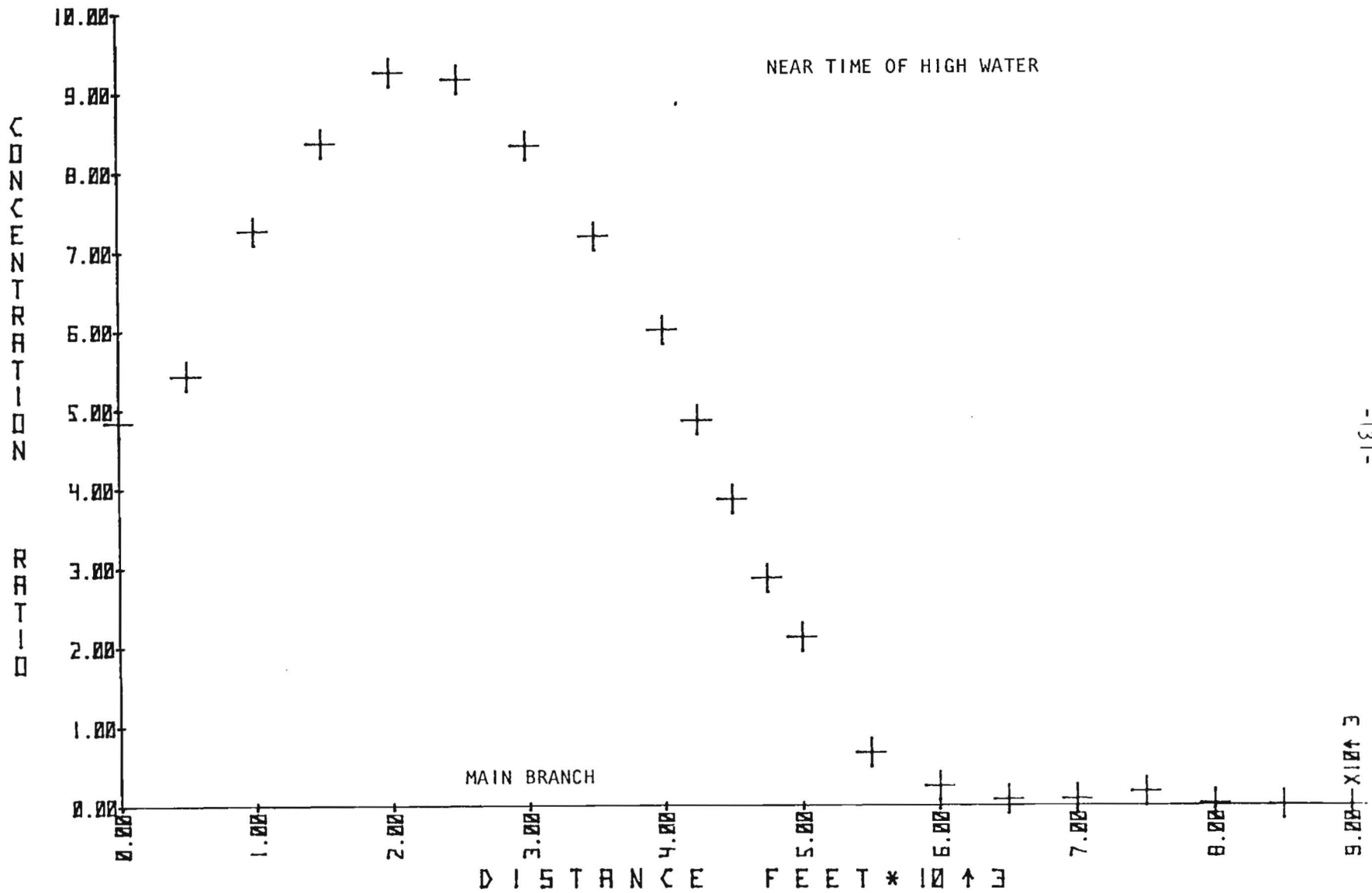


Figure 19. Variation in concentration ratio (PPB/lbs per day) with distance along the indicated reach of Chicone Creek and its tributary tidal waterways, near the time of High Water.

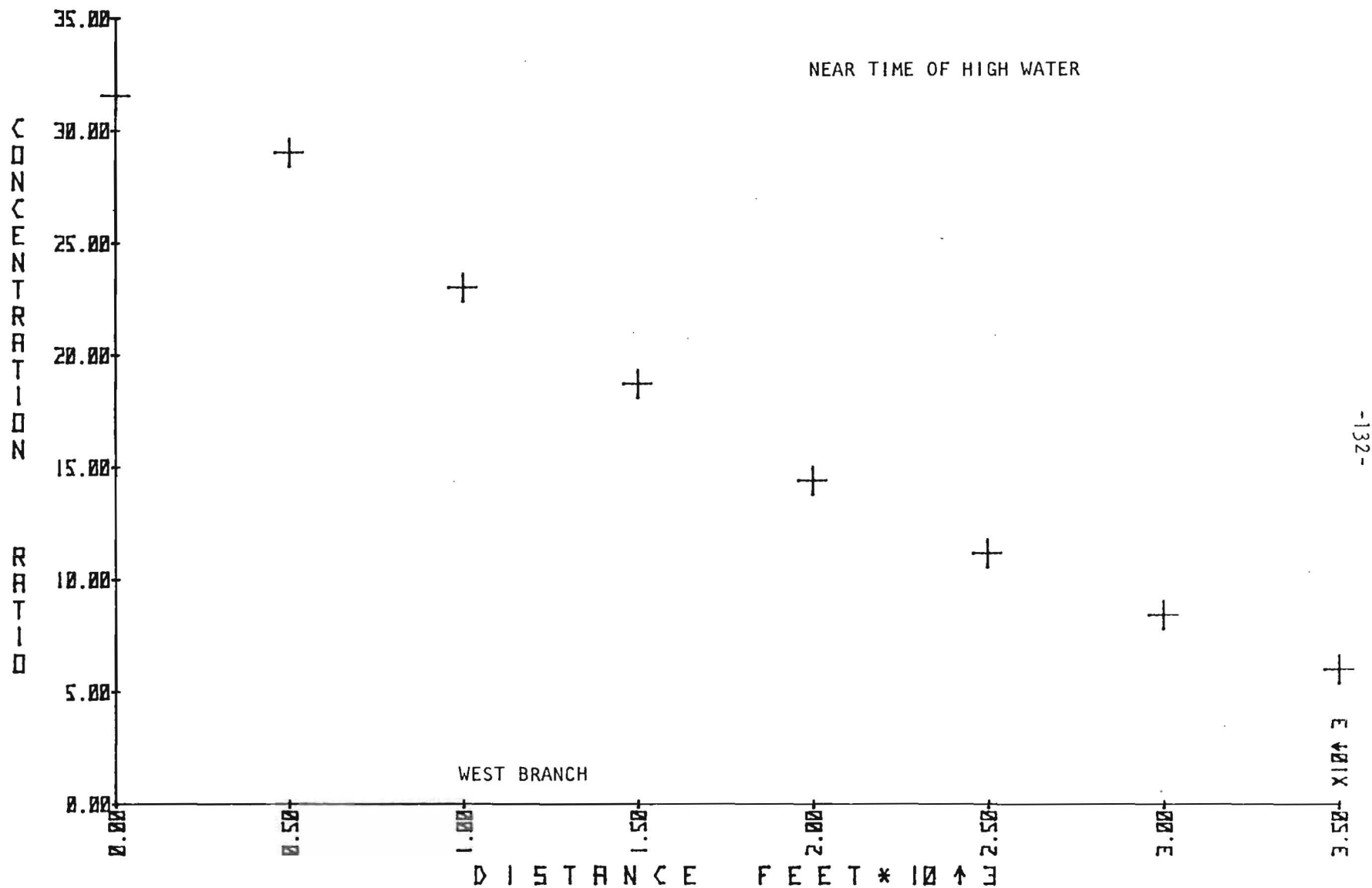


Figure 20. Variation in concentration ratio (PPB/lbs per day) with distance along the indicated reach of Chicone Creek and its tributary tidal waterways, near the time of High Water.

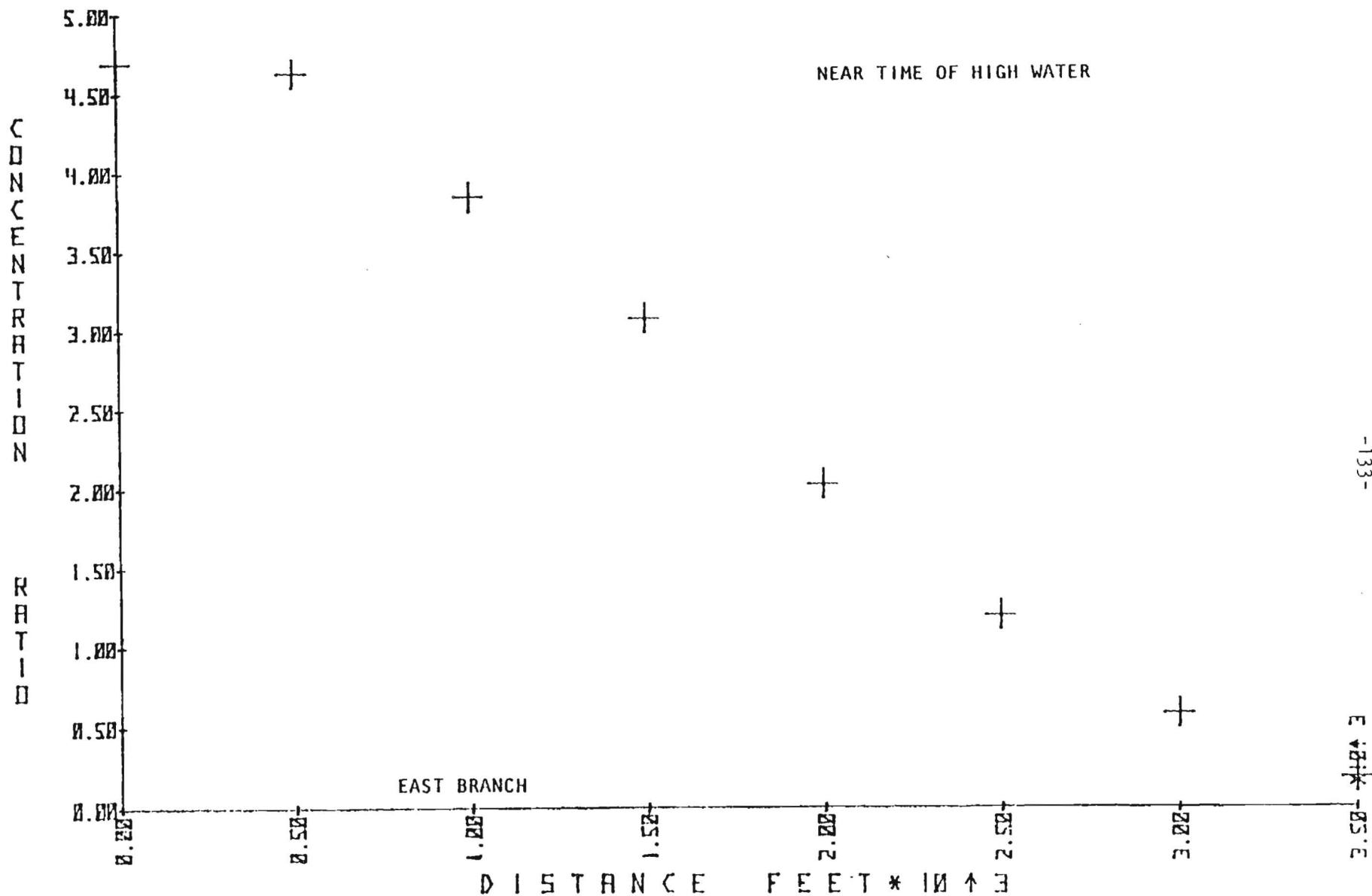


Figure 21. Variation in concentration ratio (PPB/lbs per day) with distance along the indicated reach of Chicone Creek and its tributary tidal waterways, near the time of High Water.

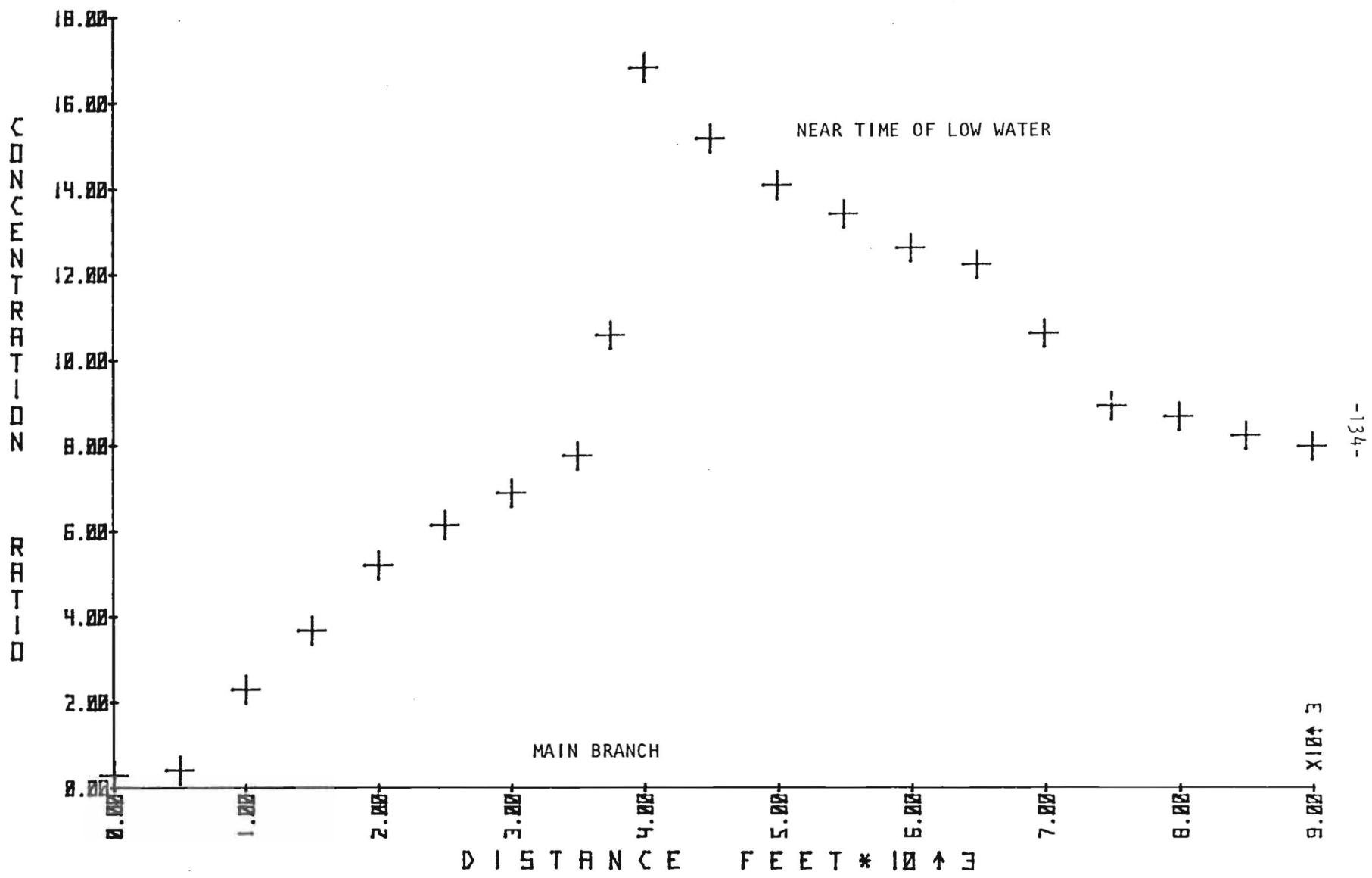


Figure 22, Variation in concentration ratio (PPB/lbs per day) with distance along the indicated reach of Chicone Creek and its tributary waterways, near the time of Low Water.

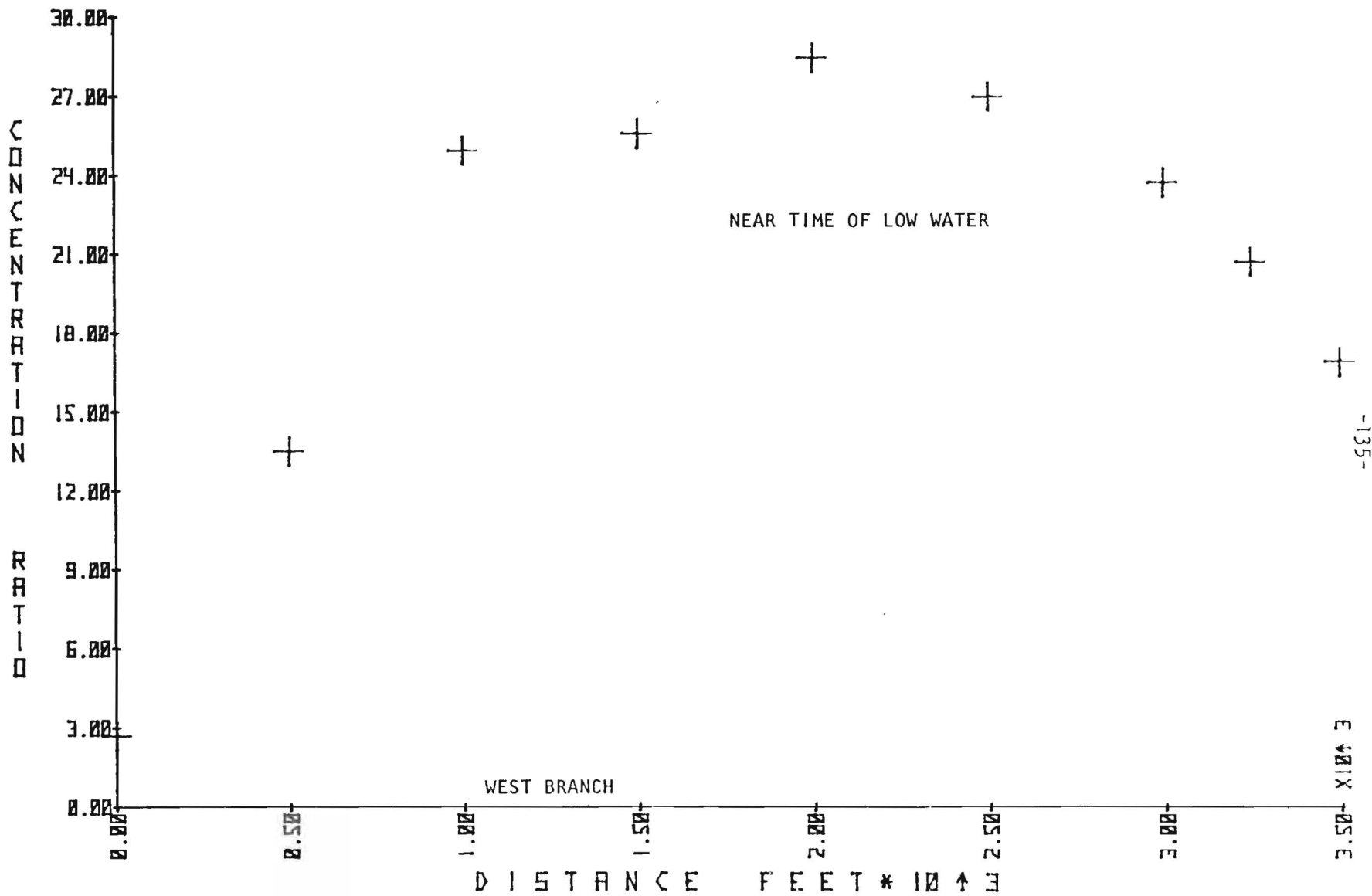


Figure 23. Variation in concentration ratio (PPB/lbs per day) with distance along the indicated reach of Chicone Creek and its tributary waterways, near the time of Low Water.

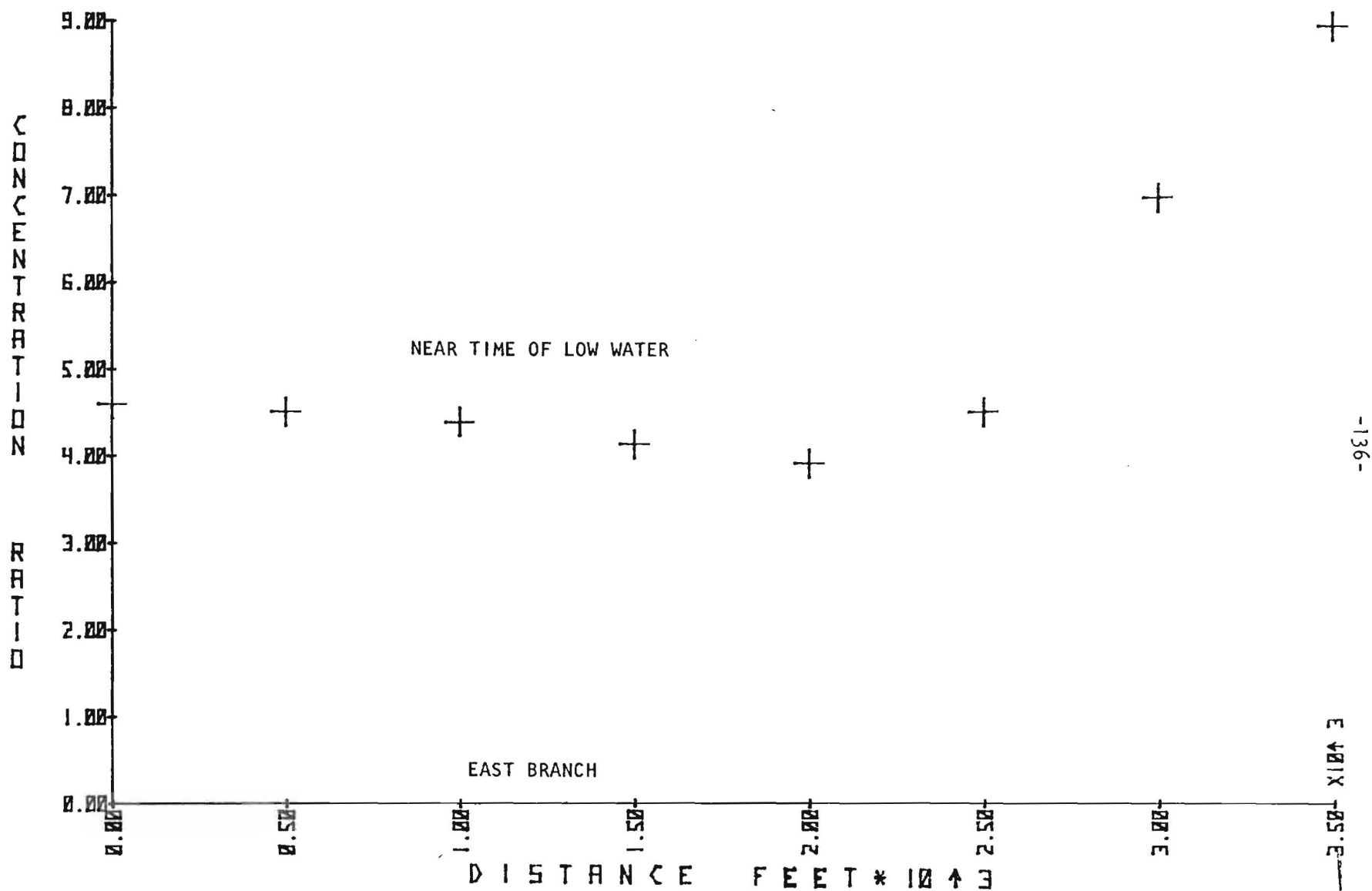


Figure 24. Variation in concentration ratio (PPB/lbs per day) with distance along the indicated reach of Chicone Creek and its tributary waterways, near the time of Low Water.

Table 1

QUALITY GRAPH FOR REACH SECTION 1 x = UPPER REACH CHICONE CREEK  
2 x = 500.0 DURING PERIOD 10

TIME SECONDS	SALIN. PPM	CON RATIO
0.	150.	4.06
1355.	156.	4.22
2710.	162.	4.39
4065.	167.	4.56
5420.	172.	4.74
6775.	177.	4.92
8129.	181.	5.10
9484.	185.	5.28
10839.	188.	5.44
12194.	192.	5.57
13549.	195.	5.67
14904.	197.	5.73
16259.	199.	5.76
17614.	199.	5.76
18969.	198.	5.74
20324.	197.	5.68
21679.	193.	5.60
23033.	189.	5.50
24388.	185.	5.41
25743.	183.	5.38
27098.	189.	5.52
28453.	168.	4.78
29808.	101.	2.78
31163.	33.	.85
32518.	12.	.35
33873.	14.	.41
35228.	17.	.48
36583.	26.	.74
37937.	47.	1.29
39292.	88.	2.43
40647.	136.	3.73
42002.	140.	3.81
43357.	144.	3.90
44712.	150.	4.05

AVERAGE CONCENTRATIONS

0. 145. 4.11



Table 2

QUALITY GRAPH FOR REACH SECTION 9 x = 1 UPPER REACH CHICONE CREEK 3500.C DURING PERIOD 10

TIME SECONDS	SAL IN. PPM	CON. RATIO
0.	362.	13.15
1355.	401.	12.10
2710.	444.	10.89
4065.	485.	9.73
5420.	520.	8.76
6775.	545.	8.06
8129.	562.	7.59
9484.	571.	7.31
10839.	572.	7.20
12194.	568.	7.22
13549.	559.	7.31
14904.	546.	7.45
16259.	529.	7.62
17614.	511.	7.80
18969.	491.	7.96
20324.	470.	8.08
21679.	448.	8.17
23033.	426.	8.22
24388.	405.	8.22
25743.	384.	8.19
27098.	363.	8.13
28453.	344.	8.05
29808.	328.	7.92
31163.	314.	7.74
32518.	305.	7.65
33873.	298.	7.76
35228.	295.	8.20
36583.	293.	9.08
37937.	293.	10.21
39292.	293.	11.42
40647.	298.	12.87
42002.	311.	13.87
43357.	332.	13.84
44712.	362.	13.14

AVERAGE CONCENTRATIONS

0. 420. 9.02

Table 3

QUALITY GRAPH FOR REACH SECTION 2 x = WEST BRANCH CHICONE CREEK 500.0 DURING PERIOD 10

TIME SECONDS	SAL IN. PPM	CON. RATIO
0.	147.	38.30
13 55.	160.	36.16
27 10.	171.	34.55
40 65.	181.	33.24
54 20.	190.	32.17
67 75.	199.	31.24
81 29.	208.	30.41
94 84.	217.	29.67
1 08 39.	225.	29.04
1 21 94.	232.	28.52
1 35 49.	237.	28.12
1 49 04.	242.	27.85
1 62 59.	244.	27.73
1 76 14.	245.	27.74
1 89 69.	245.	27.87
2 03 24.	243.	28.12
2 16 79.	239.	28.46
2 30 33.	234.	28.90
2 43 88.	228.	29.43
2 57 43.	223.	30.10
2 70 98.	221.	31.13
2 84 53.	225.	32.99
2 98 08.	197.	30.61
3 11 63.	143.	24.74
3 25 18.	97.	21.62
3 38 73.	22.	13.47
3 52 28.	7.	10.54
3 65 83.	6.	12.43
3 79 37.	5.	17.33
3 92 92.	29.	28.86
4 06 47.	89.	50.49
4 20 02.	115.	45.72
4 33 57.	132.	41.07
4 47 12.	147.	38.29

AVERAGE CONCENTRATIONS

0. 169. 29.35

Table 4

QUALITY GRAPH FOR REACH SECTION 7<sup>2</sup> x = WEST BRANCH CHICONE CREEK 2500.0 DURING PERIOD 10

TIME SECONDS	SAL IN. PPM	CON. RATIO
0.	310.	17.45
13 55.	339.	16.06
27 10.	374.	14.70
40 65.	411.	13.45
54 20.	445.	12.43
67 75.	472.	11.69
81 29.	491.	11.24
94 84.	503.	11.08
108 39.	507.	11.17
121 94.	506.	11.48
135 49.	500.	11.97
149 04.	491.	12.62
162 59.	478.	13.43
176 14.	461.	14.40
189 69.	443.	15.51
203 24.	423.	16.74
216 79.	401.	18.09
230 33.	379.	19.55
243 88.	355.	21.08
257 43.	331.	22.68
270 98.	307.	24.33
284 53.	283.	25.91
298 08.	260.	27.24
311 63.	239.	27.75
325 18.	224.	27.40
338 73.	219.	26.92
352 28.	219.	26.48
365 83.	221.	25.88
379 37.	226.	25.12
392 92.	235.	24.06
406 47.	248.	22.53
420 02.	264.	20.65
433 57.	285.	18.92
447 12.	309.	17.44

AVERAGE CONCENTRATIONS

0. 359. 18.79

Table 5

QUALITY GRAPH FOR REACH SECTION 7<sup>3</sup> x = MIDDLE REACH CHICONE CREEK  
2000.C DURING PERIOD 10

TIME SECONDS	SAL IN. PPM	CON. RATIO
0.	764.	2.19
1355.	820.	1.25
2710.	864.	.70
4065.	895.	.41
5420.	914.	.30
6775.	927.	.24
8129.	934.	.22
9484.	937.	.21
10839.	935.	.25
12194.	926.	.40
13549.	906.	.73
14904.	875.	1.32
16259.	834.	2.15
17614.	786.	3.15
18969.	734.	4.27
20324.	680.	5.44
21679.	629.	6.60
23033.	581.	7.68
24388.	541.	8.66
25743.	506.	9.54
27098.	475.	10.34
28453.	449.	11.06
29808.	428.	11.70
31163.	412.	12.17
32518.	402.	12.46
33873.	396.	12.62
35228.	394.	12.62
36583.	402.	12.34
37937.	426.	11.67
39292.	464.	10.66
40647.	515.	9.21
42002.	590.	6.92
43357.	683.	4.14
44712.	763.	2.19

AVERAGE CONCENTRATIONS

0. 667. 5.87

Table 6

QUALITY GRAPH FOR REACH SECTION 2<sup>4</sup> x = EAST BRANCH CHICONE CREEK 500.0 DURING PERIOD 10

TIME SECONDS	SALIN. PPM	CON. RATIO
0.	697.	4.46
13 55.	690.	4.56
27 10.	684.	4.69
40 65.	679.	4.80
54 20.	677.	4.85
67 75.	678.	4.83
81 29.	680.	4.78
94 84.	684.	4.70
108 39.	689.	4.63
121 94.	693.	4.56
135 49.	698.	4.49
149 04.	701.	4.43
162 59.	704.	4.39
176 14.	707.	4.36
189 69.	708.	4.35
203 24.	709.	4.35
216 79.	710.	4.36
230 33.	710.	4.38
243 88.	710.	4.39
257 43.	711.	4.41
270 98.	714.	4.42
284 53.	717.	4.43
298 08.	721.	4.45
311 63.	724.	4.48
325 18.	727.	4.50
338 73.	729.	4.51
352 28.	719.	4.44
365 83.	718.	4.43
379 37.	716.	4.43
392 92.	714.	4.40
406 47.	712.	4.35
420 02.	708.	4.31
433 57.	703.	4.35
447 12.	696.	4.44

AVERAGE CONCENTRATIONS

0. 704. 4.49

Table 7

QUALITY GRAPH FOR REACH SECTION 5 x = LOWER CHICONE CREEK 1000.0 DURING PERIOD 10

TIME SECONDS	SALIN. PPM	CON. RATIO
0.	935.	.08
1355.	949.	.03
2710.	959.	.03
4065.	966.	.02
5420.	970.	.00
6775.	973.	.03
8129.	975.	.02
9484.	977.	.01
10839.	979.	.01
12194.	984.	.00
13549.	986.	.00
14904.	980.	.02
16259.	967.	.10
17614.	953.	.22
18969.	938.	.37
20324.	912.	.70
21679.	868.	1.43
23033.	811.	2.50
24388.	757.	3.60
25743.	706.	4.68
27098.	659.	5.72
28453.	619.	6.61
29808.	589.	7.32
31163.	569.	7.84
32518.	559.	8.12
33873.	558.	8.21
35228.	569.	7.53
36583.	642.	3.87
37937.	744.	.70
39292.	803.	.48
40647.	855.	.06
42002.	892.	.12
43357.	917.	.08
44712.	935.	.08

AVERAGE CONCENTRATIONS

0. 834. 2.13

Table 8

QUALITY GRAPH FOR REACH SECTION 5 LOWER CHICONE CREEK  
7 x = 1500.0 DURING PERIOD 10

TIME SECONDS	SALIN. PPM	CON. RATIO
0.	955.	.00
1355.	966.	.00
2710.	975.	.00
4065.	981.	.00
5420.	986.	.00
6775.	989.	.00
8129.	992.	.00
9484.	994.	.00
10839.	995.	.00
12194.	991.	.00
13549.	992.	.00
14904.	996.	.00
16259.	996.	.02
17614.	985.	.11
18969.	968.	.25
20324.	948.	.48
21679.	914.	.97
23033.	862.	1.88
24388.	805.	3.03
25743.	751.	4.17
27098.	702.	5.24
28453.	659.	6.22
29808.	625.	7.00
31163.	602.	7.55
32518.	588.	7.86
33873.	583.	7.96
35228.	672.	.00
36583.	753.	.00
37937.	814.	.00
39292.	860.	.00
40647.	895.	.00
42002.	921.	.00
43357.	940.	.00
44712.	955.	.00

AVERAGE CONCENTRATIONS

0. 868. 1.60

Table 9

CONCENTRATION PROFILE, REACH 1 UPPER REACH CHICONE CREEK  
AT TIME 10839.3 OF PERIOD 10

DISTANCE FEET	SAL IN. PPM	CON. RATIO
0.	174.	4.84
500.	188.	5.44
1000.	238.	7.27
1500.	280.	8.37
2000.	352.	9.27
2500.	413.	9.18
3000.	496.	8.34
3250.	533.	7.81
3500.	572.	7.20
3750.	611.	6.58
4000.	648.	6.01

CONCENTRATION PROFILE, REACH 2 WEST BRANCH CHICONE CREEK  
AT TIME 10839.3 OF PERIOD 10

DISTANCE FEET	SAL IN. PPM	CON. RATIO
0.	203.	31.56
500.	225.	29.04
1000.	291.	23.02
1500.	350.	18.74
2000.	433.	14.41
2250.	468.	12.77
2500.	507.	11.17
2750.	543.	9.78
3000.	581.	8.43
3250.	615.	7.19
3500.	648.	6.01

CONCENTRATION PROFILE, REACH 3 MIDDLE REACH CHICONE CREEK  
AT TIME 10839.3 OF PERIOD 10

DISTANCE FEET	SAL IN. PPM	CON. RATIO
0.	648.	6.01
250.	697.	4.87
500.	741.	3.87
750.	787.	2.87
1000.	823.	2.12
1500.	903.	.67
2000.	935.	.25
2500.	963.	.08
3000.	968.	.09
3250.	973.	.09
3500.	967.	.18



Table 10

CONCENTRATION PROFILE, REACH 4 EAST BRANCH CHICONE CREEK  
AT TIME 10839.3 OF PERIOD 10

DISTANCE FEET	SALIN. PPM	CON. RATIO
0.	683.	4.69
500.	689.	4.63
1000.	731.	3.85
1500.	772.	3.08
2000.	831.	2.03
2500.	884.	1.20
3000.	931.	.58
3250.	953.	.34
3500.	967.	.18

CONCENTRATION PROFILE, REACH 5 LOWER CHICONE CREEK  
AT TIME 10839.3 OF PERIOD 10

DISTANCE FEET	SALIN. PPM	CON. RATIO
0.	967.	.18
250.	987.	.03
500.	979.	.03
750.	989.	.02
1000.	979.	.01
1250.	984.	.00
1500.	995.	.00

Table 11

CONCENTRATION PROFILE, REACH 1 OF UPPER REACH CHICONE CREEK  
AT TIME 33872.7 OF PERIOD 10

DISTANCE FEET	SALIN. PPM	CON. RATIO
0.	11.	.30
500.	14.	.41
1000.	82.	2.30
1500.	132.	3.68
2000.	193.	5.21
2500.	237.	6.15
3000.	275.	6.89
3250.	284.	7.13
3500.	298.	7.76
3750.	317.	10.58
4000.	309.	16.84

CONCENTRATION PROFILE, REACH 2 OF WEST BRANCH CHICONE CREEK  
AT TIME 33872.7 OF PERIOD 10

DISTANCE FEET	SALIN. PPM	CON. RATIO
0.	40.	2.66
500.	22.	13.47
1000.	95.	24.89
1500.	114.	25.53
2000.	173.	28.42
2250.	187.	27.33
2500.	219.	26.92
2750.	243.	26.03
3000.	267.	23.66
3250.	287.	20.62
3500.	309.	16.84

CONCENTRATION PROFILE, REACH 3 OF MIDDLE REACH CHICONE CREEK  
AT TIME 33872.7 OF PERIOD 10

DISTANCE FEET	SALIN. PPM	CON. RATIO
0.	309.	16.84
250.	325.	15.89
500.	336.	15.18
750.	347.	14.58
1000.	357.	14.10
1500.	371.	13.43
2000.	396.	12.62
2500.	406.	12.23
3000.	467.	10.61
3250.	495.	9.89
3500.	533.	8.92

Table 12

CONCENTRATION PROFILE, REACH 4 EAST BRANCH CHICONE CREEK  
AT TIME 33872.7 OF PERIOD 10

DISTANCE FEET	SALIN. PPM	CON. RATIO
0.	744.	4.60
500.	729.	4.51
1000.	719.	4.39
1500.	714.	4.13
2000.	731.	3.91
2500.	709.	4.50
3000.	611.	6.96
3250.	576.	7.86
3500.	533.	8.92

CONCENTRATION PROFILE, REACH 5 LOWER CHICONE CREEK  
AT TIME 33872.7 OF PERIOD 10

DISTANCE FEET	SALIN. PPM	CON. RATIO
0.	533.	8.92
250.	538.	8.81
500.	543.	8.66
750.	546.	8.46
1000.	558.	8.21
1250.	568.	8.09

minimum of 0.35 ppb to a maximum of 5.76 ppb over the tidal cycle. The tidal mean value would be 4.11 ppb.

(b) The concentration at a distance of 3500 feet from the upper end of the main stem of Chicone Creek would vary from a minimum of 7.20 ppb to a maximum of 13.87 ppb., with a tidal mean value of 9.02 ppb.

(c) The concentration at a distance of 500 feet from the upper end of the West Branch would vary from a minimum of 10.54 ppb to a maximum of 50.49 ppb, with a tidal mean value of 29.35 ppb.

(d) The concentration at a distance of 2500 feet from the upper end of the West Branch would vary from a minimum of 11.08 ppb to a maximum of 27.75 ppb, with a tidal mean value of 18.79 ppb.

(e) The concentration at a distance of 5500 feet from the upper end of the main stem (3500 feet from the mouth) of Chicone Creek would vary from a minimum of 0.21 ppb to a maximum of 12.62 ppb with a tidal mean value of 5.87 ppb.

(f) The concentration at a distance of 500 feet from the upper end of East Branch would vary from a minimum of 4.31 ppb and a maximum of 4.67 ppb over the tidal cycle, with a tidal mean value of 4.49 ppb.

(g) The concentration at a distance of 500 feet up from the mouth of Chicone Creek would vary from a minimum of zero to a maximum of 8.21 ppb over the tidal cycle, with a tidal mean value of 2.13 ppb.

(h) The concentration at the mouth of Chicone Creek would vary from a minimum of zero to a maximum of 7.86 ppb over the tidal cycle, with a tidal mean concentration of 1.60 ppb.

These concentration values would be proportionately increased or decreased by the ratio of the actual mass immission rate to the value 1.0 lbs per day.

REFERENCES

- Carter, H.H. and R. Regier. 1974. The three dimensional heated surface jet in a cross flow. Chesapeake Bay Institute, The Johns Hopkins University, Tech. Report #88, Ref. 74-8.
- \_\_\_\_\_, and R. Regier. 1975. The distribution of excess temperature from the Vienna Generating Station on the Nanticoke River. Chesapeake Bay Institute, The Johns Hopkins University, Tech. Report #90, Ref. 75-5.
- \_\_\_\_\_, J.R. Schubel, R.E. Wilson and P.M.J. Woodhead. 1977. A rationale for evaluating thermally induced biological effects due to once-through cooling systems. Marine Sciences Research Center, SUNY at Stony Brook, Special Report #7, Ref. 77-3.
- \_\_\_\_\_, R.E. Wilson and G.E. Carroll. 1979. An assessment of the thermal effects on striped bass larvae entrained in the heated discharge of the Indian Point generating facilities Units 2 & 3. Marine Sciences Research Center, SUNY at Stony Brook, Special Report 24, Ref. 79-7.
- Harleman, D.R.F., J.E. Dailey, M.L. Thatcher, T.O. Najarian, D.N. Brocard, and R.A. Ferrara. 1977. User's manual for the M.I.T. transient water quality network model.
- Pritchard, D.W. 1960. The application of existing oceanographic knowledge to the problem of radioactive waste disposal into the sea, *In Disposal of radioactive wastes*. Vol. 2. International Atomic Energy Agency, Vienna, pp. 229-248.
- Rives, S.R. and D.W. Pritchard. 1978. Adaptation of J.R. Hunter's one-dimensional model to the Chesapeake and Delaware Canal System. Chesapeake Bay Institute, The Johns Hopkins University, Special Report #66, Ref. 78-6.
- Thatcher, M.L. and D.R.F. Harleman. 1972. Mathematical models for the prediction of unsteady salinity intrusion in estuaries. Tech. Report #144, R.M. Parsons Laboratory for Water Resources and Hydrodynamics, Department of Civil Engineering, M.I.T.

